

**Mucus and Surfactant as Barriers for the Pulmonary Delivery of  
Anti-infectives: Challenges, Models and Strategies for Overcoming them**

Dissertation  
Zur Erlangung des Grades  
des Doktors der Naturwissenschaften  
der Naturwissenschaftlich-Technischen Fakultät  
der Universität des Saarlandes

Von  
Benedikt Constantin Huck

Saarbrücken

2022

Tag des Kolloquiums: 22.07.2022

Dekan: Prof. Dr. Jörn Walter

Berichterstatter: Prof. Dr. Claus-Michael Lehr

Vorsitz: Prof. Dr. Thorsten Lehr

Akademischer Mitarbeiter: Dr. Britta Diesel

Die vorliegende Arbeit wurde von Januar 2018 bis Juni 2021 unter der Leitung von Herrn Prof. Dr. Claus-Michael Lehr am Institut für Pharmazeutische Technologie der Universität des Saarlandes und am Helmholtz-Institut für Pharmazeutische Forschung Saarland (HIPS) in der Abteilung für Wirkstoff-Transport angefertigt.

## Table of Contents

<b>I. Summary</b> .....	<b>V</b>
<b>II. Zusammenfassung</b> .....	<b>VI</b>
<b>III. Abbreviations</b> .....	<b>VII</b>
<b>1 Introduction</b> .....	<b>1</b>
1.1 Lung physiology and barriers .....	1
1.2 Respiratory tract infections and anti-infectives .....	5
1.3 Challenges in pulmonary drug delivery of anti-infectives .....	7
1.4 Models and methods to investigate pulmonary mucus and surfactant interactions ..	12
1.5 Recent advances and strategies to overcome the pulmonary barriers .....	16
<b>2 Aims of the thesis</b> .....	<b>19</b>
<b>3 Main outcomes of the thesis</b> .....	<b>20</b>
3.1 Native pulmonary mucus and surrogates: Characterization and interaction with nanomaterials and pathogens to predict pulmonary delivery of anti-infectives .....	20
3.2 Role of composition, interfacial activity and barrier properties of pulmonary surfactant preparations for the uptake and toxicity of aerosolized nanomaterials .....	24
3.3 <i>In vitro</i> characterization and interaction of respirable liposomal dry powder formulations with cellular and non-cellular lung barriers .....	29
<b>4 Conclusion and future perspectives</b> .....	<b>37</b>
<b>5 Original publications – scientific output</b> .....	<b>38</b>
5.1 Macro- and microrheological properties of mucus surrogates in comparison to native intestinal and pulmonary mucus .....	38
5.2 A surrogate of pulmonary mucus for investigating antibiotic permeation and activity against <i>Pseudomonas aeruginosa</i> biofilms .....	53
5.3 Systematic Analysis of Composition and Performance of Pulmonary Surfactant Preparations on Cellular Uptake and Cytotoxicity of Aerosolized Nanomaterials .....	76
5.4 Nano-in-Microparticles for Aerosol Delivery of Antibiotic-loaded, Fucose- derivatized and Macrophage-targeted Liposomes to Combat Mycobacterial Infections: <i>In</i> <i>Vitro</i> deposition, Pulmonary Barrier Interactions and Targeted Delivery .....	97
<b>6 References</b> .....	<b>125</b>
<b>7 List of scientific publications</b> .....	<b>140</b>
<b>8 Scientific collaborations</b> .....	<b>142</b>
<b>9 Acknowledgements</b> .....	<b>143</b>

## I. Summary

Pulmonary administration of anti-infectives is an appealing non-invasive delivery route for the treatment of respiratory tract infections. However, the sophisticated cellular and non-cellular barriers of the lungs remain a major challenge for the success of inhalation therapy. Pulmonary mucus protects the lungs from inhaled materials by physical and chemical entrapment in the conducting airways. In the respiratory airways, the thin pulmonary surfactant (PS) layer enables the process of breathing and determines the fate of inhaled nanomaterials by particle corona formation. There is, however, a lack of pulmonary mucus and surfactant models to investigate nanoparticle interactions. This work investigates the macro- and microrheology of native and surrogate mucus to predict nanoparticle mobility, antibiotic permeability and pathogen growth. PS preparations were analyzed for their composition and biophysical activity and the key parameters that influence nanoparticle aggregation, internalization and toxicity were determined *in vitro*. As part of the ANTI-TB project, the models described in this thesis were used to investigate novel inhalable formulations for the treatment of pulmonary tuberculosis. An inhalable nano-in-micro dry powder formulation comprised of bedaquiline-loaded liposomes was tested *in vitro* for its potential to treat mycobacterial infections and to overcome the pulmonary barriers and the ever-increasing challenge of antimicrobial resistance.

## II. Zusammenfassung

Die Inhalation von Antiinfektiva ist ein nicht-invasiver Verabreichungsweg zur Behandlung von Atemwegsinfektionen. Die Überwindung der ausgeklügelten zellulären und nicht-zellulären Barrieren der Lunge bleibt eine der größten Herausforderung für den Erfolg der Inhalationstherapie. Mukus schützt die Lunge vor eingeatmeten Materialien durch physikochemische Wechselwirkung. In der tiefen Lunge ermöglicht eine dünne Schicht aus Lungensurfactant den Atmungsprozess und bestimmt das Schicksal eingeatmeter Nanomaterialien durch Partikelkoronabildung. Um diese Interaktionen zu untersuchen werden geeignete *in vitro* Modelle benötigt. Diese Arbeit untersucht die Rheologie von nativem und künstlichem Mukus, um Nanopartikelmobilität, Antibiotikapermeabilität und Pathogenwachstum vorherzusagen. Eine Auswahl an Lungensurfactants wurde auf ihre Zusammensetzung und biophysikalische Aktivität analysiert und die Schlüsselparameter, die die Aggregation, Internalisierung und Toxizität von Nanopartikeln beeinflussen, wurden bestimmt. Im Rahmen des ANTI-TB-Projekts wurden die in dieser Arbeit beschriebenen Modelle verwendet, um neuartige inhalierbare Formulierungen zur Behandlung von Lungentuberkulose zu untersuchen. Eine inhalierbare Nano-in-Mikro-Trockenpulverformulierung aus Antibiotika-beladenen Liposomen wurde auf ihr Potenzial zur Behandlung mykobakterieller Infektionen und zur Überwindung der Lungenbarrieren getestet, um der ständig wachsenden Herausforderung der Antibiotikaresistenz entgegenzuwirken.

### III. Abbreviations

AT I / AT II	Alveolar Type I /II cells
API	Active Pharmaceutical Ingredient
BDQ	Bedaquiline
BALF	Bronchoalveolar Lavage Fluid
COPD	Chronic Obstructive Pulmonary Disease
CF	Cystic Fibrosis
CFTR	Cystic Fibrosis Transmembrane Conductance Regulator
DLS	Dynamic Light Scattering
DPPC	Dipalmitoyl Phosphatidylcholine
LVX	Levofloxacin
MSD	Mean Squared Displacement
MIC	Minimal Inhibitory Concentration
MUC	Mucin Glycoprotein
MCC	Mucociliary Clearance
MDR	Multi Drug Resistance
MPT	Multiple Particle Tracking
Mtb	Mycobacterium Tuberculosis
NGA	Next Generation Impactor
PA	Pseudomonas Aeruginosa
PADDOCC	Pharmaceutical Aerosol Deposition Device on Cell Cultures
PEG	Polyethylene Glycol
PLGA	Polylactic-co-glycolic Acid
PS	Pulmonary Surfactant
RTI	Respiratory Tract Infection
SP	Surfactant Protein
TEER	Transepithelial Electrical Resistance

# 1 Introduction

## 1.1 Lung physiology and barriers

The lung is the entry port of the surrounding air into the human body and the organ in charge of gas exchange. Its main function is to transfer life-giving oxygen to the body while removing exhaled air ( $\text{CO}_2$ ). Considering an average breathing rate of  $15 \text{ min}^{-1}$  for adults and a tidal volume of 500 mL, the volume of inhaled air exceeds a number of 10,000 liters per day [1]. This bears a significant risk of exposure to pollutants, allergens, pathogens as well as dust and other particles. Therefore, the inhaled air must be appropriately conditioned and filtered on its way to the alveolar capillaries, where gas exchange takes place. The exchange of fresh  $\text{O}_2$  with  $\text{CO}_2$  from the blood stream at the air-blood interface and the subsequent elimination of carbon dioxide from the lungs by expiration completes the respiratory cycle.

As it travels along the branched bifurcations to the deep lungs, the inhaled air is surrounded by well-differentiated epithelia with specialized functions, distinguishable as conducting and respiratory airways. The former consists of a ciliated and pseudostratified columnar epithelium, starting to branch from the trachea into more than 20 generations of bronchi and even smaller bronchioles with progressively decreasing airway cross-sections [2]. Opening out to the alveolar region, the gas flow becomes laminar and the total lung surface with an area of  $140 \text{ m}^2$  offers exceptional conditions for pulmonary absorption and gas exchange [3]. The approximately  $10\text{--}30 \mu\text{m}$  thick airway epithelium, consisting mainly of goblet, basal and ciliated cells, not only reduces in diameter, but also significantly in epithelial thickness [4]. In the alveolar region, the epithelium is less than  $1 \mu\text{m}$  thick, allowing for efficient diffusion of gases to and from the blood stream facilitated by the orchestrated in- and deflation of the alveolar air sacks (alveoli) [5]. The inner, luminal side of the alveolus consists of a non-ciliated epithelium composed of squamous alveolar type (AT) I cells, covering about 95% of the airway surface. AT II cells, which are round to cuboidal in shape, account for the remaining 5%, however greatly outnumber the number of AT I cells. AT I and II cells exhibit alveolar tight-junctions that form an extremely tight epithelium, limiting the transition of most materials to the blood stream [6]. Separated from the alveolus by a thin endothelial layer, they collectively form the so-called air-blood-barrier. Alveolar macrophages, present in the alveolar lumen and connective tissues, clear up debris and inhaled materials by phagocytosis, displaying an efficient pulmonary protection mechanism [7].

On the non-cellular level, the lung is covered and protected by surface lining fluids, that greatly differ in their function and composition between respiratory and conducting airways. The latter are covered by **pulmonary mucus**, a dense polymer network consisting of water, inorganic salts, DNA, proteins, cell debris and the gel-forming macromolecular mucins [8]. Mucus, secreted from goblet cells and submucosal glands, entraps inhaled materials and continuously removes them from the lungs by the coordinated beating of ciliated cells, a process referred to as mucociliary clearance (MCC **Figure 1**). Mucus can be separated into two distinct layers, the inner, low-viscosity layer ( $5\text{--}10 \mu\text{m}$  thick periciliary layer) directed towards the ciliated



epithelium and an outer viscoelastic layer composed mainly of the gel-forming mucins (20 – 25  $\mu\text{m}$  thickness) [9].

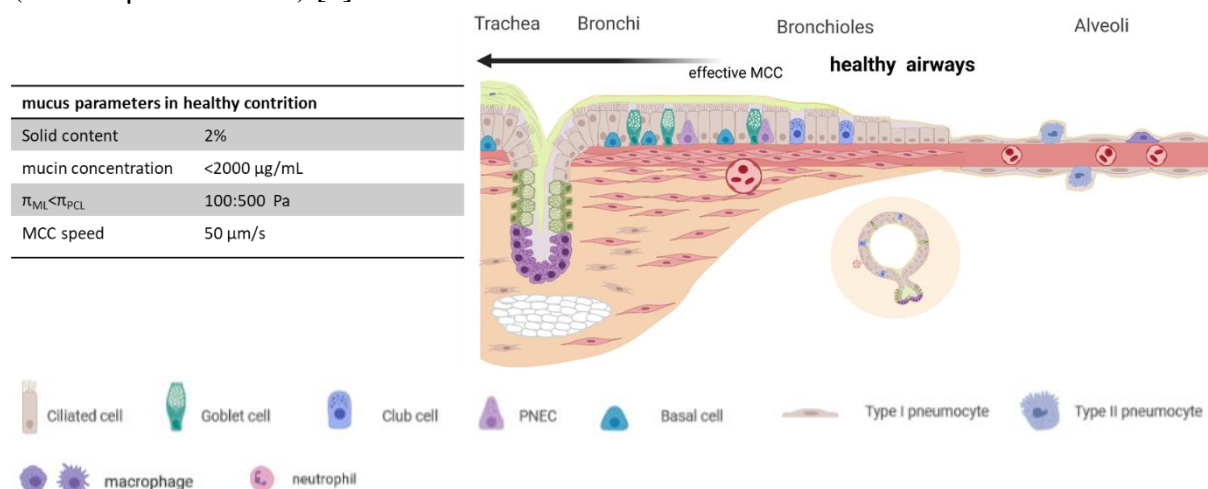


**Figure 1) Mucus in health.** Mucus in healthy airways is continuously secreted and replenished, enabling efficient removal of inhaled materials. The figure summarizes and depicts normal lung parameters. Osmotic pressure of the mucociliary ( $\pi_{\text{ML}}$ ) vs. the periciliary layer ( $\pi_{\text{PCL}}$ ) – the ratio ensures that the periciliary layer is stable in health. Adapted with permission from Huck *et al.* [10].

Mucin glycoproteins (MUC) are the main constituents of mucus. The secreted MUC5AC and MUC5B and the cell-bound mucins (MUC16; MUC1) are the predominant mucins in the human airways [11,12]. They consist of a polypeptide backbone decorated with oligosaccharide side chains and are covalently linked via disulfide bonds present in cysteine rich regions. Mucus has a net negative charge since the carboxyl- and sulfate groups of terminal sugars of the oligosaccharide branches are deprotonated at the physiological pH range of pulmonary mucus (pH range 7-9) [13]. With each approximately 1%, lipids and proteins represent only a small proportion of the total mucus mass, however, they are extremely diverse in composition. With more than 250 species each, the mucus lipidome [14] and proteome [15] is far from being understood. Lipids play a role mainly in maintaining wettability and stabilization of the conducting airways by a reduction of the airway's surface tension [16,17], whereas most of the proteins found in human mucus can be categorized either as antimicrobial peptides, chemokines or immunomodulators, almost all of them associated with innate host defense mechanisms [18]. The collective interplay of mucus constituents and particularly the high-molecular mucins create a three-dimensional biopolymeric network with diverse chemical (hydrogen bonding, hydrophobic and Van der Waal interactions), physical (electrostatic interactions and size filtering) and immunomodulatory (lipids, proteins) interaction potential. As such, mucus acts as an efficient barrier to inhaled pathogens and nano-sized materials, which are sterically trapped in the mucus meshwork (**Figure 2**) [19].

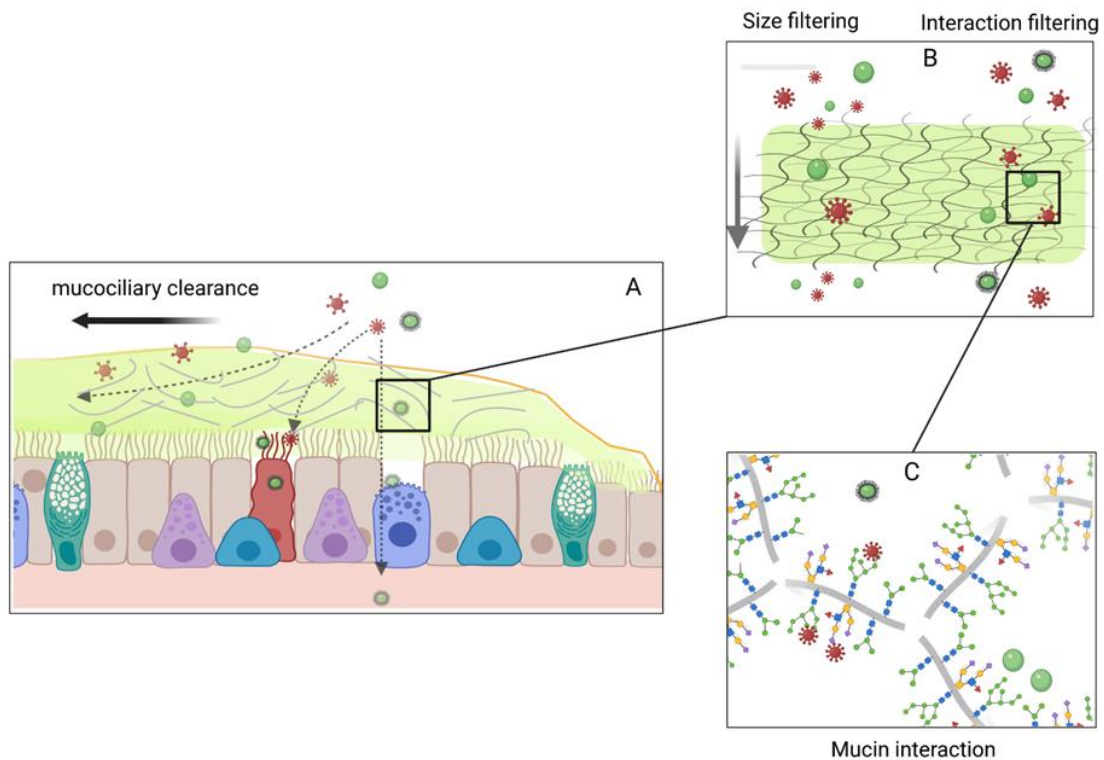


**Figure 2)** *How the mucus barrier works.* Mucus entraps most inhaled materials - both hazardous (red) or therapeutic (green) - and the coordinated ciliary beating transports them out of the lungs (A). Only if the physicochemical parameters are within a certain range, inhaled materials can penetrate the mucus barrier (B). This includes a size  $< 200$  nm and a non-interacting (stealth or mucoinert) surface chemistry that complies with the size- and interaction filtering mechanisms of mucus. In addition, the complex glycosylation pattern of the mucin backbone allows for specific interactions, thereby attenuating the virulence of inhaled pathogens (C). Reprinted with permission from Huck *et al.* [10].

With the transition from the bronchial to the alveolar airways alongside the respiratory tract, the composition and biophysical function of the surface lining fluid changes dramatically to suffice the complex process of alveolar ventilation. An extremely thin layer of **pulmonary surfactant (PS)** covers the whole respiratory surface and protects the lungs from collapsing by a reduction in surface tension during exhalation – a mechanisms paramount to breathing [20]. PS is secreted from AT II cells as lamellar bodies, unravelling into intermediate structures such as tubular myelin and large surfactant layers before adsorbing and spreading along the alveolar air-liquid interface (**Figure 3**) [21].

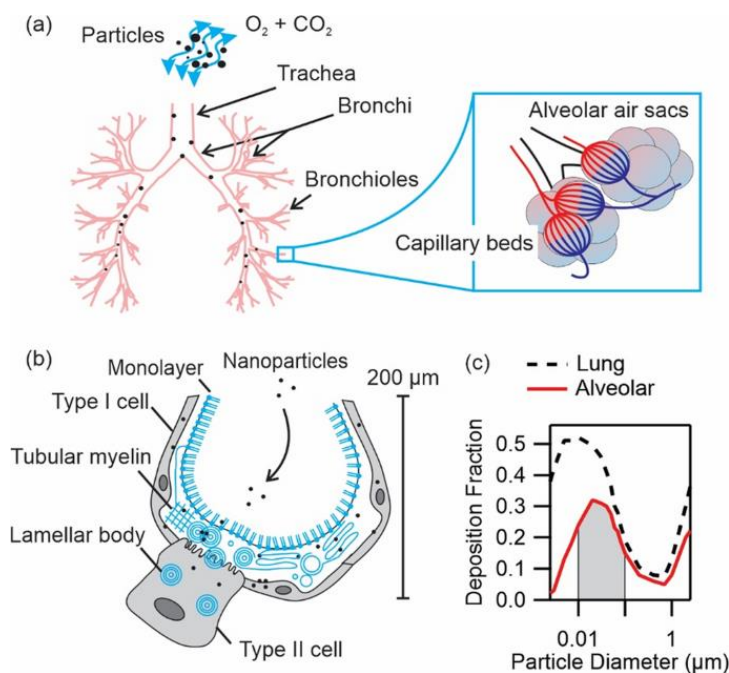


**Figure 3)** *Particles entering the lungs during respiration.* a) Lung sections of trachea, bronchi, bronchioles and alveolar air sacs decrease in diameter from 12 mm to 200  $\mu\text{m}$ . b) Deposition of nanoparticles in the alveolus. c) Deposited fractions in the bronchial (black line) and alveolar region (red line) of the lungs depending on the particle diameter. Preprinted with permission from Radiom *et al.* [22].

Although used surfactant can be found in the upper airways, it is to the largest extent recycled by alveolar macrophages via receptor-mediated mechanism and returned to the cycle [14]. PS is a membrane-based lipid-protein material consisting of 90% phospholipids and 10% proteins by mass. The lipid fraction consists of saturated dipalmitoylphosphatidylcholine (DPPC), phosphatidylglycerols and other lipids including sphingomyelins and cholesterol [23]. Surfactant proteins (SP) can be divided in two classes, the hydrophobic SP-B and SP-C and the hydrophilic SP-A and SP-D. The latter predominantly contribute to host protection via the innate immune system by opsonization and subsequent internalization by macrophages, thus clearing unwanted materials from the lungs. SP-B and SP-C support the rapid adsorption to the air-interface, the packaging of DPPC to high-ordered states and the lateral diffusion of surfactant membranes [24,25]. Collectively, surfactant proteins and phospholipids facilitate the biophysical activity of PS and its ability to reduce surface tension to values close to 0 mN/m [26].

The respiratory epithelium that is covered by PS represents the largest and thinnest surface in the body exposed to the environment. Thus, the fate of inhaled materials is determined by the interplay with PS constituents promoting nanoparticle deposition, entrapment, toxicity, pulmonary absorption and clearance [27–29]. Together with pulmonary mucus, PS constitutes an important renewable non-cellular barrier to inhaled materials, be it to harmful pollutants and pathogens or (nano)-materials for on purpose delivery of medicines to the lungs.

## 1.2 Respiratory tract infections and anti-infectives

Pathogens such as viruses and bacteria that circumvent the lung's sophisticated barriers can cause severe respiratory tract infections (RTI), typically classified as upper and lower RTIs. Infections of the respiratory tract are the leading cause of death among all infectious diseases according to WHO [30]. Although viral infections such as influenza, viral pneumonia and SARS-CoV-2 are on the rise, there is an equal threat and health-care burden caused by bacterial pathogens. In several pulmonary pathologies, including bronchitis, pneumonia and asthma, both viral and bacterial pathogens are involved. The majority of bacterial infections are caused by three major pathogen classes: *streptococci*, *haemophilus* species and *mycobacteria* and generally treated with antibiotics (**Figure 4**) [31–33]. In 2019, worryingly, the deaths caused by antibiotic resistance have outnumbered that of AIDS and Malaria together, imposing a major and increasing threat to human health [34].

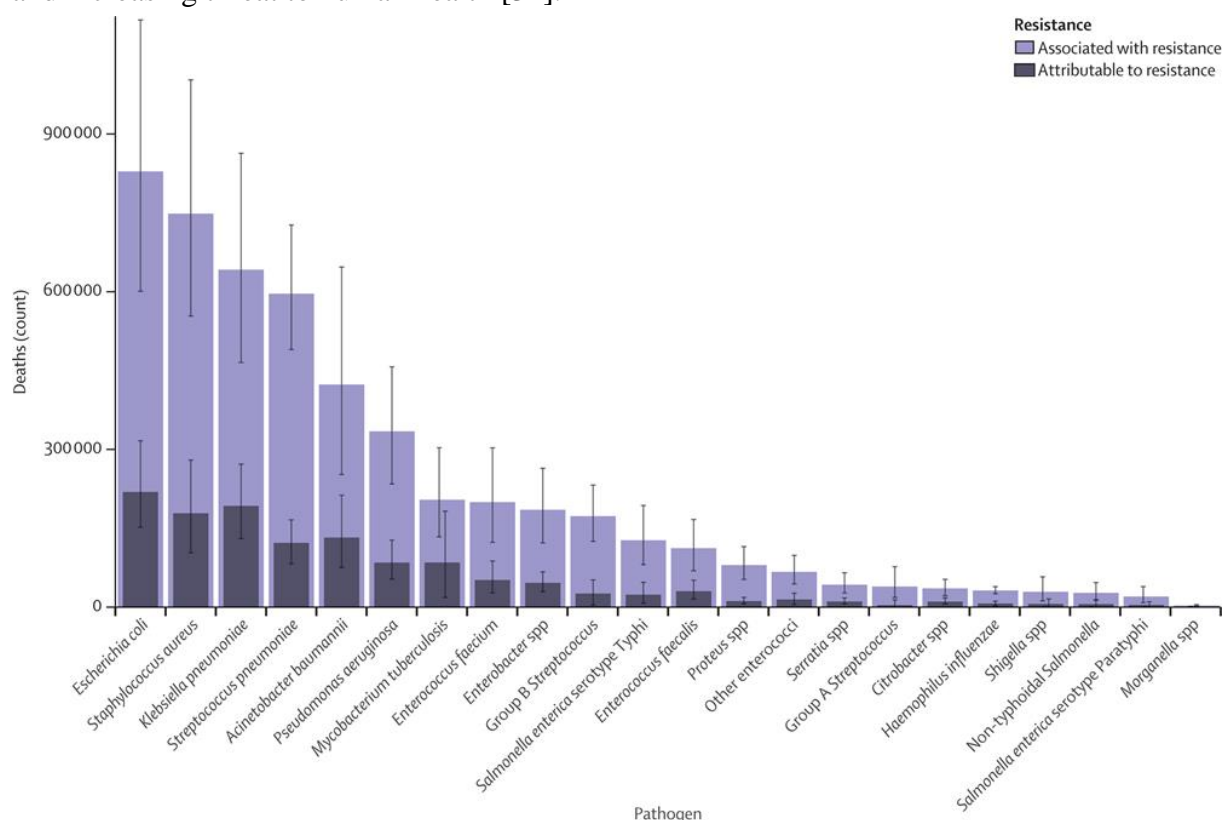


**Figure 4)** Deaths associated or attributable to antimicrobial resistance sorted by their causative pathogens. Reprinted with permission from Murray *et al.* [34].

Particularly in patients with reduced immunity and pre-existing lung conditions, the risk of severe infections and development of antibiotic resistance is dramatically increased. Oftentimes, this applies to disorders associated with the occurrence of exacerbations and impaired MCC, offering an ideal matrix and seeding ground for respiratory pathogens [35]. Mucus hypersecretion, accumulation of cell debris, mucins, DNA and impaired MCC in chronic obstructive pulmonary disease (COPD) and cystic fibrosis (CF) lead to an imbalanced lung homeostasis (**Figure 5**) [36]. Alterations in pH, protein oxidation, protease activity and neutrophil dysfunction – the main contributors to host-pathogen interactions – thus lead to acute

lung inflammation, airway obstruction and severe pulmonary infections [37]. In CF patients, a mutation in the CF transmembrane conductance regulator (CFTR) hampers the hydration and the maintenance of the osmotic pressure of the mucus layer, impairing the above-described homeostasis and host defense mechanisms while facilitating bacterial colonization [38]. Still nowadays, CF is a disease without curative, and in 60-80% of the cases, infections with *Pseudomonas aeruginosa* (PA) ultimately lead to death [39].

The most prevalent lung pathogen with almost 2 billion infected people – almost one fourth of the world's population – however, is *Mycobacterium tuberculosis* (*Mtb*) [40]. When mycobacteria, typically transmitted from person-to-person as liquid aerosols, deposit in the lower respiratory tract, they are phagocytosed by macrophages and dendritic cells via a multitude of different receptors including complement receptors, toll-like receptors and C-type lectin receptors such as the DC-SIGN and macrophage-mannose (CD206) receptors [41]. The latter is of high clinical significance for diagnosis and therapy of *Mtb* infections, and exploited to deliver medicines to intracellular phagosomal compartments [42,43]. During disease progression, the formation of granuloma via the attraction and aggregation of immune cells – the hallmark of *Mtb* infections – offer a perfect niche for bacterial replication and persistence, making them difficult to reach and treat [44]. Strikingly, there is another emerging class of non-tuberculous mycobacteria, such as *M. avium* and *M. abscessus*, for instance, that have transformed from harmless saprophytics to dangerous pathogens even for immunocompetent patients, now becoming extensively antibiotic-resistant [45].

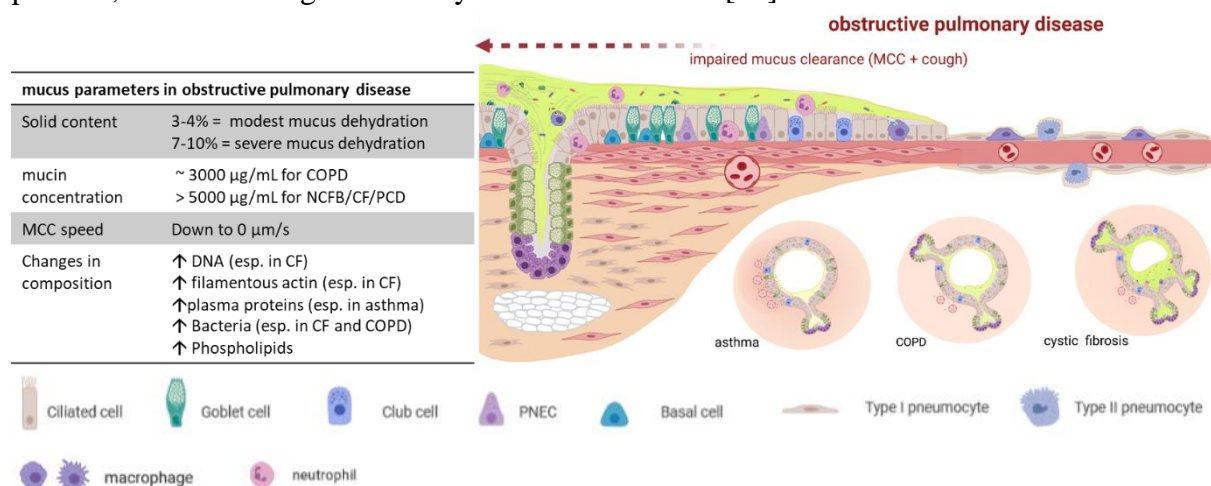


**Figure 5) Mucus in disease.** Altered mucus hydration, composition, and viscoelasticity significantly contribute to obstructive pulmonary diseases. Mucus hyperproduction, accumulation and increased risk for infections is observed in asthma and even more in chronic obstructive pulmonary disease (COPD) and cystic fibrosis (CF). The table highlights the crucial solid components with increased contributions for the respective diseases. The airway cross sections represent the three main obstructive pulmonary diseases with their differences in mucus origin (glands or airway cells), extent of mucus plugging and increased risk of infections. Adapted with permission from Huck *et al.* [10].

Since the prevention of such bacterial infections by vaccination is not established yet, the treatment with antibiotics is the greatest hope for combatting infectious diseases. The standard first-line treatment regimen for *Mtb* infections, for instance, requires the simultaneous co-treatment with a variety of antibiotics (e.g., rifampicin, ethambutol, pyrazinamide, isoniazid) to prevent and cope with resistance [46]. On the downside, such an oral antibiotic therapy may

take up to 6 months and is associated with severe systemic side effects and low patient compliance, at a success rate of only 50%, that worsens if bacteria become multi (MDR)- or even extensive drug resistant [47]. This creates a strong need to innovate new treatment strategies, delivery platforms as well as novel antibiotics and anti-infectives [48]. The development of second-line antibiotics such as the well-known streptomycin and levofloxacin (LVX) and the highly potent MDR drugs bedaquiline (BDQ), linezolid and BTZ043, however, can only be the first step in a cascade of strategies for improving pulmonary infection therapy. Particularly the hydrophobicity and poor water solubility of such antibiotics makes them hard to be adequately formulated and administered [49]. It is therefore of paramount interest to develop new delivery systems for oral inhalation therapy that deliver their cargo in sufficient amounts to the target site. Such a loco-regional delivery requires formulations that ideally can cope with or even overcome the various cellular (e.g., macrophages and epithelial cells) and non-cellular (e.g., mucus and surfactant) barriers of the lungs that challenge pulmonary drug delivery of anti-infectives.

### 1.3 Challenges in pulmonary drug delivery of anti-infectives

Treating infectious diseases via the lungs is appealing since the lungs offer an exceptional non-invasive delivery route with an extremely large surface area available for absorption of the inhaled molecules. Inhalation medicines are currently the best option for the treatment of pulmonary disorders such as asthma, COPD and CF, represented by an array of formulations approved to treat such diseases [50,51]. Local pulmonary delivery can direct molecules to their target, thereby circumventing systemic administration, reducing side effects and the dose required to achieve therapeutic concentrations [52]. However, the development of new chemical and biological (e.g., proteins and small molecules) anti-infectives more than ever requires sophisticated carriers that protect the cargo, control the release and direct drugs to the lungs: the drug delivery system. The essential barriers for the successful pulmonary delivery are depicted in **Figure 6**.

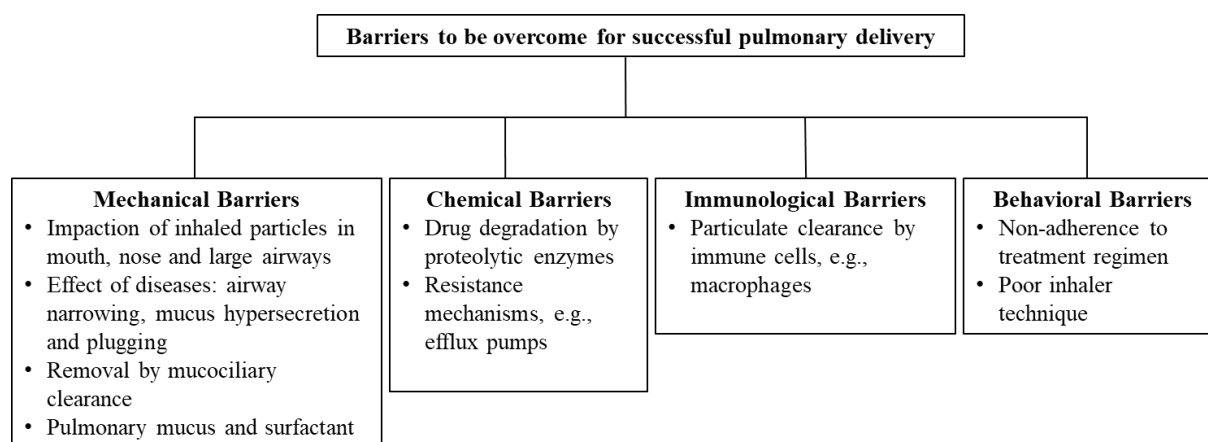


**Figure 6)** Barriers to be overcome for successful pulmonary delivery.

The pharmacological response strongly depends on the amount of active pharmaceutical ingredient (API) binding to its target, thus maximizing the locally deposited dose should be the ultimate goal of pulmonary administration. The deposition in the lungs occurs via three main mechanisms: inertial impaction, gravitational sedimentation and Brownian diffusion [53], all of them critically affected by the size, density and shape of the inhaled aerosol particles, that can be classified by i) the mass median aerodynamic diameter, which defines the particle diameter at which 50% of the aerosol mass is above and 50% is below, ii) the geometric standard deviation describing the spread of particle size of an aerosol and iii) the fine particle fraction, which is the mass percentage of particles with a diameter below a size of 4.7  $\mu\text{m}$  [54]. Thus, the particle's diameter dictates whether it settles in the throat or upper airways (size  $> 5 \mu\text{m}$ ), the central and small airways (size between 2-5  $\mu\text{m}$ ) or the alveolar region (size  $< 2 \mu\text{m}$ ). Due to airway narrowing and mucus plugging in obstructive pulmonary diseases, the dose delivered to the deep lung can be reduced by up to 50%, whereas the deposition is typically increased in the upper compared to lower airways [55]. In fact, the doses required for the treatment of pulmonary infections are as high as 1000 mg per single inhalation and quickly reach a non-tolerable limit, leaving only little space for dose adjustments. Thus, the selection of an appropriate inhaler strategy (liquid vs. dry powder aerosol) is crucial and must allow for accurate and repeated dosing while ensuring patient adherence (**Figure 7**). The latter is referred to as the behavioral barrier – the last hurdle to be taken for a successful inhalation therapy [56]. Fortunately, recent advances in inhaler technologies have quite successfully addressed this issue and increased deposited amounts tremendously [57], while shifting the focus of inhalation therapy towards a deeper understanding of the fate of the inhaled particle upon landing in the lungs.

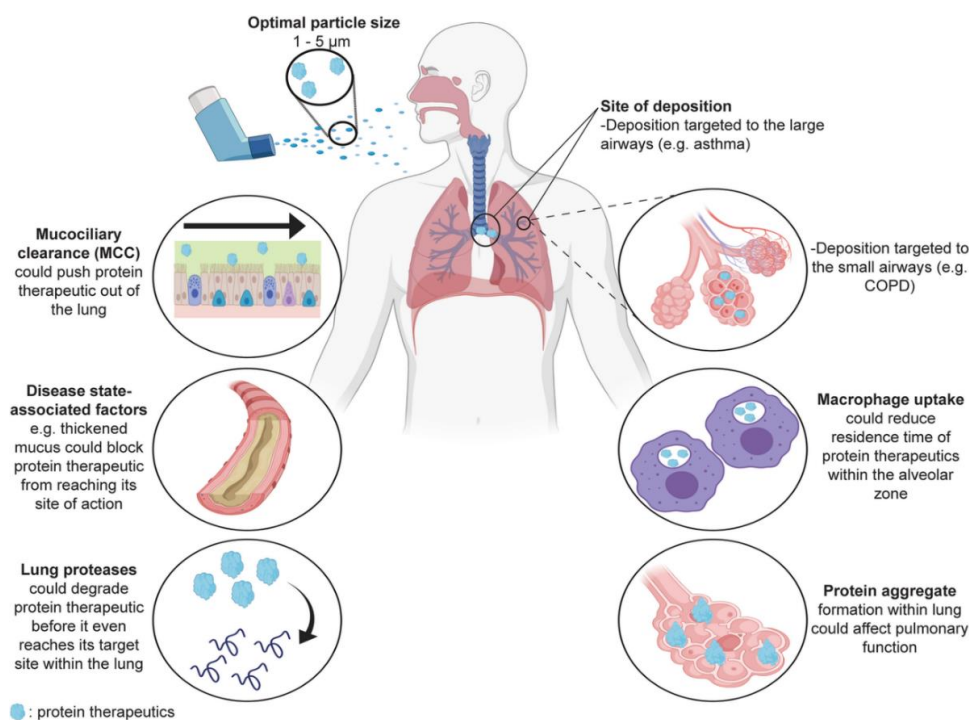


**Figure 7)** Major challenges for inhalation on the example of protein-based medicines intended for lung targeting. Targeted deposition sites within the lung (large or small airways) will vary depending on the specific lung disease being treated. Reprinted with permission from Matthews *et al.* [58].

The interactions with the cellular and non-cellular pulmonary barriers determine whether a particle reaches its therapeutic target and successfully delivers the incorporated cargo or if it is trapped and cleared from the lungs. Thus, one aim of this thesis is to understand and elucidate the mechanisms and contributing factors to the molecular and microscale interactions of nanoparticle-based drug delivery systems with the non-cellular and cellular pulmonary barriers. While for deep lung targeting, the loss of particles within the mucus layer should be minimal, for the treatment of upper airway infections, the delivery system must efficiently penetrate the pulmonary mucus layer at a speed higher than MCC rates in order to access the therapeutic target in the airway epithelium [59]. Recent studies by Schuster *et al.* have demonstrated a cut-off size of < 500 nm for such diffusive or “mobile” particles, while objects larger than this size are sterically trapped within the mucus meshwork and transported out of the lungs [19]. Similarly, positively charged and hydrophobic particles adhere to the mucus layer via electrostatic and hydrophobic interactions, thereby limiting lung residence time due to rapid mucus turnover [60]. Dehydration and accumulation of mucins, cellular debris and DNA in pulmonary pathologies such as COPD and CF lead to thickening and a decreased mean mucus pore size, necessitating delivery systems tunable in size, charge and hydrophobicity [61,62]. In *Pseudomonas aeruginosa* infections, the polysaccharide and protein-rich bacterial biofilms additionally protect the embedded bacteria from the environment, thereby increasing antimicrobial resistance 10-1000 times [63]. Recently, the combination of tobramycin and a novel quorum-sensing inhibitor with a squalene-based muco-adhesive delivery system effectively reduced bacterial colonization by lowering the minimal inhibitory concentration (MIC) of the delivered antibiotic up to 32-fold [64]. Similarly, successful lectin targeting of PA biofilms using glycomimetic liposomes [65] clearly outlines that efficient antibiotic delivery using innovative approaches is key to a successful antimicrobial therapy.

When the inhaled nanomedicine is designed to favor deposition in the respiratory airways where PS lines the interface, the formation of a protein-lipid shell, the so-called corona, determines the fate of the inhaled materials in the lungs. The new molecular identity acquired by lipid and protein adsorption may affect pulmonary absorption, distribution, particle aggregation and clearance as well as cytotoxicity [66,67]. This process depends on a variety of factors, such as the particle’s size, charge, curvature, hydrophobicity and surface properties [68,69]. Interestingly, the lipids adsorbed to the surface of polyethylene glycol (PEG), polylactic-co-glycolic acid (PLGA) and lipid nanoparticles are similar to the greatest extent, whereas the surfactant proteins seem to mediate the corona formation on different surfaces by acting as a “primer” [70]. Upon binding to the surface of inhaled materials, SP-A and D – both belonging to the collectin subtype of pattern-recognition receptors – act as modulators of the immune system and facilitate receptor-mediated phagocytosis mainly by macrophages and dendritic cells [71]. Profiting from improved cellular internalization and intracellular routing, these mechanisms have been exploited for on purpose delivery of the therapeutic cargo to intracellular compartments. For instance, surface-decoration of drug delivery systems with surfactant proteins has been investigated in mycobacterial infections and cellular transfection



studies [72–75]. However, the corona formation upon contact with PS might also limit therapeutic effects of surface-targeted nanoparticles by masking the particle's surface while facilitating rapid macrophage clearance (**Figure 8**) [76]. The fusogenic proteins SP-B and SP-C modulate permeability and lipid dynamics after intercalation into phospholipid membranes. Thus, it is to be expected that similar effects can lead to disintegration and rapid payload release of lipid-based (e.g., liposomal) delivery systems [77]. On the other hand, the lipid-rich milieu of PS exhibits exceptional properties for the solubilization of hydrophobic drugs, such as corticosteroids and antibiotics. The inherent interfacial activity of PS facilitates spreading of drugs along the respiratory surface, with the potential to act as a delivery vehicle on its own [78,79].

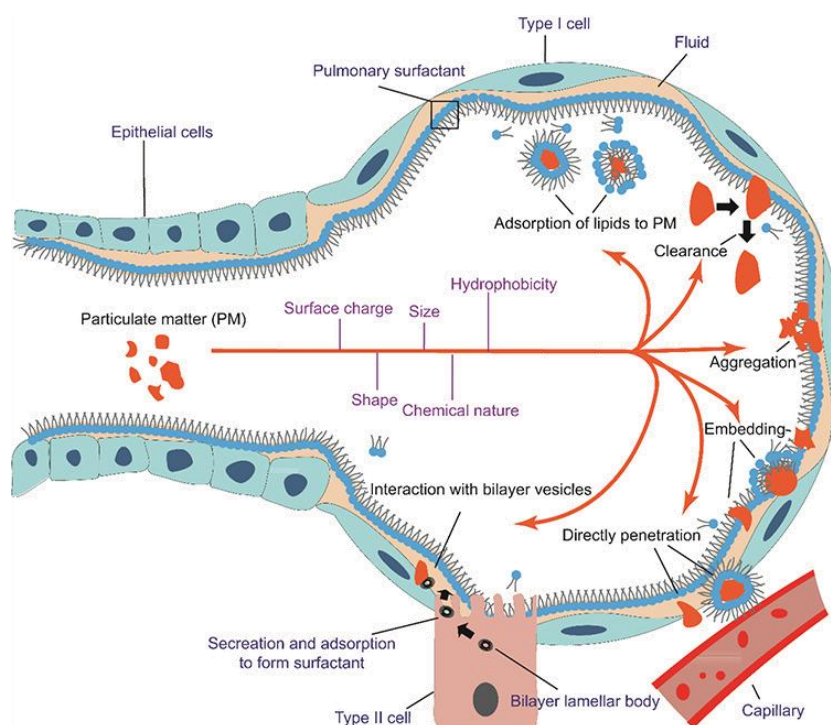


**Figure 8)** Interactions of inhaled particulate matter with pulmonary surfactant. Reprinted with permission from Wang *et al.* [80].

Surfactants such as Alveofact<sup>®</sup> and Curosurf<sup>®</sup> are commercially available and clinically used for the treatment of neonatal respiratory disorders [81] and to study nanoparticle interactions. They have been shown to reduce the cytotoxicity of multiwalled carbon nanotubes [28] and silica nanoparticles [82], however, some nanomaterials are capable of intercalating into the surfactant layer while inhibiting PS's biophysical function, in particular the ability to reduce surface tension that prevents the lungs from collapsing [83,84]. Thus, predicting the interaction of inhaled nanomaterials with PS in a case-by-case study appears necessary to estimate the efficacy and safety of novel delivery systems, ideally by including lung lining fluids into *in vitro* models of the lungs that allow for an extrapolation to the *in vivo* scenario.

On the cellular level, the factors that limit the success of inhalation therapy include i) clearance by phagocytic cells/macrophages, ii) absorption across the alveolar epithelium and iii) the permeability across the bacterial cell membrane. Specific proteolytic enzymes and the surfactant proteins present in pulmonary mucus and surfactant are linking mechanical to

immunological barrier properties [85]. The prevention of macrophage clearance is important to enhance lung residence time and is typically achieved by rendering “stealth” properties via surface PEGylation, in a fashion similar to mucopenetration [86,87]. On the contrary, such non-interacting particles may cause a dilemma; on the one hand they minimize barrier interactions and facilitate drug transport while on the other hand the uptake by phagocytic cells such as macrophages and dendritic cells has been shown to be significantly reduced [88]. This is of high relevance for the treatment of *Mtb* infections with surface-targeted particles intended for efficient macrophage uptake and cellular routing to mycobacterial habitats in endosomal compartments. In endosomal compartments, mycobacteria are extremely difficult to be addressed via oral and intravenous administration, that solely rely on passive diffusion of the drug to the cellular compartments [89]. The formation of granuloma displays an additional diffusion barrier, as well as the mycobacterial cell wall itself, collectively limiting the access of the drug to the intracellular target. Noteworthy, the permeability across the bacterial cell wall is the rate limiting step for antibiotic availability and is counterbalanced by various efflux mechanisms, a major contributor to bacterial resistance [90]. Similarly, the clearance from the alveolar lumen depends on the ability of a material to be able to cross the air-blood interface, causing subtherapeutic drug concentrations and systemic side effects.

The active molecule must be sufficiently solubilized in order to be therapeutically active, especially when the volume of absorption is low, as is the case for the alveolar lining fluid [91]. This is particularly relevant for new antibiotics such as the anti-tuberculosis drugs BDQ and BTZ043 that are both extremely hydrophobic and poorly water soluble [92–94]. To maximize therapeutic effects and minimize resistance, the drug concentration in the pulmonary compartment has to be above the MIC as long as possible, without clearance and absorption to cellular compartments or the systemic circulation. Therefore, the following parameters for the *in vitro* testing of orally inhaled drug products are suggested [95]:

- Particle dissolution in the lung and *in vitro* testing
- Lung permeability and transport
- The role of fluid mechanics in pulmonary drug deposition
- PK/PD modeling for lung delivery

These efforts towards a pulmonary biopharmaceutical classification system require standardized lining fluids, reflecting as much as possible the composition (phospholipids, antioxidants and surfactant proteins) and the biophysical activity (e.g., surface tension reduction) of the native lung lining fluid, such as that of PS [96]. Guidance on the design and testing of novel delivery system should aim to minimize pulmonary barrier interactions and clearance mechanisms while maximizing the dose available at the intracellular target. Hence, advanced *in vitro* models that incorporate essential cellular and non-cellular barriers are required to investigate the complex interplay and thus the fate of aerosolized nanomaterials in the human lungs.

#### 1.4 Models and methods to investigate pulmonary mucus and surfactant interactions

A major limitation of investigating nano-bio interactions of nanoparticles with pulmonary mucus and surfactant is the availability of human material at sufficient quality and quantity. Both, the sampling of mucus by the endotracheal tube method [97] and that of PS by bronchoalveolar lavage [98] are invasive techniques, making native material, especially from patients without lung diseases, not readily accessible. Moreover, careful handling and sample preparation by trained specialists to prevent contamination with saliva, blood, serum and cellular components is required to maintain the original structure and function of both PS and mucus. The cleavage of disulfide bonds during the purification of mucins and insufficient inhibition of protease activity, for instance, can significantly alter the mucus meshwork, potentially overestimating the diffusion of dispersed nanoparticles [99,100]. The development of easy-to-use, standardized and reproducible surrogates is therefore desired; some mucus model based on reconstituted porcine mucins [101,102] and crosslinking polymers [103–105] already exist. Although a variety of nanomaterials has been investigated with such surrogates [106,107], an adequate rheological characterization of the applied mucus surrogate is often lacking.

Novel delivery systems are typically designed to either bind/adhere to mucins or mucus [108], or to penetrate the latter [109], while nano-sized particles have also been applied to gain meaningful insights of the mucus layer itself [110]. Multiple Particle Tracking (MPT) in this respect is a useful tool to study the nanoscale interactions of hundreds of nanoparticles with their surrounding (mucus) matrix, simultaneously and at an individual particle level (**Figure 9**). Video microscopy of the x-y movement of the particles using a high-magnification microscope equipped with a high-speed camera allows to reconstruct individual particle trajectories from which the mean squared displacement (MSD or  $\Delta r^2(\tau)$ ) and the diffusion can be calculated according to the formula [8]:

$$(\Delta r^2(\tau)) = (\Delta x^2 + \Delta y^2) \quad (1)$$

$$\Delta r^2(\tau) = 4D\tau \quad (2)$$

The slope  $\alpha$  of the resulting MSD curve classifies particle diffusion in dependence of viscous and elastic proportions of the tracking medium. In literature, a cut-off value of 0.5 is typically defined to discriminate between mobile ( $> 0.5$ ) and immobile ( $< 0.5$ ) particles [19,111].

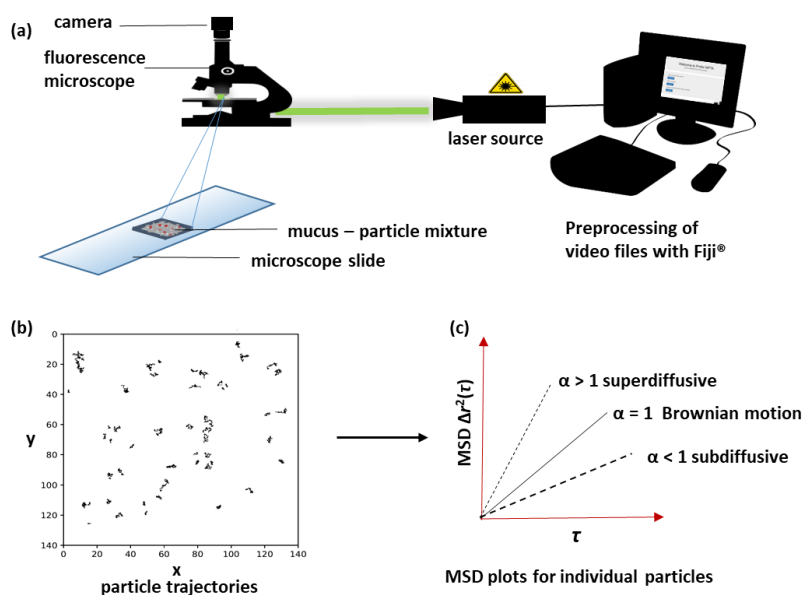


**Figure 9)** Workflow of particle tracking analysis. a) A fluorescence microscope equipped with a high-speed camera is used to monitor the movement of nanoparticles embedded in mucus. b) Individual trajectories obtained after evaluation of tracking data with a custom-made script. c) MSD plots of individual particles classifying the mobility according to the slope of the MSD curve.

On the other hand, bulk particle transport is studied as the time-resolved transport of molecules over a membrane-separated interface. In such systems, including the Franz-diffusion chamber, Ussing-chamber, and Transwell<sup>®</sup>-based approaches, the transport rate depends strongly on the homogeneity, height and origin of the mucus layer [112–115]. The connection of a deposition device such as the PennCentury<sup>™</sup> Dry Powder Insufflator, the MicroSprayer<sup>®</sup> aerosolizer or the Pharmaceutical Aerosol Deposition Device on Cell Cultures (PADDOCC) to the Transwell-system allows to investigate the dissolution and permeation of deposited materials in early drug development [116–118]. Interestingly, 100 nm sized polystyrene particles deposited as aerosols are entrapped by the mucus layer, whereas the same particles were mobile upon mechanical dispersion, suggesting a condensed mucus layer at the air-interface [111].

In the context of infectious diseases, mucus may not only act as a diffusional barrier for antibiotics and other small molecules, but also facilitate growth and adaptation of pathogenic bacteria, collectively limiting anti-infective susceptibility [119]. Thus, mucosal cultivation media such as homogenized sputum and *ex vivo* mucus have been employed to meet both, an environment for pathogen growth and the mechanical barrier properties of mucus [120]. Such mucus models, however, are likely contaminated with host-derived microorganisms that need to be eliminated by UV-sterilization, autoclavation or filtration before experiments can be performed. None of these techniques, however, are satisfactorily applicable without compromising the viscoelastic nature of mucus, driving the design of artificial sputum media to grow, for instance, PA and other bacteria [121] and to study rheology, diffusion and susceptibility of antibiotics as well as mucus-microbe interactions under controlled conditions *in vitro* (**Figure 10**) [122,123]. The complexity of such models and potential readouts can be increased by incorporation of epithelial cells, such as Calu-3, A549, 16HBE14o- and CFBE41o cells or even ciliated cells, modeling MCC and respiratory barrier properties both in health and

disease [124–126]. Some cells, including Calu-3, are secreting mucus on their own, however, the addition of *ex vivo* or synthetic mucus to such models allows for controlling layer thickness and a better distinction of the cell and mucus layer. Furthermore, bronchial epithelial (Calu-3) as well as alveolar epithelial cells such as hAELVi cells find wide application in drug permeation studies because of the expression of tight-junctions, that are functionally assessed as the transepithelial electrical resistance (TEER) [127,128].

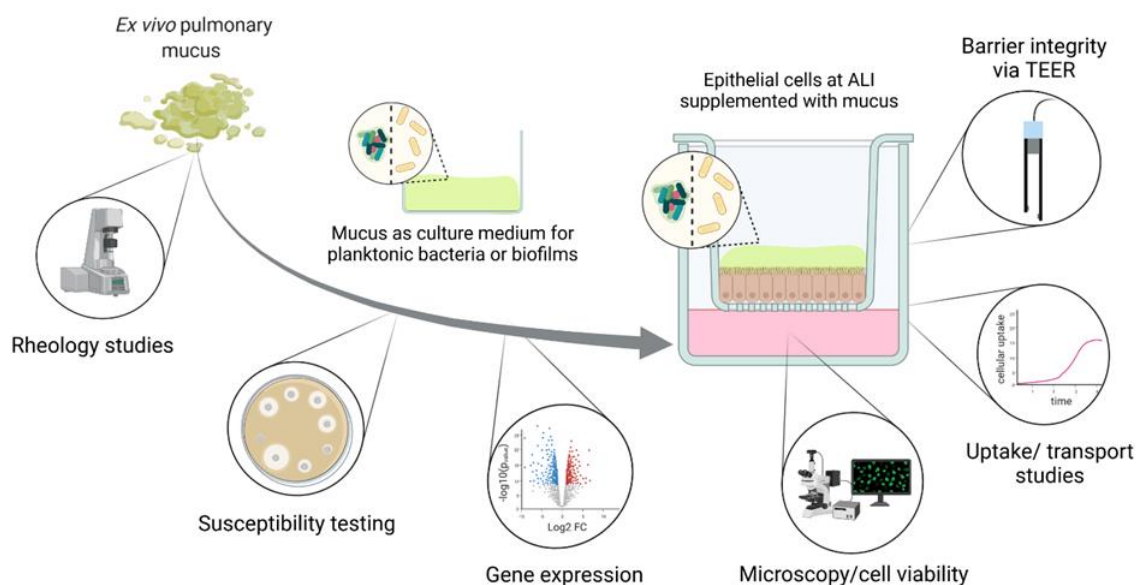


**Figure 10)** *Overview of mucus assays.* Use of native human mucus in models with increasing complexity. Mucus rheology can be studied on the macro- and microscale. Moreover, mucus is used to study microbe-mucus interactions, biofilm interactions and gene expression. The combination of lung cells with *ex vivo* mucus allows to create 3D models to study cellular uptake, drug transport, cellular interactions, and barrier integrity by means of fluorescence microscopy, flow cytometry and transepithelial electrical resistance, respectively. Reprinted with permission from Huck *et al.* [10].

To model particle-interactions in the alveolar airways, various surfactant preparations are available ranging from simple synthetic lipid mixtures containing mainly DPPC and DPPG [129–131], animal-derived surfactants which are used in clinic [132] and native material of bovine and porcine origin [133,134]. For evaluation of the quality of PS preparations, the reduction of surface tension upon compression as a functional readout is preferred over the analysis of lipid and protein composition by quantitative methods due to a complex structure-function relationship [24].

The behavior of individual phospholipids, their mixtures and complete surfactant preparations is studied upon dynamic compression and expansion of an interfacial layer, typically using a Langmuir surface balance [79,129]. The decrease in surface area is then related to the reduction in surface tension  $\gamma$  or, more commonly, an increase in the reciprocal surface pressure  $\pi$ , resulting in a specific pressure-area isotherm from which the phase transitions of the lipid layer can be concluded (**Figure 11**) [135]. Since this setup is extremely sensitive to external factors such as temperature, vibrations and the surrounding atmosphere, only few studies have successfully managed to investigate particle interactions with surfactant films, particularly after aerosol deposition. Broichsitter *et al.* could demonstrate that PLA nanoparticles inhibited the

reduction of surface tension of Alveofact<sup>®</sup> in a dose dependent manner, that was significantly improved when the particle's surface was coated with PEG [86]. Interestingly, the particle size becomes relevant only when the particles reach a size of approx. 20 nm, while above this size (particles of 40 and 500 nm, respectively), the  $\pi$ -area isotherms are similar to those of a surfactant not exposed to particles [136]. A negative zeta potential, in contrast, facilitates the adsorption of phospholipids and proteins to the particle surface, while disturbing the lateral packing and highly ordered states of the interfacial film [137].

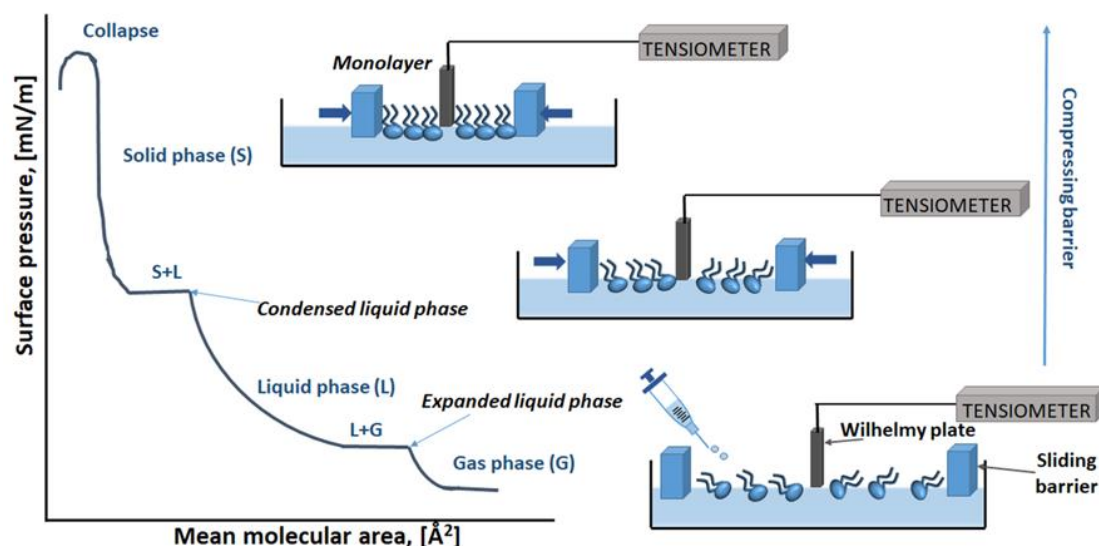


**Figure 11** Surface pressure–area isotherms ( $\pi$ – $A$ ) of a Langmuir monolayer and molecules in different phases. Reprinted with permission from Rojewska *et al.* [138].

The only few nanometer thin corona that forms around the particle can be assessed via a change in the particle size by methods including high-resolution electron microscopy, density gradient centrifugation [139] or fluorescent-based surface staining methods [140]. The biological consequences of the molecular corona that trigger cellular interactions is studied by flow cytometry [14] to quantify particle uptake into cells and/or cytokine and chemokine release [141]. Protective effects of PS against silica [22], zinc oxide nanowires [141], and polymeric nanoparticles [83] on A549 and other epithelial cells but also on macrophages (THP-1, MHS) have been observed by measuring cytotoxicity in MTT and LDH assays. More complex models, for instance, include PS covered cells and particle aerosol deposition, thereby reflecting both the mechanical and immunological barrier properties of PS, allowing to simultaneously study particle aggregation, uptake, toxicity and barrier integrity. Co- and multicultures of epithelial-, mucus-producing and phagocytic cells grown on permeable supports or 3D chips allow for the simultaneous readout of a multitude of parameters with the possibility to introducing breathing-like motion [142,143]. Current *in vitro* models, however, are often limited by the selection of adequate surfactant preparations or missing vivo-like particle deposition, or do not contain PS at all.

## 1.5 Recent advances and strategies to overcome the pulmonary barriers

Colloidal delivery systems, such as nanoparticles, micelles and liposomes offer a variety of advantages over other drug delivery systems due to their intrinsic biophysical properties. This includes their small size range, large surface area and tunable surface properties, leading to a wide range of applications in oral, parenteral and pulmonary therapies [144]. Early studies on the diffusion of small molecules through gastrointestinal mucus already unraveled the charge and molecular weight (equivalent to size) as important delimiters for the diffusion of small molecules [145]. The diffusion through mucus is limited when the molecule is lipophilic and positive in charge. This observation has been exploited to enhance residence time of nanomedicines after ocular, oral and pulmonary administration and is nowadays well-known as mucoadhesion [146]. Conversely, when the molecule is sufficiently small and non-interactive, typically via surface masking (e.g., by PEGylation), it can efficiently penetrate the mucus layer and even so reduce the interaction with the PS system [147,148]. In addition to mucopenetration, the linkage of mucolytic or cleaving agents, such as N-acetylcysteine, papain or DNase to the particle surface increases the ability to cross the mucus layer [149]. In a similar fashion, mucus-penetrating peptides and viral vectors can be designed to deliver, for instance, small molecules to their target in the lung tissue [150–152]. An innovative concept that focuses on the delivery of active molecules, such as glucocorticoids and antibiotics, is the “surfing” over the respiratory interface by exploiting the ability of PS to efficiently spread along this interface [79,153]. The concepts to cope with the pulmonary barriers can be summarized as i) avoiding or circumventing MCC, ii) mucoadhesion, iii) mucopenetration, iv) mucolysis by active destruction of the mucus meshwork and v) interfacial delivery by spreading over the mucus layer (**Figure 12**).

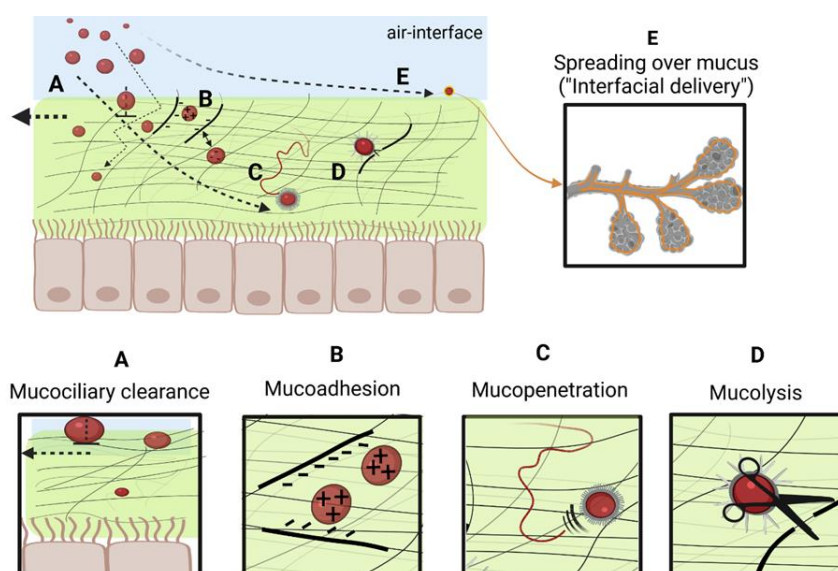


**Figure 12)** Strategies to cope with the mucus barrier. Mucociliary clearance (A) efficiently removes materials that are entrapped in or adhere (B) to mucus. Mucopenetration (C) is a concept to increase the permeation of the mucus layer as a consequence of a non-interacting surface. The use of mucolytics (D) leads to a similar effect by fluidifying the mucus layer. An emerging concept is the spreading over the mucus barrier (interfacial delivery) while exploiting surface active materials such as pulmonary surfactant (E). Reprinted with permission from Huck *et al.* [10].

The use of nanomaterials to overcome the limitations of the free drug, e.g., by increasing the solubility and bioavailability, reducing toxicity, controlling the release, enabling mucus penetration and targeted delivery, has significantly advanced the field of nanomedicine [154] with numerous promising candidates in the pipeline aiming for the treatment of infectious respiratory diseases [50]. However, until 2011, tobramycin [155] and colistin [156], and more recently, aztreonam [157] – all of them used for the management of PA infections in CF patients – were the only approved antibiotics for inhalation, followed in 2018 by the liposomal formulation of amikacine (Arikayce®) for the therapy of nontuberculous mycobacterial infections [158]. Liposomes are particularly suited for such applications due to their ability to incorporate both lipophilic and hydrophilic drugs at large amounts, while allowing to adjust the fluidity of the membrane by combining different lipids with cholesterol, most of them generally recognized as safe by regulatory authorities (**Figure 13**) [159]. Aerosol administration of rifampicin-encapsulating, ligand-decorated liposomes has been demonstrated to significantly reduce the survival of *mycobacterium smegmatis* from 46% to 7-11%, due to high drug accumulation in macrophages compared to oral therapy [160]. Aerosolization of the first-line antibiotics isoniazid, rifampicin, and ethambutol in combination with DPPC showed reduced alveolar atelectasis and a higher drug supply at the air-interface, possibly by synergistic interactions with endogenous PS [161–163]. As proposed by Misra *et al.*, such liposome-based and targeted delivery approaches might be even more successful for second-line drugs, which are only moderately potent, limited in absorption and oral bioavailability, and exhibit substantial toxicity [159].

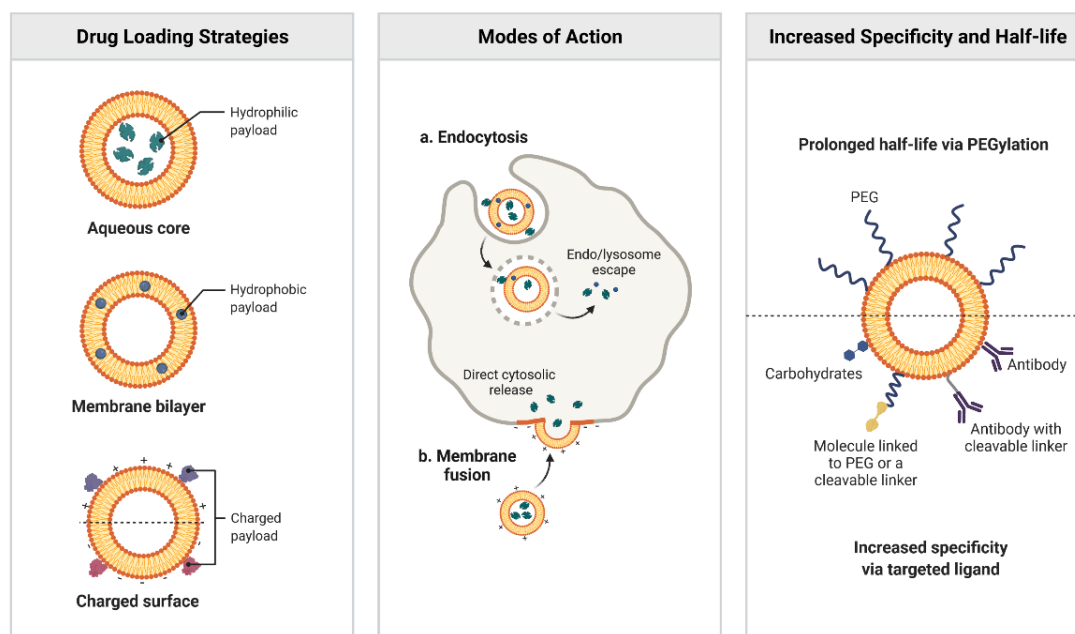


**Figure 13)** Liposome based drug delivery. Loading strategies, modes of action and surface engineering of liposomes. Reprinted with permission from Sercombe *et al.* [164].

The success of inhalation therapy, however, requires optimization of the entire system including not only the drug and the formulation, but also the inhaler device; all of them necessary to enable efficient delivery of the aerosol particle to the desired region in the lung [165]. The



inhaled aerosol consists either of liquid (droplets) or solid (powder) particles with different shapes and sizes, typically depending on the inhaler device. The most common inhaler devices include i) metered dose inhalers to aerosolize drug solutions or dispersions with the use of propellants, ii) nebulizers that use mechanical and electrical mechanisms (e.g., vibrating meshes) for aerosol generation and iii) dry powder inhalers that generate aerosols by breath actuated mechanisms [154]. Dry powder inhalers are appealing since they are relatively easy to use and provide high chemical and storage stability compared to aqueous solutions, which is of particular interest for antibiotic therapy of infectious diseases in developing countries where transport and cold storage is difficult [166,167]. However, the development of respirable dry powders requires optimization of the drying process to ensure physicochemical stability of the stock solution/dispersion, a process most commonly accomplished by freeze- or spray-drying [168]. The use of safe, biocompatible and biodegradable excipients, such as antioxidants (e.g., ascorbic acid), amino acids (e.g., L-leucine, trileucine) and sugars (e.g., trehalose, lactose) is necessary to improve chemical stability, powder dispersibility and aerodynamic properties, respectively [94,169].

Anti-infective delivery as dry powder aerosols could improve the efficacy of PA treatment when co-delivering deoxyribonuclease and ciprofloxacin [170], the killing of Mtb with spray-dried chitosan-based rifampicin and rifabutin microparticles [171], and even the delivery of proteins by spraying-drying of liposomes [172]. Dry powder aerosols containing muco-inert particles, moreover, could effectively penetrate PA mucoid biofilms after *in vitro* aerosol deposition [173]. A combination of polymeric nanoparticles with Tat protein allowed to deliver their cargo into CF-like 16-HBE14o<sup>-</sup> cells by simultaneous muco- and cell penetration, even when the nanoparticles were embedded into spray-dried microparticles [174]. Recent advances in the formulation of lipid and polymeric nanoparticles, drug nanocrystals and proteins as dry powders reduced bacterial burden, systemic absorption and toxicity in mycobacterial infections by delivering high aerosol doses to the place of infection both *in vitro* and *in vivo* [175,176]. Thus, nano-in-micro delivery system may have the potential to combine the best of both worlds, while an adequate prediction and optimization of pulmonary barrier interactions remains a major challenge.

## 2 Aims of the thesis

The overall aim of this work was to investigate the cellular and non-cellular barriers for pulmonary drug delivery. In particular, models of pulmonary mucus and surfactant have been developed to study uptake, toxicity and efficacy of nanoparticle-based anti-infectives in the context of mycobacterial infections. The delivery of nanomedicines to the place of infection in the alveolar airways requires novel delivery approaches to cope with resistance. Pulmonary administration of nanomedicines can complement conventional therapy by increasing pulmonary bioavailability, reducing systemic exposure and allows for targeted delivery of antibiotics to the site of infection. However, pulmonary delivery is challenged by the sophisticated interplay of nanocarriers with the lungs' defense mechanisms. To address this issue, surrogates and *in vitro* models of pulmonary mucus and surfactant have been developed to study the penetration, cytotoxicity and uptake of aerosolized nanocarriers. Ultimately, antibiotic-loaded and macrophage-targeted liposomes were developed in cooperation with the ANTI-TB project partners as respirable dry powders and their uptake and barrier interactions were tested with the models described above (fucosylated liposomes were provided by Rodos Biotarget and dry powder formulations developed with the help of Thiagarajan Durairaj).

The research aim of this study was to

- i) Develop a pulmonary mucus surrogate and to investigate nanoparticle mobility in dependence of size and surface decoration in native and surrogate mucus including the penetration of antibiotics through and the viability of respiratory pathogens in pulmonary mucus surrogates (see results section 3.1)
- ii) Determine the influence of pulmonary surfactant composition and biophysical properties on cytotoxicity, barrier integrity and cell uptake, and on drug release and stability of aerosolized nanoparticles (see results section 3.2)
- iii) Characterize and optimize respirable nano-in-micro dry powder formulations of antibiotic-loaded liposomes for macrophage-targeted pulmonary delivery *in vitro* (see results section 3.3)
- iv) Study the interactions of fucosylated liposomes and their nano-in-micro dry powder formulation with pulmonary mucus in the presence and absence of pulmonary surfactant with respect to the targeting of phagocytic cells (see results section 3.3).

### 3 Main outcomes of the thesis

#### 3.1 Native pulmonary mucus and surrogates: Characterization and interaction with nanomaterials and pathogens to predict pulmonary delivery of anti-infectives

Mucus' physical and chemical filtering mechanisms can significantly reduce the penetration of nanomaterials and thereby limit therapeutic outcomes. The limited access to native mucus material at high quality and quantity to study the interactions of mucus with nanomaterials was the driving force for the development of mucus surrogates. Such surrogates, ideally, should mimic both, the bulk rheological properties and the microscale properties of native mucus at small length scales. Macro- and microrheology of selected pulmonary mucus surrogates was assessed by oscillatory rheology and MPT and compared to native mucus samples obtained from human donors by means of the endotracheal tube method [97]. From previous studies, a cut-off size of approx. 500 nm was concluded, that discriminates mobile from immobile particles in human pulmonary mucus [19]. Therefore, 500 nm carboxy-modified and fluorescently labeled polystyrene particles were selected. Nanoparticle tracking experiments were conducted to spot differences between the investigated surrogates and native samples. In this study, native mucus from human lung and porcine intestine were compared to their respective surrogates previously described in literature [103,121]. Tracking the mobility of polystyrene nanoparticles in the surrounding mucus matrix allowed to calculate the transport modes and MSD curves of the suspended particles and the viscosity of the mucus matrix. Thereby, the main contributors to the viscoelastic properties of the mucus meshwork, such as the concentration and type of the macromolecular mucins and crosslinking polymers could be determined. The lung mucus surrogate developed by Dinesh *et al.* matched mucus in terms of composition, however, lacked the ability to form elastic-dominant ( $G' > G''$ ) hydrogels. Only when a biocompatible polymer, such as polyacrylic acid PAA was added to artificial airway mucus as a cross-linker, both elastic ( $G'$ ) and storage ( $G''$ ) moduli matched well and rheological profiles similar to that of native mucus could be obtained (**Figure 14**).

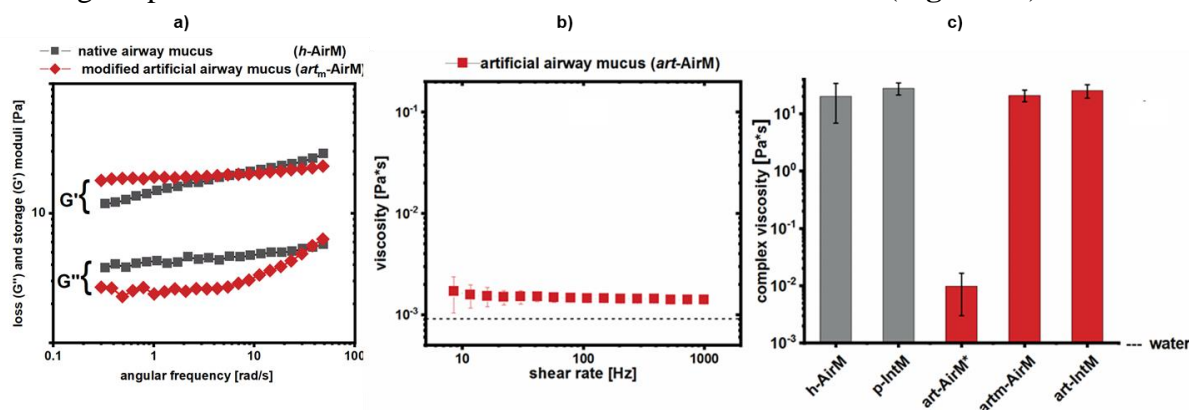


**Figure 14)** *Rheological profiling of h-AirM and art<sub>m</sub>-AirM.* a) Shows the loss and storage moduli for h-AirM and art<sub>m</sub>-AirM. Measurements were performed at a strain-amplitude of 1%, falling in the linear viscoelastic region of the samples. b) Dashed line shows the viscosity of water at RT. c) The complex viscosities of human airway mucus (h-AirM), porcine intestinal mucus (p-IntM), artificial intestinal mucus (art-IntM) and modified artificial airway mucus (art<sub>m</sub>-AirM) at an angular frequency of 62.8 rad/s (= 10 Hz) compared to the dynamic viscosity ( $\eta^*$ ) of artificial airway mucus (art-AirM) at a shear rate of 10 Hz. Adapted with permission from Huck *et al.* [8].

Interestingly,  $G'$  of modified artificial airway mucus showed a stronger dependency on the angular frequency compared to native airway mucus, whereas the opposite was the case for  $G''$ . At a fixed angular frequency of 62.6 rad/s, equivalent to a shear rate of 10 Hz, all matrices except for the artificial airway mucus, exhibited complex viscosities of  $\pm 10$  Pa\*s. In line with these findings, the mobility of tracer particles in artificial airway mucus was essentially similar to pure water, whereas the behavior of particles in native airway mucus and modified artificial airway mucus was matching to a greater extent. Native airway mucus immobilized almost all of the polystyrene tracer particles (as indicated by red lines and a  $\alpha$ -values distribution  $<0.5$ ). In contrast, particles in artificial airway surrogates behaved like in a low-viscosity aqueous environment (black lines), and the polymer-modified surrogate showed an intermediate behavior (**Figure 15**). When adding PAA at an optimal concentration (predicted to be 0.9% w/w) to the surrogate, a size-limited penetration could be achieved, sufficient to discriminate the mobility of 500 nm, but also of 200 nm sized particles. These findings clearly indicate that both, macro- and microrheology critically affect the diffusion of molecules through mucus and need to be well-characterized and optimized to predict the nanoscale interactions with delivery systems and their diffusion through mucus. The polymer-modified surrogate described herein holds the potential to complement or even replace native pulmonary mucus in future nanoparticle-mucus interaction studies.

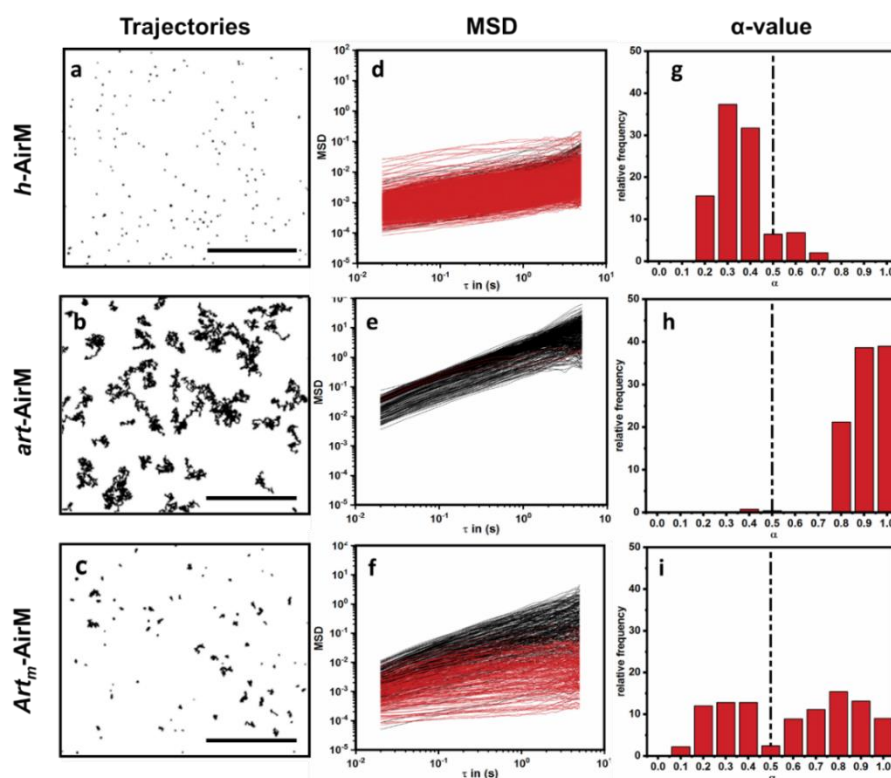


**Figure 15)** Multiple particle tracking (MPT) analysis of 500 nm carboxylated polystyrene NPs dispersed in *h-AirM*, *art-AirM* and *art<sub>m</sub>-AirM*. Depicted trajectories (a-c) show 5s of particle motion (Scale bar: 10 $\mu$ m). MSD of NPs dispersed in different hydrogels as a function of time scale (d-f). Black lines correspond to particles in a viscous environment ( $\alpha > 0.5$ ) and red lines to particles in an elastic environment ( $\alpha < 0.5$ ). The  $\alpha$ -value plots (g-i) show the number distribution of particles in elastic and viscous environment. Data represents mean of 3-6 mucus samples with a minimal amount of 350 particles/plot. Adapted with permission from Huck *et al.* [8].

In a follow-up study under the lead of Sarah Frisch, the above developed PAA-modified mucus surrogate ( $ASM_{mod}$ ) was investigated for its capacity to predict the permeability of antibiotics in a Transwell<sup>®</sup>-based setup, where the concentration of antibiotics was measured after transition from the donor (apical) to the acceptor (basolateral) compartment at defined timepoints. Colistin, tobramycin and ciprofloxacin were selected as well-established antibiotics used in pulmonary infections with mucus and/or biofilm involvement, while they have different molecular weights and surface charges [177]. For all three tested antibiotics, the penetration through PAA-modified artificial mucus was in line with that of native human airway mucus. In contrast, the permeability was significantly higher for the PBS control, indicating that the mucus surrogate appeared as an applicable model to predict antibiotic permeability. The underlying interaction mechanisms, most likely, is attributed to size and electrostatic interactions with the negatively charged PAA or mucin matrix, respectively. The discriminatory effect of the model allowed to rank the permeability of different antibiotics, particularly that of the poorly permeable colistin in contrast to ciprofloxacin and tobramycin (**Figure 16**). Hence, the model might be suitable for medium to high throughput *in vitro* screening of new active compounds intended for the treatment of bacterial infections.

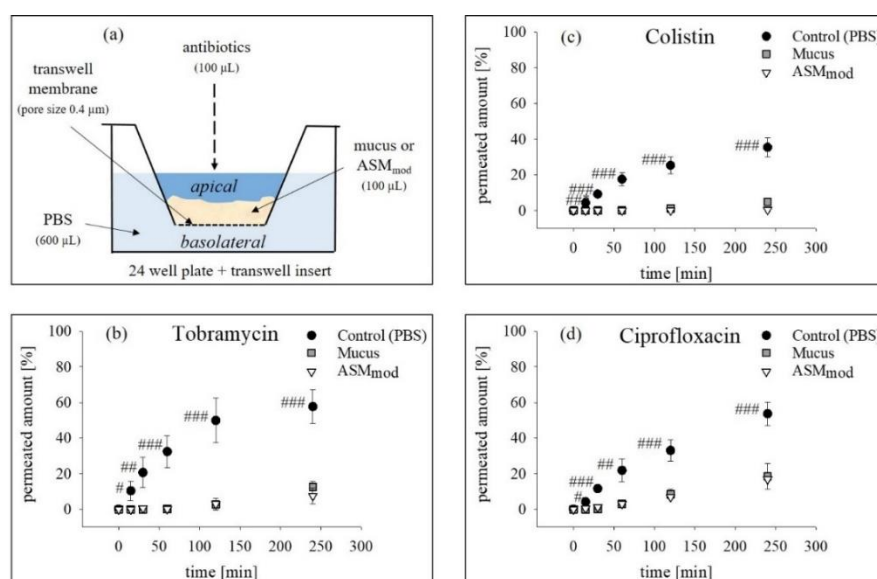


**Figure 16** Antibiotic transport through mucus and  $ASM_{mod}$ . a) Transport studies of tobramycin (b), colistin (c), and ciprofloxacin (d) through native mucus (squares) and  $ASM_{mod}$  (triangles). PBS was used as control (circles). The cumulative mass [ $\mu\text{g}$ ] was normalized to the calculated mass of the initial concentration [ $\mu\text{g}$ ]; the permeated amount [%] is shown over time [min]. Statistical significance (PBS vs. mucus and PBS vs.  $ASM_{mod}$ ) is indicated by hashes.  $N=3$  with  $n>8$ . Reprinted with permission from Frisch *et al.* [178].

Next, the growth of CF respiratory pathogens, including *Staphylococcus aureus*, *Mycobacterium abscessus* and PA, was assessed in the artificial mucus surrogate. However, only PA showed a growth behavior comparable to standard conditions (LB medium). Therefore, PA was selected to further study the effect of such a matrix on bacterial adaptation and growth and on antibiotic susceptibility. When treated with tobramycin in the presence of PAA-modified artificial mucus, the CFU/mL was reduced only 1-2 logs at concentrations up to 1028 mg/mL. In contrast, bacteria grown in LB broth or unmodified artificial mucus, were killed almost

entirely. These findings correlate with metabolic activity data, showing a lower reduction for bacteria grown in PAA modified artificial mucus than for the controls (**Figure 17**). This suggests that PAA modified artificial mucus may serve as a biomatrix compatible to grow respiratory pathogens while exerting diffusional barrier properties for common antibiotics similar to permeation data found for native mucus [122]. Such a mucus model that represents both, composition and biophysical properties of native mucus, may allow to predict interactions of inhaled nanomaterials *in vitro* at appreciable throughput rates.

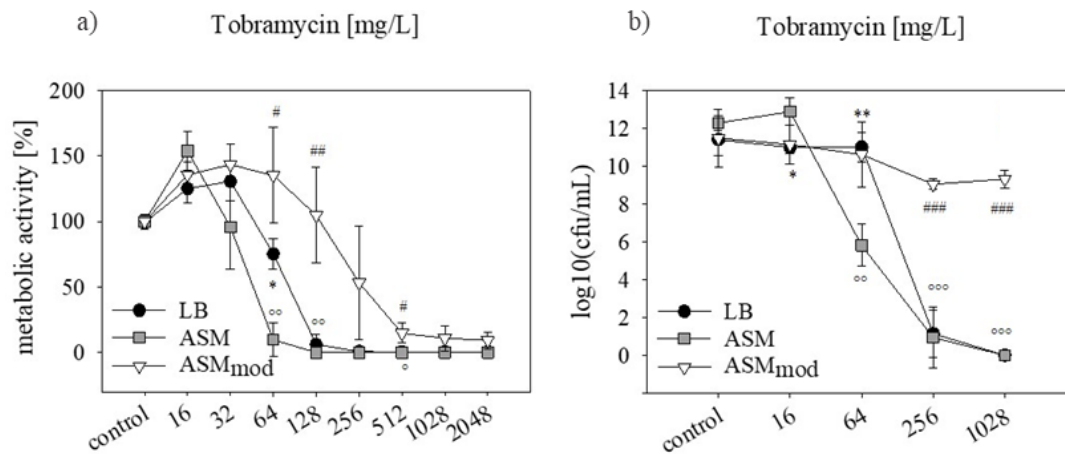
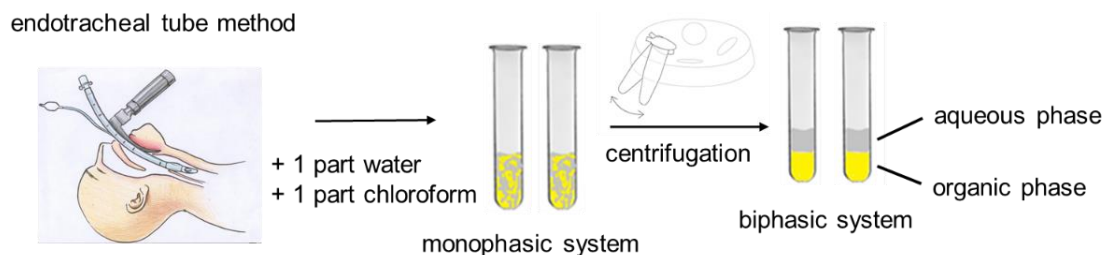


**Figure 17)** Antibiotic activity against 72-h PAO1 biofilms in various test media. a) Presto Blue™ assays and CFU analysis (b) of 72-h PAO1 in LB (circles), ASM (squares) and ASM<sub>mod</sub> (triangles) after 24 h treatment with Tobramycin. Metabolic activity [%] or log<sub>10</sub>(cfu/mL) are plotted against antibiotic concentration [mg/L]. Significance between groups is indicated by asterisks (LB vs. ASM), hashes (LB vs. ASM<sub>mod</sub>) and circles (ASM vs. ASM<sub>mod</sub>). N=3 with n=9. Adapted with permission from Frisch *et al.* [178].

### 3.2 Role of composition, interfacial activity and barrier properties of pulmonary surfactant preparations for the uptake and toxicity of aerosolized nanomaterials

Inspired by the work with pulmonary mucus, the idea to isolate PS from this material was hypothesized to open the perspective for a readily available source of PS, that would not require laborious sampling techniques. The isolation procedure and phospholipid quantities obtained from endotracheal tubes of healthy patients following organic extraction are summarized in **Figure 18**. The purpose of this work was to compare surfactant obtained from pulmonary mucus to a selection of native and commercially available PS preparations derived from human, porcine and bovine lungs, as well as an artificial lining fluid. The investigation focused on three main aspects i) the lipid and protein composition assessed by lipidomic analysis and western blotting (lipid analysis was performed at Forschungszentrum Borstel by Franziska Waldow), ii) biophysical properties investigated via surface tensiometry (at the Complutense University Madrid with the help of Jesus-Perez-Gil and Alberto Hidalgo) and iii) the interaction with aerosolized nanomaterials studied as cellular uptake and cytotoxicity.



**Quantification** of phospholipid phosphorous by Phosphorous assay

amount of mucus / patient	Phospholipids [mg] / patient	Phospholipid [%]
627 mg ( $\pm 177$ mg)	<b>1.28 mg</b>	0.2%
Min: 215 mg	Min: 0.083 mg	0.02%
Max: 1050 mg	Max: 4.4 mg	0.4%

**Figure 18)** *Extraction of surfactant from pulmonary mucus.* Mucus samples were obtained from human patients via the endotracheal tube method and subsequent surfactant isolation was performed by organic extraction (n=28).

The phospholipid composition of the various surfactant preparations was different between the investigated samples; however, major phospholipid species were relatively conserved in native surfactant preparations. The major proportion of PL are saturated Phosphatidylcholine (saturated PC) DPPC, and the (poly)unsaturated Phosphatidylcholine (unsaturated PC) POPC, POPG and POPI (**Figure 19**). The ratio of saturatedPC/unsaturatedPC is almost equal for human surfactant from bronchoalveolar lavage fluid (BALF) and mucus and porcine surfactant, but shifted to a higher proportion of unsaturated PC in bovine surfactant (Alveofact). In porcine surfactant from BALF – the biophysically best performing surfactant – POPG is elevated compared to all other surfactant preparations whereas the opposite was observed for POPI. In surfactant from mucus, interestingly, considerable amounts of sphingomyelins and lysolipids

were detected, supporting the hypothesis that surfactant isolated from mucus might be “spent” surfactant that is secreted from the alveolar region to the upper airways [179,180].

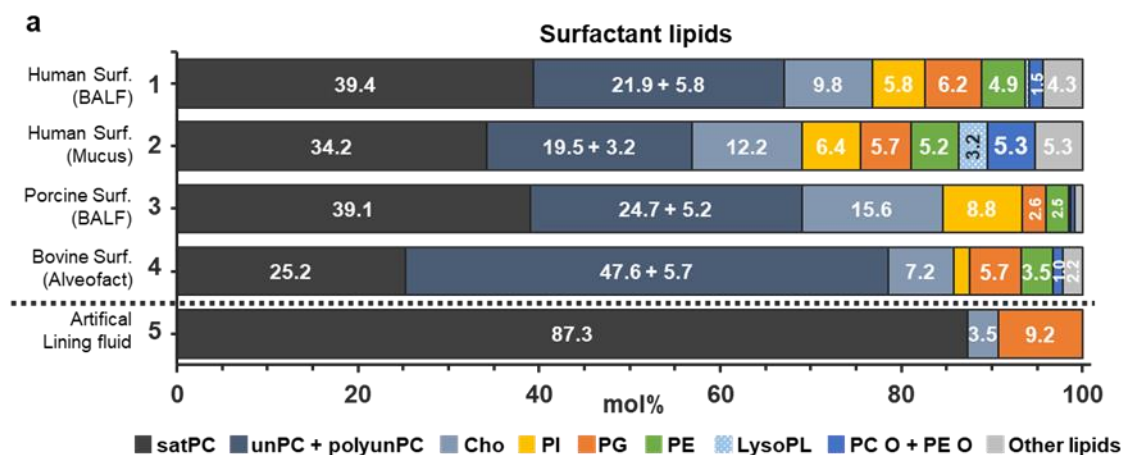


**Figure 19)** Lipid composition of pulmonary surfactant preparations. Relative molar amount of lipids. satPC: saturated phosphatidylcholine; unPC: unsaturated phosphatidylcholine ( $\leq 2$  C=C); polyunPC: polyunsaturated phosphatidylcholine ( $>2$  C=C); Chol.: free cholesterol; PI: phosphatidylinositol; PG: phosphatidylglycerol; PE: phosphatidylethanolamine; Lyso-PL: lyso phospholipids (lysoPC, lysoPG and lysoPE); PC-O: ether phosphatidyl choline; PE-O: ether phosphatidyl ethanolamine; Other lipids (sphingomyelins, ceramides, phosphatidic acid, diacylglycerols, triacylglycerols, hexosylceramide and cholesteryl esters). Adapted with permission from Huck *et al.* [14].

The relationship of the distinctive phospholipid fingerprint of the surfactant preparations to their surface activity is complex, and in most studies only individual lipids or some simple mixtures of lipids are investigated. Intriguingly, the lack of SP-B and SP-C observed in western blotting experiments might in the first place be responsible for the differences observed in biophysical properties and surface tension profile [181]. Pressure-area isotherms obtained with a Langmuir balance demonstrated that upon compression, all native surfactant preparations could achieve the maximum surface pressure (e.g., minimum surface tension) of approx. 60 mN/m. The largest plateau phase – indicating a high stability of the interfacial film – is observed for bovine and porcine surfactant. This was further reflected in a minimum hysteresis after repetitive cycling and in a surface pressure that changes only marginally after the third compression cycle (**Figure 20**).



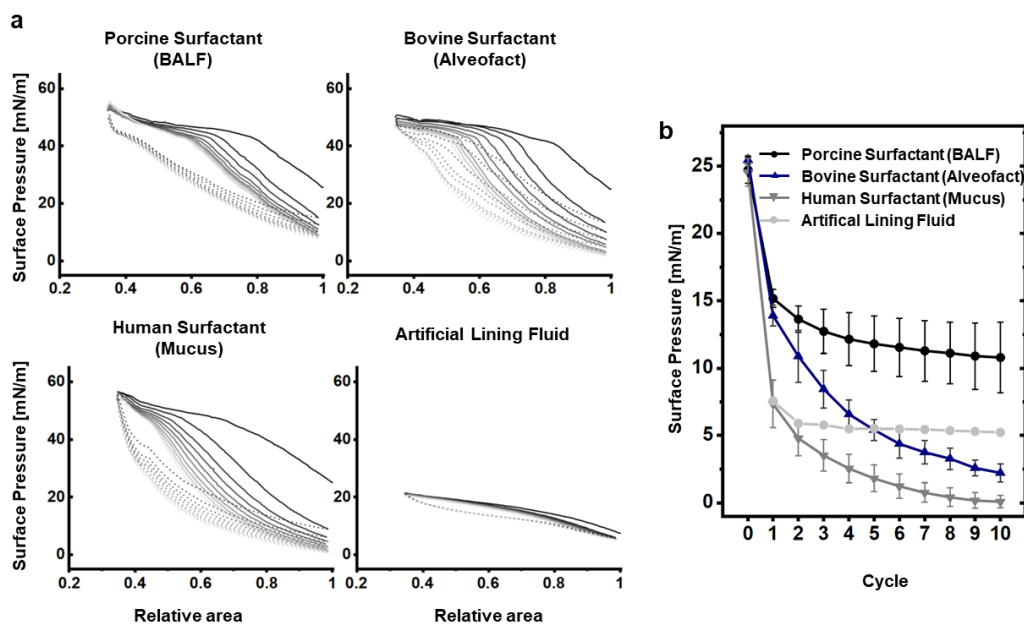


**Figure 20)** Pressure-area isotherms obtained with a Langmuir-trough. a)  $\Pi$ -area isotherms of surfactant preparations following 10 subsequent compression-expansion cycles at a barrier compression rate of  $65 \text{ cm}^2/\text{min}$ . Surfactants were dispersed in Tris/NaCl at  $5 \text{ mg/mL}$  and applied on a Tris/NaCl (pH 7.4) buffered subphase thermostated at  $25 \text{ }^\circ\text{C}$ . Surface pressure ( $\Pi$ ) is defined as the difference in surface tension between a clean air-water interface ( $\gamma_0$ ) and an interface covered by the lipid layer ( $\gamma$ ). A representative experiment of  $n=3$  is represented. b) Minimal surface pressure after each expansion. Error bars correspond to standard deviation ( $n=3$ ). Reprinted with permission from Huck *et al.* [14].

Another powerful method to study the adsorption and surface tension profiles of PS is the captive bubble surfactometer, in which an air bubble that contains the surfactant preparation is continuously compressed and expanded while the surface tension is monitored as a change in the shape of the inserted air bubble. The initial interfacial adsorption to the equilibrium value of  $20 \text{ mN/m}$  is reached for all surfactant preparations except for the artificial lining fluid, that lacks essential surfactant lipids (POPC, POPG, POPI) and hydrophobic surfactant proteins SP-B and SP-C. Under dynamic conditions mimicking compression and expansion at physiological breathing rates [182], the performance of the preparations can be ranked as porcine surfactant (BALF) > bovine surfactant (Alveofact) > surfactant from mucus from highest to lowest interfacial activity. This grading could be linked to the inverted ratio of POPG/POPI and saturated PC/unsaturated PC of Alveofact compared to PS from porcine BALF and the absence of PS proteins SP-B and SP-C in case of surfactant isolated from human mucus.

Even though the interaction of nanomaterials with PS has been reported to modulate particle aggregation, uptake and toxicity of nanomaterials, a systematic analysis of the aforementioned readouts is lacking. After nebulization of silica nanoparticles with positive, neutral and negative surface charge onto phagocytic macrophage-like THP-1 cells at the air-liquid interface, the toxicity – indicated as LDH release – was measured (**Figure 21**).

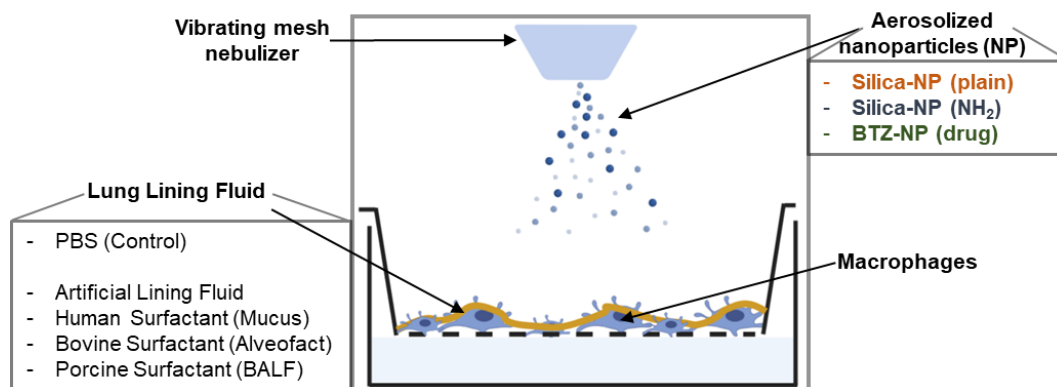


**Figure 21)** *In vitro* setup to study the interaction of aerosolized nanoparticles in the presence of various surfactant preparations and cell types. The cell surface was covered with 20  $\mu$ L of various surface lining fluids (PBS, artificial lining fluid, human surfactant obtained from mucus, Alveofact and a native porcine surfactant purified from BALF) at a concentration of 5 mg/mL. Adapted with permission from Huck *et al.* [14].

Interestingly, only when a surfactant preparation with high interfacial activity (such as Alveofact<sup>®</sup> and porcine surfactant) was added to the interface, protective effects on the underlying THP-1 cells were observed. Neutral silica particles exhibited a lower toxicity compared to amino-functionalized ones, whereas PS showed a more pronounced protective effect on the latter, most likely due to interactions of positively-charged particles with the negatively-charged phosphate-residues. This is in line with the finding that amino-functionalized silica nanoparticles exhibit stronger interactions with porcine and bovine surfactant expressed in a size increase and tendency of agglomeration.

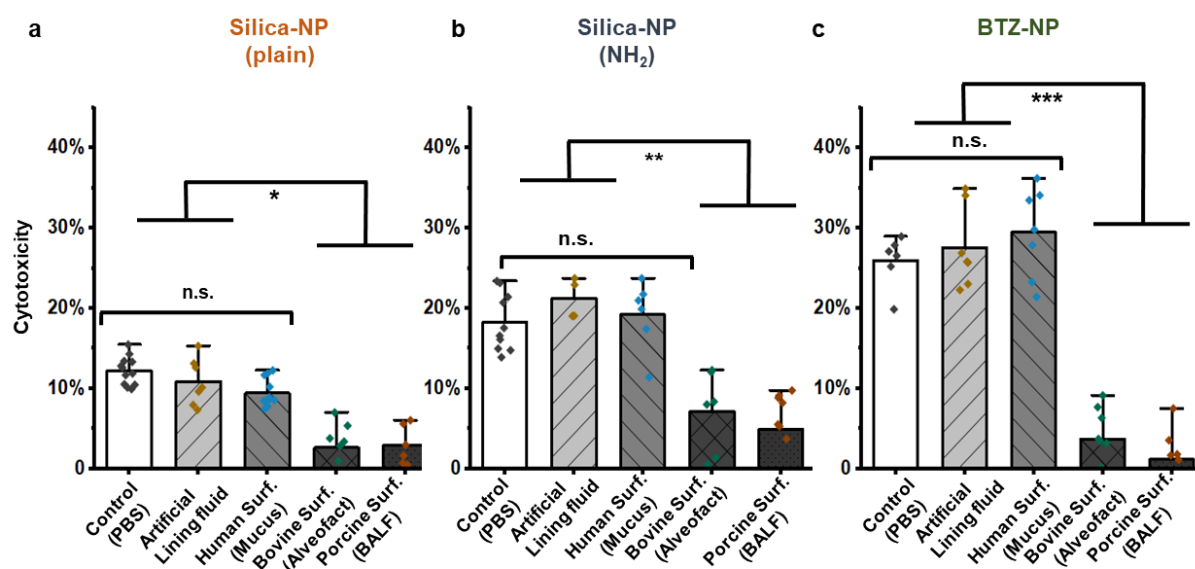


**Figure 22)** *Cytotoxicity of NPs on macrophage-like THP-1 cells.* The cells were exposed by aerosol deposition of a) 100  $\mu$ g plain silica NPs, b) 100  $\mu$ g amino-functionalized silica NPs, and c) 10  $\mu$ g BTZ043 (drug)-NPs. Values were normalized to the unexposed cultures (data not shown). Increase in gray scale indicates a tendency for more physiological pulmonary surfactant samples. Cytotoxicity was determined by flow cytometry live/dead assay. Mean of N=3 independent experiments with n=3–4 replicates are represented. Error bars represent standard deviation. One-way ANOVA, Tukey post-hoc test (\*)  $p < 0.05$ , (\*\*)  $p < 0.01$ , (\*\*\*)  $p < 0.001$ , (n.s.)  $p < 0.005$ . Adapted with permission from Huck *et al.* [14].

Most significant effects, however, were observed in case of the anti-mycobacterial BTZ-nanoformulation, where the toxicity is reduced by a factor of 5, most likely due to a shielding of the sodiumdodecylsulfate molecules (used as stabilizers) from the cell membrane (**Figure 22**). Nanoparticle tracking analysis was employed to study the interaction of fluorescently-labeled particles upon incubation with the different surfactant preparations. Interestingly, the contact of aminated-silica nanoparticles with functional surfactant such as PS from porcine BALF, caused an aggregation of the contacting nanoparticles, particularly for positively charged amino-functionalized particles.

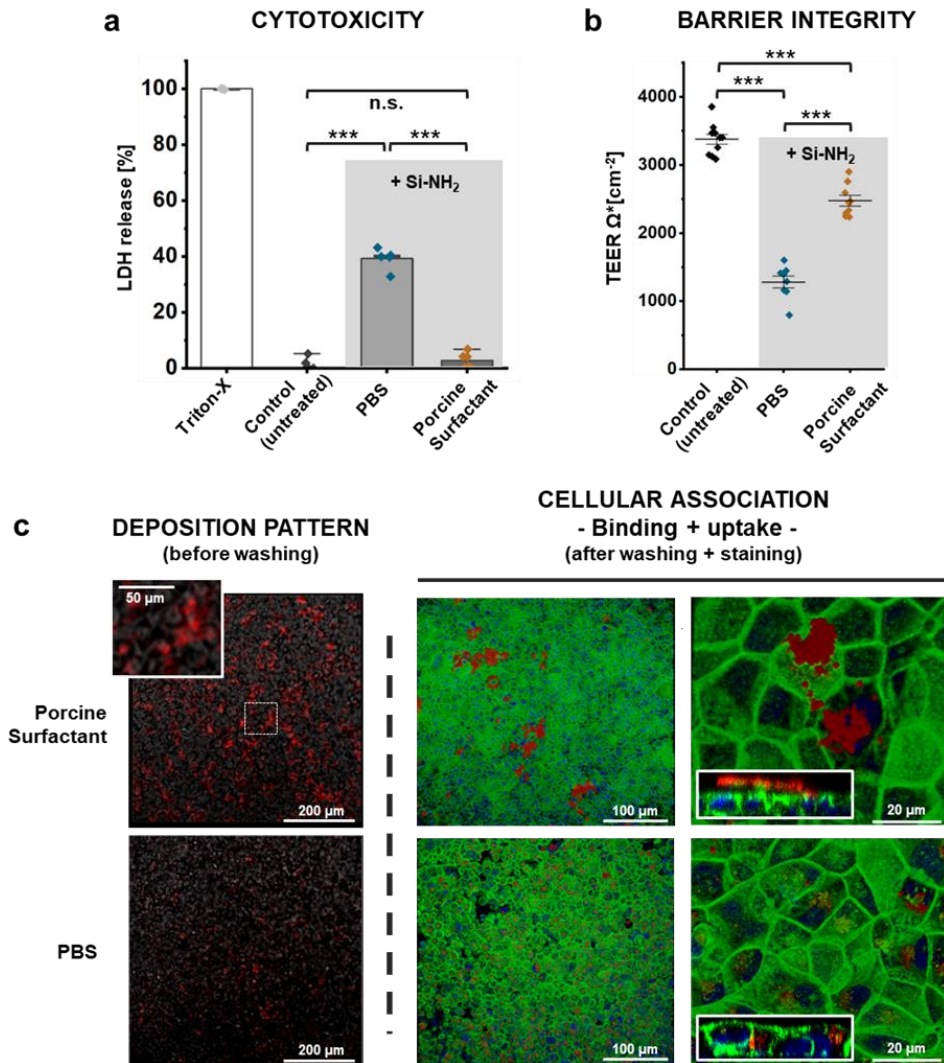


**Figure 23)** *hAELVi* cells after aerosol deposition of Silica-NH<sub>2</sub> NPs. The cytotoxicity (a) and barrier integrity (b) of *hAELVi* cells covered with 20  $\mu$ L of PBS or native porcine surfactant from BALF (20  $\mu$ L at 5 mg/mL) 24 hours after particle deposition. Untreated control did not receive aerosol deposition of NPs. Bars represent mean  $\pm$  standard deviation of the mean of N=3 independent experiments with n=3 replicates and significance levels \*\*\*  $p < 0.005$ . c) Representative confocal fluorescence micrographs of *hAELVi* cell monolayers after particle aerosol deposition showing the deposition pattern before washing (left panels) and cellular localization after washing and staining the cells (middle and right panels). Right panels correspond to a higher magnification of the middle panels and z-stacks are shown for discrimination of particle on and inside cells. Red: Silica-NH<sub>2</sub> NPs; Green: Phalloidin-Alexa 488 (Actin); Blue: DAPI (Nucleus). Reprinted with permission from Huck *et al.* [14].

Cellular studies on nanoparticle localization in hAELVi cells could demonstrate that larger, aggregated particles are only cell-associated rather than internalized into the cell, potentially explaining the decreased toxicity of nanomaterials in the presence of a thin layer of PS (**Figure 23**). This is in line with a higher barrier integrity – measured as TEER  $> 2000 \Omega \cdot \text{cm}^{-2}$  – of cells covered with porcine surfactant. The link of PS composition (content of DPPC and presence of surfactant proteins SP-B and SP-C) and biophysical function on the investigated biological readouts may guide the systematic selection of suitable surfactant preparations and their implementation into *in vitro* models of the human lungs.

### **3.3 *In vitro* characterization and interaction of respirable liposomal dry powder formulations with cellular and non-cellular lung barriers**

Mycobacterial infections that persist in phagocytic cells (e.g., resident and monocyte-derived macrophages) are difficult to reach and treat with conventional oral therapies [183]. The goal of the ANTI-TB project and in particular of this thesis therefore was to characterize and optimize respirable nano-in-micro formulations of BDQ encapsulating liposomes that are targeted towards phagocytic cells in the alveolar region of the deep lung. A main focus was the *in vitro* assessment of fucosylated liposomes and their respective dry powder formulations using the above-described models and novel fucose-binding assays. By receptor mediated endocytosis via fucose ligands, a high and selective cellular uptake into macrophages was intended, as described recently by Duran *et al.* [43]. To deliver the encapsulated drug BDQ, dry powder microparticles based on fucosylated liposomes were developed with aerodynamic properties optimized to favor deep lung deposition. This task was accomplished in close collaboration with the ANTI-TB project partners, who provided fucosylated liposomes (employees of Rodos Biotarget), supported in dry powder development and spray drying of liposomes (Durairaj Thiagarajan). The challenge here was to maintain liposomes' integrity and fucose-mediated targeting while prevent leakage of BDQ from the inside of the liposome. Moreover, the interaction with pulmonary mucus and surfactant that may eventually limit therapeutic outcomes and the efficacy of the final formulation on cultured *Mycobacterium abscessus*, were assessed (**Figure 24**). The scope of this study can be summarized as i) assessment of fucose surface functionalization and receptor-mediated internalization of targeted liposomes into myeloid cells under submerged and air-liquid interface conditions and ii) the interaction of liposomes with various types of macrophages in the presence of mucus and surfactant and, iii) the optimization and characterization of respirable nano-in-micro particles obtained by spray-drying of BDQ-loaded liposomes, and iv) the assessment of antimycobacterial activity against extracellular and intracellular *Mycobacterium abscessus*.

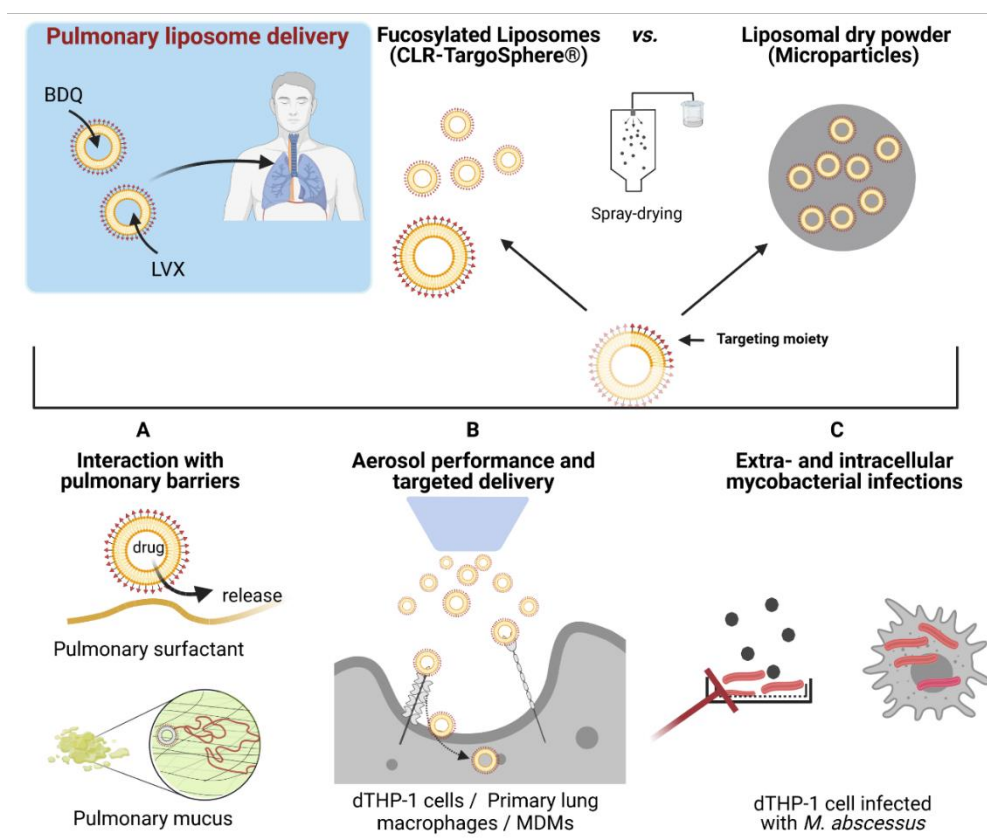


**Figure 24) Research strategy.** Targeted liposomes and liposomal dry-powder formulations loaded with bedaquiline (BDQ) or levofloxacin (LVX), respectively, were developed to overcome the pulmonary barriers. Abbreviations: MDMs: Peripheral blood monocyte-derived macrophages, dTHP-1: differentiated THP-1 cells. Reprinted with permission from Huck *et al.* [184].

In a first step, the fucose-binding capacity of liposomes was assessed in cell free assays. Both assays relied on the interaction of fucose-decorated liposomes with the fucose-binding lectin LecB, which was recently published by Metelkina and Huck *et al.* [65]. In the first assay, fucosylated liposomes were exposed to LecB at a molar ratio of 2:1, and the size measured by dynamic light scattering and nanoparticle tracking analysis after overnight incubation. Only in case of fucosylated liposomes, a size shift was observed due to the binding of liposomes to the multivalent LecB, leading to the formation of larger agglomerates (**Figure 25a**). In a second assay, PA C-type lectin LecB was coated to the surface of a flow chamber and subsequently flushed with targeted liposomes (**Figure 25b**) [65]. Upon contact of the fucose ligands with LecB on the chamber surface, liposomes were immobilized and subsequently quantified by confocal microscopy. This setup allowed to study the binding of fucosylated liposomes in the presence of competitive inhibitor, thereby confirming the specificity of such a sugar-based targeting. Only the competitive inhibitor L-Fucose, but not the buffer solution, removed the attached liposomes, indicating specific fucose-mediated binding of the targeted BDQ-liposomes.

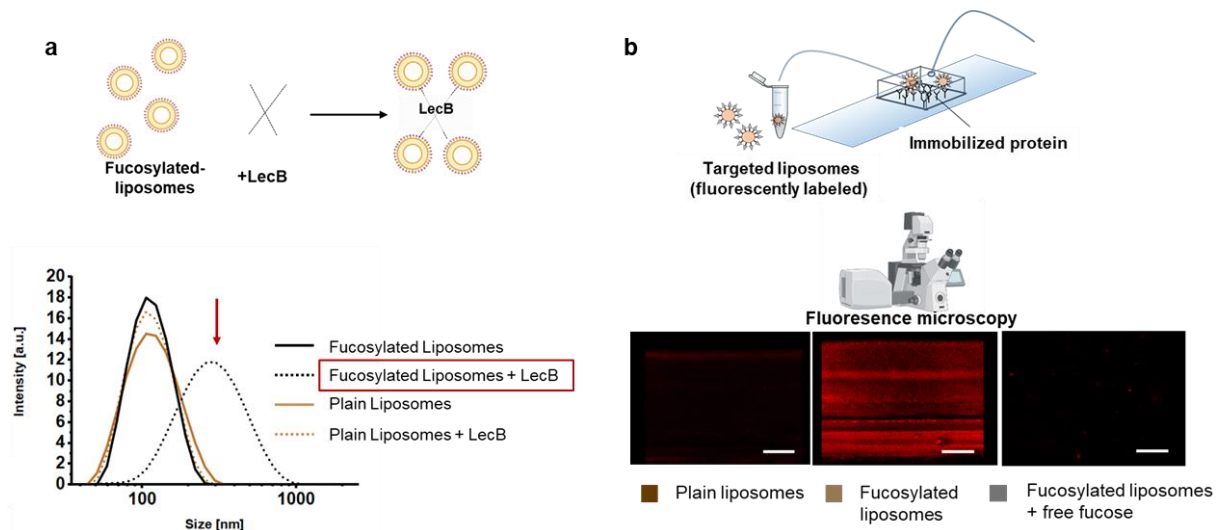


**Figure 25) Principle of lectin binding assays.** a) Incubation of fucosylated liposomes with *Pseudomonas aeruginosa* lectin LecB. Red arrow marks the size shift of fucosylated liposomes after overnight incubation with LecB, confirming the specificity of the binding and the presence of fucose residues on the liposomes' surface. Experiments were performed in triplicates. b) Fucosylated liposomes were flushed through a LecB coated flow chamber using a syringe pump. Following incubation and flushing with buffer or competitive inhibitor, the fluorescence intensity of liposomes bound to the chamber was assessed by fluorescence microscopy. Adapted with permission from Huck *et al.* [184].

After demonstration of the fucose-mediated binding in a cell-free setup, relevant phagocytic cells, including the cell line THP-1 and primary macrophages obtained from human lung tissue and blood, were selected to study cellular internalization under controlled conditions *in vitro*. These cells were selected based on their distinctive expression profiles of the C-type lectin macrophage-mannose receptor (CD206), which facilitates the receptor-mediated internalization and intracellular routing of the targeted liposomes to endosomal compartments [185]. Since several types of macrophages are involved in TB infections including resident alveolar macrophages (represented by the macrophages isolated from human lung tissue) and monocyte-derived macrophages [186] (represented by those isolated from buffy coats) both macrophage types as well as a cell line (dTHP-1) were used to study liposomal uptake. Noteworthy, the lack of competitive uptake between different cell types in the current “macrophage only model” may even underestimate the effect of a targeted delivery approach and the shift in uptake towards a certain population (e.g., phagocytic cells) might not be become visible in such a setup. On the other hand, due to an already high basal uptake of phagocytic cells, the observation of an elevated uptake of fucosylated liposomes might be challenging and requires an optimal concentration of both liposomes and cells and a careful selection of the incubation timeframe. In a first approach, the uptake of fucosylated liposomes was tested on differentiated THP-1 (dTHP-1) cells after 2 hours of incubation in the absence and presence of competitive inhibitor (L-fucose). Here, the uptake of fucosylated liposomes was significantly increased, however, remained on the same level as plain liposomes when L-fucose was present. Experiments at 4°C were performed to confirm an active, energy-dependent uptake mechanism (**Figure 26**).

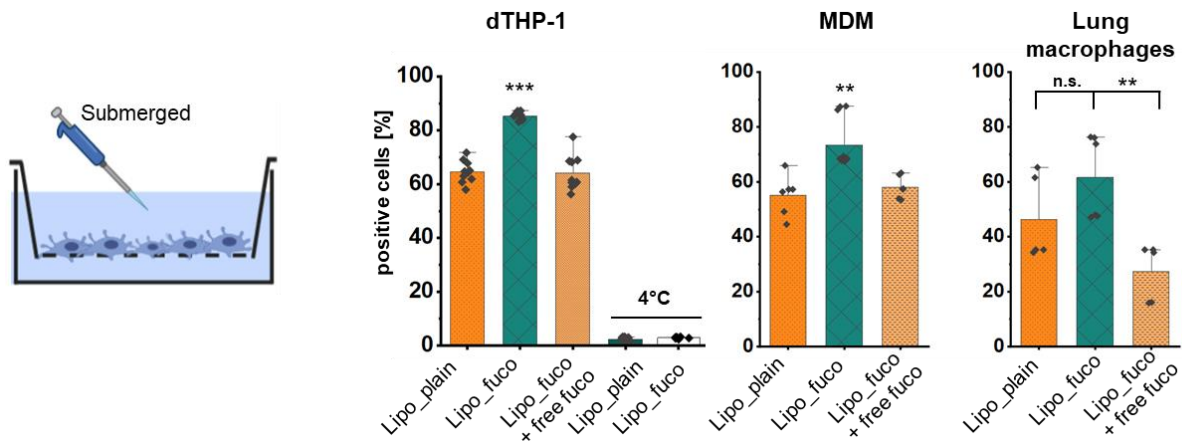


**Figure 26)** Cellular uptake of fucosylated liposomes into phagocytic cells. Fucosylated liposomes showed a higher uptake than plain liposomes. Increased uptake into human dTHP-1 cells, peripheral blood monocyte-derived macrophages (MDM) and lung tissue macrophages was reduced in the presence of free fucose (10 mM). At 4°C, the internalization was drastically reduced due to the inhibition of active uptake, thus indicating the proportion of cell-associated liposomes in this specific case. Data represent means  $\pm$  SD (n=6-9, N=3 for dTHP-1 and MDM, and n=3-5 with N=2 for lung macrophages). Significance was defined as \*\*\* ( $p < 0.001$ ), \*\* ( $p < 0.005$ ) and \* ( $p < 0.05$ ). Adapted with permission from Huck *et al.* [184].

To simulate the deposition scenario in the alveolar region more closely, liposomes were subsequently exposed to cells in aerosol form using a vibrating mesh nebulizer. Such a setup further allowed the inclusion of pulmonary surfactant (Alveofact®) to the interface to investigate the fate of the deposited liposomes upon contact with PS. Interestingly, at the same dose, the overall uptake of aerosolized liposomes was higher compared to liposomes added under submerged conditions, most likely due to the additional diffusion barrier in the latter case. More importantly, the presence of PS in the interface seems to modulate liposomal internalization, since no additional uptake of fucosylated liposomes was observed when PS was present at the air-liquid interface (**Figure 27**). This is most likely attributed to a masking of the liposomes' surface by PS components. From this *in vitro* study, the potential limitations observed in *in vivo* studies was deduced, owing to the control of various contributing aspects in such a setup.

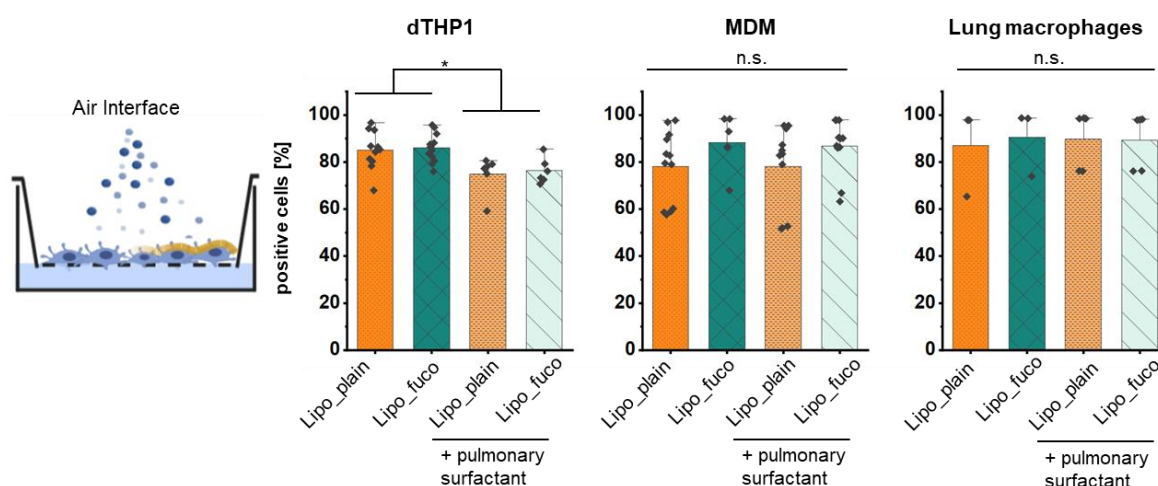


**Figure 27)** Cellular uptake of fucosylated liposomes into phagocytic cells after aerosol deposition. In the presence of pulmonary surfactant, no additional uptake of fucosylated uptake is observed. Data represent means  $\pm$  SD ( $n=6-9$ ,  $N=3$  for dTHP-1 and MDM, and  $n=3-5$  with  $N=2$  for lung macrophages). Significance was defined as \*\*\* ( $p < 0.001$ ), \*\* ( $p < 0.005$ ) and \* ( $p < 0.05$ ). Adapted with permission from Huck *et al.* [184].

Having shown that PS can mitigate the uptake of aerosolized liposomes in a variety of phagocytic cells, in a next step, the release of the incorporated antibiotic upon contact with PS was assessed. In order to so, a suitable system consisting of two compartments separated by a 10,000 Dalton molecular weight cut-off membrane was developed using a Slide-A-Lyzer<sup>®</sup> placed into a 24 well plate equipped with a magnetic stirrer. The time-dependent release of the antibiotic from the donor to the acceptor compartment was then tested for bedaquiline (BDQ) and levofloxacin (LVX, used as control) either in the presence or absence of PS in the release medium. LVX is entirely released after 96 h of incubation and the presence of PS accelerates drug release, indicated by a more than two-fold increased release after 24 h compared to a release medium without PS (**Figure 28**).

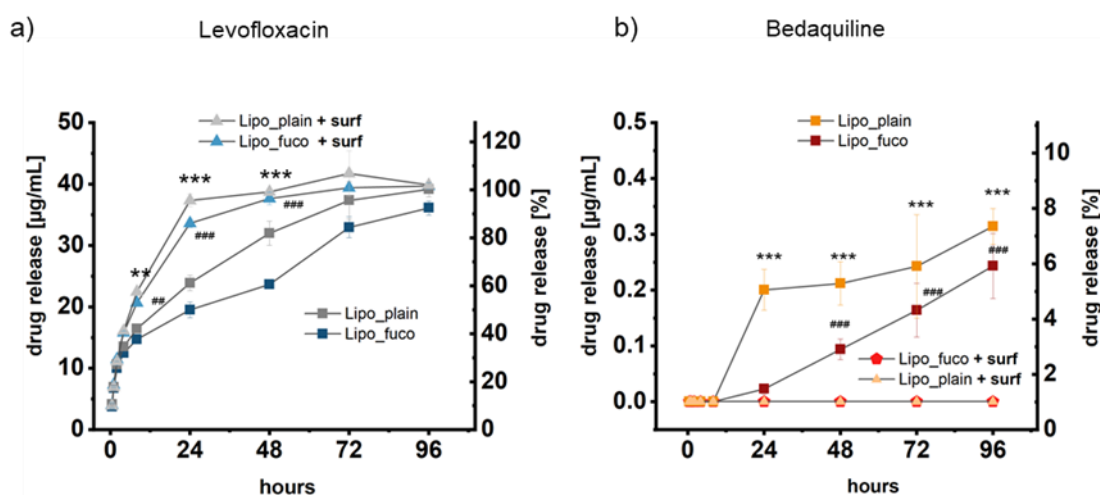


**Figure 28)** Drug release from liposomes. Release profiles of levofloxacin (LVX) (a) and bedaquiline (BDQ) (b) from fucosylated (Lipo\_fuco) and plain liposomes (Lipo\_plain) in the presence and absence of pulmonary surfactant (Alveofact<sup>®</sup>), respectively. LVX was released more rapidly in the presence of pulmonary surfactant (PS) and compared to BDQ. The release of BDQ did not exceed 10% after 96 h and was not detectable when PS was present in the donor medium. Error bars represent means  $\pm$  SD ( $n=9$ ,  $N=3$ ). Significance was defined as \*\*\* / ### ( $p < 0.001$ ) and \*\* / ## ( $p < 0.005$ ). Adapted with permission from Huck *et al.* [184].



In case of BDQ, the overall release did not exceed 10% even after 96 h, and in the presence of PS, literally no release was observed. This might be explained by the localization of BDQ in the hydrophobic liposomal bilayer, associating with the phospholipids present in PS, thereby hampering the release. The presence of a fucose targeting moiety on the liposomes' surface, in contrast, seems to be of minor relevance for the release.

To transfer BDQ-loaded liposomes into respirable microparticles within a size range of 1-5  $\mu\text{m}$ , spray-drying was performed. Optimization of the biocompatible excipients lactose and leucine as previously published by Thiyagarajan and Huck *et al.* [94] resulted in stable, round-shaped microparticles with a high respirable portion (>70%) and drug load. Cryo-TEM and confocal microscopy confirmed the intactness of the liposomal outer layer after spray drying and a uniform distribution of liposomes within the dry powder. This was in line with dynamic light scattering (DLS) size measurements of liposomes after spray drying, which displayed a narrow size distribution with a mean size of  $100 \pm 5$  nm. Subsequent flow cytometry and confocal image analysis could confirm that the targeting function of the fucosylated liposomes was preserved when formulated as microparticles. The elevated uptake into dTHP-1 cells was comparable to the liposomes before spray drying (**Figure 29**).

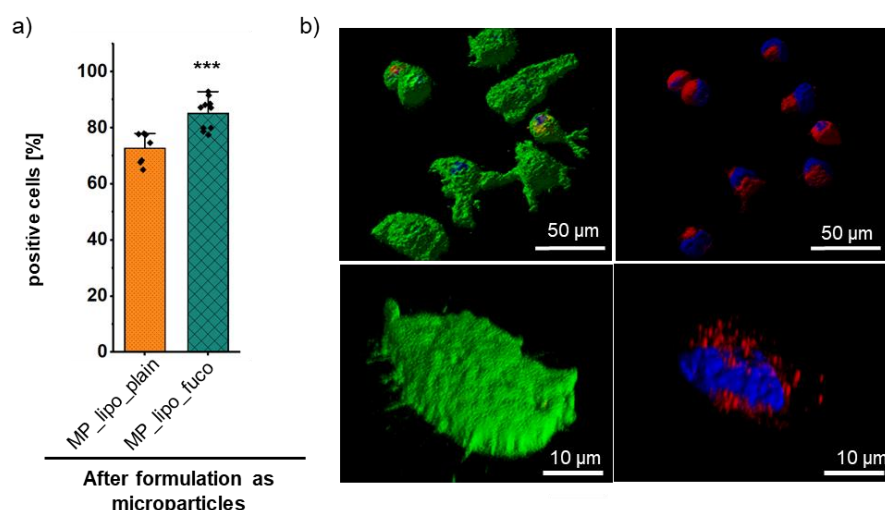


**Figure 29)** Cellular uptake of the liposomal dry powder formulation. a) Uptake after 2 h incubation at 37°C by dTHP-1 cells evidenced by flow cytometry confirmed that active targeting was preserved. b) Representative confocal images analyzed for dissolved dry powders containing fucosylated liposomes show the intracellular localization of liposomes. Nuclei were stained with DAPI (blue), actin with phalloidin (green), and liposomes with PE-Texas red. Data represent means  $\pm$  SD (N=3, n=9) with significance defined as \*\*\* ( $p < 0.001$ ). Adapted with permission from Huck *et al.* [184].

Next, the interaction of the liposome-based dry powder formulations with native pulmonary mucus after dry powder aerosol deposition in the next generation impactor (NGA) served to spot the fraction that is excluded from deposition as consequence of entrapment in the mucus meshwork. The mobility of the liposomes released from microparticles, which were deposited on mucus-covered inserts inside the NGA, was then assessed by MPT. Considerable fractions of 71.4% and 66.5% of plain and fucosylated liposomes, respectively, were immobilized in the mucus layer (**Figure 30**). From this data one can conclude that the formation of granuloma and mucus microaggregate biofilms at the place of mycobacterial infections may impose a

significant barrier for the delivery of such particles to the place of infection in the respiratory bronchioles [187]. On the other hand, the fact that a large fraction of dry powder is immobilized in the mucus meshwork could in parts be counterbalanced by the comparably high mobility of fucosylated liposome. This might be related to the PEG-residues used to link the fucose-derivates to the liposome's surface. Such studies are key to predict the fate of inhaled nanomedicines, while dissecting numerous contributing aspects, such as the composition and barrier properties of pulmonary mucus and surfactant *in vitro*.

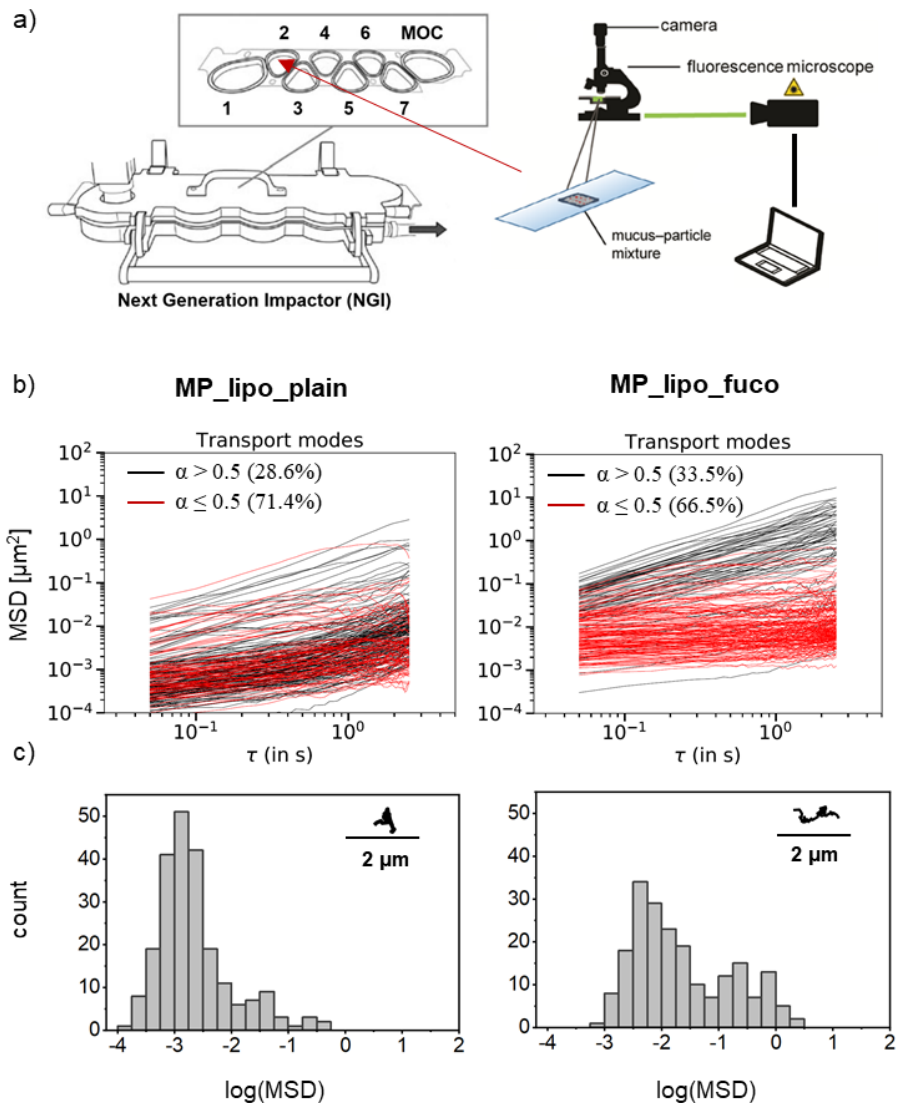


**Figure 30) Mucus interaction studies.** An objective slide containing tracheobronchial mucus was placed into stage 2 of the next generation impactor and analyzed by video microscopy after deposition of the dry powder to study the mobility of plain (MP\_lipo\_plain) and fucosylated (MP\_lipo\_fuco) liposomes released from microparticles. b) The slope of individual mean squared displacement (MSD) curves discriminates between mobile (black line,  $\alpha > 0.5$ ) and immobile (red line,  $\alpha \leq 0.5$ ) particles. Percentages indicate the mobile/immobile fraction of all tracked particles. c) The distribution of log(MSD) values at a timescale of  $t = 0.5$  s indicates a higher mobility of fucosylated liposomes; see also representative trajectories. Three independent experiments were performed with at least  $>150$  particles/frame. Reprinted with permission from Huck *et al.* [184].

In a final evaluation, the killing of *M. abscessus* was assessed both intra- and extracellularly under submerged and air-interface conditions. The PADDOCC systems was used to study the killing of extracellular mycobacteria after dry powder aerosol deposition at a BDQ dose of 0.5  $\mu\text{g}$  (Figure 31).

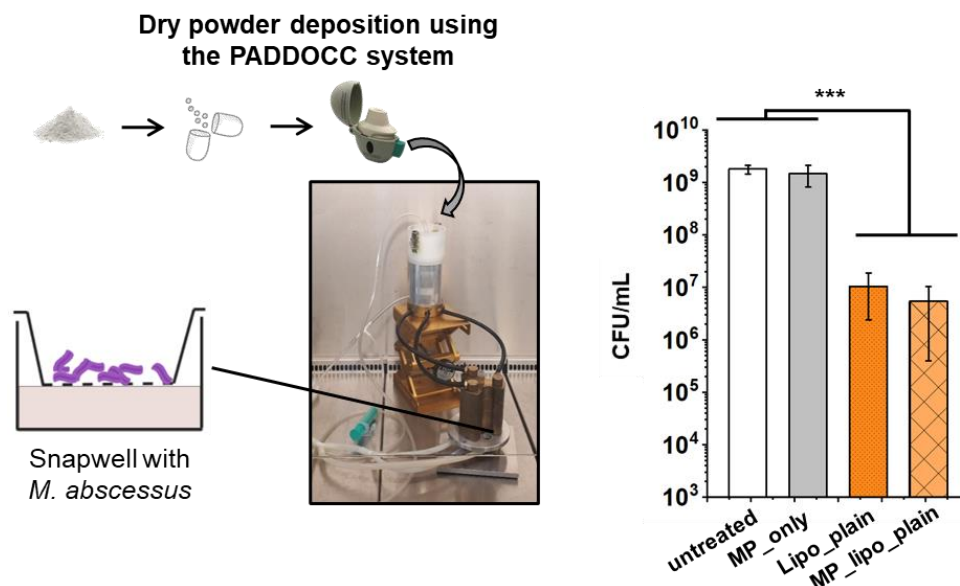


**Figure 31)** Dry powder aerosol deposition for the treatment of extracellular *M. abscessus* using the PADDOCC system. The CFU is reduced by several logs after 72 h of treatment with the BDQ-loaded nano-in-micro formulation. Data represent means  $\pm$  SD (N=3, n=9) with significance defined as \*\*\* ( $p < 0.001$ ).

The treatment resulted in a significant reduction in CFU, already at doses in the sub-microgram range. Control microparticles without BDQ (MP\_only) served to exclude matrix effects derived from the lactose-leucine dry powder excipients. The CFU reduction was similar to that obtained under sub-merged conditions, demonstrating a successful killing of extracellular bacteria with the nano-in-micro formulation under relevant deposition conditions. To study the efficacy of the targeted formulations, a more complex *in vitro* model mimicking the intracellular infection of the targeted cells was developed and liposomes tested in cooperation with Aghiad Bali. The slow growth of the *M. abscessus* revealed a benefit of fucose-mediated targeting of infected dTHP-1 cells after 72 h of treatment. When improving the delivery to intracellular bacteria, targeted aerosolized nano-in-micro delivery systems could help to overcome the pulmonary barriers and the increasing challenge of mycobacterial resistance. While this study may provide the basis for a future translation to clinics, further investigations should focus on the correlation of *in vitro* results obtained in this study with data obtained in animal studies.

## 4 Conclusion and future perspectives

This work investigated the interactions of nanomaterials and anti-infective drug delivery systems with cellular and non-cellular pulmonary barriers, in particular that of pulmonary mucus and surfactant.

The first chapter (section 3.1) of this thesis focused on the characterization of pulmonary mucus and the development of mucus surrogates for the *in vitro* assessment of diverse nanomaterial interactions. Mucus barrier properties and rheology were studied as a function of composition and compared to recently published and newly designed surrogates of mucus, the latter offering a readily available source at high quantity and quality. The movement of 200 nm and 500 nm benchmark particles demonstrated a size-limited diffusion that depends on the concentration and type of cross-linking polymer, including the natural mucins as well as artificial polymers. A mucus surrogate could be developed with properties similar to that of native mucus, allowing to predict the interaction of nanomaterials at appreciable throughput rates. Moreover, this artificial mucus surrogate allowed the growth of respiratory pathogens and to study the diffusion and susceptibility of a variety of antibiotics.

The surfactant barrier was addressed in the second chapter of this thesis (section 3.2) with the aim to link composition and biophysical activity to the interaction with aerosolized nanomaterials. A comprehensive lipidomic analysis of various surfactant preparations and biophysical investigation allowed to dissect individual lipids and proteins as key parameters of a proper interfacial activity. Moreover, this observation could be linked to the uptake and toxicity of aerosolized nanomaterials with different surface functionalization in an *in vitro* model composed of phagocytic or alveolar epithelial cells. These findings may guide the selection of appropriate surfactant preparations for future studies, while emphasizing on the role of PS in relevant *in vitro* models of the human lung, such as the one described herein.

The last chapter (section 3.3 and 3.4) summarizes the characterization and optimization of a liposome-based nano-in-micro delivery system for deep lung deposition and targeting of mycobacterial infections. Fucose-mediated delivery of liposomes and liposomal dry powders in an *in vitro* model of *M. abscessus* infected macrophages demonstrated the benefit of controlled and targeted delivery using dry powder aerosols. This study is a first step towards a translation of novel drug carrier systems for aerosol therapy of mycobacterial infections, certainly requiring follow-up investigations to demonstrate the safety and efficacy of the described system *in vivo*.

Altogether, this thesis contemplates the models and tools to predict the fate of inhaled nanomedicines after interaction with the pulmonary barriers *in vitro* and guides the selection of appropriate models for such interactions. While this is considered a significant contribution for the future testing of novel nanomedicines and anti-infectives, the carrier system investigated in this thesis may potentially overcome the lung barriers and shortcomings of current inhalation therapy of mycobacterial infections.

## 5 Original publications – scientific output

### 5.1 Macro- and microrheological properties of mucus surrogates in comparison to native intestinal and pulmonary mucus

**Benedikt C. Huck**<sup>a, b, †</sup>, Olga Hartwig<sup>a, b, †</sup>, Alexander Biehl<sup>a</sup>, Konrad Schwarzkopf<sup>c</sup>, Christian Wagner<sup>d</sup>, Brigitta Loretz<sup>a</sup>, Xabier Murgia<sup>a, \*, †</sup> and Claus-Michael Lehr<sup>a, b, \*</sup>

<sup>a</sup> Helmholtz Institute for Pharmaceutical Research Saarland (HIPS), Helmholtz Center for Infection Research (HZI), Saarland University, D-66123 Saarbruecken, Germany

<sup>b</sup> Department of Pharmacy, Saarland University, D-66123 Saarbruecken, Germany

<sup>c</sup> Klinikum Saarbrücken gGmbH, Department of Anesthesia and Intensive Care, Saarbruecken, Germany

<sup>d</sup> Experimental Physics, Saarland University, 66123 Saarbruecken, Germany

<sup>†</sup> Equal contribution

*Biomacromolecules* 2019, 20, 3504-3512

<https://doi.org/10.1021/acs.biomac.9b00780>



## Macro- and Microrheological Properties of Mucus Surrogates in Comparison to Native Intestinal and Pulmonary Mucus

Benedikt C. Huck,<sup>†,‡</sup> Olga Hartwig,<sup>†,‡</sup> Alexander Biehl,<sup>†</sup> Konrad Schwarzkopf,<sup>§</sup> Christian Wagner,<sup>||</sup> Brigitta Loretz,<sup>†</sup> Xabier Murgia,<sup>\*,†,||</sup> and Claus-Michael Lehr<sup>\*,†,‡</sup>

<sup>†</sup>Helmholtz Institute for Pharmaceutical Research Saarland (HIPS), Helmholtz Center for Infection Research (HZI), and

<sup>‡</sup>Department of Pharmacy, Saarland University, D-66123 Saarbruecken, Germany

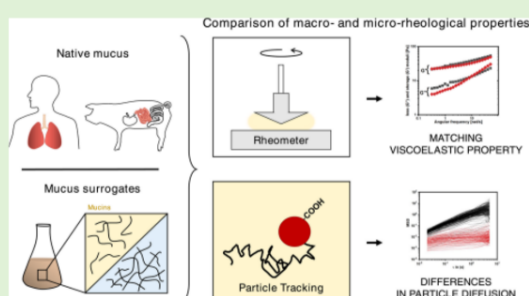
<sup>§</sup>Department of Anesthesia and Intensive Care, Klinikum Saarbrücken gGmbH, 66123 Saarbruecken, Germany

<sup>||</sup>Experimental Physics, Saarland University, 66123 Saarbruecken, Germany

### Supporting Information

**ABSTRACT:** Mucus is a complex hydrogel that acts as a protective barrier in various parts of the human body. Both composition and structural properties play a crucial role in maintaining barrier properties while dictating diffusion of molecules and (nano)materials. In this study, we compare previously described mucus surrogates with the native human airway and pig intestinal mucus. Oscillatory shear rheology was applied to characterize mucus on the bulk macro-rheological level, revealing that the artificial airway surrogate deviates from the elastic-dominant behavior of native mucus samples. We circumvented this limitation through the addition of a cross-linking polymer to the surrogate, adjusting the rheological properties closer to those of native mucus.

Applying particle tracking microrheology, we further demonstrated that the mechanical properties at the microscale differ significantly between artificial and native mucus. We conclude that proper characterization of mucus and its surrogates is vital for a reliable investigation of nanoparticle-based mucosal drug delivery.



### 1. INTRODUCTION

Mucus covers all wet epithelia throughout the human body such as the eyes, the cervicovaginal, respiratory, and gastrointestinal (GI) tracts, displaying a protective barrier that challenges the effective transport of drugs to their target.<sup>1</sup> It is continuously secreted by submucosal glands and specialized epithelial secretory cells and has been reported to form a 100–800  $\mu\text{m}$  thick layer in the GI tract<sup>2</sup> and a smaller 2–10  $\mu\text{m}$  thick layer in the pulmonary airways.<sup>3</sup> In the GI tract, mucus prevents self-digestion, acts as a lubricant, and forms a selective barrier, which is able to discriminate between beneficial substances such as nutrients while shedding away unwanted materials.<sup>4</sup> The main function of airway mucus is to entrap and remove foreign particulates by means of the so-called mucociliary clearance.<sup>5</sup>

The composition of mucus is relatively conserved across different epithelia. It is made up of water (95%), mucin glycoproteins (1–5% w/v), nonmucin proteins, lipids, salts, and cell debris.<sup>6</sup> Mucin macromolecules form an interconnected three-dimensional elastic network with a mesh-like structure. Thus, mucus features a size-limiting physicochemical barrier for molecules as well as (nano)-particles. First, this is maintained by hindering the diffusion of objects bigger than the mesh pore size (physical filtering barrier) and second, it

provides numerous interaction sites that may suppress the diffusion of objects with a size smaller than the mesh spacing (interaction barrier).<sup>7</sup> To circumvent the barrier properties that influence the penetration through mucus, different approaches such as PEGylation have focused on the design of chemically modified nanocarriers with muco-penetrating capacity.<sup>8–12</sup> Particle tracking studies conducted with native intestinal<sup>13</sup> and airway mucus<sup>4</sup> have demonstrated that a great fraction of stealth particles (e.g., PEGylated) with a size of 100–200 nm could penetrate mucus at relatively high diffusion rates. Conversely, particles with a diameter of 500 nm were found to be immobilized by mucus in both studies. These findings clearly delineate a cut-off size for therapeutic nanoparticles (NPs), aiming at crossing intestinal and pulmonary mucus.

The limited availability of native mucus of human origin has stimulated scientific interest in artificial mucus surrogates.<sup>15</sup> Ideally, such surrogates should mimic both composition and structural properties of its natural paradigm, providing a robust experimental model for drug permeation studies.<sup>16–21</sup>

Received: June 5, 2019

Revised: August 15, 2019

Published: August 16, 2019

Reconstituted, commercially available mucins from porcine stomach have been used in previous studies as physiological mucus surrogates.<sup>17,22,23</sup> Recently, such mucus models were utilized to investigate the muco-penetration of nano-sized carrier systems.<sup>24–26</sup> In these studies, mucus was mimicked in terms of biochemical composition, paying particular attention to elevated DNA levels of mucus under pathological conditions<sup>27</sup> (e.g., cystic fibrosis), without reporting its rheological properties. At physiological shear rates, mucus behaves as an elastic-dominant hydrogel. This rheological signature is primarily due to the covalent interactions in the form of disulfide bonds between mucin macromolecules.<sup>28,29</sup> Commercially available mucins in suspension are unable to establish covalent bonding and rather behave as Newtonian fluids.<sup>30,31</sup> The lack of an interconnected mucin network in such suspensions neglects the size-filtering feature of native mucus and may therefore overestimate the diffusion of NPs through mucus.

In this study, we characterized the structural properties of native mucus samples from humans and pigs and compared them to the properties of artificial mucus surrogates that have been previously proposed in the pharmaceutical literature. The GI surrogate used in this study was selected based on the macrorheological match to native porcine mucus.<sup>16</sup> The artificial sputum medium was selected based on its recent use in permeation studies of nanocarriers.<sup>17–19,23,24</sup> In addition to the macrorheological bulk characterization of mucus, we compared the mobility of fluorescent tracer particles with a diameter of 500 nm through all hydrogels to gain an insight into their microrheological behavior. Such data should reveal to what extent these artificial mucus surrogates are suitable for investigating NP–mucus interactions.

## 2. MATERIALS AND METHODS

**2.1. Isolation of Native Mucus Samples.** Native human airway mucus (h-AirM) was collected from patients undergoing elective surgery at the Klinikum Saarbrücken gGmbH according to the protocol approved by the Ethics Commission of the Chamber of Medicine Doctors of the Saarland (file number 19/15) as previously described.<sup>32,33</sup> Briefly, endotracheal tubes obtained from mechanically ventilated patients were cut in 10–15 cm pieces and centrifuged at 1000 rpm at 4 °C for 2 × 30 s to spin down the mucus. Patient age was between 40 and 77 years and male/female ratio was 2:3. Only nonsmokers were included in this study. Samples were stored at –20 °C and gradually thawed at 4 °C overnight prior to experimental use.

Native porcine intestinal mucus (p-IntM) was isolated from the small intestine of four different Swabian-Hall swine (body weight 30–40 kg) at the Institute of Clinical and Experimental Surgery (Saarland University Medical Center, Homburg). Immediately after euthanasia, around 1 m of proximal jejunum was obtained by surgical intervention. The isolation of the mucus was performed by first cutting the intestine into shorter pieces of approximately 10 cm. Small bowel fragments were cut open longitudinally and rinsed carefully with isotonic buffer [10 mM HEPES (Roth), 1.3 mM CaCl<sub>2</sub> (Sigma-Aldrich), 1.0 mM MgSO<sub>4</sub> (Sigma), and 137 mM NaCl (Sigma), pH 7.4]. The mucosal surface was gently scraped with a spatula and aliquoted. Samples were stored at –20 °C and gradually thawed at 4 °C overnight prior to experimental use.

**2.2. Preparation of Artificial Mucus Surrogates.** **2.2.1. Pulmonary Mucus Surrogates.** Artificial airway mucus (art-AirM) was prepared as described by Dinesh.<sup>27</sup> Briefly, 50 mg of porcine stomach mucin (type II mucin from porcine stomach, Sigma), 50 mg deoxyribonucleic acid (low-molecular-weight from salmon sperm, Sigma), 100 μL of a 0.15 M diethylenetriaminepentaacetic acid (Sigma-Aldrich) stock solution, 50 mg of NaCl (Sigma), 22 mg of KCl (Sigma), and 18.1 mg of Trizma base (Sigma) were added to a

volume of 8 mL of ultrapure water (Milli-Q, Advantage A10, Merck Millipore) under constant stirring. The solution was stirred for several hours at 800 rpm to dissolve the mucins completely. After adding 50 mg of casein hydrolysate (Sigma-Aldrich), the pH was adjusted to 7.0 by adding Trizma base. Finally, 50 μL of egg yolk emulsion (Oxoid) was added to the solution and the final volume made up to 10 mL. Experiments were performed immediately after preparation.

To increase the viscoelastic properties of mucus, a variation was applied to the protocol by Dinesh et al. art-AirM was modified by adding 0.9% (w/v) poly(acrylic)acid (PAA) (Carbopol 974P NF). Before adjusting the pH, 90 mg of PAA was added to the mixture and stirred for several hours until PAA was completely dissolved. Finally, the pH was adjusted to 7.0 and experiments performed immediately. We refer to this as modified art-AirM (art<sub>m</sub>-AirM).

**2.2.2. Intestinal Mucus Surrogate.** Artificial intestinal mucus (art-IntM) was prepared according to the protocol by Boegh et al.<sup>16</sup> Briefly, two different 10 mM HEPES (Roth) buffers were prepared containing 1.3 mM CaCl<sub>2</sub> (Sigma), 1.0 mM MgSO<sub>4</sub> (Sigma), with and without 137 mM NaCl, termed buffer A and B. First, 90 mg of PAA (Carbopol 974P NF) was dissolved in buffer B under magnetic stirring at 800 rpm and 500 mg (w/v) porcine gastric mucin type II (Sigma-Aldrich) was added. After complete dissolution, the pH was adjusted to 7.0 by adding NaOH. A lipid mixture was prepared separately in buffer A containing a final concentration of 0.11% (w/v) linoleic acid (Sigma-Aldrich), 0.36% (w/v) cholesterol (Sigma-Aldrich), 0.18% (w/v) phosphatidylcholine (Lipoid), and 0.16% Tween 80 (Caelo). Finally, the lipid mixture was added to the PAA/mucin solution, followed by addition of 3.1% (w/v) bovine serum albumin (Sigma) and pH adjusted to 7.4 with NaOH. After preparation, art-IntM was stored overnight at 4 °C and used the day after for experiments (Table 1).

**Table 1. Overview of Abbreviations**

abbreviations		
airways	human airway mucus	h-AirM
	artificial airway mucus	art-AirM
	modified art-AirM	art <sub>m</sub> -AirM
intestine	porcine intestinal mucus	p-IntM
	artificial intestinal mucus	art-IntM

**2.3. Bulk Rheology.** Bulk rheology was measured using an Anton Paar MCR 702 rheometer (Graz, Austria) with cone–plate geometry (diameter: 25 mm, cone angle: 2°). A volume of 150 μL of mucus was placed between the measuring units. Low viscosity silicon oil was applied to prevent potential mucus dehydration during the measurement. All experiments were performed at 25 °C within the linear viscoelastic region (Figure S2) of the samples determined by a strain amplitude (γ) sweep of 0.1–10% strain with a frequency fixed at 1 Hz. Elastic (G′) and viscous (G″) moduli were determined by frequency (ω) sweep experiments in a range of 0.5–50 rad/s at γ = 1%. Steady shear was applied to measure viscosity (η) of art-AirM and complex viscosity (η\*) was computed according to eq 1 for viscoelastic samples.

$$\eta^* = \frac{\sqrt{(G')^2 + (G'')^2}}{\omega} \quad (1)$$

**2.4. Multiple Particle Tracking Analysis.** The Brownian motion of tracer particles was investigated in native as well as in artificial mucus samples by means of multiple particle tracking (MPT). Fluorescent, carboxyl-terminated polystyrene microspheres (Fluo-Spheres) with a nominal diameter of 500 nm were purchased from Invitrogen. The hydrodynamic diameter was 537 ± 15.5 nm with a polydispersity index of 0.046 ± 0.013, and a ζ-potential of –34 ± 0.460 mV as determined by dynamic light scattering (Zetasizer Nano-ZS, Malvern Instruments, Malvern, UK).

A volume of 25 μL of either native or artificial mucus was mixed with 1 μL of the tracer particles (0.1% w/v) and placed within a 10 ×

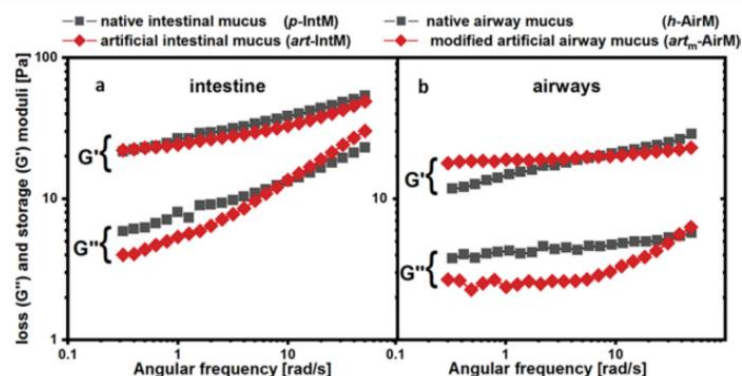


**Figure 1.** Rheological profiling of p-IntM and art-IntM (a). Loss ( $G''$ ) and storage moduli ( $G'$ ) are frequency-dependent in a frequency range of 0.3–50 rad/s. (b) shows the loss and storage moduli for the h-AirM and art<sub>m</sub>-AirM. All measurements were performed at a strain-amplitude of 1%, which falls in the linear viscoelastic region of the samples. The results show the mean of at least four measurements from three independent samples.

**Table 2. Summary of Macrorheological Properties<sup>a</sup>**

		phase-angle [deg] <sup>b</sup>	moduli <sup>b</sup>		complex viscosity [Pa·s]
			$G'$	$G''$	
airways	h-AirM	17.0 ± 1.8	14.9 ± 9.2	4.3 ± 2.7	20.3 ± 13.4
	art-AirM <sup>d</sup>	n.d.	n.d.	n.d.	0.01 ± 0.007 <sup>c</sup>
	art <sub>m</sub> -AirM <sup>c</sup>	7.4 ± 2.3	19.0 ± 2.7	2.4 ± 0.8	21.0 ± 4.7
intestine	p-IntM	18.7 ± 3.4	26.7 ± 6.3	8.1 ± 3.1	27.9 ± 6.8
	art-IntM <sup>f</sup>	16.0 ± 3.2	24.2 ± 6.5	5.4 ± 0.7	25.5 ± 6.7

<sup>a</sup>Human airway mucus (h-AirM), artificial airway mucus (art-AirM), modified artificial airway mucus (art<sub>m</sub>-AirM), porcine intestinal mucus (p-IntM), artificial intestinal mucus (art-IntM). <sup>b</sup>At angular frequency of 1 rad/s. <sup>c</sup>Dynamic viscosity. <sup>d</sup>According to the protocol by Dinesh et al. <sup>e</sup>Modified with PAA. <sup>f</sup>According to the protocol by Boegh et al.

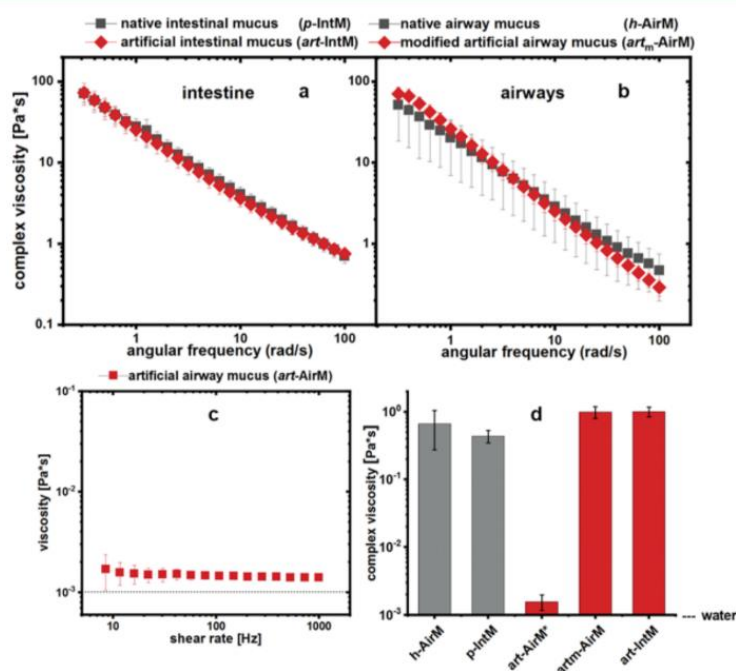


**Figure 2.** Complex viscosity of p-IntM and art-IntM intestinal mucus (a) and h-AirM and art<sub>m</sub>-AirM (b) measured in a frequency range of 0.3–100 rad/s. The viscosity of art-AirM is constant with increasing shear rates (c). The dashed line shows the viscosity of water at RT. The complex viscosities of h-AirM, p-IntM, art-IntM, and art<sub>m</sub>-AirM at an angular frequency of 62.8 rad/s (=10 Hz) compared to the dynamic viscosity (\*) of art-AirM at a shear rate of 10 Hz (d).



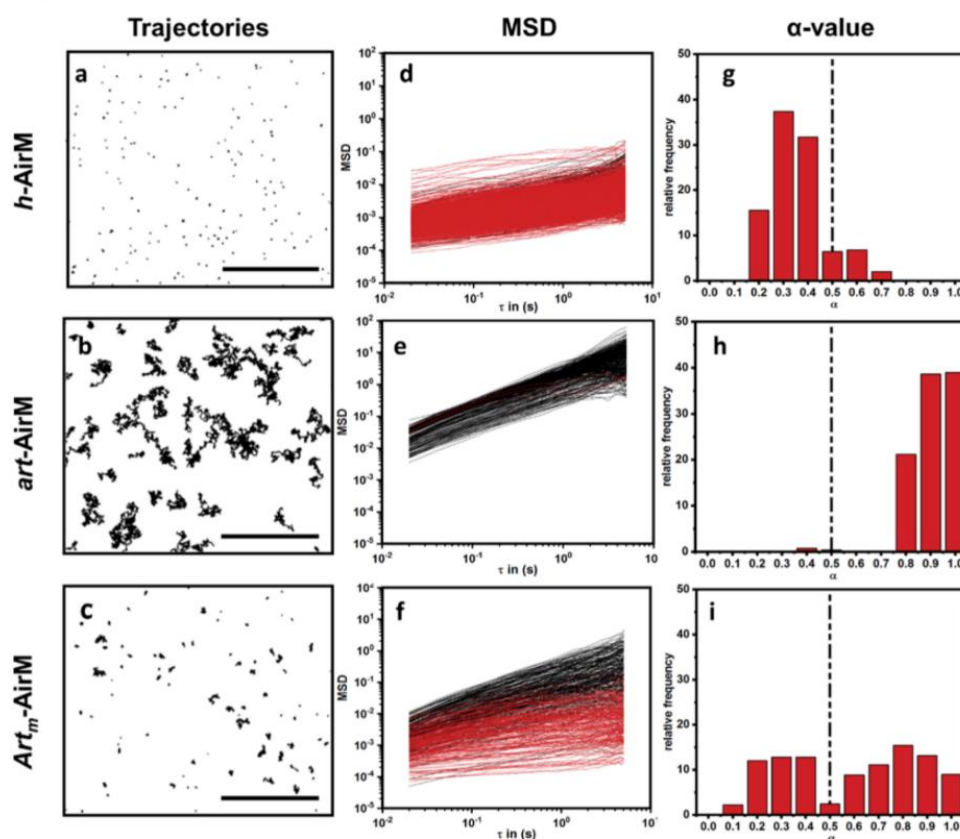


**Figure 3.** (a–i) MPT analysis of 500 nm carboxylated polystyrene NPs dispersed in h-AirM, art-AirM, and art<sub>m</sub>-AirM. Depicted trajectories (a–c) show 5 s of particle motion (scale bar: 10 μm). MSD of NPs dispersed in different hydrogels as a function of time scale (d–f). Black lines correspond to particles in a viscous environment ( $\alpha > 0.5$ ) and red lines to particles in an elastic environment ( $\alpha < 0.5$ ). The  $\alpha$ -value plots (g–i) show the number distribution of particles in elastic and viscous environments. Data represent the mean of 3–6 mucus samples with a minimal amount of 350 particles/plot.

10 mm gene frame chamber (Thermo Fisher Scientific) mounted on a microscope slide. The chamber was sealed with a cover slip and equilibrated for 2 h prior to video microscopy. Measurements were performed with an inverted fluorescence microscope (Nikon Eclipse Ti-S) equipped with a Nikon Intensilight 130 W mercury lamp and 40 × S-plan Fluor Nikon objective with a numerical aperture of 0.6. Short tracking videos of  $\geq 10$  s length were recorded at a frame rate of 50 frames per second (fps) with an Orca R2 monochrome 1.3 MP CCD camera (Hamamatsu) at a resolution of 0.135 μm per pixel. To improve the quality and digital readout of the video files, preprocessing was performed by adjusting sharpness/brightness and contrast and by applying a fast Fourier transform bandpass filter available at ImageJ as described by Ho et al.<sup>33</sup> Two-dimensional displacement in X and Y direction at each frame was obtained using ParticleTracker from MOSAIC ToolSuite (Plugin for ImageJ) developed by Sbalzarini and Koumoutsakos.<sup>34</sup> We used a custom-written Python script for the calculation of averaged mean squared displacement [MSD or  $\Delta r^2(\tau)$ ]

$$|\Delta r^2(\tau)| = (\Delta x^2 + \Delta y^2) \quad (2)$$

The slope of the resulting MSD on a double logarithmic scale is defined as

$$\alpha = \frac{d \log \Delta r^2(\tau)}{d \log(\tau)} \quad (3)$$

and describes the extent of particle diffusion depending on viscous and elastic proportions of the tracking medium: an  $\alpha$ -value equal to

one describes unrestricted thermally driven Brownian motion, whereas  $\alpha < 1$  indicates constrained (subdiffusive) motion. From  $[\Delta r^2(\tau)]$  we can assess the particle's effective diffusivity,  $D_{\text{eff}}$  which is related to MSD as

$$\Delta r^2(\tau) = 4D\tau \quad (4)$$

### 3. RESULTS AND DISCUSSION

**3.1. Macrorheology of Native Mucus and Its Surrogates.** h-AirM and p-IntM showed an elastic-dominant behavior with ( $G' > G''$ ) in the range of frequencies tested (Figure 1). This is a characteristic rheological signature of cross-linked biopolymers and is in accordance with previous characterizations of native mucus samples.<sup>35,36</sup> Bulk rheological properties of p-IntM and art-IntM are matching reproducibly, suggesting that art-IntM is a good model of p-IntM in terms of bulk rheology. Similarly, art<sub>m</sub>-AirM was found to be a good model for h-AirM (Figures 1 and S1). Notably, the loss and storage moduli of airway mucus (Figure 1b) were in general less dependent on the angular frequency than for intestinal mucus (Figure 1a). The ratio of viscous to elastic response is described by the phase angle ( $\delta$ ) and is defined as  $\tan(\delta) = G''(\omega)/G'(\omega)$ . At an angular frequency of 1 rad/s, representing the low velocity of mucociliary clearance,<sup>37</sup>  $\tan(\delta)$  was found to be 0.30 for h-AirM and is equivalent to

a phase angle of  $17^\circ$  found in earlier studies<sup>14</sup> while meeting the criteria for viscoelastic materials with  $0^\circ < \delta < 45^\circ$ .

A similar angle was found for art-IntM and p-IntM with  $16.0^\circ$  and  $18.7^\circ$ , respectively. A value of 7.4 was found for art<sub>m</sub>-AirM, indicating a marked elastic-dominant behavior compared to h-AirM (Table 2). From all the analyzed hydrogels, art<sub>m</sub>-AirM, p-IntM, art-IntM, and h-AirM showed a shear thinning behavior as expected for native mucus (Figure 2a,b).<sup>16,38</sup> Conversely, art-AirM, which has been employed in previous studies as a mimic of pulmonary mucus,<sup>17,18,24,26</sup> only showed a viscous behavior as the elastic part was too weak to be resolved by the rheometer. The viscosity of art-AirM was alternatively measured by steady shear rheology in a shear rate ranging from 1 to 1000 Hz. Regarding the detection limit of the rheometer (Figure S3), the viscosity was independent of the shear rate as typical of Newtonian fluids and only slightly higher than the viscosity of water (Figure 2c).

The results of this study so far clearly demonstrate that the mucins in the art-AirM (mucins in art-IntM as well) lack the ability of forming an interconnected network, most likely because of the industrial extraction and purification process.<sup>39</sup> This is in line with the findings of Kočevár-Nared et al., who reported a similar bulk rheological profile of native intestinal mucus, but a less pronounced elastic signature of rehydrated crude gastric porcine mucins.<sup>30</sup> Therefore, we added PAA in a similar concentration as proposed by Boegh et al. as a cross-linking polymer to increase the elastic response of art-AirM (Figure 1B). PAA has been previously used as a building block for the development of artificial mucus hydrogels.<sup>16,40,41</sup> Indeed, the resulting material, art<sub>m</sub>-AirM, showed an elastic-dominant behavior approaching the rheological signature of h-AirM (Figure 1B). PAA is a versatile polymer widely used in pharmaceutical applications<sup>42</sup> and is also well known for its mucoadhesive properties.<sup>43</sup> When combined with porcine mucins, it was shown to manifest lubricating effects on PDMS interfaces.<sup>44</sup> For both surrogates, a concentration of 0.9% PAA was adequate to render gel-like properties with  $G'/G''$  in the same range as those of native mucus. This further confirms that the mucus surrogate developed by Boegh et al. matches the bulk rheological behavior of native mucus. An important factor in designing polymer-based mucus surrogates is the mechanism of how the polymer forms the gel. In the case of PAA, the degree of physical entanglement of polymer chains, which is determined by the molecular weight, and more importantly, the protonation state of the carboxylic acid head groups, are key factors. This makes such hydrogels highly sensitive to changes in pH. A second factor intrinsic to PAA is its ability to form hydrogen bonds with sugar residues present in the mucin carbohydrate backbone, which could contribute to the interaction filtering mechanisms, in particular for hydrophilic nanomaterials.

**3.1.1. Particle Tracking Microrheology.** To gain insights into the microstructure of both native and artificial mucus matrices, we applied MPT analysis using tracer particles with a diameter of 500 nm. We have previously shown that 94% of carboxylated 500 nm particles were immobilized or severely hindered by native porcine tracheal mucus.<sup>13</sup> Similarly, Schuster et al. reported that 95% of the polyethylene glycol (PEG)-coated stealth particles with the same diameter were immobilized by native human mucus.<sup>14</sup> In the case of art-AirM, particle trajectories show increased MSD values as a function of the time-scale, indicating that particles are diffusing unimpededly through a Newtonian fluid. The results are

strikingly different for h-AirM where 500 nm particles show fairly constant MSD values irrespective of the time scale, indicative of a subdiffusive behavior (Figure 3). In line with our previous work, we set an arbitrary cutoff of 0.5 for the  $\alpha$ -values of each MSD trajectory to classify the particles as diffusive ( $\alpha$ -values  $> 0.5$ ) and nondiffusive ( $\alpha$ -values  $< 0.5$ ).<sup>13</sup> According to this criterion, 86.8% of the particles appeared immobilized in h-AirM and the remaining particles showed a diffusive behavior. Conversely, 99.2% of the particles were diffusive in art-AirM. Together with the bulk rheology, these data demonstrate that the mucus surrogate art-AirM behaves like a Newtonian fluid rather than a complex mucus hydrogel. Therefore, such a material is likely to overestimate the actual particle penetration through native mucus in particle penetration studies.<sup>18</sup>

Indeed, art-AirM was originally developed by Dinesh et al. as a medium to study bacterial growth in the cystic fibrosis airways rather than a mucus model to assess drug permeation. Compared to water, the relative diffusivity of the particles in art-AirM was decreased by just twofold, whereas in the case of h-AirM, particle diffusion was dramatically reduced by 635-fold (Table 3).

**Table 3. Summary of Microrheological Properties<sup>a</sup>**

		transport modes (mobility)		immobilization factor
		immobile particle fraction ( $\alpha < 0.5$ ) [%]	mobile particle fraction ( $\alpha > 0.5$ ) [%]	( $D_{\text{water}}/D_{\text{eff}}$ )
airways	h-AirM	86.8	13.2	635
	art-AirM <sup>b</sup>	0.8	99.2	2
	art <sub>m</sub> -AirM <sup>c</sup>	42.1	57.9	44
intestine	p-IntM	42.8	57.2	20
	art-IntM <sup>d</sup>	92.6	7.4	2570

<sup>a</sup>Human airway mucus (h-AirM), artificial airway mucus (art-AirM), modified artificial airway mucus (art<sub>m</sub>-AirM), porcine intestinal mucus (p-IntM), artificial intestinal mucus (art-IntM). <sup>b</sup>According to the protocol by Dinesh et al. <sup>c</sup>Modified with PAA. <sup>d</sup>According to the protocol by Boegh et al.

However, the addition of PAA to the original recipe of art-AirM allows to create an elastic-dominant gel with a wide pore size distribution. Some pores are compatible with the tracer NPs, as shown by a percentage of  $>50\%$  diffusive particles, whereas other pores seem to be smaller than the particle size.<sup>13,14</sup>

As it was observed at macrorheological level, there were also clear differences between native lung and native intestinal mucus in terms of microrheology. For instance, only 42.1% of the particles are in an elastic environment in the p-IntM, and double the amount (86.8%) in the h-AirM. This variability can be attributed to different species (human vs pig) as well as to the different anatomic origin of native samples (airway vs GI tract) where mucus layers fulfill distinct physiological functions<sup>1</sup> and show quantitative differences in the predominating mucin type in the lungs and the intestine. MUC5AC and MUC5B<sup>45</sup> are the main mucin types in pulmonary mucus, whereas MUC2<sup>46</sup> is the dominating mucin species in intestinal mucus. We found mucin contents ranging between 1.41 and 4.19% for native lung mucus and between 3.18 and 7.40% for p-IntM (Table S1). Furthermore, variations can occur from the

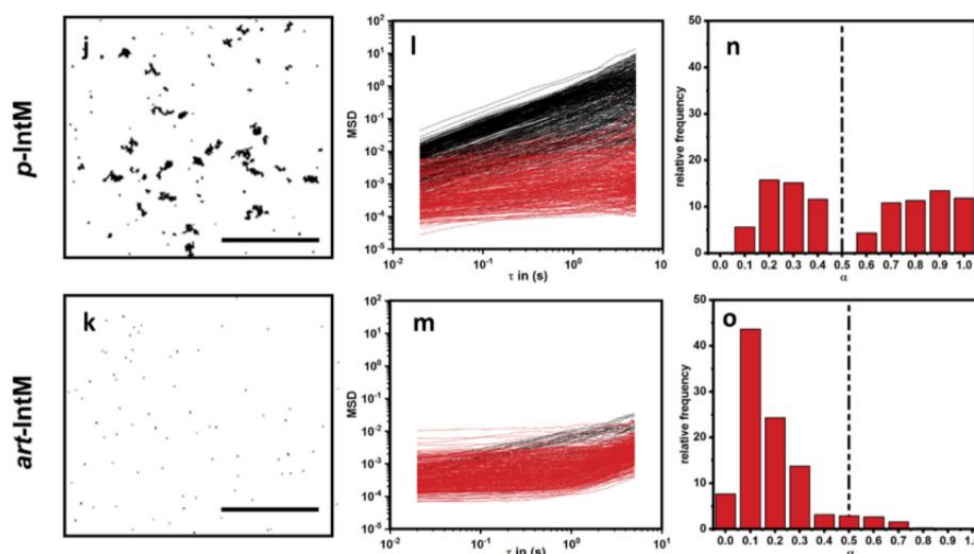


**Figure 4.** (j–o) MPT analysis of 500 nm carboxylated polystyrene NPs dispersed in p-IntM and art-IntM. Depicted trajectories (j,k) show 5 s of particle motion (scale bar: 10  $\mu$ m). MSD of NPs dispersed in different hydrogels as a function of time scale (l,m). Black lines correspond to particles in a viscous environment ( $\alpha > 0.5$ ) and red lines to particles in an elastic environment ( $\alpha < 0.5$ ). The  $\alpha$ -value plots (n,o) show the number distribution of particles in elastic and viscous environments. Data represent the mean of 3–6 mucus samples with a minimal amount of 350 particles/plot.

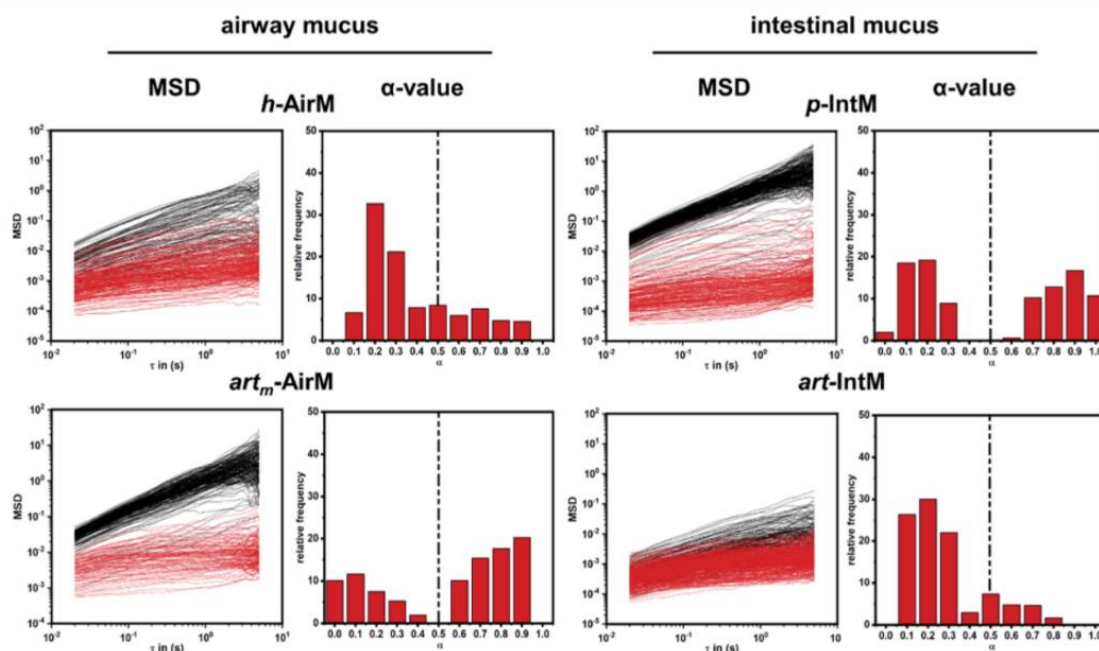


**Figure 5.** MPT analysis of 200 nm carboxylated polystyrene NPs dispersed in h-AirM, art<sub>m</sub>-AirM, art-IntM, and p-IntM. MSD of NPs dispersed in different hydrogels are depicted as a function of time scale. Black lines correspond to particles in a viscous environment ( $\alpha > 0.5$ ) and red lines to particles in an elastic environment ( $\alpha < 0.5$ ). The  $\alpha$ -value plots show the number distribution of particles in elastic and viscous environments. Data represent the mean of three samples with a minimal amount of 350 particles/plot.

collection method. Scratching mucus from the porcine intestinal walls requires diligent performance to avoid contamination of the samples with gastric contents and epithelial tissue. The endotracheal tube method is less prone to such variations.<sup>47,48</sup> Moreover, the airway environment is more homogenous than the intestinal tract with its continuous altering food/water and enzyme content. Although this might

explain the more permeable intestinal mucus in our case, an increase of barrier properties has been observed in previous studies with food-associated intestinal contents.<sup>49</sup> Even though art-IntM precisely mimics the macroscale rheology of native mucus, it is able to immobilize almost twice as many particles compared to p-IntM, suggesting a higher cross-linking density and a lower pore-size range (Figure 4).

We also observed differences regarding particle motilities between art<sub>m</sub>-AirM and art-IntM. Considering that both surrogates contain 0.9% PAA as the gel-forming polymer, these differences can be linked to the concentration of mucins. In art<sub>m</sub>-AirM, containing 0.5% mucins, particles move 44 times slower than in water, whereas in art-IntM, containing 5% mucins, the diffusivity is reduced by a factor of 2570 (Table 3). This suggests that a higher mucin concentration increases the microviscosity of the PAA pores, leading to reduced particle mobility. Mucin content of art-IntM matches well with the concentration found in native p-IntM samples, whereas the mucin concentration of artificial lung surrogates is rather at the lower end of what is found in nature. Lieleg et al. found that a concentration of 1% mucins in mucin-hydrogels can already reduce particle mobility by a factor 2500 compared to free diffusion.<sup>50</sup> On the other hand, using purified mucins without an additional polymer will not lead to an elastic-dominant structure regardless of the mucin concentration deployed. Astonishingly, the art<sub>m</sub>-AirM described above manifests a similar particle tracking profile compared to p-IntM with 57.9 and 57.2% mobile particles, respectively. Similar findings can be observed for h-AirM and art-IntM, which display a barrier to particle diffusion. On the basis of these data, art-IntM appears as a suitable model for h-AirM in terms of both macro- and microrheological properties, in the same way as art<sub>m</sub>-AirM is for p-IntM.

As most of drug carriers described in literature, including the references of this work, have a size of around 200 nm, we decided to validate our findings with particles of a similar size. Figure 5 represents the tracking results of 200 nm polystyrene particles (size  $214.4 \pm 3.4$  nm,  $\zeta$ -potential  $-28.7 \pm 2.37$  mV) for native samples compared to their surrogates.

The tracking results confirm the trends that we observe for 500 nm particles, with the difference that in all samples the percentage of mobile particles is slightly higher for 200 nm particles.

#### 4. CONCLUSIONS

The limited access to native mucus in order to perform drug interaction studies has stimulated the development of artificial mucus surrogates. However, an appropriate surrogate should not only mimic the biochemical composition of mucus but must also resemble its mechanical properties.

In this study, we characterized the rheological properties of some mucus surrogates that have already been used to study the interaction with drugs and drug carrier systems, and compared them with those of native mucus. By combining mucins and other macromolecular constituents of native mucus with the gel-forming polymer PAA, an improved surrogate for pulmonary mucus could be developed with elastic-dominant behavior. Although matching mechanical properties at the bulk level, there remain differences in cross-linking density between native and artificial mucus, which critically affect the diffusion of molecules and particles. For instance, the fraction of mobile NPs in artificial intestinal and artificial pulmonary mucus varied between 7.4 and 99.2%, respectively. This means, only if properly characterized can mucus surrogates be helpful as models to investigate transport and mobility of (nano)-materials. However, we recommend to validate such data with native mucus whenever possible.

#### ■ ASSOCIATED CONTENT

##### 📄 Supporting Information

The Supporting Information is available free of charge on the ACS Publications website at DOI: 10.1021/acs.biomac.9b00780.

Representative strain-sweep experiments to determine the linear-viscoelastic region; individual oscillatory measurements of native mucus and artificial surrogates; oscillatory measurements of samples containing 0.5% and increasing concentrations of PAA; shear rate versus viscosity of water and art-AirM showing increasing viscosity values at lower shear rates when approaching the rheometer detection limit; standard calibration curve of mucin quantification; and mucin concentrations for native mucus samples determined by PAS assay (PDF)

#### ■ AUTHOR INFORMATION

##### Corresponding Authors

\*E-mail: [xmurgia@kusudama.eu](mailto:xmurgia@kusudama.eu) (X.M.).

\*E-mail: [Claus-Michael.Lehr@helmholtz-hips.de](mailto:Claus-Michael.Lehr@helmholtz-hips.de) (C.-M.L.).

##### ORCID

Xabier Murgia: 0000-0002-6370-9047

##### Present Address

<sup>†</sup>Kusudama Therapeutics, Parque Científico y Tecnológico de Gipuzkoa, 20014 Donostia-San Sebastián, Spain.

##### Author Contributions

B.H. and O.H. contributed equally. The paper was written through contributions of all the authors. All the authors have given approval to the final version of the paper.

##### Funding

O.H. and B.C.H. gratefully acknowledge financial support from the EU Horizon 2020 research and innovation programme under grant agreement no. 720905-2 and the BMBF ANTI-TB project under grant agreement GWANTA 20, respectively.

##### Notes

The authors declare no competing financial interest.

#### ■ ACKNOWLEDGMENTS

The authors acknowledge Prof. Dr. Matthias Laschke from the Institute for Clinical and Experimental Surgery (Saarland University, Homburg/Saar, Germany) for providing porcine intestines.

#### ■ REFERENCES

- (1) Murgia, X.; Loretz, B.; Hartwig, O.; Hittinger, M.; Lehr, C.-M. The role of mucus on drug transport and its potential to affect therapeutic outcomes. *Adv. Drug Delivery Rev.* **2018**, *124*, 82–97.
- (2) Atuma, C.; Strugala, V.; Allen, A.; Holm, L. The adherent gastrointestinal mucus gel layer: Thickness and physical state in vivo. *Am. J. Physiol.: Gastrointest. Liver Physiol.* **2001**, *280*, G922–G929.
- (3) Mercer, R.; Russel, M.; Carpo, J. Mucus lining layer in human and rat airways. *Am. Rev. Respir. Dis.* **1992**, *145*, 355.
- (4) Johansson, M. E. V.; Sjövall, H.; Hansson, G. C. The gastrointestinal mucus system in health and disease. *Nat. Rev. Gastroenterol. Hepatol.* **2013**, *10*, 352–361.
- (5) Button, B.; Cai, L.-H.; Ehre, C.; Kesimer, M.; Hill, D. B.; Sheehan, J. K.; Boucher, R. C.; Rubinstein, M. A periciliary brush promotes the lung health by separating the mucus layer from airway epithelia. *Science* **2012**, *337*, 937–941.
- (6) Bansil, R.; Turner, B. S. Mucin structure, aggregation, physiological functions and biomedical applications. *Curr. Opin. Colloid Interface Sci.* **2006**, *11*, 164–170.

- (7) Witten, J.; Ribbeck, K. The particle in the spider's web: Transport through biological hydrogels. *Nanoscale* **2017**, *9*, 8080–8095.
- (8) Craparo, E. F.; Porsio, B.; Sardo, C.; Giammona, G.; Cavallaro, G. Pegylated Polyaspartamide-Polylactide-Based Nanoparticles Penetrating Cystic Fibrosis Artificial Mucus. *Biomacromolecules* **2016**, *17*, 767–777.
- (9) Suk, J. S.; Xu, Q.; Kim, N.; Hanes, J.; Ensign, L. M. PEGylation as a strategy for improving nanoparticle-based drug and gene delivery. *Adv. Drug Delivery Rev.* **2016**, *99*, 28–51.
- (10) Liu, M.; Zhang, J.; Shan, W.; Huang, Y. Developments of mucus penetrating nanoparticles. *Asian J. Pharm. Sci.* **2015**, *10*, 275–282.
- (11) Dünnhaupt, S.; Kammona, O.; Waldner, C.; Kiparissides, C.; Bernkop-Schnürch, A. Nano-carrier systems: Strategies to overcome the mucus gel barrier. *Eur. J. Pharm. Biopharm.* **2015**, *96*, 447–453.
- (12) Zhang, H.; Bahamondez-Canas, T. F.; Zhang, Y.; Leal, J.; Smyth, H. D. C. PEGylated Chitosan for Nonviral Aerosol and Mucosal Delivery of the CRISPR/Cas9 System in Vitro. *Mol. Pharmaceutics* **2018**, *15*, 4814–4826.
- (13) Murgia, X.; Pawelczyk, P.; Schaefer, U. F.; Wagner, C.; Willenbacher, N.; Lehr, C.-M. Size-Limited Penetration of Nanoparticles into Porcine Respiratory Mucus after Aerosol Deposition. *Biomacromolecules* **2016**, *17*, 1536–1542.
- (14) Schuster, B. S.; Suk, J. S.; Woodworth, G. F.; Hanes, J. Nanoparticle diffusion in respiratory mucus from humans without lung disease. *Biomaterials* **2013**, *34*, 3439–3446.
- (15) Lock, J. Y.; Carlson, T. L.; Carrier, R. L. Mucus models to evaluate the diffusion of drugs and particles. *Adv. Drug Delivery Rev.* **2018**, *124*, 34–49.
- (16) Boegh, M.; Baldursdóttir, S. G.; Müllertz, A.; Nielsen, H. M. Property profiling of biosimilar mucus in a novel mucus-containing in vitro model for assessment of intestinal drug absorption. *Eur. J. Pharm. Biopharm.* **2014**, *87*, 227–235.
- (17) Nafee, N.; Forier, K.; Braeckmans, K.; Schneider, M. Mucus-penetrating solid lipid nanoparticles for the treatment of cystic fibrosis: Proof of concept, challenges and pitfalls. *Eur. J. Pharm. Biopharm.* **2018**, *124*, 125–137.
- (18) Yang, Y.; Tsifansky, M. D.; Shin, S.; Lin, Q.; Yeo, Y. Mannitol-guided delivery of Ciprofloxacin in artificial cystic fibrosis mucus model. *Biotechnol. Bioeng.* **2011**, *108*, 1441–1449.
- (19) Torge, A.; Wagner, S.; Chaves, P. S.; Oliveira, E. G.; Guterres, S. S.; Pohlmann, A. R.; Titz, A.; Schneider, M.; Beck, R. C. R. Ciprofloxacin-loaded lipid-core nanocapsules as mucus penetrating drug delivery system intended for the treatment of bacterial infections in cystic fibrosis. *Int. J. Pharm.* **2017**, *527*, 92–102.
- (20) Larhed, A. W.; Artursson, P.; Björk, E. The influence of intestinal mucus components on the diffusion of drugs. *Pharm. Res.* **1998**, *15*, 66–71.
- (21) Hamed, R.; Fiegel, J. Synthetic tracheal mucus with native rheological and surface tension properties. *J. Biomed. Mater. Res., Part A* **2014**, *102*, 1788–1798.
- (22) Leal, J.; Dong, T.; Taylor, A.; Siegrist, E.; Gao, F.; Smyth, H. D. C.; Ghosh, D. Mucus-penetrating phage-displayed peptides for improved transport across a mucus-like model. *Int. J. Pharm.* **2018**, *553*, 57–64.
- (23) Yang, Y.; Tsifansky, M. D.; Wu, C.-J.; Yang, H. I.; Schmidt, G.; Yeo, Y. Inhalable antibiotic delivery using a dry powder co-delivering recombinant deoxyribonuclease and ciprofloxacin for treatment of cystic fibrosis. *Pharm. Res.* **2010**, *27*, 151–160.
- (24) Ernst, J.; Klinger-Strobel, M.; Arnold, K.; Thamm, J.; Hartung, A.; Pletz, M. W.; Makarewicz, O.; Fischer, D. Polyester-based particles to overcome the obstacles of mucus and biofilms in the lung for tobramycin application under static and dynamic fluidic conditions. *Eur. J. Pharm. Biopharm.* **2018**, *131*, 120–129.
- (25) Cristallini, C.; Barbani, N.; Ventrelli, L.; Summa, C.; Filippi, S.; Capelôa, T.; Vitale, E.; Albera, C.; Messore, B.; Giachino, C. Biodegradable microparticles designed to efficiently reach and act on cystic fibrosis mucus barrier. *Mater. Sci. Eng., C* **2019**, *95*, 19–28.
- (26) Pellosi, D. S.; d'Angelo, I.; Maiolino, S.; Mitidieri, E.; d'Emmanuele di Villa Bianca, R.; Sorrentino, R.; Quaglia, F.; Ungaro, F. In vitro/in vivo investigation on the potential of Pluronic mixed micelles for pulmonary drug delivery. *Eur. J. Pharm. Biopharm.* **2018**, *130*, 30–38.
- (27) Dinesh, S. D. Artificial Sputum Medium. *Protocol Exchange* **2010**, DOI: 10.1038/protex.2010.212.
- (28) Dinesh, C. E. D.; Wheeler, K. M.; Ribbeck, K. Mucins and Their Role in Shaping the Functions of Mucus Barriers. *Annu. Rev. Cell Dev. Biol.* **2018**, *34*, 189–215.
- (29) Demouveau, B.; Gouyer, V.; Gottrand, F.; Narita, T.; Dessey, J.-L. Gel-forming mucin interactome drives mucus viscoelasticity. *Adv. Colloid Interface Sci.* **2018**, *252*, 69–82.
- (30) Kočevár-Nared, J.; Kristl, J.; Šmid-Korbar, J. Comparative rheological investigation of crude gastric mucin and natural gastric mucus. *Biomaterials* **1997**, *18*, 677–681.
- (31) Celli, J.; Gregor, B.; Turner, B.; Afdhal, N. H.; Bansil, R.; Erramilli, S. Viscoelastic properties and dynamics of porcine gastric mucin. *Biomacromolecules* **2005**, *6*, 1329–1333.
- (32) Murgia, X.; Yasar, H.; Carvalho-Wodarz, C.; Loretz, B.; Gordon, S.; Schwarzkopf, K.; Schaefer, U.; Lehr, C.-M. Modelling the bronchial barrier in pulmonary drug delivery: A human bronchial epithelial cell line supplemented with human tracheal mucus. *Eur. J. Pharm. Biopharm.* **2017**, *118*, 79–88.
- (33) Ho, D.-K.; Frisch, S.; Biehl, A.; Terriac, E.; De Rossi, C.; Schwarzkopf, K.; Lautenschläger, F.; Loretz, B.; Murgia, X.; Lehr, C.-M. Farnesylated Glycol Chitosan as a Platform for Drug Delivery: Synthesis, Characterization, and Investigation of Mucus-Particle Interactions. *Biomacromolecules* **2018**, *19*, 3489–3501.
- (34) Sbalzarini, I. F.; Koumoutsakos, P. Feature point tracking and trajectory analysis for video imaging in cell biology. *J. Struct. Biol.* **2005**, *151*, 182–195.
- (35) Vasquez, E. S.; Bowser, J.; Swiderski, C.; Walters, K. B.; Kundu, S. Rheological characterization of mammalian lung mucus. *RSC Adv.* **2014**, *4*, 34780–34783.
- (36) Litt, M.; Khan, M. A.; Wolf, D. P. Mucus rheology: Relation to structure and function I. *Biorheology* **1976**, *13*, 37–48.
- (37) King, M. Experimental models for studying mucociliary clearance. *Eur. Respir. J.* **1998**, *11*, 222–228.
- (38) Lai, S. K.; Wang, Y.-Y.; Wirtz, D.; Hanes, J. Micro- and macrorheology of mucus. *Adv. Drug Delivery Rev.* **2009**, *61*, 86–100.
- (39) Schömig, V. J.; Käs Dorf, B. T.; Scholz, C.; Bidmon, K.; Lielie, O.; Berensmeier, S. An optimized purification process for porcine gastric mucin with preservation of its native functional properties. *RSC Adv.* **2016**, *6*, 44932–44943.
- (40) Schenck, D. M.; Fiegel, J. Tensiometric and Phase Domain Behavior of Lung Surfactant on Mucus-like Viscoelastic Hydrogels. *ACS Appl. Mater. Interfaces* **2016**, *8*, 5917–5928.
- (41) Donnelly, R.; Shaikh, R.; Singh, T. R.; Garland, M.; Woolfson, A. Mucoadhesive drug delivery systems. *J. Pharm. BioAllied Sci.* **2011**, *3*, 89–100.
- (42) Kadajji, V. G.; Betageri, G. V. Water Soluble Polymers for Pharmaceutical Applications. *Polymers* **2011**, *3*, 1972–2009.
- (43) Jones, D. S.; Muldoon, B. C. O.; Woolfson, A. D.; Sanderson, F. D. An examination of the rheological and mucoadhesive properties of poly(acrylic acid) organogels designed as platforms for local drug delivery to the oral cavity. *J. Pharm. Sci.* **2007**, *96*, 2632–2646.
- (44) Røn, T.; Patil, N. J.; Ajallouiean, F.; Rishikesan, S.; Zappone, B.; Chronakis, I. S.; Lee, S. Gastric mucus and mucuslike hydrogels: Thin film lubricating properties at soft interfaces. *Biointerphases* **2017**, *12*, 051001.
- (45) Wickström, C.; Davies, J. R.; Eriksen, G. V.; Veerman, E. C. I.; Carlstedt, I. MUCSB is a major gel-forming, oligomeric mucin from human salivary gland, respiratory tract and endocervix: Identification of glycoforms and C-terminal cleavage. *Biochem. J.* **1998**, *334*, 685–693.
- (46) Round, A. N.; Rigby, N. M.; Garcia de la Torre, A.; Macierzanka, A.; Mills, E. N. C.; Mackie, A. R. Lamellar structures of MUC2-rich mucin: A potential role in governing the barrier and

lubricating functions of intestinal mucus. *Biomacromolecules* **2012**, *13*, 3253–3261.

(47) Rubin, B. K.; Ramirez, O.; Zayas, J. G.; Finegan, B.; King, M. Collection and analysis of respiratory mucus from subjects without lung disease. *Am. Rev. Respir. Dis.* **1990**, *141*, 1040–1043.

(48) Rubin, B. K.; Finegan, B.; Ramirez, O.; King, M. General anesthesia does not alter the viscoelastic or transport properties of human respiratory mucus. *Chest* **1990**, *98*, 101–104.

(49) Yildiz, H. M.; Speciner, L.; Ozdemir, C.; Cohen, D. E.; Carrier, R. L. Food-associated stimuli enhance barrier properties of gastrointestinal mucus. *Biomaterials* **2015**, *54*, 1–8.

(50) Lieleg, O.; Vladescu, I.; Ribbeck, K. Characterization of particle translocation through mucin hydrogels. *Biophys. J.* **2010**, *98*, 1782–1789.

# Macro- and microrheological properties of mucus surrogates in comparison to native intestinal and pulmonary mucus

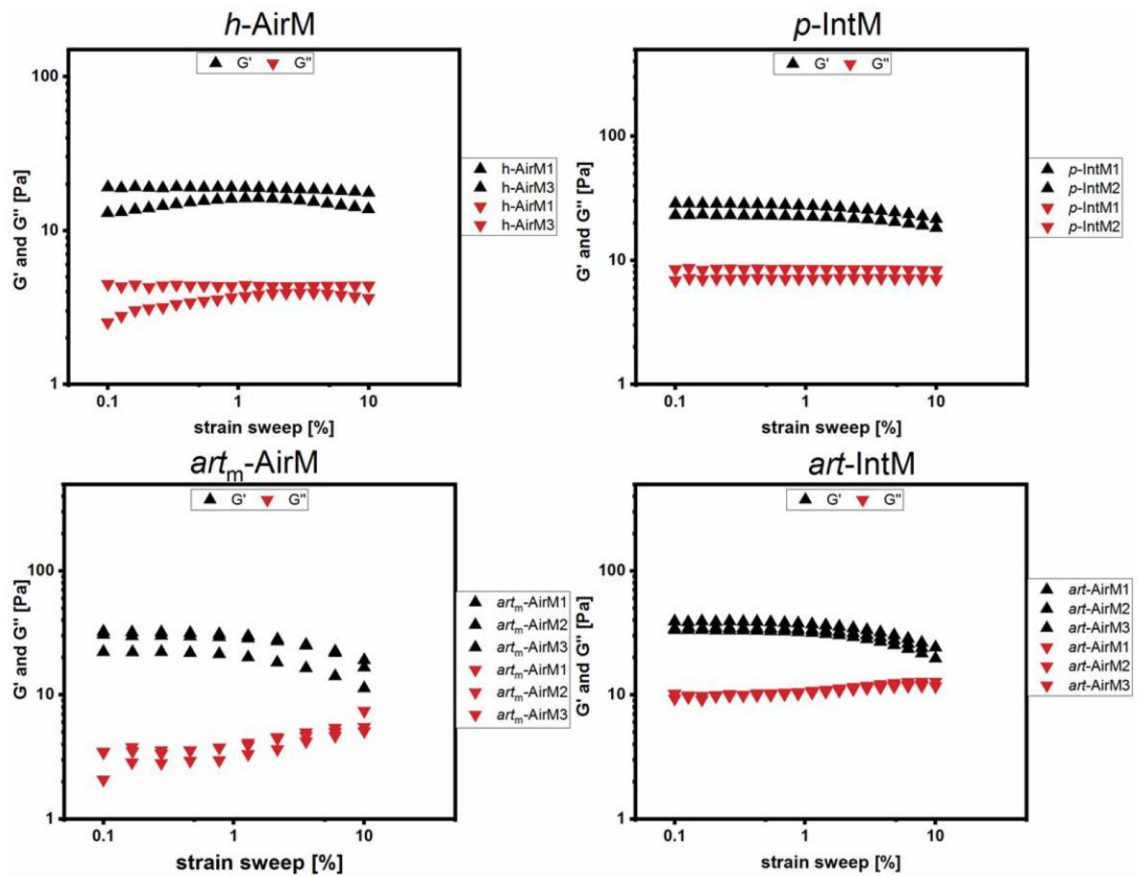
*Benedikt C. Huck<sup>a, b, †</sup>, Olga Hartwig<sup>a, b, †</sup>, Alexander Biehl<sup>a</sup>, Konrad Schwarzkopf<sup>c</sup>,  
Christian Wagner<sup>d</sup>, Brigitta Loretz<sup>a</sup>, Xabier Murgia<sup>a, \*, ‡</sup> and Claus-Michael Lehr<sup>a, b, \*</sup>*

<sup>a</sup> Helmholtz Institute for Pharmaceutical Research Saarland (HIPS), Helmholtz Center for Infection  
Research (HZI), Saarland University, D-66123 Saarbruecken, Germany

<sup>b</sup> Department of Pharmacy, Saarland University, D-66123 Saarbruecken, Germany

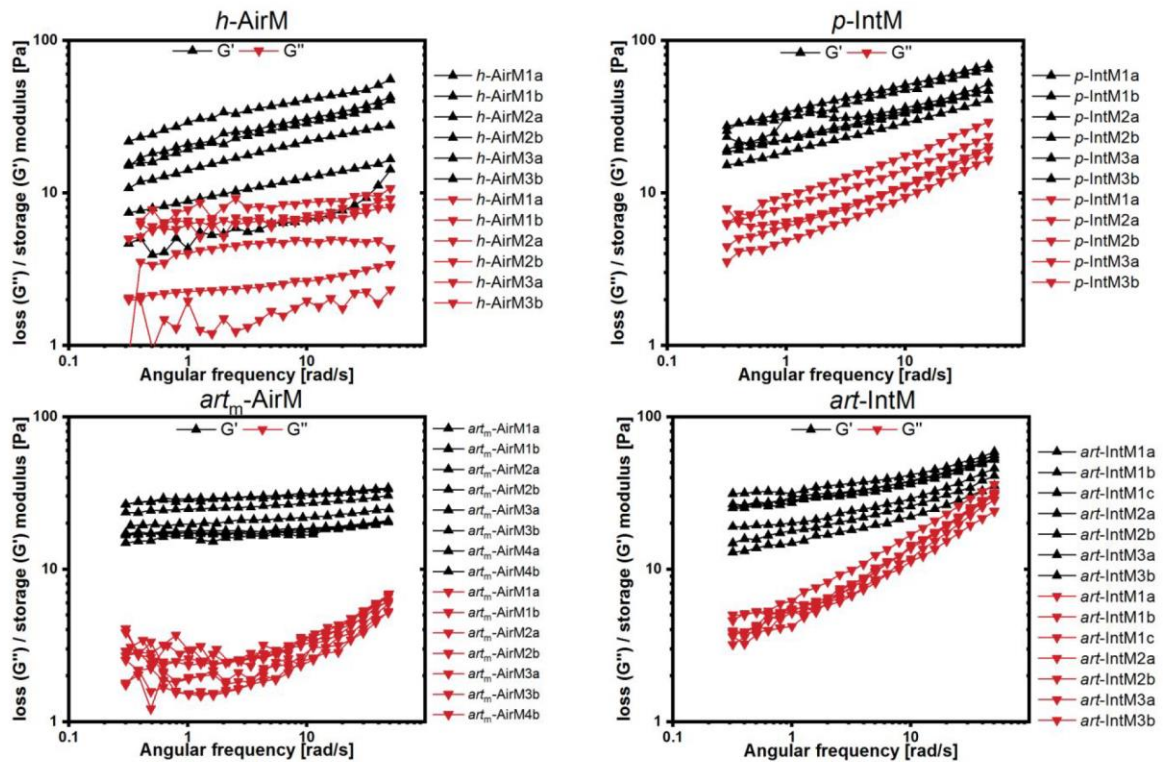
<sup>c</sup> Klinikum Saarbrücken gGmbH, Department of Anesthesia and Intensive Care, Saarbruecken,  
Germany

<sup>d</sup> Experimental Physics, Saarland University, 66123 Saarbruecken, Germany

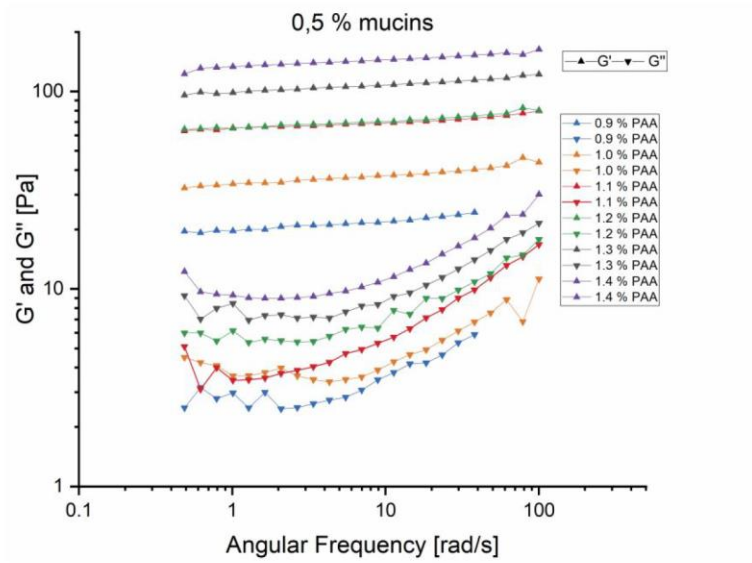


**Supplementary Figure 1.** Representative strain-sweep experiments performed to determine the linear viscoelastic region of human airway mucus ( $h$ -AirM), porcine intestinal mucus ( $p$ -IntM), modified artificial airway mucus ( $art_m$ -AirM) and artificial intestinal mucus ( $art$ -IntM).

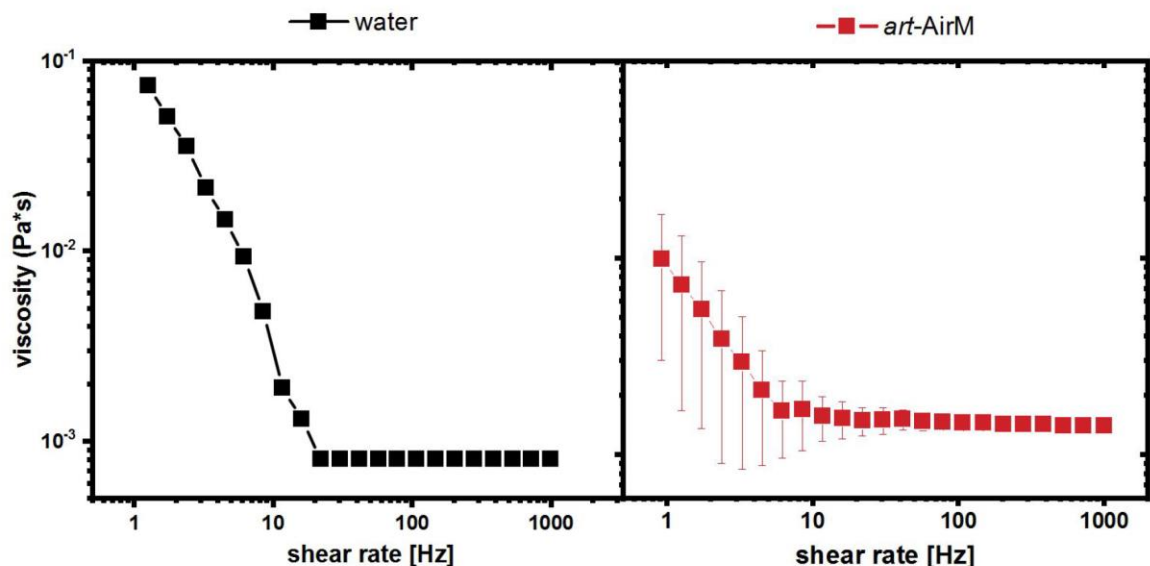




**Supplementary Figure 2.** Oscillatory measurements of human airway mucus (*h*-AirM), porcine intestinal mucus (*p*-IntM), modified artificial airway mucus (*art<sub>m</sub>*-AirM) and artificial intestinal mucus (*art*-IntM). Loss ( $G''$ ) and storage moduli ( $G'$ ) are frequency-dependent in a frequency range of 0.3 – 50 rad/s. All measurements were performed at a strain-amplitude of 1%, which falls in the linear viscoelastic region of the samples.



**Supplementary Figure 3.** Oscillatory measurements of PAA modified artificial airway mucus (*art<sub>m</sub>-AirM*). *Loss* ( $G''$ ) and *storage moduli* ( $G'$ ) are frequency-dependent in a frequency range of 0.3 – 100 rad/s and strongly influence by the PAA concentration. All measurements were performed at a strain-amplitude of 1%, which falls in the linear viscoelastic region of the samples..

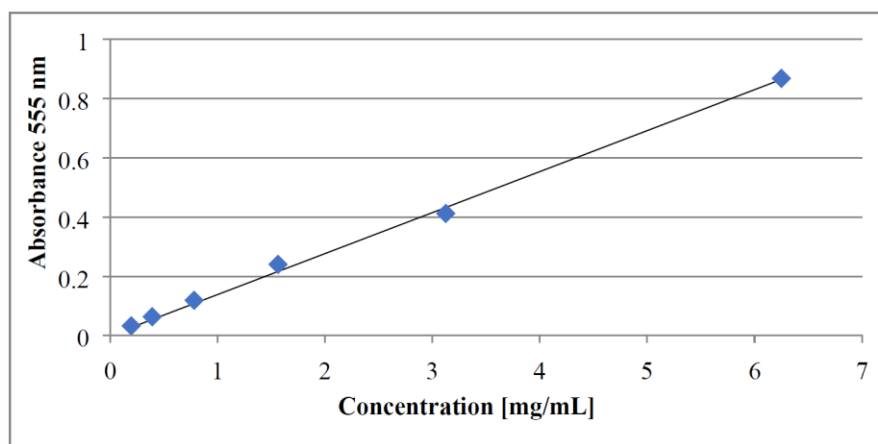


**Supplementary Figure 4.** Viscosity of water and artificial airway mucus (*art-AirM*) measured in a shear rate range from 1 to 1000 Hz. At small shear rates < 10 Hz the viscosity values are increased when approaching the rheometer detection limit.

**Supplementary Table 1 and Figure 5** Quantification of mucin content in native mucus samples from human airways and porcine intestine. (mean  $\pm$  SD of triplicates).

	<i>h</i> -AirM				<i>p</i> -IntM		
Sample	1	2	3	4	1	2	3
Mucin conc. [mg/mL]	34.3 $\pm$ 3.3	26.2 $\pm$ 2.6	14.1 $\pm$ 3.0	41.9 $\pm$ 4.4	31.8 $\pm$ 0.4	53.5 $\pm$ 4.7	73.4 $\pm$ 10.6
[%] of mucins	3.43 $\pm$ 0.33	2.62 $\pm$ 0.26	1.41 $\pm$ 0.3	4.19 $\pm$ 0.44	3.18 $\pm$ 0.04	5.35 $\pm$ 0.47	7.4 $\pm$ 1.06

PAS assay, according to the protocol of Kilcoyne et al., Anal Biochem. 2011. (oxidized with 0.06% periodic acid in 7% acetic acid at 37°C for 1.5h and incubated with Schiff's Reagent for 40 min at RT). Absorbance at 555 nm shows a linear range from 0,2 to 6.25 mg/mL of mucin concentration. (absorbance scan has been performed to confirm 555 nm as the measurement wavelength)



**Supplementary Figure 5** Standard curve of porcine gastric mucins (Sigma)

**5.2 A surrogate of pulmonary mucus for investigating antibiotic permeation and activity against *Pseudomonas aeruginosa* biofilms**

Sarah Frisch<sup>1,2</sup>, Annette Boese<sup>1</sup>, **Benedikt Huck**<sup>1,2</sup>, Justus Horstmann<sup>1,2</sup>, Duy-Khiet Ho<sup>1,3</sup>, Konrad Schwarzkopf<sup>4</sup>, Xabier Murgia<sup>1,5</sup>, Brigitta Loretz<sup>1</sup>, Cristiane de Souza Carvalho-Wodarz<sup>1</sup>, Claus-Michael Lehr<sup>1,2</sup>

<sup>1</sup>Helmholtz-Institute for Pharmaceutical Research Saarland, Saarbrücken, Germany

<sup>2</sup>Department of Pharmacy, Saarland University, Saarbrücken, Germany

<sup>3</sup>Current Address: Department of Bioengineering; University of Washington, School of Medicine, Seattle, USA

<sup>4</sup>Department of Anaesthesia and Intensive Care, Klinikum Saarbrücken, Germany

<sup>5</sup>Current Address: Kusudama Therapeutics, San Sebastian, Spain

*Journal of Antimicrobial Chemotherapy*, March 2021

<https://doi.org/10.1093/jac/dkab068>

## A pulmonary mucus surrogate for investigating antibiotic permeation and activity against *Pseudomonas aeruginosa* biofilms

Sarah Frisch<sup>1,2</sup>, Annette Boese<sup>1</sup>, Benedikt Huck<sup>1,2</sup>, Justus C. Horstmann<sup>1,2</sup>, Duy-Khiet Ho<sup>1,†</sup>, Konrad Schwarzkopf<sup>3</sup>, Xabier Murgia<sup>1,‡</sup>, Brigitta Loretz<sup>1</sup>, Cristiane de Souza Carvalho-Wodarz<sup>1\*</sup> and Claus-Michael Lehr<sup>1,2</sup>

<sup>1</sup>Helmholtz-Institute for Pharmaceutical Research Saarland, Saarbrücken, Germany; <sup>2</sup>Department of Pharmacy, Saarland University, Saarbrücken, Germany; <sup>3</sup>Department of Anaesthesia and Intensive Care, Klinikum Saarbrücken, Germany

\*Corresponding author. E-mail: cristiane.carvalho@helmholtz-hips.de

†Present address: Department of Bioengineering; University of Washington, School of Medicine, Seattle, USA.

‡Present address: Kusudama Therapeutics, San Sebastian, Spain.

Received 4 September 2020; accepted 15 February 2021

**Background:** Pulmonary infections associated with *Pseudomonas aeruginosa* can be life-threatening for patients suffering from chronic lung diseases such as cystic fibrosis. In this scenario, the formation of biofilms embedded in a mucus layer can limit the permeation and the activity of anti-infectives.

**Objectives:** Native human pulmonary mucus can be isolated from endotracheal tubes, but this source is limited for large-scale testing. This study, therefore, aimed to evaluate a modified artificial sputum medium (ASM<sub>mod</sub>) with mucus-like viscoelastic properties as a surrogate for testing anti-infectives against *P. aeruginosa* biofilms.

**Methods:** Bacterial growth in conventional broth cultures was compared with that in ASM<sub>mod</sub>, and PAO1-GFP biofilms were imaged by confocal microscopy. Transport kinetics of three antibiotics, tobramycin, colistin, and ciprofloxacin, through native mucus and ASM<sub>mod</sub> were studied, and their activity against PAO1 biofilms grown in different media was assessed by determination of metabolic activity and cfu.

**Results:** PAO1(-GFP) cultured in human pulmonary mucus or ASM<sub>mod</sub> showed similarities in bacterial growth and biofilm morphology. A limited permeation of antibiotics through ASM<sub>mod</sub> was observed, indicating its strong barrier properties, which are comparable to those of native human mucus. Reduced susceptibility of PAO1 biofilms was observed in ASM<sub>mod</sub> compared with LB medium for tobramycin and colistin, but less for ciprofloxacin.

**Conclusions:** These findings underline the importance of mucus as a biological barrier to antibiotics. ASM<sub>mod</sub> appears to be a valuable surrogate for studying mucus permeation of anti-infectives and their efficacy against PAO1 biofilms.

### Introduction

In the airways, mucus fulfils a protective function by entrapping particles and pathogens and removing them from the lungs through mucociliary clearance.<sup>1</sup> Once this mechanism is impaired, a sticky and relatively static mucus layer is formed and potentially provides a breeding ground for bacteria such as *Pseudomonas aeruginosa*, *Staphylococcus aureus*, or *Mycobacterium abscessus*.<sup>2</sup> Such pathogens are responsible for severe infections in patients suffering from chronic lung diseases such as cystic fibrosis (CF).<sup>3</sup> In CF, an aggravation is caused by the formation of biofilms, which exhibit increased antibiotic tolerance.<sup>4</sup> The typical assessment of susceptibility via MIC, however, neglects the pathophysiological situation with bacterial biofilms being embedded in mucus.<sup>5</sup>

Mucus consists mainly of water (95%), mucins (2%–5%), salts, lipids, DNA, other proteins, and cell debris.<sup>6,7</sup> Samples of human

tracheobronchial mucus can be used to investigate its barrier function and different interaction mechanisms.<sup>8–10</sup> The latter is mainly associated with mucins, a class of high molecular weight glycoproteins, which are negatively charged at neutral pH.<sup>7</sup> The non-glycosylated and cysteine-rich regions are furthermore responsible for crosslinking via intermolecular disulphide bonds,<sup>11</sup> providing mucus with viscoelastic properties.<sup>12</sup> These polymerized proteins form a heterogeneous mesh, limiting the penetration of particles bigger than the pore size of pulmonary mucus, which has been estimated to be approximately 500 nm.<sup>10,13</sup> However, the diffusion of molecules or smaller particles may be hindered by electrostatic as well as hydrophobic interactions.<sup>1,14</sup>

Therefore, it is crucial to address the permeability through the mucus barrier in order to be able to target bacteria inside the biofilms efficiently. Human tracheal mucus can indeed be used for such studies,<sup>15,16</sup> but high-throughput assays are not favoured

due to its limited availability. The use of standardized surrogates—such as the artificial sputum medium (ASM)—can be a favourable alternative,<sup>17</sup> and such media are also applied for the development of anti-infective delivery systems.<sup>18,19</sup> Rheologically, ASM is however, a Newtonian liquid.<sup>14</sup> In order to obtain gel-like viscoelastic properties, poly(acrylic)acid (PAA)—a biocompatible polymer, which forms a gel at neutral or slightly basic pH—can here be added as a supplement.<sup>20</sup> As earlier reported, such modified ASM (=ASM<sub>mod</sub>) has rheological properties comparable to those of native human pulmonary mucus.<sup>21</sup> In this study, we investigated the application of ASM<sub>mod</sub> for studying drug transport and bacterial biofilm infections.

## Materials and methods

An expanded version is provided in the [Supplementary data](#) (available at JAC Online).

### Mucus samples

Native human pulmonary mucus, non-related to pulmonary diseases, was obtained from endotracheal tubes of patients undergoing elective surgery (Klinikum Saarbrücken GmbH) according to the protocol approved by the Ethics Commission of the Chamber of Medicine Doctors of the Saarland (file number 19/15). In brief, mucus was extracted by centrifugation, and native samples were used for transport studies, while freeze-dried mucus discs were prepared as described previously<sup>9,15</sup> for bacteria cultivation.

### Preparation of mucus surrogates

ASM and ASM<sub>mod</sub> preparation was conducted as described before.<sup>17,21</sup> Mucin, DNA, NaCl, KCl, Trizma base, and casamino acids (all from Sigma-Aldrich, Germany) were dissolved in ultra-pure water (Milli-Q<sup>®</sup>, Advantage A10, Merck Millipore, Germany). When solubilized, 0.15 M diethylenetriaminepentaacetic acid (Sigma-Aldrich, Germany) was added. ASM<sub>mod</sub> was further supplemented with 0.9% (w/v) Carbopol (PAA, Lubrizol, UK). After adjustment to pH 7, the surrogates were autoclaved, and sterile filtered egg yolk emulsion (Oxoid, UK) was added.

### Bacterial strains

In this work, *Pseudomonas aeruginosa* PAO1 (ATCC 1562) and PAO1-GFP (ATCC 15692GFP), *Staphylococcus aureus* Newman (SA Newman, ATCC 25904), and *Mycobacterium abscessus* smooth variant were used. The latter was isolated from CF patients' sputum and kindly provided by Prof Dr John Perry, Newcastle University, UK.

### Bacterial growth experiments

Bacterial overnight cultures were diluted and added in a small volume (5–10 µL, for a final OD of 0.01 or 0.001) to 100 µL of the respective standard medium (LB, BHI, 7H9), ASM or ASM<sub>mod</sub> in 96-well plates. The outer rim was filled with 200 µL water or PBS and wet tissues were placed next to the plates to prevent dry-out. After 72 h incubation at 37°C, 100 µL PBS was added to each well containing the biofilm cultures and resuspended by pipetting up and down. The content was transferred to Eppendorf tubes and vortexed for 10–15 min at medium speed to disrupt the biofilm. The bacterial number was determined via dilution plating and counting of colony-forming units (cfu).

### Confocal microscopy

Biofilm morphology of PAO1-GFP was investigated via confocal laser scanning microscopy (CLSM). Bacteria were cultivated in different media using

an 8-well chambered coverglass system (155411, Thermo Scientific, USA). After 72 h incubation, live imaging of bacterial biofilms was performed with a DMi8 inverted microscope and a TCS SP 8 confocal laser scanning unit with an AOBs beam splitter and HyD detector (Leica, Germany). An argon laser (20%) was used for excitation at 476 nm; emission was detected at 580 nm. 200-plane z-stacks were acquired at a resolution of 1024 × 1024 and a speed of 400 Hz, using a Fluotar VIZIR 24×/0.95 water objective.

### Antibiotics

Tobramycin and ciprofloxacin (free base and hydrochloride) were purchased from Sigma-Aldrich (Germany), colistin sulfate was from Adipogen (Switzerland). Some essential characteristics are given in Table S1.

### Transport studies

Transport studies were performed in 24-well plates with transwell<sup>®</sup> inserts (3470, Corning, USA) with 100 µL mucus or ASM<sub>mod</sub> being added to the membrane; PBS was used as a control. Figure 3(a) shows the schematic experimental setup. Stock solutions of antibiotics in PBS of 600 mg/L<sup>15</sup> for tobramycin and colistin sulfate or 100 mg/L for the less-soluble ciprofloxacin were added to the apical compartment. Samples of 100 µL were taken from the basolateral compartment at specific time-points and replaced with PBS. Tobramycin and colistin were quantified via LC-MS and HPLC, respectively, and ciprofloxacin quantification was done by fluorescence intensity.

### Antibiotic activity

Antibiotics in PBS were diluted 1 : 1 in LB, followed by serial dilution. Without mixing, 100 µL of the respective dilutions was transferred to 72 h PAO1 biofilm or planktonic cultures (OD 0.01, ~10<sup>7</sup> cfu/mL) in 96-well plates. The plates were incubated for 24 h at 37°C without shaking, and viability after treatment was assessed by adding 10% (v/v) Presto Blue<sup>™</sup> (Invitrogen, USA) and measuring OD at 570 and 600 nm. Additionally, cfu experiments were performed for selected concentrations.

### Statistical analysis

For each experiment, at least three independent runs (N = 3) with triplicates or duplicates (mucus control experiments) (n > 6) were performed. The statistical analysis was conducted using SigmaPlot (SigmaPlot 14, Systat Software Inc.) with One Way ANOVA followed by the Tukey test. Statistical difference was considered significant for P < 0.05 and is indicated by asterisks (\*), hashes (#) or circles (°) with significance level: \*|#|°, P < 0.05; \*\*|##|°°, P < 0.01; and \*\*\*|###|°°°, P < 0.001, respectively.

## Results

### Effect of ASM<sub>mod</sub> on bacterial growth

Rheology experiments with ASM<sub>mod</sub> (Figure S1) confirmed that the process of sterilization did not alter its viscoelasticity, ensuring its suitability as growth medium for bacteria. The viability of PAO1, SA Newman, and *M. abscessus* in different media was determined after 72 h incubation (Figure 1). The log<sub>10</sub> cfu/mL for PAO1 in standard medium and ASM was comparable, and growth in ASM<sub>mod</sub> was only slightly lower. SA Newman cultures in standard medium and ASM also reached a similar bacterial count; the growth in ASM<sub>mod</sub> was, however, significantly reduced. *M. abscessus* showed a significant 2 log reduction when cultured in ASM, and the bacterial number was even lower in ASM<sub>mod</sub>.

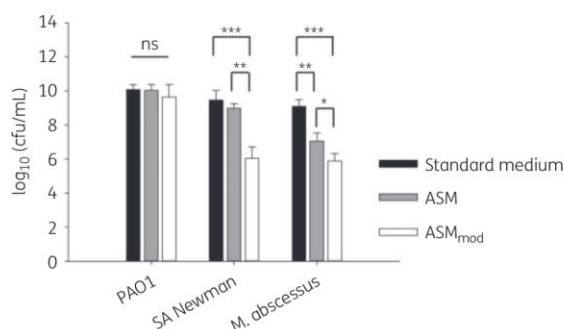


**Figure 1.** Growth of CF-relevant bacteria in various test media. Colony-forming units (cfu) of *Pseudomonas aeruginosa* (strain PAO1), *Staphylococcus aureus* Newman (SA Newman) and *Mycobacterium abscessus* after 72 h incubation in different media (standard medium, ASM, ASM<sub>mod</sub>). Significance is indicated by asterisks; ns=not significant. N=3 with n=9.

### Confocal analysis of PAO1-GFP biofilm morphology

All three bacteria used in this study are known to be biofilm-forming. However, the unaffected growth rate of PAO1 guided the selection for biofilm investigations via CLSM (Figure 2 and Figure S2). In liquid cultures, bacteria most often attach to solid surfaces and proliferate to microcolonies.<sup>4</sup> Accordingly, 72 h biofilms in LB and ASM were observed as attachments to the well bottoms (Figure 2a and b). In contrast, in ASM<sub>mod</sub>, biofilm structures were found relatively equally distributed throughout the medium, similar to mucus (Figure 2c and d). Although the bacterial density seemed to differ, Figure S2, which covers a more sizable z-axis up to 1 mm, shows a distinct distribution in a liquid (ASM) or a viscoelastic medium (ASM<sub>mod</sub>). Also, the cfu data confirmed that the bacterial number in all conditions was not significantly different (Table 1).

### Antibiotic permeation is highly reduced by mucus and ASM<sub>mod</sub>

Transport studies through mucus and ASM<sub>mod</sub> were performed with tobramycin, colistin, and ciprofloxacin (Figure 3 and Figure S3). In comparison with control experiments (PBS), antibiotic diffusion started delayed and showed a significant decrease in the presence of mucus or ASM<sub>mod</sub>. Both hydrogels revealed a similar time course and no significant differences. Tobramycin was only detected after 2 h in the presence of mucus or ASM<sub>mod</sub> but reached 12.4% and 7.6% permeation, respectively (Figure 3b). An even more pronounced hindrance in transport was observed for colistin with overall <5% permeation (Figure 3c). Ciprofloxacin diffusion through both hydrogels was also retarded, but steadily increased to 18.4% and 16.8% (Figure 3d).

### Viscoelastic properties of mucus surrogates affect antibiotic activity

Antibiotic efficacy was determined by measuring bacterial metabolic activity via a resazurin-based assay (Presto Blue™). With a metabolic activity below 10%, the following inhibiting

concentrations were determined for planktonic PAO1: 8 mg/L for tobramycin and colistin and 0.5 mg/L for ciprofloxacin (Figure S4). The same method and additional cfu experiments were further applied on 72 h PAO1 biofilms (Figure 4). Here, we could ensure a correlation between a metabolic activity below 10% and bacteria eradication. A decrease in metabolic activity was, however, not forcibly related to a lower bacterial count or vice versa.

Tobramycin completely reduced the metabolic activity of PAO1 biofilms (Figure 4a) and eradicated the bacteria in standard LB medium at 64 mg/L (Figure 4b). The cultivation in ASM already revealed some reduced efficacy; however, this effect was pronounced in ASM<sub>mod</sub>, pointing to the fact that the medium's viscoelasticity has an additional impact on tobramycin activity. For colistin, the metabolic activity of PAO1 biofilms was inhibited at 64 and 128 mg/L in ASM and LB (Figure 4c). Using ASM<sub>mod</sub>, the metabolic activity was also decreasing, but the bacterial count was still high at 256 and 1024 mg/L, while eradication was achieved with the other tested media (Figure 4d). Due to its limited solubility in PBS, the activity of ciprofloxacin was only tested up to 128 mg/L. The effect on metabolic activity was marginal (Figure 4e). However, there was already some cfu reduction starting at 4 mg/L, which was comparable in all tested media (Figure 4f).

As tobramycin activity was most affected by the mucus surrogates, we selected this drug for a confirmative test with native mucus. Treatment with 64 mg/L tobramycin reduced the cfu drastically in LB and ASM, while in ASM<sub>mod</sub> as well as in native mucus, the cfu count was only slightly diminished (Table 2).

## Discussion

### ASM<sub>mod</sub> serves as a growth medium for relevant bacteria

Different models exist to address mucosal biofilms' susceptibility *in vitro* which, for instance, use human pulmonary mucus<sup>15</sup> or CF sputum<sup>22</sup> as a growth medium. Such *ex vivo* samples provide a natural environment for the cultivation of bacterial biofilms. However, for both, there is a limitation regarding their availability and sample homogeneity. Therefore, mucus surrogates such as ASM are of interest for high-throughput assays,<sup>23</sup> but this medium does not feature mucin cross-linking and shows rather Newtonian behaviour. ASM<sub>mod</sub> does not show a dense and heterogeneous protein network either, but the supplement with PAA provides the medium with relevant elasticity.<sup>21</sup>

The potential of ASM<sub>mod</sub> was further investigated by addressing bacterial counts. For PAO1(-GFP) only minor changes were determined for all tested conditions, and we hypothesize that this outcome is caused by metabolic diversity and capability to adapt to environmental conditions.<sup>24,25</sup> *P. aeruginosa*, therefore, seems to be able to grow well even when being hindered by mucus or some viscoelastic surrogate. The other tested bacteria showed, however, a substantial reduction of growth in ASM<sub>mod</sub>. For *S. aureus*, we suppose that this effect is mainly based on the addition of PAA since no significant reduction was detected in liquid ASM. A low amount of biomass and lower metabolic activity of *S. aureus* was also observed in another modified version of ASM, supplemented with agar.<sup>26</sup> *M. abscessus* growth was significantly lower in both ASM and ASM<sub>mod</sub>, which might be related to its slower growth and/or a switch to survival mode in both surrogates. Other groups also

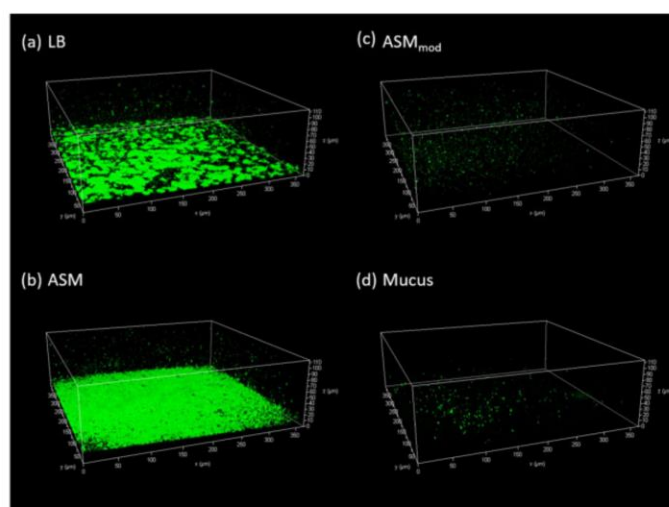


**Figure 2.** 72 h PAO1-GFP biofilm structure in different media. Three-dimensional confocal images of PAO1-GFP (green) after 72 h incubation in LB (a), ASM (b), ASM<sub>mod</sub> (c) and freeze-dried, resuspended human mucus (d). Z-stacks of 115 µm are shown. This figure appears in colour in the online version of JAC and in black and white in the print version of JAC.

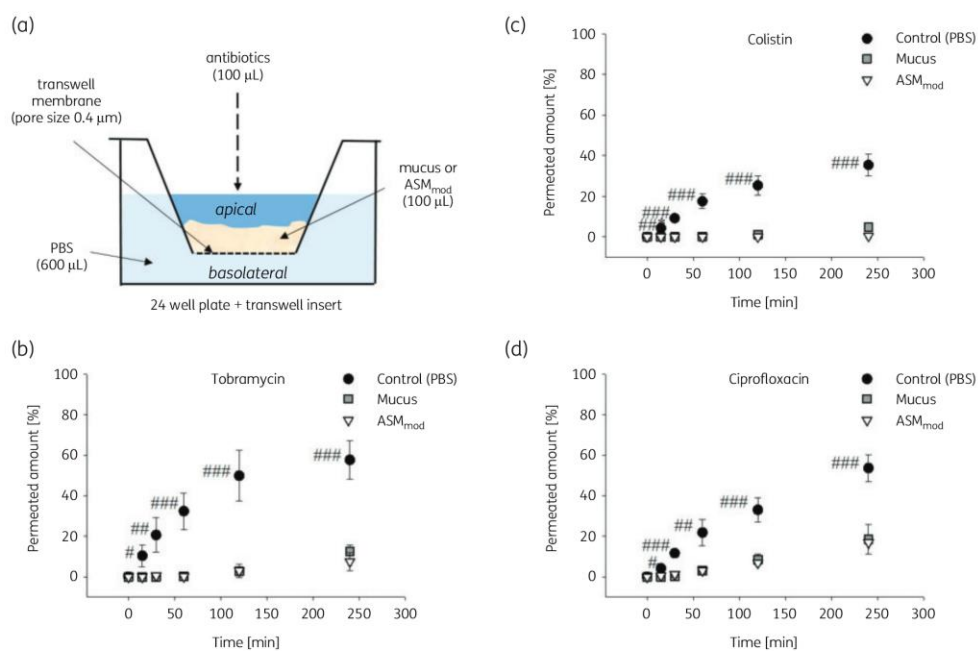


**Figure 3.** Antibiotic transport through mucus and ASM<sub>mod</sub>. (a) Diagram of transport study set up. Results are shown for tobramycin (b), colistin (c), and ciprofloxacin (d) permeation through native mucus (squares) and ASM<sub>mod</sub> (triangles), PBS was used as control (circles). The cumulative mass [µg] was normalized to the calculated mass of the initial concentration [µg]; the permeated amount [%] is shown over time [min]. Statistical significance (PBS versus mucus and PBS versus ASM<sub>mod</sub>) is indicated by hashes.  $N=3$  with  $n>8$ . This figure appears in colour in the online version of JAC and in black and white in the print version of JAC.



**Table 1.** Bacterial count of PAO1-GFP in different media

Condition	Log <sub>10</sub> cfu/mL (mean±SD)			Mucus
	LB	ASM	ASM <sub>mod</sub>	
PAO1-GFP	9.52 ± 0.78	9.25 ± 0.09	8.34 ± 1.25	9.76 ± 0.75

PAO1-GFP bacterial survival after 72 h in different media (LB, ASM, ASM<sub>mod</sub>, freeze-dried, resuspended mucus), determined by cfu. No significant difference was detected.  $N = 3$  with  $n = 9$ .

reported impaired *M. abscessus* growth once cultured in artificial CF sputum medium.<sup>27</sup> It is noteworthy that ASM was initially developed for the cultivation of *P. aeruginosa*.<sup>23,28</sup> Moreover, the bacterium is listed by the WHO as a class I critical bacterium and therefore causing substantial interest in models suitable for testing and developing antibiotics. Consequently, we focused on PAO1 for further investigations.

### PAO1-GFP biofilm morphology correlates to the rheological properties of the growth medium

In the next step, the biofilm morphology of PAO1-GFP was addressed by confocal imaging. Here, major differences were observed using a liquid (LB, ASM) or a viscoelastic medium (ASM<sub>mod</sub>, mucus). It has been reported that *P. aeruginosa* grows as aggregates within mucus in the airways of CF patients.<sup>29,30</sup> We made similar observations with ASM<sub>mod</sub> or mucus as a growth medium, which indicates that mucosal *P. aeruginosa* biofilms consist of microcolonies being attached rather to mucins or other matrices instead of a solid surface. Therefore, ASM<sub>mod</sub> simulates the growth conditions of *P. aeruginosa* in mucus with high resemblance regarding bacterial count and biofilm morphology.

### ASM<sub>mod</sub> resembles the mucus barrier for antibiotics

Mucus acts as an essential biological barrier for the delivery of anti-infectives in the airways, and our results confirm that the diffusion of antibiotics is highly reduced by human pulmonary mucus.<sup>15,31</sup> Its 3D polymeric network appears to be a relevant factor, with an increased lag-phase and slowed permeation of the antibiotics, and a similar drastically hindered permeation through ASM<sub>mod</sub> was observed. Additionally, we noted drug-dependent differences. Mucus is also a selective barrier and offers different interaction mechanisms with mucin proteins, especially of electrostatic nature.<sup>32</sup> As a hydrophilic and positively charged antibiotic, tobramycin can bind in such a manner to mucins and other negatively charged mucus components such as DNA, causing entrapment of drug molecules in the mucus layer. The same mechanism may also apply to the cationic colistin. The fatty acid part of the peptide antibiotic may lead to additional hydrophobic interactions with the non-glycosylated regions of mucins, reducing the permeation even more. The highest percentage of mucus permeation was observed for ciprofloxacin whose net charge is neutral at physiological pH. Therefore, we assume that the fluoroquinolone shows less interaction, and the reduction is rather a matter of slowed-down diffusion based on the hydrogels' elasticity. Although the micro-rheology of mucus and ASM<sub>mod</sub> differs, as observed by

multiple particle tracking,<sup>21</sup> a comparable constitution and elasticity seem to be adequate to address drug permeation. It is noteworthy that our testing conditions may overestimate the thickness of the mucus layer *in vivo*. Still, this comparably easy and fast protocol has the potential to address the mucus-penetrating properties of novel drugs or carrier systems already at an early stage of development.

### Antibiotic activity is altered in a mucosal environment

The activity of the same antibiotics was tested by addressing the minimal metabolic inhibiting concentrations for planktonic PAO1 and 72 h biofilms in different media. Our results are based on bacterial metabolic activity rather than on visible growth inhibition via OD or inhibition zones on agar, which explains higher values than those reported for MIC in the literature.<sup>33–35</sup> An increased tolerance of 72 h biofilms in the standard medium was observed, which is multi-factorial and is related to slower bacterial growth, low metabolic activity and reduced diffusion through the extracellular polysaccharide (EPS) matrix.<sup>25,36</sup> These factors may be amplified for mucosal biofilms due to an altered environment and an even more substantial reduction of drug diffusion by the mucus barrier.<sup>37</sup>

This effect was mainly observed for tobramycin treatment of PAO1 biofilms in ASM<sub>mod</sub>, similar to our previously reported findings with native mucus.<sup>15</sup> The biochemical surroundings might affect the susceptibility of *P. aeruginosa* to tobramycin since a higher tolerance could also be noted in liquid ASM. The bacterial metabolism can indeed be altered by environmental changes such as the presence of mucins.<sup>28,38</sup> However, the reduced diffusion of tobramycin through mucus or ASM<sub>mod</sub> seemingly enhances this effect.

For colistin, results for PAO1 grown in LB and ASM showed only small variations, and biofilm eradication could be achieved for both conditions. Nevertheless, the reduced antibiotic permeation through ASM<sub>mod</sub> resulted in less antibiotic reaching the bacteria inside the biofilm, favouring their survival. This might also explain discrepancies with the results from Müller et al.,<sup>15</sup> who achieved eradication of mucosal biofilms at much lower concentrations. In this case, ASM<sub>mod</sub> may overestimate the mucus barrier for a strongly interacting drug, such as colistin.

In contrast ciprofloxacin showed much better penetration. Within our tested concentration range, which was limited by the solubility in PBS, similar results for activity against PAO1 biofilms were obtained for all tested media, with the bacterial number being reduced comparably. Here, the discrepancies between Presto Blue™ assays (no inhibition) and counting of cfu (reduction of bacterial count) are most likely based on an altered determination of viability using a rather qualitative or quantitative approach, respectively.

The mechanism of action is another factor that needs to be considered regarding an altered susceptibility in biofilms. For instance, colistin—which disrupts the outer membrane of Gram-negative bacteria—is also effective against bacterial biofilms, causing reduced growth and metabolic activity. Therefore, lower susceptibility of ASM<sub>mod</sub> biofilms probably results from the reduced permeation. The efficacy of ciprofloxacin (inhibition of DNA gyrase) and tobramycin (binding to 30S subunit of ribosomes) is, in contrast, based on effective concentrations at the intracellular targets, making permeation through the bacterial cell membrane inevitable. For this reason, an overexpression of efflux pumps in

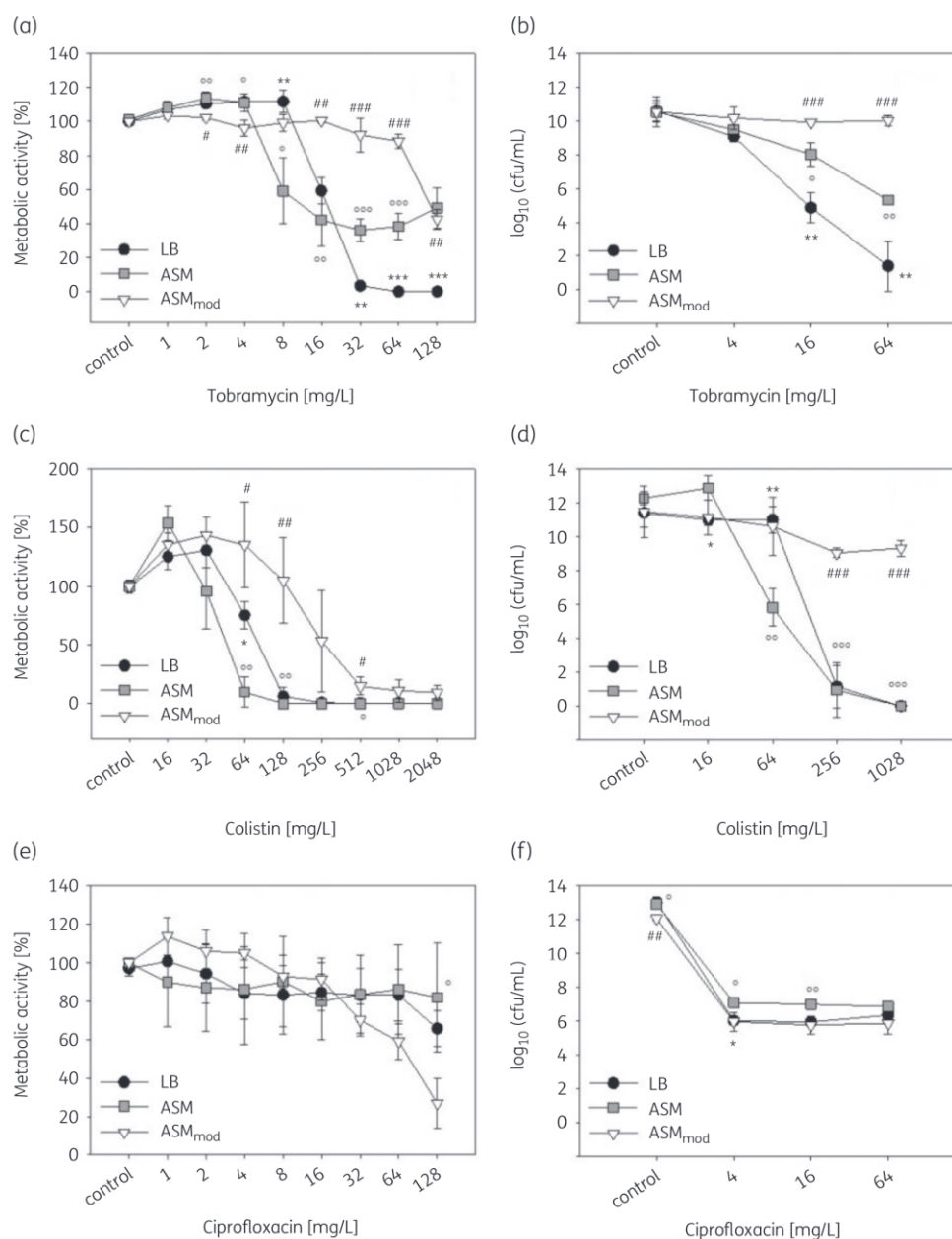


**Figure 4.** Antibiotic activity against 72 h PAO1 biofilms in various test media. Presto Blue™ assays (a, c, e) and cfu analysis (b, d, f) of 72 h PAO1 in LB (circles), ASM (squares) and ASM<sub>mod</sub> (triangles) after 24 h treatment with tobramycin (a, b), colistin (c, d) or ciprofloxacin (e, f). Metabolic activity [%] or log<sub>10</sub> (cfu/mL) are plotted against antibiotic concentration [mg/L]. Significance between groups is indicated by asterisks (LB versus ASM), hashes (LB versus ASM<sub>mod</sub>) and circles (ASM versus ASM<sub>mod</sub>). N = 3 with n = 9.

Frisch et al.

**Table 2.** Tobramycin efficacy against PAO1 biofilms—mucus control experiment

Condition	Log <sub>10</sub> cfu/mL (mean±SD)			
	LB	ASM	ASM <sub>mod</sub>	Mucus
Control	10.59 ± 0.65	10.53 ± 0.52	10.55 ± 0.91	11.67 ± 1.45
Tobramycin 64 mg/L	1.41 ± 1.48 <sup>a, b, c</sup>	5.33 ± 0.04 <sup>a, d, e</sup>	10.04 ± 0.30 <sup>b, d</sup>	9.32 ± 0.29 <sup>c, e</sup>

PAO1 (72 h biofilm) survival in different media (LB, ASM, ASM<sub>mod</sub>, freeze-dried, resuspended mucus) after 24 h treatment with 64 mg/L tobramycin. As a control, PBS mixed with LB was used. *N* = 3 with *n* = 9. Significant difference between the groups (*P* ≤ 0.001) is indicated as:

<sup>a</sup>LB versus ASM, significant difference between groups (*P* ≤ 0.001).

<sup>b</sup>LB versus ASM<sub>mod</sub>, significant difference between groups (*P* ≤ 0.001).

<sup>c</sup>LB versus mucus, significant difference between groups (*P* ≤ 0.001).

<sup>d</sup>ASM versus ASM<sub>mod</sub>, significant difference between groups (*P* ≤ 0.001).

<sup>e</sup>ASM versus mucus, significant difference between groups (*P* ≤ 0.001).

*P. aeruginosa* biofilms contributes to sub-inhibitory concentrations reaching the targets and consequently leads to the higher tolerance of biofilms.<sup>39</sup>

### Conclusions

Our findings underline the importance of the medium when testing anti-infectives against mucosal biofilms, and ASM<sub>mod</sub> appears to be a useful alternative for an *in vitro* simulation of such infections, especially with *P. aeruginosa*. So far, our model covers the formation of mature biofilms and the mucus-like environment in which these are embedded. Despite the limited access to human pulmonary mucus, experiments with native mucus should not be entirely replaced. ASM<sub>mod</sub>, however, enables exploratory studies to be conducted at a much higher throughput to screen for novel compounds or delivery systems and takes the viscoelastic properties of mucus into account, making this medium more biosimilar. Finally, our results suggest that it is not only mucus rheology that is of high importance, but also its molecular interactions with antibiotics, which may influence their permeation.

### Acknowledgements

We would like to acknowledge the excellent technical support of Dr Chiara de Rossi and Pascal Paul. We further thank Prof Dr John Perry, Newcastle University, for providing *Mycobacterium abscessus* smooth variant, isolated from the sputum of CF patients.

### Funding

This work was supported by the Helmholtz Institute for Pharmaceutical Research Saarland. Further funding was received from the Bundesministerium für Bildung und Forschung (BMBF) - ANTI-TB project under grant agreement GWANTA 20.

### Transparency declarations

None to declare.

### Supplementary data

Extended Methods, Table S1 and Figures S1 to S4 are available as [Supplementary data](#) at JAC Online.

### References

- Murgia X, Loretz B, Hartwig O et al. The role of mucus on drug transport and its potential to affect therapeutic outcomes. *Adv Drug Deliv Rev* 2018; **124**: 82–97.
- Lyczak JB, Cannon CL, Pier GB. Lung Infections Associated with Cystic Fibrosis. *Cmr* 2002; **15**: 194–222.
- Ratjen F, Bell SC, Rowe SM et al. Cystic fibrosis. *Nat Rev Dis Primers* 2015; **1**: 15010.
- Hall CW, Mah T-F. Molecular mechanisms of biofilm-based antibiotic resistance and tolerance in pathogenic bacteria. *FEMS Microbiol Rev* 2017; **41**: 276–301.
- Moreau-Marquis S, Stanton BA, O'Toole GA. *Pseudomonas aeruginosa* biofilm formation in the cystic fibrosis airway. *Pulm Pharmacol Ther* 2008; **21**: 595–9.
- Boegh M, Nielsen HM. Mucus as a barrier to drug delivery – understanding and mimicking the barrier properties. *Basic Clin Pharmacol Toxicol* 2015; **116**: 179–86.
- Bansil R, Turner BS. Mucin structure, aggregation, physiological functions and biomedical applications. *Curr Opin Colloid Interface Sci* 2006; **11**: 164–70.
- Rubin BK, Ramirez O, Zayas JG et al. Collection and analysis of respiratory mucus from subjects without lung disease. *Am Rev Respir Dis* 1990; **141**: 1040–3.
- Murgia X, Yasar H, Carvalho-Wodarz C et al. Modelling the bronchial barrier in pulmonary drug delivery: a human bronchial epithelial cell line supplemented with human tracheal mucus. *Eur J Pharm Biopharm* 2017; **118**: 79–88.
- Schuster BS, Suk JS, Woodworth GF et al. Nanoparticle diffusion in respiratory mucus from humans without lung disease. *Biomaterials* 2013; **34**: 3439–46.
- Perez-Vilar J, Hill RL. The structure and assembly of secreted mucins. *J Biol Chem* 1999; **274**: 31751–4.
- Lai SK, Wang Y-Y, Wirtz D et al. Micro- and macrorheology of mucus. *Adv Drug Deliv Rev* 2009; **61**: 86–100.
- Murgia X, Pawelzyk P, Schaefer UF et al. Size-limited penetration of nanoparticles into porcine respiratory mucus after aerosol deposition. *Biomacromolecules* 2016; **17**: 1536–42.

- 14 Lock JY, Carlson T, Carrier RL. Mucus models to evaluate the diffusion of drugs and particles. *Adv Drug Deliv Rev* 2017; **124**: 34–49.
- 15 Müller L, Murgia X, Siebenbürger L et al. Human airway mucus alters susceptibility of *Pseudomonas aeruginosa* biofilms to tobramycin, but not colistin. *J Antimicrob Chemother* 2018; **73**: 2762–9.
- 16 Ho D-K, Frisch S, Biehl A et al. Farnesylated glycol chitosan as a platform for drug delivery: synthesis, characterization, and investigation of mucus-particle interactions. *Biomacromolecules* 2018; **19**: 3489–501.
- 17 Diraviam Dinesh S. Artificial Sputum Medium. *Protocol Exchange* 2010. <https://protocols.scienceexchange.com/protocols/artificial-sputum-medium>.
- 18 Porsio B, Cusimano MG, Schillaci D et al. Nano into micro formulations of tobramycin for the treatment of *Pseudomonas aeruginosa* infections in cystic fibrosis. *Biomacromolecules* 2017; **18**: 3924–35.
- 19 Tran T-T, Yu H, Vidailac C et al. An evaluation of inhaled antibiotic liposome versus antibiotic nanoplex in controlling infection in bronchiectasis. *Int J Pharm* 2019; **559**: 382–92.
- 20 Boegh M, Baldursdóttir SG, Müllertz A et al. Property profiling of biosimilar mucus in a novel mucus-containing in vitro model for assessment of intestinal drug absorption. *Eur J Pharm Biopharm* 2014; **87**: 227–35.
- 21 Huck BC, Hartwig O, Biehl A et al. Macro- and microrheological properties of mucus surrogates in comparison to native intestinal and pulmonary mucus. *Biomacromolecules* 2019; **20**: 3504–12.
- 22 Palmer KL, Mashburn LM, Singh PK et al. Cystic fibrosis sputum supports growth and cues key aspects of *Pseudomonas aeruginosa* Physiology. *J Bacteriol* 2005; **187**: 5267–77.
- 23 Kirchner S, Fothergill JL, Wright EA et al. Use of artificial sputum medium to test antibiotic efficacy against *Pseudomonas aeruginosa* in conditions more relevant to the cystic fibrosis lung. *J Vis Exp* 2012; **64**: 3857.
- 24 Moradali MF, Ghods S, Rehm BHA. *Pseudomonas aeruginosa* lifestyle: a paradigm for adaptation, survival, and persistence. *Front Cell Infect Microbiol* 2017; **7**: 39.
- 25 Pang Z, Raudonis R, Glick BR et al. Antibiotic resistance in *Pseudomonas aeruginosa*: mechanisms and alternative therapeutic strategies. *Biotechnol Adv* 2019; **37**: 177–92.
- 26 Diaz Iglesias Y, Wilms T, Vanbever R et al. Activity of antibiotics against *Staphylococcus aureus* in an in vitro model of biofilms in the context of cystic fibrosis: influence of the culture medium. *Antimicrob Agents Chemother* 2019; **63**: e00602-19.
- 27 Hunt-Serracin AC, Parks BJ, Boll J et al. *Mycobacterium abscessus* cells have altered antibiotic tolerance and surface glycolipids in artificial cystic fibrosis sputum medium. *Antimicrob Agents Chemother* 2019; **63**: e02488-18.
- 28 Sriramulu DD, Lünsdorf H, Lam JS et al. Microcolony formation: a novel biofilm model of *Pseudomonas aeruginosa* for the cystic fibrosis lung. *J Med Microbiol* 2005; **54**: 667–76.
- 29 Bjarnsholt T, Jensen PØ, Fiandaca MJ et al. *Pseudomonas aeruginosa* biofilms in the respiratory tract of cystic fibrosis patients. *Pediatr Pulmonol* 2009; **44**: 547–58.
- 30 Worlitzsch D, Tarran R, Ulrich M et al. Effects of reduced mucus oxygen concentration in airway *Pseudomonas* infections of cystic fibrosis patients. *J Clin Invest* 2002; **109**: 317–25.
- 31 Bhat PG, Flanagan DR, Donovan MD. Drug diffusion through cystic fibrotic mucus: steady-state permeation, rheologic properties, and glycoprotein morphology. *J Pharm Sci* 1996; **85**: 624–30.
- 32 Lieleg O, Ribbeck K. Biological hydrogels as selective diffusion barriers. *Trends Cell Biol* 2011; **21**: 543–51.
- 33 Louie A, Liu W, Fikes S et al. Impact of meropenem in combination with tobramycin in a murine model of *Pseudomonas aeruginosa* pneumonia. *Antimicrob Agents Chemother* 2013; **57**: 2788–92.
- 34 Walkty A, DeCorby M, Nichol K et al. In vitro activity of colistin (Polymyxin E) against 3,480 isolates of gram-negative bacilli obtained from patients in Canadian Hospitals in the CANWARD Study, 2007–2008. *Antimicrob Agents Chemother* 2009; **53**: 4924–6.
- 35 Brazas MD, Hancock R. Ciprofloxacin induction of a susceptibility determinant in *Pseudomonas aeruginosa*. *Antimicrob Agents Chemother* 2005; **49**: 3222–7.
- 36 Højby N. Understanding bacterial biofilms in patients with cystic fibrosis: current and innovative approaches to potential therapies. *J Cyst Fibros* 2002; **1**: 249–54.
- 37 Bos AC, Passé KM, Mouton JW et al. The fate of inhaled antibiotics after deposition in cystic fibrosis: how to get drug to the bug? *J Cyst Fibros* 2017; **16**: 13–23.
- 38 Wheeler KM, Cárcamo-Oyarce G, Turner BS et al. Mucin glycans attenuate the virulence of *Pseudomonas aeruginosa* in infection. *Nat Microbiol* 2019; **4**: 2146–54.
- 39 Morita Y, Tomida J, Kawamura Y. Responses of *Pseudomonas aeruginosa* to antimicrobials. *Front Microbiol* 2014; **4**: 422.

## SUPPLEMENTARY DATA

### MATERIALS AND METHODS (expanded)

#### *Mucus samples*

Native human pulmonary mucus, non-related to pulmonary diseases, was obtained from the endotracheal tubes of patients undergoing elective surgery (Klinikum Saarbrücken GmbH) according to the protocol approved by the Ethics Commission of the Chamber of Medicine Doctors of the Saarland (file number 19/15). In brief, endotracheal tubes were cut (5-10 cm) and transferred to 50 mL falcons for centrifugation (30 s at 140 x g, twice). The mucus was extracted and transferred to 2 mL Eppendorf tubes with samples showing visible blood contamination being excluded. Mucus samples were stored at - 20 °C and thawed overnight at 4 °C before use. Native mucus was used for antibiotic transport studies; for the use as a bacterial medium, so-called mucus discs were prepared as described previously (Murgia *et al.* 2017, Müller *et al.* 2018). Therefore, mucus samples were weighed with 40-60 mg per disc and frozen for a minimum of 2 h at - 80 °C. After freeze-drying overnight (Alpha 2-4 LSC from Christ and vacuum pump from Pfeiffer, Germany), sterilization was conducted via 1 h of UV radiation. Samples were transferred to a sterile petri dish and stored dry at room temperature. Before experimental use, 2-3 discs were resuspended in the corresponding volume of sterile PBS (1x PBS, pH 7.4, Sigma-Aldrich, Germany) in a 96 well plate for a total volume of 100 µL.

#### *Preparation of mucus surrogates*

The preparation of artificial sputum medium (ASM) and its modified version (ASM<sub>mod</sub>) was conducted as described before (Dinesh 2010; Huck *et al.* 2019). For 50 mL, 250 mg mucin from porcine stomach, 200 mg low molecular-weight salmon sperm DNA, 250 mg NaCl, 110 mg KCl, 90.5 mg Trizma base, and 250 mg casamino acids from casein hydrolysate (all from Sigma-Aldrich, Germany) were dissolved in 40 mL ultra-pure water (Milli-Q<sup>®</sup>, Advantage

A10, Merck Millipore, Germany). When solubilized, 0.15 M diethylenetriaminepentaacetic acid (DTPA, Sigma-Aldrich, Germany) was added, and media were stirred for 2-3 h at 600 rpm. ASM<sub>mod</sub> was additionally supplemented with 0.9 % (w/v) Carbopol (Poly(acrylic)acid, PAA, Lubrizol, UK), and both media were stirred overnight at 600 rpm. After adjusted to pH 7 using 1 M Trizma base, the volume was filled up to 50 mL with ultra-pure water, and the surrogates were autoclaved for 20 min at 121 °C. When cooled down, egg yolk emulsion (Oxoid, UK) was sterile filtered (Minisart<sup>®</sup>, Sartorius Stedium, pore size 0.2 µm, Germany) and 250 µL were added to ASM as well as ASM<sub>mod</sub>. The media were stored at 4 °C and could be used for up to one month.

### ***Bulk rheology***

Bulk rheology of ASM<sub>mod</sub> was determined by a Discovery HR-2 Hybrid Rheometer (Waters/TA Instruments, USA) with Smart Swap<sup>™</sup> Peltier Plate geometry (diameter: 20 mm, cone angle: 1 °). After placing 100 µL of ASM<sub>mod</sub> between the measuring units, frequency sweep experiments in a range of 0.1 to 100 rad/s were performed at 25 °C. The elastic ( $G'$ ) and viscous ( $G''$ ) moduli were determined before and after sterilization to show that this process does not change the viscoelastic properties of the medium.

### ***Bacteria strains and cultivation***

*Pseudomonas aeruginosa*. The followings strains were used in this work: *P. aeruginosa* PAO1 (ATCC 1562) and PAO1-GFP (ATCC 15692GFP). Overnight cultures were prepared by incubating a single bacteria colony in Luria-Bertani (LB) broth (Sigma-Aldrich, Germany). For PAO1-GFP cultures, the LB medium was supplemented with 300 mg/L Ampicillin sodium salt (Carl Roth, Germany). Bacteria were grown overnight at 37 °C at 180 rpm.

*Staphylococcus aureus*. The strain *S. aureus* Newman (SA Newman, ATCC 25904) was used and cultured in brain heart infusion (BHI) broth (BD, USA) for overnight cultures, which were prepared and incubated as described for *P. aeruginosa*.

*Mycobacterium abscessus*. *M. abscessus* smooth variants were isolated from CF patients' sputum and kindly provided by Prof. Dr. John Perry, Newcastle University. Prior to experiments, the bacteria obtained from single colonies were cultured for 72 h in 7H9 medium (Sigma-Aldrich, Germany), supplemented with 10 % (v/v) Middlebrook OADC Enrichment (BD, USA). Bacteria cultures were centrifuged (10 min, 2000 x g) and the pellet resuspended in 1 mL PBS, together with glass beads (2.5-3.5 mm, VWR chemical), to disrupt the bacteria clumps. After 15 min vortexing, 9 mL 7H9 were added and centrifuged again (5 min, 300 x g). The supernatant was used for biofilm preparation.

### ***Bacteria growth experiments***

Bacterial growth was investigated via colony-forming units (cfu) experiments. In brief, 96 well plates were filled with 100  $\mu$ L medium, using the respective standard medium (LB, BHI, 7H9), ASM, or ASM<sub>mod</sub>. Bacterial overnight cultures of PAO1, SA Newman or *M. abscessus* were diluted and added in a small volume (5-10  $\mu$ L) to the medium to achieve a final OD of 0.01 for PAO1(-GFP) and *M. abscessus* ( $\sim 10^7$  cfu/mL) or an OD of 0.001 ( $\sim 10^6$  cfu/mL) for SA Newman. The outer rim was filled with 200  $\mu$ L water or PBS and wet tissues were placed next to the plates to prevent dry-out. For these experiments, no washing step was added, to avoid disturb the biofilms. Only in the final time point after 72 h incubation at 37 °C, 100  $\mu$ L PBS were added to each well containing the biofilm cultures and resuspended by pipetting up and down to disperse the biofilm for further plating. The content was transferred to 2 mL Eppendorf tubes and vortexed for 10-15 min at medium speed to completely disrupt the biofilm. The bacterial number was furthermore determined via serial dilution in PBS/Tween80 (0.05 %) and plating on agar (LB, BHI, 7H9). The cfu were counted after overnight incubation at 30 °C for PAO1(-GFP) and SA Newman; *M. abscessus* was incubated for 72 h at 37 °C.

### ***Confocal microscopy***

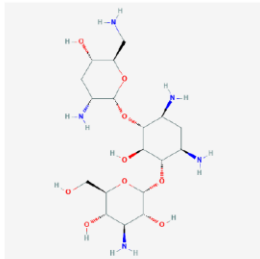
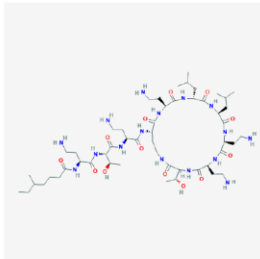
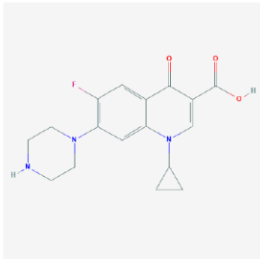
To compare the morphology and biofilm formation of bacteria in different media, confocal laser scanning microscopy (CLSM) was used. PAO1-GFP was cultivated in an 8-well chambered coverglass system (155411, Thermo Scientific, USA) in a total volume of 200  $\mu$ L LB, ASM, ASM<sub>mod</sub> or resuspended mucus. Starting with an OD of 0.01 ( $\sim 10^7$  cfu/mL), the slides were incubated at 37 °C and images were taken after 72 h incubation. Live imaging of bacteria was performed using a DMI8 inverted microscope and a TCS SP 8 confocal laser scanning unit with an AOBS beam splitter and a Leica HyD detector (Leica, Germany). For excitation, an argon laser (4 %) was used at 476 nm, emission was detected at a wavelength of 580 nm. 200-plane z-stacks were acquired at a resolution of 1024x1024 and a speed of 400 Hz, using a Fluotar VIZIR 24x/0.95 water objective.

### ***Antibiotics***

Three antibiotics with different physico-chemical properties were used for transport studies and antibiotic activity assays: Tobramycin (Sigma-Aldrich, Germany), Colistin sulfate (Adipogen, Switzerland), and Ciprofloxacin or Ciprofloxacin-Hydrochloride (both Sigma-Aldrich, Germany). Ciprofloxacin was used for transport studies, while better soluble Ciprofloxacin-Hydrochloride was used for antibiotic activity tests to achieve high stock concentrations in water, which were in a next step diluted in PBS to a concentration of 512 mg/L (for a final treatment concentration of 128 mg/L). Some essential characteristics of the used antibiotics are given in Table S1.



Table S1: Biochemical characteristics (chemical formula (PubChem), molecular weight (g/mol), solubility (g/L), and classification) of the tested antibiotics Tobramycin, Colistin and Ciprofloxacin.

	<b>Tobramycin</b>	<b>Colistin</b>	<b>Ciprofloxacin</b>
<b><i>Chemical formula</i></b>			
<b><i>Molecular weight</i></b>	467.52 g/mol	1155.43 g/mol	331.35 g/mol
<b><i>Solubility</i></b>	53.7 g/L	0.238 g/L	1.35 g/L
		50 g/L for Colistin sulfate	30 g/L for Ciprofloxacin HCl
<b><i>Classification</i></b>	Aminoglycoside	Peptide antibiotic	Fluoroquinolone

### ***Transport studies***

Transport studies were performed in 24 well plates with transwell<sup>®</sup> inserts with a surface of 0.33 cm<sup>2</sup> and a pore size of 0.4 μm (3470, Corning, USA), which divide the system to a basolateral and an apical compartment. Figure 3a shows the schematic experimental setup. To obtain the actual mass of mucus and ASM<sub>mod</sub>, transwells were weighed before and after 100 μL of mucus or ASM<sub>mod</sub> were added to the membrane. Therefore, the exact amount in the apical compartment could be determined and a corresponding correction factor was applied to the results after analysis. For experiments, the basolateral chamber was filled with 600 μL pre-warmed PBS. Stock solutions of antibiotics in PBS (600 mg/L for Tobramycin and Colistin sulfate, 100 mg/L for less soluble Ciprofloxacin) were added to the apical compartment. The well plates were incubated at 37 °C during the study and samples of 100 μL were taken after 0, 15 and 30 min as well as 1, 2, 4 and 24 h and replaced with 100 μL fresh PBS, respectively. As a control, 100 μL PBS, replacing mucus or ASM<sub>mod</sub>, were added to the apical compartment, indicating diffusion only hindered by the transwell filter membrane.

### ***Antibiotic quantification***

*Tobramycin.* For LC-MS analysis, a Dionex UltiMate 3000 Binary Rapid Separation LC System (Thermo Scientific, USA) coupled with a TSQ Quantum Access Max (QQQ, Thermo Scientific, USA) was used. The analytical column was a Zorbax Eclipse xdb C-18 column (5 μm, 50\*4,6 mm, Agilent, USA) with C18 guard column. As mobile phase acetonitrile (eluent A) and water (eluent B), each supplemented with 0.1 % trifluoroacetic acid, 0.1 % heptafluorobutyric acid and 0.1 % pentafluoro propionic acid, were used. Samples were run with a flow of 0.7 mL/min at 40 °C, using a gradient of eluents A and B, starting with a ratio of 20:80 in the first minute. From 1 to 3.5 min, the ratio changed to 70:30 and was restored to 20:80 between 3.5 and 4.5 min. 3 μL of the samples were injected and Tobramycin was

quantified by electro spray ionization (ESI+) and the selected reaction monitoring of the ion with the  $m/z$  ratio 468.184  $\rightarrow$  323.960. For quantification, the area under the curve was used.

*Colistin*. For Colistin quantification, an Ultimate 3000 HPLC with diode array detector, autosampler and pump (Thermo Scientific, USA) was used. As stationary phase, a Synchronis C18 (1.7  $\mu\text{m}$ , 50\*2.1 mm, Thermo Fisher, USA) and additional guard column Synchronis C18 (2.1  $\mu\text{m}$ , 10\*2.1 mm, Thermo Fisher, USA) were used at 40 °C. For the mobile phase, acetonitrile and 30 mM  $\text{Na}_2\text{SO}_4$  buffer (pH 2.4) were used. With an isocratic ratio of 22:78, respectively, the run time amounted to 5 min per sample with an injection volume of 25  $\mu\text{L}$  and a flow of 0.6 mL/min. Colistin was detected at a wavelength of 215 nm. For quantification, the area under the peak (Colistin A + Colistin B) was used.

*Ciprofloxacin*. Samples were measured by fluorescence intensity with a Plate Reader (Infinite M200 Pro, Tecan, Austria) at wavelengths of 330 nm for extinction and 430 nm for emission. PBS was used as a blank.

### ***Antibiotic activity***

*Antibiotic treatment*. To assess the activity of antibiotics, 72 h PAO1 biofilms were cultivated in different media (LB, ASM, ASM<sub>mod</sub>) as described above. For Tobramycin and Colistin 4x concentrated stocks (512 mg/L and 8192 mg/L, respectively) were prepared in PBS and sterile filtered. Due to the low solubility of Ciprofloxacin in PBS, a stock of Ciprofloxacin Hydrochloride was prepared in ultra-pure water (2048 mg/L), sterile filtered and diluted in 1:4 sterile PBS, reaching 4x of the final concentration (512 mg/L for treatment concentration of 128 mg/L). 100  $\mu\text{L}$  of the antibiotic solutions were diluted 1:1 in LB medium, followed by a serial dilution. Without mixing, 100  $\mu\text{L}$  of different concentrations (2x) of the respective antibiotic solutions were transferred to 72 h PAO1 biofilms. The procedure was the same for the treatment of planktonic cultures, using 100  $\mu\text{L}$  PAO1 (OD 0.01,  $\sim 10^7$  cfu/mL) in LB

medium instead. As an untreated control, 100  $\mu$ L of antibiotic-free PBS 1:1 mixed with LB were used. 96 well plates were incubated for 24 h at 37 °C without shaking.

*Presto Blue<sup>TM</sup> assays:* The viability of planktonic bacteria as well as 72-h biofilms after 24 h antibiotic treatment was assessed via Presto Blue<sup>TM</sup> assays. Therefore, 10 % (v/v) Presto Blue<sup>TM</sup> (Invitrogen, USA) were added to each well with the blue dye turning pink due to a reduction of resazurin by metabolically active bacteria. The well plates were incubated for 30-60 min at 37 °C and 300 rpm; for samples in ASM<sub>mod</sub> incubation time was prolonged up to 120 min until the dye was visibly equally distributed in the viscoelastic medium. The OD was measured at 570 and 600 nm, the difference between both values was calculated and values were normalized to the mean of the untreated control to obtain the percentage of metabolic activity.

*cfu analysis.* cfu experiments were performed for selected concentrations obtained from Presto Blue<sup>TM</sup> assays of 72 h PAO1 biofilms to determine the bacterial number after treatment in different media. cfu plating and analysis were performed as described above.

*Mucus control.* As a control experiment, 100  $\mu$ L of freeze-dried mucus, resuspended in PBS, were infected with PAO1 (final OD 0.01,  $\sim 10^7$  cfu/mL). After 72 h incubation at 37 °C, the biofilm was treated with 64 mg/L Tobramycin; as untreated control, PBS mixed 1:1 with LB was used. After 24 h incubation at 37 °C, cfu experiments were performed as described above.

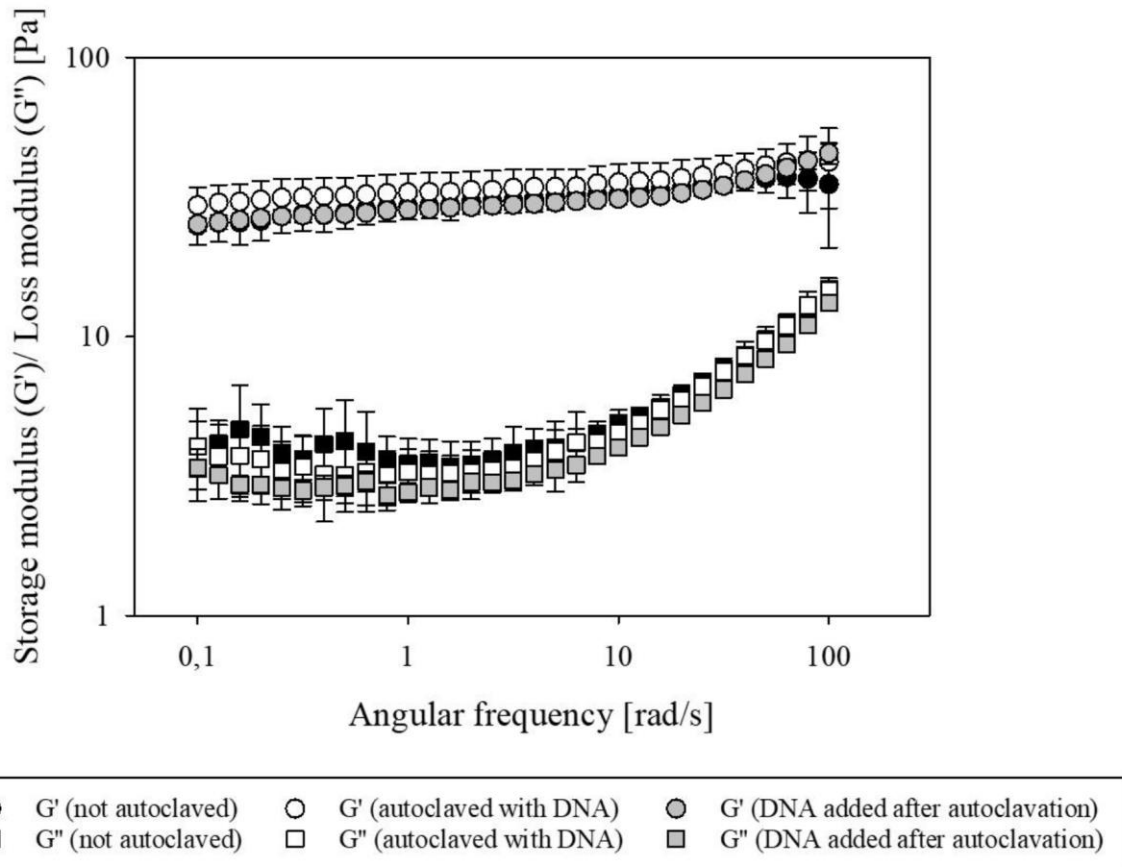
### ***Statistical analysis***

For each experiment, at least three independent runs (N=3) with triplicates or duplicates (mucus control experiments) (n>6) were performed. The statistical analysis was conducted using SigmaPlot (SigmaPlot 14, Systat Software Inc.) with One Way ANOVA followed by the Tukey test. Statistical difference was considered significant for  $p < 0.05$  and is indicated by asterisks (\*), hashes (#) or circles (°) with significance level \*/#/° $p < 0.05$ , \*\*/##/°° $p < 0.01$  and \*\*\*/###/°°° $p < 0.001$ , respectively.

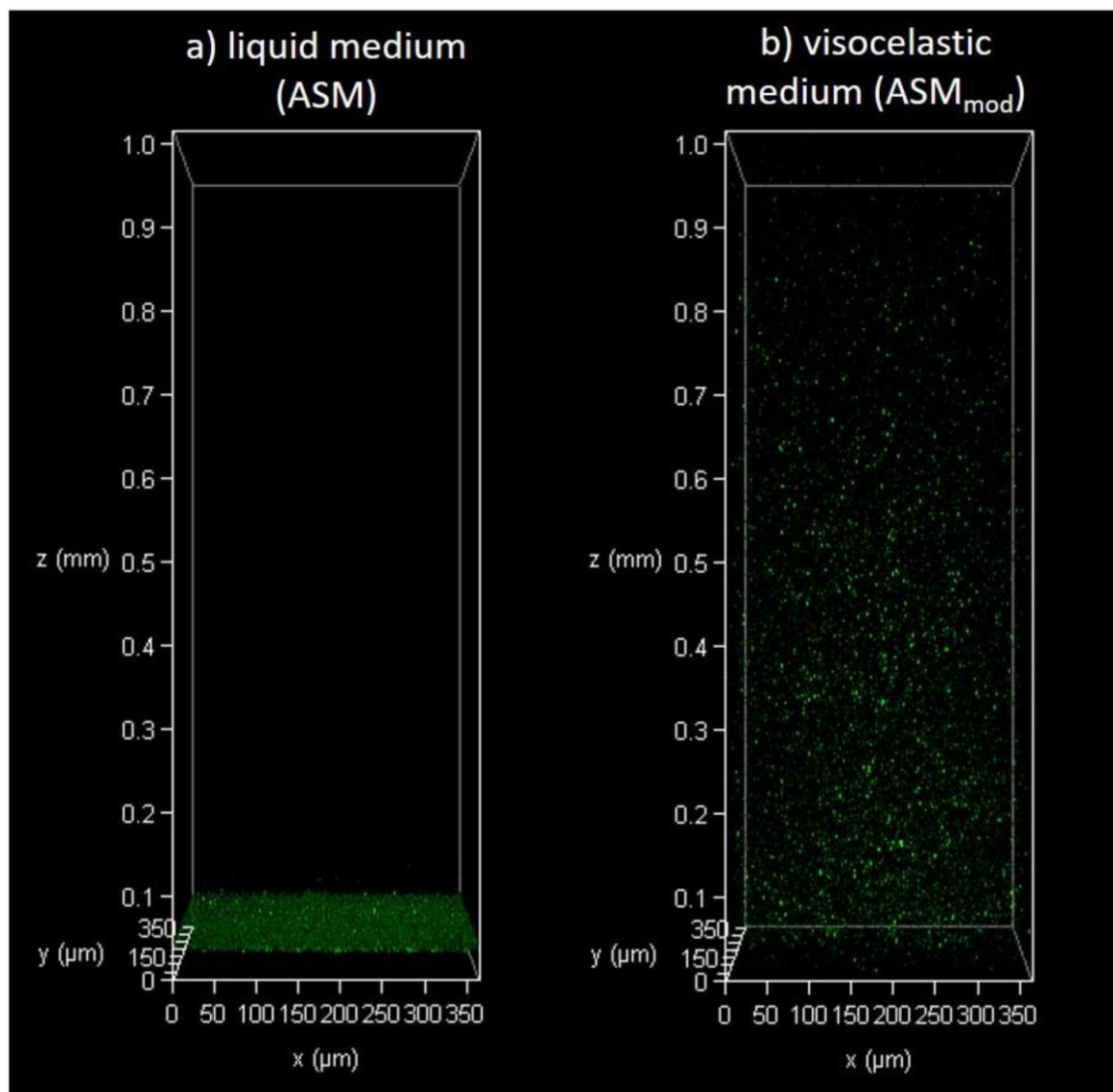
## RESULTS (supplementary)

### *ASM<sub>mod</sub> rheology*

A comparable rheological profile of ASM<sub>mod</sub> and human native tracheal mucus was shown by Huck *et al.* (2019). However, for the growth of bacteria, the ASM<sub>mod</sub> must be sterile. The standard procedure to sterilize bacteria medium is via autoclavation, 20 min, 121 °C. To ensure that this process does not affect the rheological properties of ASM<sub>mod</sub>, we performed frequency sweep experiments in a range of 0.1 to 100 rad/s. Additionally, the rheology of ASM<sub>mod</sub> with subsequently added DNA (after autoclaving) was investigated. As shown in Figure S1, an elastic-dominant profile ( $G' > G''$ ) was observed for all conditions.



**Figure S1:** Rheology of  $ASM_{mod}$  determined by frequency sweep experiments before (black) and after autoclaving (white). Additionally, the rheology of  $ASM_{mod}$  with subsequently added DNA (after autoclaving) was determined (grey). Storage modulus ( $G'$ ) and loss modulus ( $G''$ ) [Pa] are shown in a frequency range of 0.1 to 100 rad/s (log scale). With  $G' > G''$  an elastic dominant behaviour can be observed for all conditions.  $N > 3$  with  $n > 9$

*Additional confocal images of PAO1-GFP in different media*

**Figure S2:** Additional three-dimensional confocal images of PAO1-GFP after 72 h incubation in a liquid medium (ASM) (a) or a viscoelastic medium (ASM<sub>mod</sub>) (b). Wide z-stack of 1 mm are shown from front view to demonstrate different distribution of bacteria in a liquid or viscoelastic medium.

*Antibiotic transport studies - normalization*

For a better comparison of permeation profiles of the three tested drugs – Tobramycin, Colistin and Ciprofloxacin – a normalisation to the respective control experiment (PBS) was conducted after an incubation time of 4 h and 24 h. Therefore, the data obtained for the diffusion through mucus and ASM<sub>mod</sub> was normalized to the mean of the respective PBS control for all antibiotics. Figure S3 shows the percentage of permeation (%) after 4 h (Figure S3a) incubation and after 24 h (Figure S3b).

A clear trend can be observed regarding the permeability of the drugs: Ciprofloxacin shows highest percentage of permeation, followed by Tobramycin and only comparably low drug diffusion through mucus and ASM<sub>mod</sub> was detected for Colistin. In general, the total percentage of permeation is higher for mucus than for the surrogate. After 4 h, the values are still in a comparable range. However, after 24 h drug diffusion through mucus is clearly higher, especially for Colistin. The peptide antibiotic shows almost no penetration though ASM<sub>mod</sub>, which might explain the high tolerance of PAO1 biofilms cultured in this substrate.



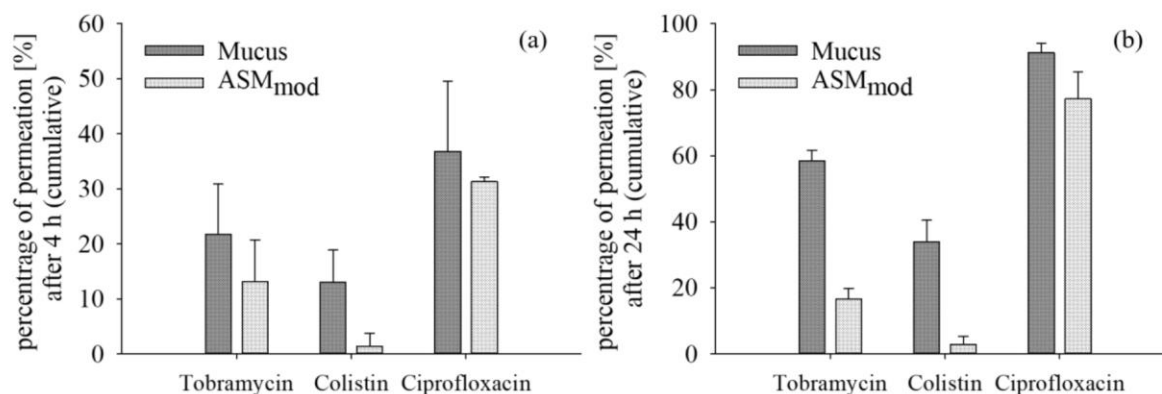


**Figure S3:** Normalized data for transport studies of Tobramycin, Colistin and Ciprofloxacin through native mucus and ASM<sub>mod</sub>, PBS was used as control. The cumulative mass [ $\mu\text{g}$ ] was normalized to the calculated mass of the initial concentration [ $\mu\text{g}$ ]; the percentage of permeation [%] was further normalized to the mean percentage of the respective PBS control after 4 h (a) and 24 h (b). N=3 with n>8.

#### Minimal metabolic inhibiting concentration of planktonic PAO1 (Presto Blue™ assays)

For better comparability, Presto Blue™ assays were performed using planktonic PAO1 (start OD 0.01,  $\sim 10^7$  cfu/mL) after 24 h antibiotic treatment. A metabolic activity of planktonic bacteria below 10 % was considered as inhibition and the following concentrations were determined: 8 mg/L for Tobramycin and Colistin and 0.5 mg/L for Ciprofloxacin (Figure S4).

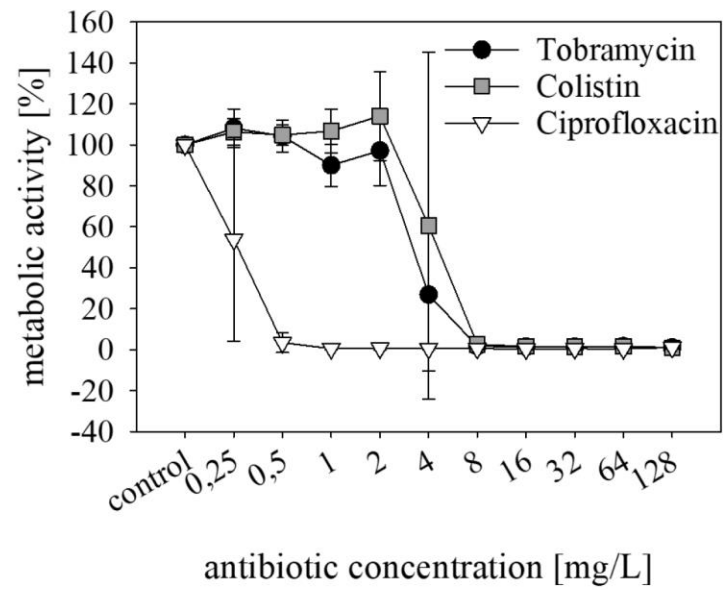


**Figure S4:** Presto Blue™ assays were performed for minimal metabolic inhibiting concentration of planktonic PAO1 (OD 0.01,  $\sim 10^7$  cfu/mL) in standard LB medium after 24 h treatment with Tobramycin (circles), Colistin (squares) or Ciprofloxacin (triangles). Metabolic activity [%] is plotted against antibiotic concentration [mg/L]. N=2 with n=6.

### **5.3 Systematic Analysis of Composition and Performance of Pulmonary Surfactant Preparations on Cellular Uptake and Cytotoxicity of Aerosolized Nanomaterials**

**Benedikt Huck**§, Alberto Hidalgo§\*, Franziska Waldow, Dominik Schwudke, Karoline I. Gaede, Claus Feldmann, Patrick Carius, Chiara Autilio, Jesus Perez-Gil, Konrad Schwarzkopf, Xabier Murgia, Brigitta Loretz and Claus-Michael Lehr\*

Benedikt Huck, Patrick Carius, Helmholtz Center for Infection Research, Helmholtz Institute for Pharmaceutical Research Saarland, Department of Drug Delivery. Department of Pharmacy, Saarland University, Campus E8 1, 66123 Saarbrücken, Germany.

Dr. Alberto Hidalgo<sup>\*</sup>, Dr. Brigitta Loretz, Helmholtz Center for Infection Research, Helmholtz Institute for Pharmaceutical Research Saarland, Department of Drug Delivery. Saarland University, Campus E8.1, 66123 Saarbrücken, Germany. E-Mail: alberto.hidalgo@helmholtz-hips.de

Dr. Franziska Waldow, Dr. Dominik Schwudke, Research Center Borstel, Leibniz Lung Center, Parkallee 1-40, 23845 Borstel, Germany; German Center for Infection Research, Thematic Translational Unit Tuberculosis, Partner Site Hamburg-Lübeck-Borstel-Riems, Borstel, Germany. German Center for Lung Research (DZL), Airway Research Center North (ARCN), Research Center Borstel, Leibniz Lung Center, Borstel, Germany.

Dr. Karoline Gaede, BioMaterialBank Nord, Research Center Borstel, Leibniz Lung Center, Parkallee 35, 23845 Borstel, Germany. German Center for Lung Research (DZL), Airway Research Center North (ARCN), Research Center Borstel, Leibniz Lung Center, Borstel, Germany.

Prof. Claus Feldmann, Institute of Inorganic Chemistry, Karlsruhe Institute of Technology, 76131 Karlsruhe, Germany.

Prof. Jesus Perez-Gil, Dr. Chiara Autilio, Department of Biochemistry and Molecular Biology, Faculty of Biology, and Research Institute “Hospital 12 de Octubre (imas12)”, Complutense University, 28040 Madrid, Spain.

Prof. Konrad Schwarzkopf, Klinikum Saarbrücken, Department of Anaesthesia and Intensive Care, 66119 Saarbrücken, Germany.

Dr. Xabier Murgia, Biotechnology Area, GAIKER Technology Centre, 48170 Zamudio, Spain.

Prof. Claus-Michael Lehr<sup>\*</sup>, Helmholtz Center for Infection Research, Helmholtz Institute for Pharmaceutical Research Saarland, Department of Drug Delivery. Saarland University, Campus E8.1, Saarbrücken, Germany. Department of Pharmacy, Saarland University, Campus E8 1, 66123 Saarbrücken, Germany. E-Mail: claus-michael.lehr@helmholtz-hips.de

\* Corresponding author

§ Equal contribution

*Small Science*, October 2021, 1: 2100067

<https://doi.org/10.1002/smsc.202100067>

# Systematic Analysis of Composition, Interfacial Performance and Effects of Pulmonary Surfactant Preparations on Cellular Uptake and Cytotoxicity of Aerosolized Nanomaterials

Benedikt Huck, Alberto Hidalgo,\* Franziska Waldow, Dominik Schwudke, Karoline I. Gaede, Claus Feldmann, Patrick Carius, Chiara Autilio, Jesus Pérez-Gil, Konrad Schwarzkopf, Xabier Murgia, Brigitta Loretz, and Claus-Michael Lehr\*


The interplay of particles with pulmonary surfactant, a lipid-protein material pivotal for lung function, is hypothesized as a key factor that has not been routinely considered in the current *in vitro* models when determining the fate of inhaled nanomaterials. To explain its influence on cellular uptake and protective effects, nanoparticles are studied on two models of alveolar cells, in the absence or presence of pulmonary surfactant. Composition and interfacial performance of native human and porcine surfactants, a commercially available bovine surfactant (Alveofact), and an artificial lung lining fluid are characterized using shotgun lipidomics and biophysical approaches (i.e., Langmuir surface balances and captive bubble surfactometry). Plain and aminofunctionalized silica nanoparticles and a novel antimycobacterial nanoformulated benzothiazinone (BTZ043) are selected as examples of neutral, positively charged and therapeutically relevant nanoparticles, respectively. They are deposited onto monocultures of human alveolar epithelial and phagocytic cell lines in the presence or absence of the surfactant preparations, modeling the alveolar milieu. Only surfactant preparations with high interfacial activity and distinctive composition mitigated the toxicity of aerosolized particles, along with a tendency of aerosolized particles to aggregate. Key requirements of surfactant preparations needed when studying interactions of nanomaterials with the pulmonary air-blood barrier *in vitro* are identified.

## 1. Introduction

With the rapid growth of nanotechnology and engineered nanomaterials, the implications of lung exposure as one of the main entry routes into the body have received increasing attention, especially the potential risks derived from exposure to engineered nanomaterials and the benefits of controlled pulmonary delivery systems.<sup>[1]</sup> The epithelium forming the respiratory surface in the lungs represents the most extensive and thinnest barrier in the body in direct contact with the external environment. Therefore, to ensure a proper lung performance while preserving the barrier integrity, the lungs have developed different cellular (e.g., immune system and epithelium) and noncellular (e.g., branched architecture, mucus, and pulmonary surfactant) mechanisms that protect the lungs from undesirable airborne matter by physicochemical entrapment and immune clearance. The branching lung geometry and mucus covering the tracheobronchial epithelium are considered the first barriers against potential airborne matter entering

the lungs by promoting their deposition, entrapment, and

B. Huck, A. Hidalgo, P. Carius, B. Loretz, C.-M. Lehr  
Helmholtz Center for Infection Research, Helmholtz Institute for  
Pharmaceutical Research Saarland, Department of Drug Delivery  
Saarland University  
Campus E8.1, 66123 Saarbrücken, Germany  
E-mail: alberto.hidalgo@helmholtz-hips.de;  
claus-michael.lehr@helmholtz-hips.de

 The ORCID identification number(s) for the author(s) of this article can be found under <https://doi.org/10.1002/smsc.202100067>.

© 2021 The Authors. Small Science published by Wiley-VCH GmbH. This is an open access article under the terms of the Creative Commons Attribution License, which permits use, distribution and reproduction in any medium, provided the original work is properly cited.

DOI: 10.1002/smsc.202100067

B. Huck, P. Carius, B. Loretz, C.-M. Lehr  
Department of Pharmacy  
Saarland University  
Campus E8 1, 66123 Saarbrücken, Germany

F. Waldow, D. Schwudke  
Research Center Borstel  
Leibniz Lung Center  
Parkallee 1-40, 23845 Borstel, Germany

F. Waldow, D. Schwudke  
German Center for Infection Research  
Thematic Translational Unit Tuberculosis  
Site Research Center Borstel  
Parkallee 1-40, 23845 Borstel, Germany

clearance.<sup>[2,3]</sup> The mucociliary escalator transports mucus out of the lungs and quite effectively removes any entrapped material deposited in the airways. In addition, pulmonary surfactant, a thin but essential lining fluid covering the whole respiratory surface,<sup>[4,5]</sup> constitutes an important barrier against airborne matter entering the lungs, especially in the alveolar region.<sup>[6]</sup>

Pulmonary surfactant is a lipid–protein complex essential for the process of breathing and is composed of  $\approx 90\%$  lipids and 10% proteins by mass, with negative zeta potentials.<sup>[7,8]</sup> The majority of lipids are phospholipids, dipalmitoylphosphatidylcholine (DPPC, PC 16:0\_16:0) being the most abundant.<sup>[9]</sup> The protein fraction counts four major proteins, two hydrophobic (surfactant protein [SP]-B and SP-C) and two hydrophilic (SP-A and SP-D). The former two are mainly involved in the interfacial performance of pulmonary surfactant, and the hydrophilic in innate immune defense.<sup>[10]</sup> Pulmonary surfactant prevents the lungs from collapsing during exhalation by reducing the surface tension of the aqueous lining fluid covering the distal airways to values below  $2 \text{ mN m}^{-1}$ , thereby minimizing the work of breathing. This is mainly due to 1) the high-ordered states supported by DPPC at the air–liquid interface under interfacial compression (expiration) and 2) the interplay of SP-B and SP-C that stabilize pulmonary surfactant components at the air–liquid interface and enable efficient interfacial spreading and readsorption to stabilize the respiratory surface.<sup>[10,11]</sup> In addition, pulmonary surfactant is the first barrier against airborne particles and microorganisms reaching distal airways or alveoli. Under this scenario, inhaled nanomaterials reaching alveoli will be covered with surfactant components, forming the so-called biomolecular corona.<sup>[12]</sup> Recent studies highlighted that the protein corona renders the particle's biological identity and, as a consequence, determines the fate and interactions at cellular as well as subcellular levels.<sup>[12–14]</sup>

Nowadays, *in vitro* models of the human lungs are commonly used to test the effects of drug compounds, particles or airborne contaminants on single cells or complex co-/multicultures of different types of lung cells.<sup>[15]</sup> *In vitro* models allow for studying the essential parameters that determine the air–blood barrier (e.g., representative cells, air–liquid culture conditions, breathing-like dynamics, etc.) in a systematic way to facilitate mechanistic and structural effects, in contrast to the complex *in vivo* scenario where one observes the overall effect without detailed knowledge or controlling contributing characteristics. Surprisingly, to the best of our knowledge, almost none of those approaches considers the presence of pulmonary surfactant and

even less contemplate which are the most suitable surfactant preparations that could potentially be used (e.g., natural or synthetic, human or animal). Particularly in cellular uptake and toxicity studies, pulmonary surfactant has been shown to have modulatory effects on the internalization of nanoparticles (NPs) into alveolar macrophages, mainly triggered by SP-A and SP-D.<sup>[16]</sup> Gasser et al. demonstrated that reactive oxygen species (ROS), inflammatory chemokine release, and apoptosis in primary blood monocyte-derived macrophages was augmented when exposed to multi-walled carbon nanotubes coated with Poractant alpha (Curosurf).<sup>[17]</sup> Similar effects were described for silica NPs coated with Bovactant (Alveofact) in an *in vitro* model of the air–blood barrier.<sup>[18]</sup> Further, the incubation of silica particles with the porcine clinical surfactant Curosurf was found to promote particle aggregation while reducing cellular internalization dramatically.<sup>[19]</sup> Such experimental studies, however, are often performed under liquid-covered conditions and upon preincubation of NPs with surfactant. Ideally, a setup that aims to investigate biological effects in an *in vivo* relevant context should consider both the presence of pulmonary surfactant already at the air–liquid interface and particle deposition on top.

Thus, this work aims to explore the role of pulmonary surfactant upon deposition of aerosolized matter on the respiratory surface and the essential features to model the alveolar lining fluid *in vitro* closer to *in vivo* scenarios. We systemically investigated the profile of different animal- and human-derived surfactant preparations based on their composition and interfacial activity and, ultimately, the relevance to include them in *in vitro* cellular models to study particle–cell interactions. Particularly, a clinically used and commercially available pulmonary surfactant (Alveofact), porcine and human pulmonary surfactant purified from bronchoalveolar lavage (BAL) fluids (BALFs) have been compared. Nevertheless, protocols to obtain human BALF require highly invasive procedures and entail several ethical concerns, making the access to human pulmonary surfactant extremely limited. Therefore, other alternative sources, such as tracheobronchial mucus or artificial surrogates, would be of high interest to emulate the alveolar lining fluid. Thus, pulmonary surfactant purified from human tracheobronchial mucus, as well as an artificial lining fluid proposed in the literature,<sup>[20]</sup> were also included. **Figure 1** shows the surfactant sources, sampling procedures, and exclusion criteria.

To study the potential influence of the different pulmonary surfactants on particle–cell interactions, plain and amino-functionalized silica NPs, a nanomaterial commercially available

K. I. Gaede  
BioMaterialBank Nord, Research Center Borstel  
Leibniz Lung Center  
Parkallee 35, 23845 Borstel, Germany

D. Schwudke, K. I. Gaede  
German Center for Lung Research (DZL), Airway Research Center North (ARCN)  
Research Center Borstel  
Leibniz Lung Center  
Site Research Center Borstel Parkallee 1-40, Borstel 23845, Germany

C. Feldmann  
Institute of Inorganic Chemistry  
Karlsruhe Institute of Technology  
76131 Karlsruhe, Germany

C. Autilio, J. Pérez-Gil  
Department of Biochemistry and Molecular Biology, Faculty of Biology, and Research Institute "Hospital 12 de Octubre (imas12)"  
Complutense University  
28040 Madrid, Spain

K. Schwarzkopf  
Klinikum Saarbrücken  
Department of Anaesthesia and Intensive Care  
66119 Saarbrücken, Germany

X. Murgia  
Biotechnology Area  
GAIKER Technology Centre  
48170 Zamudio, Spain

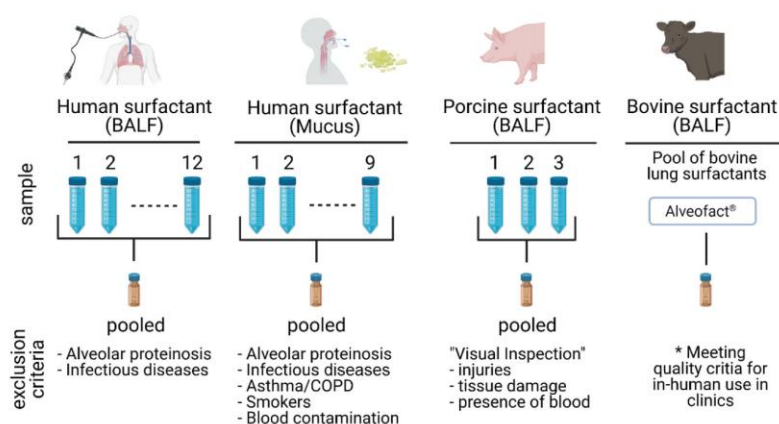


Figure 1. Surfactant sources, sampling, and exclusion criteria (Created with BioRender.com).

in high quality and frequently used to determine the interactions with biological materials, as well as a novel nanocarrier of the antimycobacterial drug benzothiazinone (BTZ043) developed for inhalation therapy, were selected as examples of neutral, positively charged and therapeutic-relevant NPs, respectively. As a proof of concept, each NP was aerosolized and deposited on separate monocultures of macrophage-like THP-1 cells and a human alveolar epithelial lentivirus-immortalized cell line (hAELVi), under air–liquid culture conditions in the presence or absence of the different pulmonary surfactant preparations. The former mimicks phagocytic cells in the lungs, while the latter represents the respiratory epithelial barrier.

## 2. Results

### 2.1. Lipid and Protein Composition

To understand and evaluate the potential use of pulmonary surfactant in human cellular *in vitro* models of the lungs, the differential lipid and protein composition of several animal- and human-derived surfactant preparations was characterized by shotgun lipidomics and western blotting.

Figure 2a,b shows that the presence of the most representative lipids are highly conserved between pulmonary surfactant samples, though the proportion varies between species and location within the lungs (i.e., upper or distal airways by means of tracheobronchial mucus or BALF, respectively). A predominance of total phosphatidylcholine (PC) is observed in all the samples, regardless the species or location. However, as shown in Figure 2c, the satPC/(unPC + polyunPC) ratio was practically inverted in Alveofact ( $\approx 30:70$ ) compared with porcine and human samples ( $\approx 60:40$ ). In all the samples analyzed, the most abundant and conserved PC species were PC 32:0 and the unsaturated PC 34:1, mostly corresponding to DPPC (PC 16:0\_16:0) and palmitoleoyl glycerophosphocholine (POPC; PC 16:0\_18:1), respectively (Figure 2d and S1, and Table S3, Supporting Information). Cholesterol was found in all samples, with highest amounts in porcine pulmonary surfactant (15.6 mol%), followed by human mucus (12.2 mol%), human surfactant

from BALF (9.8 mol%) and Alveofact (7.2 mol%). The anionic phosphatidylglycerol (PG) and phosphatidylinositol (PI) were also detected in all the samples. Nevertheless, in porcine pulmonary surfactant, PG was reduced by half, balanced by an increase of PI. The zwitterionic phosphatidylethanolamine (PE) was also present in similar proportions regardless of the species or location within the lung (i.e., upper or distal airways). Interestingly, the lipid fraction obtained from human mucus in the upper airways showed a remarkable major proportion of lysoPL ( $>3$  mol%), mostly lysoPC 16:0 ( $>2$  mol%). In addition, higher amounts of sphingomyelin, ceramides, and phosphatidic acid, were found in human mucus in comparison with the rest of the surfactant samples (data not shown). PC-O and PE-O were also increased in human mucus, particularly species of PE-O and long-chain polyunsaturated PC-O (Figure 2a,b).

The artificial lining fluid, in contrast, completely differs from the rest of the samples. It only contains three different lipids (i.e., 87.3 mol% DPPC, 9.2 mol% dipalmitoylphosphatidylglycerol [DPPG (PG 16:0\_16:0)] and 3.5 mol% cholesterol; Figure 2a) and a variety of proteins, but no surfactant proteins (see Experimental Section).

Even though the lipid composition showed several dissimilarities (Figure 2a–d and S1, Supporting Information), the differences in the protein fraction are also evident. As assessed by western blotting, only traces of SP-C ( $<6$  ng  $\mu\text{g PL}^{-1}$ ) and no SP-B were detected on pulmonary mucus (Figure 2e). This contrasts with pulmonary surfactant obtained from porcine BALF, as well as human or commercially available surfactants (e.g., Alveofact), which contain, at least, the hydrophobic proteins SP-B and SP-C in greater amounts.<sup>[21–24]</sup> The lack of enough SP-B and SP-C in material purified from human mucus and the artificial lining fluid suggests that these preparations may have reduced interfacial performance and may not be considered as a proper or fully-functional pulmonary surfactant.

### 2.2. Interfacial Performance

Due to the different origin and composition of the investigated pulmonary surfactant preparations, we next investigated to what



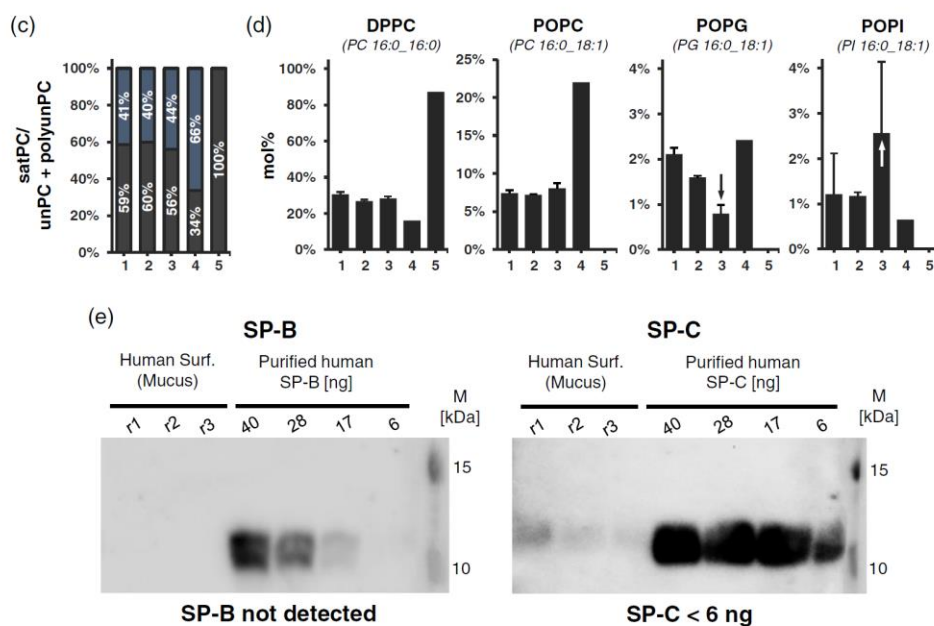
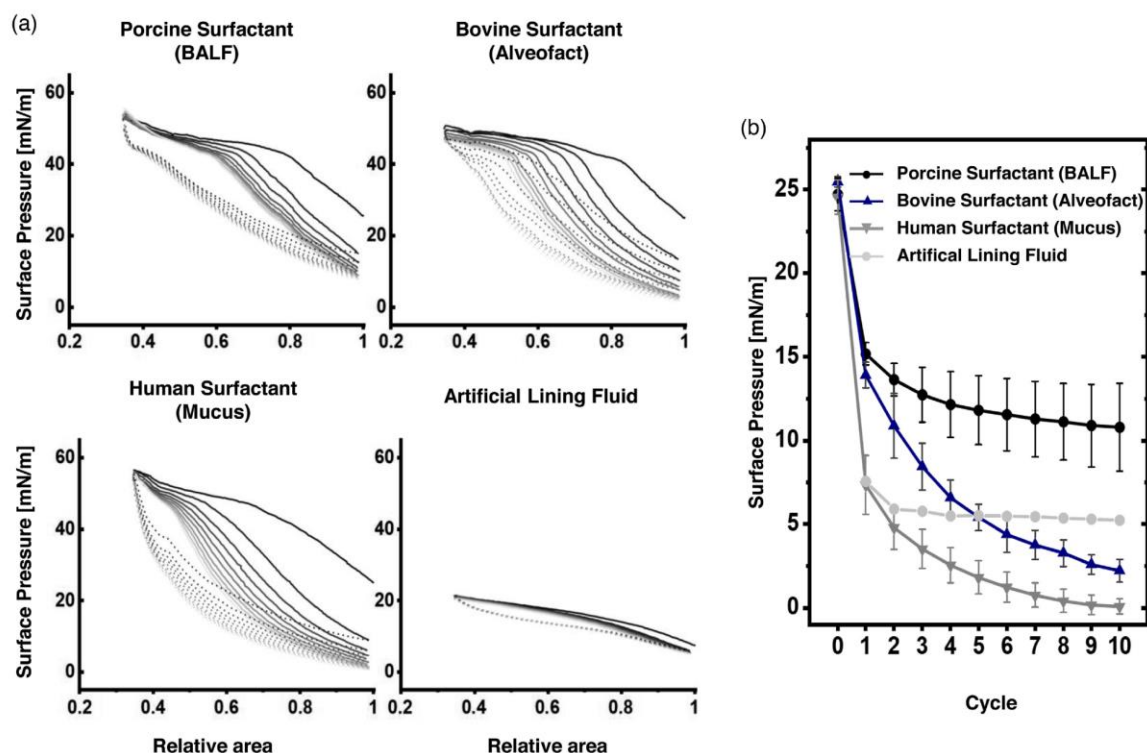


Figure 2. Continued.



**Figure 3.** a)  $\Pi$ -area isotherms of surfactant preparations following 10 subsequent compression–expansion cycles at a barrier compression rate of  $65 \text{ cm}^2 \text{ min}^{-1}$ . Surfactants were dispersed in Tris/NaCl at  $5 \text{ mg mL}^{-1}$  and applied on a Tris/NaCl (pH 7.4) buffered subphase thermostatted at  $25^\circ \text{C}$ . Surface pressure ( $\Pi$ ) is defined as the difference in surface tension between a clean air–water interface ( $\gamma_0$ ) and covered by the lipid layer ( $\gamma$ ). A representative experiment of  $n = 3$  is represented. b) Minimal surface pressure after each expansion. Error bars correspond to standard deviation ( $n = 3$ ).



samples but not the artificial lining fluid show a plateau at  $\approx 42\text{--}50\text{ mN m}^{-1}$  upon compression. During this plateau,  $\Pi$  remains constant as a consequence of the exclusion of interfacial material that cannot support such steric forces. During expansion, the small plateau indicates that the material that remains folded and closely attached to the interfacial film spreads out over the interface again, compensating the  $\Pi$  reduction.<sup>[25]</sup> In other words, the longer the plateau during compression and expansion, the higher the interfacial exclusion and readsorption, respectively. Both compression and expansion plateaus progressively reduce over cycling, which coincides with a progressive decrease in the  $\Pi$  observed at the end of each expansion (Figure 3b), likely because of the progressive loss of interface-associated material. In this line, the reduction of minimal  $\Pi$  seems to be greater as the plateaus both during compression and expansion shorten, indicating that part of the material excluded during compressions does not readsorb again into the interface. Intriguingly, these observations show different patterns depending on the pulmonary surfactant sample. Porcine surfactant from BALF, which contains the whole components of native surfactant (both lipids and surfactant proteins), presents the lowest reduction both in plateaus and minimal  $\Pi$ . Human surfactant from mucus, having similar lipid composition but only traces of SP-C and no SP-B, shows the greatest reductions. In addition, the plateaus observed during expansions of the surfactant purified from mucus are the smallest, suggesting that the lack of surfactant proteins burden the readsorption of excluded material and stability of the interfacial film during dynamics. Then, Alveofact, which has no hydrophilic surfactant proteins but comparable amounts of SP-B and SP-C and major proportions of unPC and polyunPC, also shows higher reductions than the porcine surfactant but less accentuated than the human surfactant from mucus. In the case of the artificial lining fluid, which completely differs from pulmonary surfactant, clear differences are evidenced. It does not show an increase in  $\Pi$  during compression above  $20\text{ mN m}^{-1}$  and remains relatively stable during cycling, suggesting that the material adsorbing to the air–water interface greatly differs from any of the pulmonary surfactant samples.

The previous experiments indicated that each type of pulmonary surfactant exerted distinct interfacial performance influenced by lipid and protein composition. To confirm it under relevant *in vivo*-like conditions, we used a captive bubble surfactometer, which allows for emulating alveolar dynamics under physiological conditions of compression–expansion rates, temperature, pH and humidity.

As shown in Figure 4a (initial adsorption), upon addition of each type of pulmonary surfactant, surface tension ( $\gamma$ ) decreased sharply until reaching equilibrium at  $\approx 20\text{--}22\text{ mN m}^{-1}$  ( $\Pi \approx 45\text{--}50\text{ mN m}^{-1}$ ), a value that coincides with the exclusion plateau observed in the Langmuir isotherms (Figure 4a) and indicates proper interfacial adsorption. Nevertheless, porcine surfactant shows the fastest adsorption kinetics, whereas Alveofact and human surfactant from mucus exert a minimal initial delay of few seconds. When the bubble is expanded from  $0.05\text{ cm}^3$  to a maximum volume of  $0.15\text{ cm}^3$  (i.e., increasing the air–liquid interface; Figure 4b postexpansion adsorption), all types of pulmonary surfactant remain stable, meaning that the material already adsorbed efficiently respreads over the newly opened interface. New nonadsorbed material accumulated in the reservoir at the subphase and closely associated to the interface may

also adsorb during those 5 min. This behavior is expected from a pulmonary surfactant with proper adsorption and respreading properties, ensuring stable and saturated interfaces during breathing dynamics.

Subsequently, the air bubble was subjected to successive slow quasistatic (Figure 4c) and rapid breathing-like (Figure 4d) compression–expansion dynamics, with great differences between samples. Porcine surfactant, considered as the reference in this study, reached minimal surface tensions below  $2\text{ mN m}^{-1}$  after a long exclusion plateau exhibited during the first compression at  $\approx 20\text{--}22\text{ mN m}^{-1}$ . During the subsequent quasistatic and dynamic cycles, minimal surface tensions below  $2\text{ mN m}^{-1}$  were reached with less than 20% area reduction and practically no hysteresis. The rest of materials could not reach such minimal surface tensions even after long plateaus. In the case of the human surfactant from mucus, which only contains traces of SP-C and lacks SP-B, compressions of more than 50% of the relative area were not enough to lower surface tensions below the equilibrium ( $\gamma \approx 20\text{--}22\text{ mN m}^{-1}$ ) both during quasistatic and breathing-like dynamic cycles. In fact, the long plateaus observed during compressions induced a  $\gamma$  increase during expansions. Apart from the native porcine surfactant, only Alveofact was able to reach  $\gamma < 2\text{ mN m}^{-1}$  during breathing-like dynamic cycles, but only under area reductions of more than 25%. This behavior could be derived from the lower proportions of DPPC and higher unPC and polyunPC compared with the porcine surfactant that burden the highly packed state of DPPC at the air–liquid interface. The artificial lining fluid, containing only DPPC, DPPG, and cholesterol as the lipid fraction and no surfactant proteins, does not exert an interfacial activity comparable to pulmonary surfactant. It is not able to reduce  $\gamma$  to values below  $45\text{ mN m}^{-1}$  ( $\Pi$  above  $20\text{ mN m}^{-1}$ ) under static conditions nor  $30\text{ mN m}^{-1}$  during interfacial dynamics. This evidences a poor interfacial activity that advances the formation of weak interfacial films unable to prevent the penetration of aerosolized NP, as addressed in the next section.

### 2.3. Pulmonary Surfactant as a Barrier to Protect Alveolar Cells against Deposition of Aerosolized NPs

Finally, we evaluated to what extent the presence of several lining fluids with different composition and interfacial activity may modulate cytotoxicity and cellular uptake of aerosolized NPs. Studying such bionano interactions in adequate *in vitro* models may allow to better understand and eventually predict the effects of such nanomaterials once reaching the deep lung *in vivo*. Positively and negatively charged silica NPs with sizes of 144.3 and 183.7 nm, respectively, were selected as models to set the framework for toxicity and uptake experiments. In addition, a novel nanocarrier for the antimycobacteria drug BTZ043 with 60.0 nm size and negative charge was also evaluated. Characterization of the NPs and deposited doses are shown in Table 1. Moreover, nanoparticle tracking analysis (NTA) was carried out to determine the potential interactions of plain and amino-functionalized silica NPs with different media at a 1:1 w/w ratio: 1) phosphate buffer saline (PBS), 2) artificial lining fluid, 3) human surfactant obtained from mucus, 4) Alveofact, and 5) a native pulmonary surfactant purified from porcine

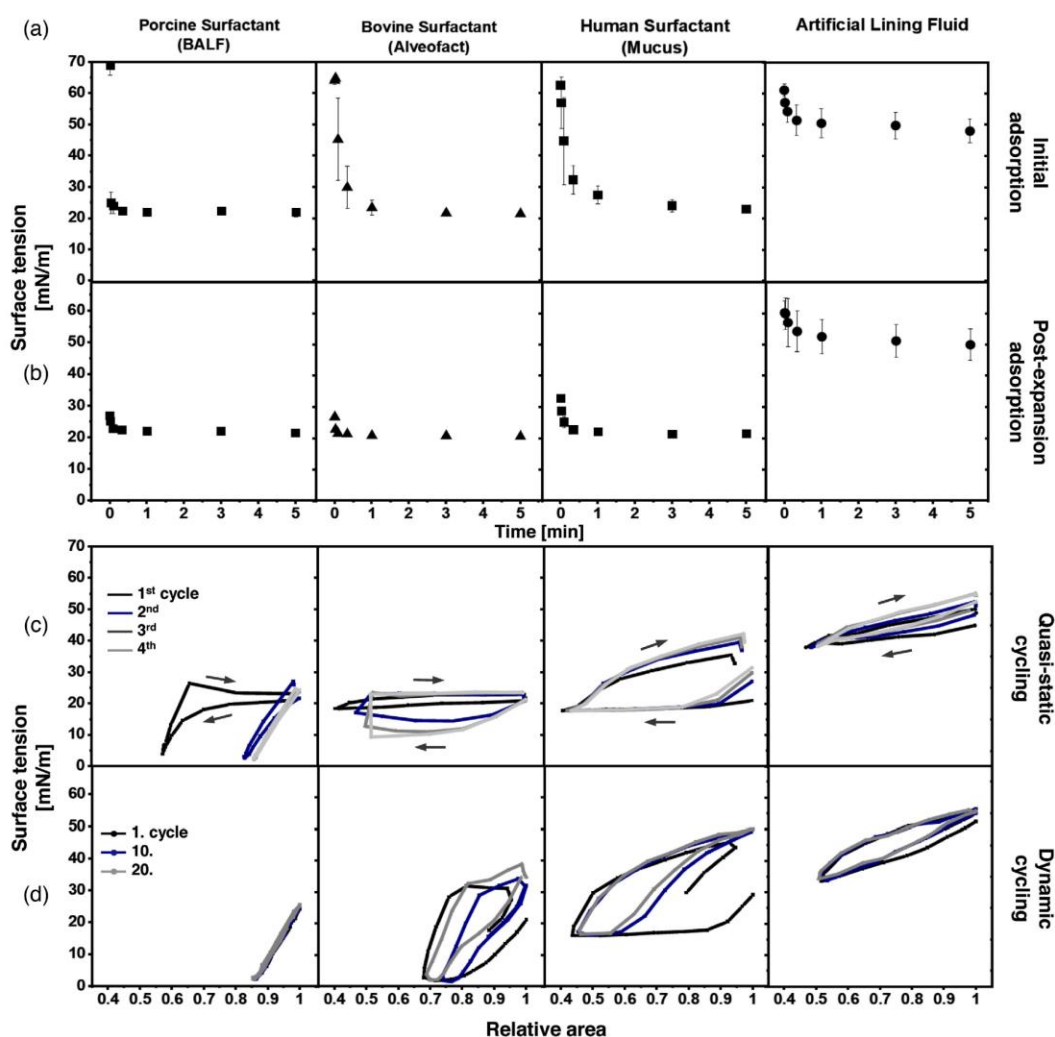


**Figure 4.** Comparison of interfacial performance as assessed in a captive bubble surfactometer. Porcine surfactant from BALF, bovine surfactant (Alveofact), human surfactant from mucus and artificial lining fluid are compared. Aliquots of 200 nL were applied close to the air-liquid interface at a concentration of  $20 \text{ mg mL}^{-1}$ . a,b) Interfacial adsorption kinetics is represented as surface tension–time ( $\gamma$ -time) isotherms right a) after application and b) after a fast expansion. Mean of three experiments is represented. Error bars represent the standard deviation. c,d) Representative  $\gamma$ -area isotherms of three independent experiments are compared during four slow quasistatic (c) and 20 breathing-like rapid dynamic cycles carried out at a rhythm of 20 cycles  $\text{min}^{-1}$  (d). First to fourth for quasistatic cycles and 1st, 10th, and 20th for dynamic are represented.

**Table 1.** Overview of particle characteristics. Particle size, polydispersity index (Pdl), and zeta potential were measured by dynamic and electrophoretic light scattering in PBS. Deposited dose of silica or BTZ043 NPs per well was determined by fluorescence and HPLC, respectively. Mean  $\pm$  SD of three independent experiments is represented.

NP	Size in PBS [nm]	Pdl	$\zeta$ -potential [mV]	Deposited dose [ $\mu\text{g}$ ]
BTZ-NP	$60.0 \pm 25$	$0.253 \pm 0.12$	$-32.1 \pm 2.48$	$10 \pm 0.53$ (BTZ)
Silica-NP ( $\text{NH}_2$ )	$144.3 \pm 1.85$	$0.11 \pm 0.03$	$4.43 \pm 0.6$	$100 \pm 4.75$
Silica-NP (plain)	$183.7 \pm 0.21$	$0.01 \pm 0.006$	$-16.5 \pm 3.32$	$100 \pm 4.03$

BALF. **Figure 5** and Table S4, Supporting Information, show a size increment of silica NPs in the presence of both porcine (BALF) and bovine (Alveofact) surfactants, but not in the presence of surfactant from human mucus nor synthetic lining fluid, indicating a major interaction with the former surfactants. This increase in size seems to be more prominent in the case of amino-functionalized NPs, which may indicate a higher electrostatic interaction with the negatively charged surfactants.

Then, the three different NPs were deposited on THP-1 macrophage-like cells grown on permeable supports and covered by distinct aqueous lining layers: 1) PBS, 2) artificial lining fluid, 3) human surfactant obtained from mucus, 4) Alveofact, and 5) a

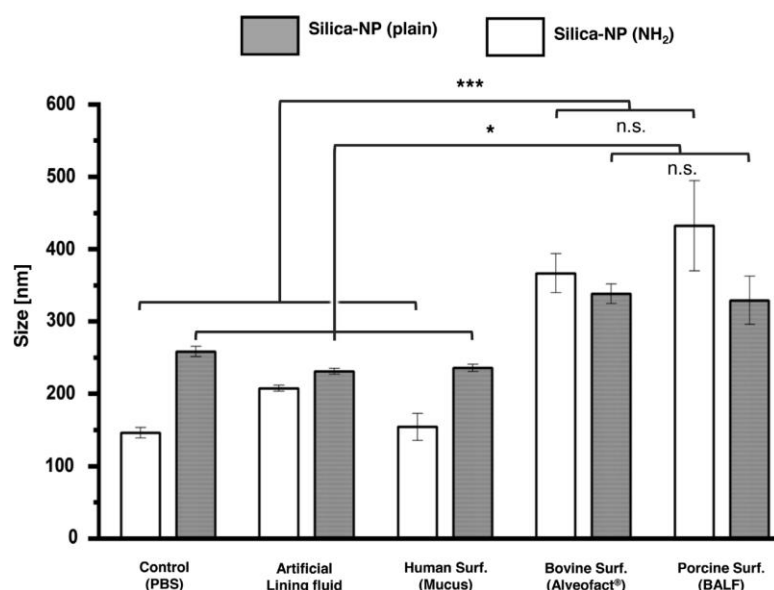


**Figure 5.** Size determination of plain and amino-functionalized silica NPs in various surfactant preparations. NTA of fluorescently labeled NPs was carried out in porcine surfactant from BALF, bovine surfactant (Alveofact), human surfactant from mucus and artificial lining fluid. PBS served as a control. Silica NPs were incubated in respective surfactant preparations and PBS at a ratio of 1:1. Experiments were carried out in triplicates. Error bars represent standard deviation. One-way ANOVA, Tukey post-hoc test: (\*, silica-NP plain);  $p < 0.05$ ; (\*\*\*, silica-NP NH<sub>2</sub>)  $p < 0.001$ .

native pulmonary surfactant purified from porcine BALF. A limited access to human BALF prevented testing a true human surfactant. As shown in **Figure 6b–d**, each NP exerted different cytotoxicity depending on the lining layer, as assessed using live/dead staining and subsequent flow cytometry analysis, whereas the lining layer per se did not affect the viability of the cells (**Figure S3**, Supporting Information). On PBS lining layers, plain silica NPs increased the cytotoxicity by 12%, amino-functionalized silica NPs by 19% and BTZ-NPs by 28% with respect to unexposed cell cultures. Similar results were obtained when covering the cells with the artificial lining fluid and pulmonary surfactant obtained from human mucus. This indicates that they do not act as proper barriers, likely because the lack of essential components of pulmonary surfactant prevents the formation of stable interfacial layers and hampers the interaction with airborne NPs. Interestingly, Alveofact and native porcine pulmonary surfactant, which represent functional pulmonary surfactant (**Figure 4**) and showed higher interactions with silica NPs (**Figure 5**), promoted a significant reduction of cytotoxicity upon exposure to all types of NPs. These results evidence that only the lining fluids containing proper pulmonary surfactant preparations may exert a protective function likely by forming interfacial films that act as physical and molecular barriers against external matter.

Based on these results, we exemplarily selected amino-functionalized silica particles to study their effect on the barrier properties of the human alveolar epithelial lentivirus-immortalized cell line (hAELVi) in the presence or in the absence of the porcine pulmonary surfactant. The latter was chosen because of its most prominent protective effect on macrophage-like THP-1 cells. In this case, the exposure time was

increased to 24 h to detect more prominent detrimental effects on barrier integrity of epithelial cells. **Figure 7a** shows that, upon particle deposition, the presence of porcine pulmonary surfactant covering the cells significantly reduced lactate dehydrogenase (LDH) release from hAELVi cells, in contrast to coverage by PBS only (**Figure 7a**). Furthermore, **Figure 7b** shows that the presence of porcine pulmonary surfactant in the lining fluid markedly preserved the integrity of the epithelial barrier upon NPs exposure in comparison with PBS. Only covered by PBS, the TEER decreased significantly upon exposure to silica-NH<sub>2</sub> NPs from  $\approx 3500$  to not more than some  $1200 \Omega \text{ cm}^{-2}$ . In the presence of porcine pulmonary surfactant covering the cells, however, TEER only decreased to  $2800 \Omega \text{ cm}^{-2}$ , demonstrating significant protection of epithelial barrier integrity by pulmonary surfactant.

**Figure 7c** shows confocal light scanning micrographs revealing the distribution pattern and cellular association (binding + uptake) of aerosolized silica-NH<sub>2</sub> NPs after deposition on hAELVi cells coated with a thin layer ( $179 \mu\text{m}$ ; mathematical estimation for a volume of  $20 \text{ mm}^3$  in Transwells with a surface of  $112 \text{ mm}^2$ ) of native porcine pulmonary surfactant at  $5 \text{ mg mL}^{-1}$  (upper panels) or PBS (lower panels). Right after deposition and prior to washing out the lining layer (left panels), the presence of porcine pulmonary surfactant seems to promote greater aggregation of silica-NH<sub>2</sub> NPs (red fluorescent aggregates) in comparison with PBS, indicating that they may interact with pulmonary surfactant before contacting the cells. Interestingly, only in the presence of pulmonary surfactant, these aggregates persisted on top of the cells after washing to remove noninternalized particles (middle and right panels). As visualized on the confocal z-stacks (micrographs at the bottom left in right panels), the

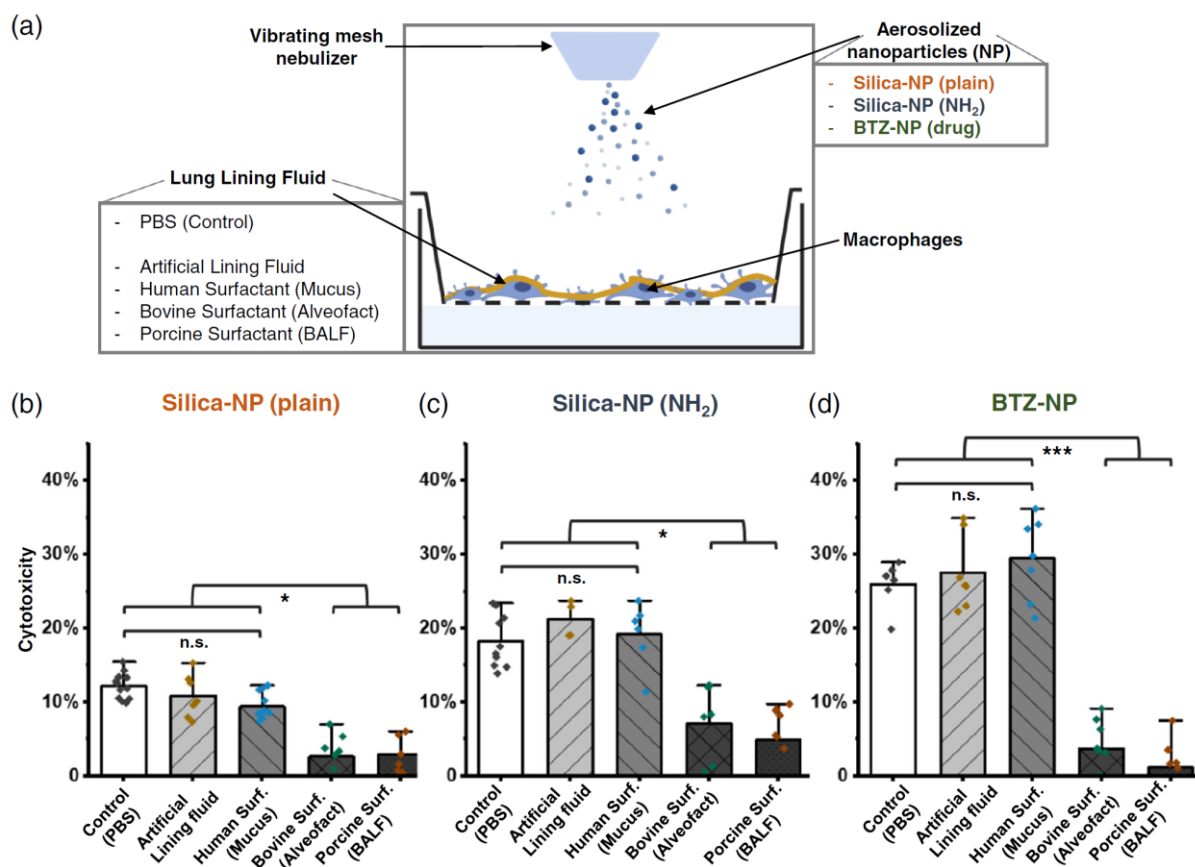


**Figure 6.** Deposition of NPs. a) Schematic representation of the air-liquid interface exposure of plain and amino-functionalized silica particles and BTZ043 NPs. b-d) Cytotoxicity of NPs on macrophage-like THP-1 cells. The cell surface was covered with 20  $\mu\text{L}$  of various aqueous lining layers (PBS, artificial lining fluid, human surfactant obtained from mucus, Alveofact and a native porcine surfactant purified from BALF). Each surfactant preparation at 5  $\text{mg mL}^{-1}$ . b) The cells were exposed to aerosol deposition of 100  $\mu\text{g}$  plain silica NPs, c) 100  $\mu\text{g}$  amino-functionalized silica NPs, and d) 10  $\mu\text{g}$  BTZ043 (drug)-NPs. Values were normalized to the unexposed cultures (data not shown). Increase in gray scale indicates a tendency for more physiological pulmonary surfactant samples. Cytotoxicity was determined by flow cytometry live/dead assay. Mean of  $N = 3$  independent experiments with  $n = 3-4$  replicates are represented. Error bars represent standard deviation. One-way ANOVA, Tukey post-hoc test (\*)  $p < 0.05$ , (\*\*);  $p < 0.001$ , (\*\*\*)  $p < 0.005$ .

majority of fluorescent NPs was located outside the cells forming aggregates. However, in the absence of pulmonary surfactant, most of the NPs were internalized (lower right panel). These results are in line with cytotoxicity/LDH release and TEER measurements, where the protective effect of pulmonary surfactant may be related to lower cellular uptake.

### 3. Discussion

The implementation of pulmonary surfactant into cell culture models requires access to suitable material in sufficient amount and quality. Nowadays, there is a plethora of pulmonary surfactants available in the market, most of them for the treatment of premature neonates with respiratory distress syndrome. The majority of them derives from animal sources, mostly from porcine and bovine BALFs (e.g., Alveofact from InfectoPharm,

Surfacen from CENSA, BLES from BLES Biochemicals Inc., or Infasurf from Forest Laboratory) or minced lungs (e.g., Curosurf from Chiesi Farmaceutici or Survanta from Abbot Laboratories).<sup>[9]</sup> However, when it comes to design human-relevant in vitro models of the respiratory air-blood barrier, human surfactants are desirable. The most common protocols to obtain pulmonary surfactant imply BALs, a procedure that is highly invasive, time consuming, expensive, and entails several ethical concerns, making the access to human pulmonary surfactant extremely limited. Therefore, additional sources other than human BALF could be beneficial. Interestingly, the presence of pulmonary surfactant in the upper airways interacting with pulmonary mucus is known since the early 1990s, though it has been poorly studied in comparison with pulmonary surfactant in the deep lung.<sup>[4,5,26,27]</sup> With this in mind, apart from pulmonary surfactant samples from the distal airways, we also explored pulmonary mucus from mechanically ventilated patients as a

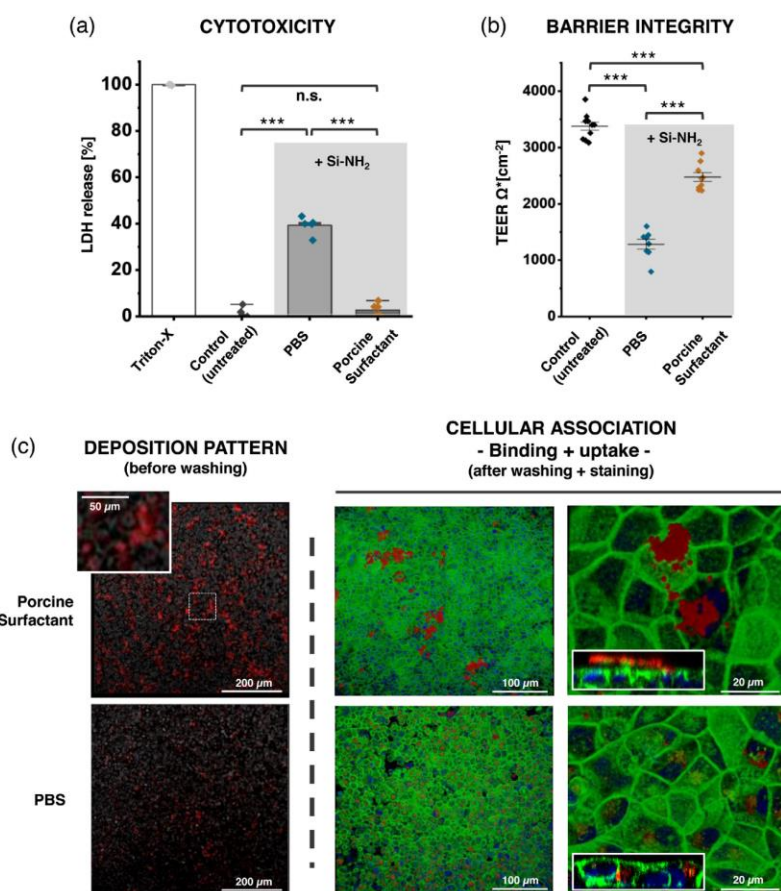


**Figure 7.** hAELVi cells after aerosol deposition of silica-NH<sub>2</sub> NPs. a) The cytotoxicity and b) barrier integrity of hAELVi cells covered with 20  $\mu$ L of PBS or native porcine surfactant from BALF (20  $\mu$ L at 5 mg mL<sup>-1</sup>) 24 h after particle deposition. Untreated control did not receive aerosol deposition of NPs. Bars represent mean  $\pm$  standard deviation of the mean of  $N=3$  independent experiments with  $n=3$  replicates and significance levels \*\*\* $p < 0.005$ . c) Representative confocal fluorescence micrographs of hAELVi cell monolayers after particle aerosol deposition showing the deposition pattern before washing (left panels) and cellular localization after washing and staining the cells (middle and right panels). Right panels correspond to a higher magnification of the middle panels and z-stacks are shown for discrimination of particle on and inside cells. Red: silica-NH<sub>2</sub> NPs; Green: phalloidin-Alexa 488 (Actin); Blue: 4',6-diamidino-2-phenylindole (DAPI) (Nucleus).

potential source of human-derived pulmonary surfactant preparations. The collection of tracheobronchial mucus does not require lung lavage and is routinely collected and discarded during clinical practice.

We systematically addressed the lipid/protein composition and interfacial performance of different pulmonary surfactant preparations isolated from human and animal sources, as well as an artificial lining fluid described in the literature,<sup>[20]</sup> to understand how this may relate to predict bio-nano interactions of aerosolized NPs on in vitro cellular models. Then, aerosol particle deposition, viability, cellular uptake, and barrier integrity were studied for differentiated macrophage-like THP-1 cells and human alveolar epithelial lentivirus-immortalized cells (hAELVi) in the presence of lining fluids of different origins containing or not pulmonary surfactant.

The composition of animal-derived pulmonary surfactant has been exhaustively characterized in the literature,<sup>[24,28,29]</sup> whereas

human pulmonary surfactant either from tracheobronchial mucus or BALF has been poorly studied mainly because of the extremely limited access and highly invasive methods required to obtain it. We found several differences in terms of lipid composition regarding the species (i.e., humans, pigs, and calves) and location within the lung (i.e., upper vs distal airways) that affect the interfacial properties of the different surfactant materials. However, the presence of surfactant proteins SP-B and SP-C are the critical components that confer the lining fluid with appropriate interfacial performance, stability, and barrier properties. All the analyzed samples but the artificial lining fluid adsorbed to the air-liquid interface in a similar fashion, though under breathing-like dynamic conditions, only those having SP-B and SP-C were able to reproducibly reach surface tensions below 2 mN m<sup>-1</sup>. The saturated PL, mainly represented by DPPC in all analyzed samples, are essential for reaching minimal surface tensions during expiration due to the highly packed states supported by the saturated acyl chains.<sup>[30]</sup>

Unsaturated PL, as well as neutral lipids like cholesterol, are indispensable to fluidify pulmonary surfactant membranes, enhancing adsorption and spreading into the air–liquid interface. However, excessive amounts of unPL and polyunPC, such as those found in Alveofact, or cholesterol may hinder the proper functionality of pulmonary surfactant under dynamic conditions.<sup>[31]</sup> In fact, the large plateaus observed in the Langmuir (Figure 3) and CBS (Figure 4) assays for Alveofact could be explained by the high proportions of unPL. Nevertheless, during the compression–expansion dynamics, the interfacial film seems to be refined and minimal surface tensions can be reached. As proposed by the squeeze-out model, this is mainly explained by a selective exclusion of the excess of unPL while maintaining stable interfacial films by means of a steric process mainly governed by SP-B and SP-C.<sup>[10,32]</sup> The lack of enough amounts of SP-B and SP-C, such as in human surfactant from mucus, affects the proper interfacial performance of pulmonary surfactant and promote lipid desorption,<sup>[7]</sup> visually observable by means of high reduction of surface pressure (Figure 3) and increase in surface tension (Figure 4) over compression–expansion cycles. Consequently, we propose that commercially available surfactants like Alveofact, as well as pulmonary surfactant purified from healthy BALFs may be good candidates to exert protective effects against deposition of aerosolized NPs on cellular models. In contrast, the artificial lining fluid lacking surfactant lipids and proteins, as well as the surfactant purified from human pulmonary mucus, which lacks enough SP-B and SP-C, might not be the best materials to mimic the alveolar lining fluid.

Knowing this, we evaluated whether the composition and interfacial characteristics of different lining fluids may affect the interaction of nanomaterials with cells (Figure 6 and 7). Interactions with pulmonary surfactant have been demonstrated for different inhaled nanomaterials including silica NPs that may inhibit the interplay of surfactant lipids and proteins, which can be reduced by introducing less-interactive polyethylene glycol particle surface coating.<sup>[33,34]</sup> Beck-Broichsitter et al. observed that the NP-promoted inactivation of pulmonary surfactant depends on the composition and type of pulmonary surfactant preparations used (i.e., synthetic or native).<sup>[35]</sup> Mousseau et al. described that Curosurf, a clinically used porcine surfactant, interacts with positively charged alumina and silica NPs, inducing particle aggregation essentially by electrostatic forces.<sup>[8]</sup> Wohlleben et al. have demonstrated that surface-functionalized silica particles only interact with lipid samples in the presence of surfactant proteins, while fostering particle agglomeration and short-term toxicity.<sup>[36]</sup> Studies by Ruge et al., which exclusively focused on surfactant proteins SP-A and SP-D, found that the uptake of polymer-coated NPs in contact with these proteins is enhanced in alveolar macrophages (MH-S).<sup>[16]</sup> The particle uptake depends on the type of polymer surface coating, which determines corona formation by adsorption of lipids and proteins onto the surface. We addressed the influence of surface charge and functionalization by selecting two types of silica NPs (plain and amino-functionalized). The positively charged particles exerted a twofold higher cytotoxicity compared to plain particles (10% vs 20%), which was reduced in the presence of bovine or porcine surfactant preparations by a factor of three. Such silica NPs have a controlled surface chemistry and were selected for being inert and well characterized. They were used at doses higher than physiological exposure to evidence such effects. Our data suggest that under the investigated conditions, pulmonary surfactant

constitutes a barrier to aerosolized particles mainly by physical interactions, especially those that are positively charged and interact with negatively charged components of pulmonary surfactant. To support the relevance of our study for pharmaceutically engineered drug delivery systems, BTZ-NPs, developed in the context of pulmonary tuberculosis therapy, were investigated. For BTZ-NPs, cytotoxic effects were more pronounced compared with silica particles, even at lower doses (10 µg for BTZ and 100 µg for silica particles). Interestingly, the presence of lining fluids containing proper pulmonary surfactant reduced drastically the cytotoxicity, demonstrating once again that pulmonary surfactant exerts protective effects influencing the NP–cell interactions, at least under static conditions. As recently demonstrated by Hidalgo et al., interfacial dynamics is a critical aspect that enhances distribution, release from the interface and cellular internalization of compounds associated to pulmonary surfactant.<sup>[25]</sup> Therefore, further research would be desirable to evaluate the influence of breathing-like dynamics on aggregation, distribution or even release of NPs to the subphase and subsequent particle–cell interactions.

To emulate the NP corona formation upon contact with pulmonary surfactant and how it influences the cellular uptake,<sup>[37]</sup> most of the current studies usually preincubate the particles with pulmonary surfactant preparations or some of its main components (e.g., DPPC) prior to deposition on pulmonary surfactant-free cultures. Moore et al. demonstrated that premixing NPs with medium, depositing the particles at high concentration or resuspending the culture medium after deposition, had also an effect on particle–cell interaction. They suggested that by premixing NPs with medium, higher dispersion of NP was reached, enhancing the corona formation and reducing the interactions with cells.<sup>[38]</sup> Li et al. reported that preincubating silica particles with DPPC, the toxicity of high doses comparable with those used in our study ( $\approx 100$  µg) on two types of lung epithelial cells, A549 and 16HBE, was reduced.<sup>[39]</sup>

In contrast to these previous studies, we only covered the macrophage-like THP-1 and epithelial cells with small volume of lining fluids containing pulmonary surfactant. When NPs are deposited on top of such stable interfacial films, they must first penetrate it and then diffuse through the lining layer prior to contacting the cells. This diffusion may be influenced by the interaction with the lining fluid promoting the corona formation. In fact, the NTA assays (Figure 5 and Table S4, Supporting Information), demonstrated that the surfactant preparations containing the essential components of pulmonary surfactant and exerting the best interfacial performance (i.e., porcine surfactant from BALF and Alveofact), promoted an increase in the particle size. This is especially true for positively charged NPs as the ones used in this work (silica–NH<sub>2</sub> NPs), which indicates that the diffusion of particles may be subjected, at least in part, to electrostatic interactions with positively charged surfactant components. Both by slowing down the diffusion upon interaction with NPs and acting as a stable lining barrier at the air–liquid interface, lining fluids containing proper pulmonary surfactants provided the best protection to the cells, likely by preventing the uptake and masking some cationic charges upon corona formation. Further investigations of this hypothesis, also including breathing-like dynamics might be of high interest for developing more relevant models closer to the in vivo situation.

Altogether, when studying the toxicity or therapeutic effects of inhaled nanomaterials on cellular models, using adequate pulmonary surfactant preparations turns critical. Simple or complex lipid mixtures lacking SP-B and SP-C with low interfacial activity are not enough to form stable barriers. Native pulmonary surfactant samples may be considered ideal as they contain the whole lipid and protein fractions, but the purification process is tedious, they are subjected to interindividual variabilities and ensuring contaminant-free materials is rather time consuming and costly. However, in this study we did not observe remarkable differences between native porcine pulmonary surfactant (BALF) and the clinical surfactant preparation Alveofact in the cellular studies. This demonstrates that commercially available clinical surfactant preparations may well be suitable for cellular in vitro models. In contrast, simple synthetic lining fluids lacking essential phospholipids and surfactant proteins appear to be less suitable. Standardized surfactant preparations for such purposes must minimally contain the functionally relevant phospholipids DPPC, POPC, and POPG, as well as the essential lung surfactant proteins SP-B and SP-C. For the latter, recombinant or synthetic proteins could become an interesting alternative while ensuring contaminant-free production and lower production costs.

#### 4. Conclusions

As this study demonstrates, appropriate pulmonary surfactant preparations are crucial to set and optimize in vitro cellular models of the lung to study the interaction with inhaled particles. Artificial lining fluids that do not contain the essential pulmonary surfactant components appear to be of limited relevance. Pulmonary surfactant obtained from pulmonary mucus preserves phospholipid composition compared with native surfactant from BALF, but lacks the surfactant proteins and does not show proper barrier function. Lipid and protein composition determine interfacial properties and are therefore essential to select the appropriate surfactant preparations. Key quality parameters including the presence of DPPC, minor phospholipids, and surfactant proteins must be addressed when routinely implementing pulmonary surfactant to understand and predict nanoscale lung interactions. Only preparations displaying sufficiently high interfacial activity, by means of the interplay between phospholipids and proteins, markedly influence the cellular interactions of nanomaterials. In this sense, full native pulmonary surfactant preparations are the best candidates, though they are limited by the conditions imposed by the purification procedures. Therefore, commercially available and clinically used surfactant preparations may provide a compromise.

#### 5. Experimental Section

**Pulmonary Surfactant from Porcine BALF:** Porcine surfactant was obtained from BAL of freshly slaughtered pigs according to an established protocol.<sup>[25,40,41]</sup> Briefly, BALs were carried out by intratracheal instillation of a buffer solution (5 mM Tris, 150 mM NaCl, pH 7.4), while massaging the lungs. Each batch of BALF was filtered to remove the tissue debris and centrifuged at 1000 × g, 4 °C for 5 min to eliminate cells and debris. Subsequently, BALFs were ultracentrifuged in an angular rotor (100 000 × g; 1 h; 4 °C). Pellets were pooled and homogenized in a 16% NaBr solution and ultracentrifuged (2 h: 120 000 × g; swinging-bucket rotor;

no break) in a discontinuous NaBr density gradient (16% NaBr + NaCl 0.9%; 13% NaBr + NaCl 0.9%; NaCl 0.9%). The band located between NaCl 0.9% layer (top) and 13% NaBr + NaCl 0.9% (middle) was collected, pooled, and homogenized, storing them as small aliquots at –80 °C until used. Phospholipid content was determined by phosphorous assay.<sup>[42]</sup> Sampling and exclusion criteria are shown in Figure 6.

**Bovactant (Alveofact):** It was purchased from Lyomark Pharma GmbH (Oberhaching, Germany) at a concentration of 45 mg mL<sup>-1</sup> phospholipids. It derived from bovine lung lavages. Sampling and exclusion criteria are shown in Figure 6.

**Pulmonary Surfactant from Human Mucus:** Human pulmonary mucus was collected from patients undergoing elective surgery at the Klinikum Saarbrücken gGmbH as previously described<sup>[43]</sup> and surfactant isolated thereof. In short, endotracheal tubes obtained from mechanically ventilated patients were cut in 10–15 cm pieces and centrifuged at 1000 rpm at 4 °C for 2 × 30 s to spin down the mucus. Only nonsmokers without lung diseases were included in this study. Samples were stored at –20 °C and gradually thawed at 4 °C overnight prior to surfactant isolation. Surfactant was isolated by chloroform/methanol organic extraction following the method of Bligh and Dyer<sup>[44]</sup> and phospholipid content was determined by a colorimetric phosphorous assay.<sup>[42]</sup> Mucus sampling was approved by the Ethics Commission of the Chamber of Medicine Doctors of the Saarland (file number 19/15). Sampling and exclusion criteria are shown in Figure 6.

**Pulmonary Surfactant from Human BALF:** BALF was collected from patients undergoing flexible bronchoscopy for diagnostic reasons according to current German guidelines.<sup>[45]</sup> BAL was carried out in 20 mL fractions of 0.9% sterile saline up to a max total volume of 300 mL. Pooled BAL fractions of one patient were used for diagnostic purposes. BALF samples of donors with known R3 and/or R4 pathogens or proteinosis were not included. Leftover anonymized BAL samples were centrifuged at 400 × g with brake at 4 °C for 10 min. BALF supernatants were stored at –80 °C. The project-specific MTA of the BioMaterialBank Nord was approved by the Ethics Commission of the Chamber of the University of Luebeck (file number 20-128). Surfactant purification was carried out following the protocol described in Section 5.1.4. Sampling and exclusion criteria are shown in Figure 6.

**Artificial Lining Fluid:** The synthetic lining fluid was prepared by mixing 48 mg DPPC, 5 mg DPPG, and 1 mg cholesterol diluted in chloroform. The solvent was evaporated under nitrogen flow and proteins and antioxidants (i.e., albumin, IgG, transferrin, ascorbate, urate, and glutathione) dissolved in an aqueous solution (HBSS buffer, Sigma) added at the concentrations described by Kumar et al.<sup>[20]</sup> The formulation was freeze-dried and stored at –20 °C until experimental use. DPPC and DPPG (25 mg mL<sup>-1</sup> diluted in chloroform) were purchased from Avanti Polar Lipids (Alabaster, AL). All other chemicals were purchased from Sigma Aldrich (St. Louis, MO) at the highest purity.

**Lipid and Protein Composition—Lipidomics:** Extracted phospholipids were further diluted in 700 μL in a mixture of chloroform, methanol, and water (60:30:4.5; v/v/v). Afterward, 100 μL sample solution were diluted in 870 μL in a mix of 2-propanol, methanol with 0.1% ammonia acetate, and chloroform (4:2:1, v/v/v). For quantification 30 μL SPLASH Lipidomix Mass Spec Standard (Table S1, Supporting Information; 330707, Avanti Polar Lipids, Alabaster, USA) were spiked to the samples post extraction. Shotgun lipidomics measurements were carried out using a Q Exactive (Thermo Fisher Scientific, Bremen, Germany) equipped with a TriVersa NanoMate (Advion BioSciences, Ithaca, NY, USA) as autosampler and ion source.<sup>[46,47]</sup>

Free cholesterol was quantified after acetylation as reported earlier.<sup>[48]</sup> Briefly, 100 μL lipid extracts were dried in the speed vac. To the dried samples, 100 μL of a mixture of acetyl chloride and chloroform (1:5, v/v) were added. The samples were incubated at room temperature for one hour with continuous shaking. Afterward, the samples were dried in the speed vac and subsequently resolved in solvent mixture of 2-propanol, methanol with 0.1% ammonia acetate, and chloroform (4:2:1, v/v/v).

Lipid identification was carried out using LipidXplorer.<sup>[49]</sup> Table S2, Supporting Information, shows the standards used for shotgun Lipidomics including the quantified ions, quantitation mode, and quantitation ion. LipidXplorer settings and MFQL will be made available via LIFS webportal.<sup>[50]</sup>

**Lipid and Protein Composition—Western Blotting:** Human SP-B and SP-C, used as WB internal references, were purified from a patient with alveolar proteinosis by two-step molecular exclusion chromatography, using the organic extract of a purified pulmonary surfactant from the human BAL, as previously described.<sup>[22]</sup> Different volumes of the purified proteins corresponding to different masses (40, 28, 17, and 6 ng) as quantified by amino acids analysis (Biochrom 30+amino acid analyzer, Harvard Bioscience, Holliston, MA, USA) were dried and resuspended in a buffer solution (5 mM Tris and 150 mM NaCl at pH 7.4). A volume corresponding to 6  $\mu\text{g}$  of phospholipids in mucus organic extract was dried under nitrogen flux and resuspended in the same buffer solution. Electrophoresis Laemmli buffer (2% sodium dodecyl sulfate, 62.5 mM Tris, pH 6.8, 10% glycerol, and 0.03% bromophenol blue), containing 4%  $\beta$ -mercaptoethanol was added to mucus samples and the human purified proteins, before incubating the tubes 15 min at 90 °C. Subsequently, samples were loaded into a polyacrylamide gel (16%) that was run for around 1 h, and proteins were transferred onto polyvinylidene fluoride membranes with a humid chamber (1 h; 4 °C; 300 mA) and blocked in PBS-T (100 mM  $\text{Na}_2\text{HPO}_4/\text{KH}_2\text{PO}_4$ -1% Tween) with 5% skim milk at room temperature for 2 h. Membranes were then incubated overnight with the primary polyclonal antibodies (anti SP-B: polyclonal rabbit, WRAB-48604; anti SP-C: rabbit, WRAB-76696; Seven Hills, Cincinnati, USA) in PBS-T 5% milk at 4 °C, washed thoroughly in PBS-T, and incubated with the secondary antibody (polyclonal swain anti-rabbit Ig [P0217]; Dako, Agilent Technologies, Santa Clara, USA) for 1 h at room temperature. Membranes were then developed (1 min of exposition) using a commercial ECL system for horseradish peroxidase (HRP) substrate and chemiluminescence was read in ImageQuant LAS 500 (GE Healthcare Life Sciences, Logan, USA). Bands densitometry was carried out using ImageJ for Mac OS X.

**Interfacial Performance Assays—Langmuir Trough:** Pressure–area ( $\Pi$ - $a$ ) isotherms were carried out with a ribbon-barrier Langmuir trough (NIMA Technologies, Coventry, UK; area variable from 185 to 58  $\text{cm}^2$ ) equipped with a Wilhelmy plate connected to a pressure sensor (NIMA Technologies, Coventry, UK) to track the surface tension. A Tris/NaCl buffer (5 mM/150 mM) at pH 7.4 served as the subphase (25 °C) and to suspend the surfactants at a final concentration of 5  $\text{mg mL}^{-1}$ . Ten subsequent compression–expansion cycles were carried out at 65  $\text{cm}^2 \text{min}^{-1}$ .

**Interfacial Performance Assays—Captive-Bubble Surfactometer:** To analyze and compare the interfacial performance of different surfactant preparations, a custom-made captive bubble surfactometer (CBS) was used. CBS models the alveolar dynamics under physiological-like conditions of temperature, humidity, and pH, and compression–expansion cycling rates. It consists of an air-bubble (5 mm diameter, 0.05  $\text{cm}^3$ ) settled at the bottom of an agarose cap placed in a sealed thermostated (37 °C) chamber surrounded by a dense, temperature-controlled saline solution. A 200 nL aliquot of each surfactant preparation, dispersed in Tris/NaCl buffer (5 mM/150 mM) at pH 7.4 at a concentration of 20  $\text{mg mL}^{-1}$ , was injected close to the air bubble. Then, the bubble is subjected to several compression–expansion cycles by moving up and down a piston driven by a computer-controlled engine. Surface tension is deduced from the change in bubble shape, which is monitored by a high-speed camera during the whole experiment.

**Particle Characterization:** Plain and amino-modified, fluorescently labeled silica particles were purchased from Kisker Biotech (Steinfurt, Germany). Prof. Feldmann's group (Karlsruhe Institute of Technology, Karlsruhe, Germany) provided the antibiotic (Benzothiazinone, BTZ043) containing nanosuspension. It consists of three components: sodiumdodecylsulfate (SDS) to stabilize drug colloids buffered with ammoniumacetate and the drug, to overcome the poor solubility of BTZ043. Particle size and zeta-potential were determined in PBS using Zetasizer Nano (Malvern Analytical, Malvern, UK). Reported is the intensity-based z-average of three independent measurements  $\pm$  standard deviation (Table S3, Supporting Information). Size determination of silica NPs in various surfactant preparations was carried out by NTA using a NanoSight (Malvern Analytical, Malvern, UK) and analyzed using the NTA 3.3 software. In brief, particles were diluted in the respective surfactant preparations at a final concentration of 100  $\mu\text{g mL}^{-1}$  NPs and surfactant, respectively, yielding a 1:1 w/w ratio.

**Cell Cultures—THP-1 Cells:** They were passaged in culture 25  $\pm$  8 times in T75 flasks with RPMI-medium supplemented with 10% fetal calf serum (FCS) not exceeding a density of  $1 \times 10^6$  cells  $\text{mL}^{-1}$ . Transwells (1.12  $\text{cm}^2$ ) permeable supports (3460; Corning Costar, Corning, NY) at a density of 200 000 cells per well and differentiated into macrophage-like (dTHP-1) cells using 25  $\text{ng mL}^{-1}$  phorbol-12-myristate-13-acetate (PMA, SIGMA, Germany) for 48 h, followed by a resting period of 24 h (Medium without PMA). Prior to each experiment, cells were washed twice with PBS from the apical compartment to remove cell culture medium containing FCS.

**Cell Cultures—hAELVi cells:** Previously established in our group,<sup>[15]</sup> were cultured during passages 13–18 in SAGM medium (Lonza, Cleveland, OH) containing 1% v/v FCS and 1% v/v penicillin/streptomycin. Cells were transferred onto fibronectin/collagen-coated Transwells (surface area 1.12  $\text{cm}^2$ ) at a number of 100 000 cells  $\text{cm}^{-2}$  with 500  $\mu\text{L}$  medium in the apical and 1500  $\mu\text{L}$  in the basolateral compartment. On day 3, medium was removed from the apical side and cells cultured at air-liquid interface (ALI) conditions until day 14–16 with medium change every second day.

**Cell Cultures—NP Aerosol Deposition Experiments:** Transwells supports containing dTHP-1 or hAELVi cell monocultures were transferred to the sample holders of a Vitrocell Cloud12 system (Vitrocell, Waldkirchen, Germany) and medium was removed from the apical compartment by washing with PBS twice. Cells were kept at 37 °C prior to addition or not of 20  $\mu\text{L}$  of different lining fluid containing or not pulmonary surfactant. This volume ensures a full coverage of the cells with a theoretical thickness of the lining layer of 179  $\mu\text{m}$  in Transwells with a surface of 112  $\text{mm}^2$ . Only PBS was added on top of the cells by drop deposition as a control for nonsurfactant-containing lining fluid. Surfactant preparations at 5  $\text{mg mL}^{-1}$  of phospholipids dispersed in PBS were added on top by drop deposition. After 30 min for the system to equilibrate, 200  $\mu\text{L}$  of the respective NP dispersed in PBS were nebulized on top of the cells using the Vitrocell Cloud 12 system (Vitrocell, Waldkirchen, Germany). Nebulization was carried out using an Aeroneb nebulizer with a mesh size of 2.5–4  $\mu\text{m}$ . After aerosol generation, the cloud was allowed to settle for 10 min to guarantee spatially uniform and complete sedimentation. Particle concentrations were adjusted to meet a final dose of 100  $\mu\text{g}$  silica NPs or 10  $\mu\text{g}$  BTZ043 per well. Notice that, the final dose of silica NPs exposed to cells was higher than expected in vivo to evidence toxic effects. Silica NP concentration was determined by nebulizing fluorescent silica NPs into Transwells containing 500  $\mu\text{L}$  PBS. Comparison of the fluorescence intensity of the working stock solution, at a concentration of 1  $\text{mg mL}^{-1}$ , with the fluorescence intensity after aerosol deposition into Transwells allowed to calculate the deposited amount/well (dose). BTZ043 dose was detected by HPLC as described previously.<sup>[15]</sup> Transwells support were mounted back into well plates and further processed as described in the following text for the respective assays/analysis.

**Cytotoxicity—Live–Dead Staining:** After 4 h incubation time, dTHP-1 cells were washed twice with PBS and detached using 100  $\mu\text{L}$  of Accutase solution (Sigma, Taufkirchen, Germany) for 15–20 min. Cells were centrifuged twice and resuspended in 500  $\mu\text{L}$  FACS buffer containing 4% v/v FCS in PBS. For live cell staining, 5  $\mu\text{L}$  of a 10  $\mu\text{M}$  working solution of Calcein-AM (Molecular Probes, viability/cytotoxicity kit, Invitrogen, CA, USA) and a final concentration of 1  $\mu\text{g mL}^{-1}$  DAPI (Sigma, Germany) for dead cell staining were used. Cells grown under submerged conditions were used as negative control and heat inactivated cells (35 min, 70 °C) as positive control. Samples were analyzed by flow cytometry (LSRFortessa, BD Bioscience, San Jose, CA, USA) with a minimum count of 10 000 cells per sample. Results were analyzed with Flowjo v10.6.1 (BD) software and gating strategy is shown in Figure S3, Supporting Information.

**Cytotoxicity—LDH Assay:** hAELVi cells strongly adhere to the transwell membranes and can only be detached incompletely and with scraping, which would interfere with cell viability. Therefore, we measured the release of intracellular LDH, which is secreted into the basolateral compartment after 24 h. From this supernatant, 100  $\mu\text{L}$  were transferred to a 96-well plate and 100  $\mu\text{L}$  of a mixture of 11.25 mL solution A and 250  $\mu\text{L}$  solution B from LDH Cytotoxicity Detection KIT (Roche, Basel, CH) was added to the well. Untreated cells were used as negative control and 0.1% Triton-X 100 (Sigma, USA) treated cells as positive control and medium without cells served as blank.



Cytotoxicity (LDH-release) was calculated after subtracting the blank as

$$\text{Cytotoxicity (\%)} = \left( \frac{\text{experimental value} - \text{low control}}{\text{high control} - \text{low control}} \right) \times 100 \quad (1)$$

**Measurement of Barrier Integrity:** hAELVi cells were cultured as indicated in the cytotoxicity section and transepithelial electrical resistance (TEER) values were measured before and 24 h after nebulization of the silica-NH<sub>2</sub> NPs. Two hours before resistance measurements, old cell culture medium was aspirated and 0.5 mL fresh medium was added to the apical compartment as well as 1.5 mL to the basolateral compartment, to allow cells to equilibrate before the measurement. Ohmic resistance values were measured using an epithelial Volt/Ohm meter (EVOM<sub>2</sub>; World Precision Instruments, Sarasota, USA). Reported TEER values (Ohm cm<sup>2</sup>) were calculated subtracting a blank (well without cells) followed by normalization for the surface area (1.12 cm<sup>2</sup> for 3460 Transwell).

**Confocal Microscopy:** Confocal images were acquired 24 h after nebulization without washing to investigate particle deposition and with washing and subsequent staining to verify cellular internalization. Z-stacks were obtained with a Leica DMI8 Confocal Microscope (Leica Microsystems, Germany) equipped with a 25× water immersion objective at a 1024 × 1024 resolution and a step size of 0.25 μm per image plane. Imaris software (Imaris x64 v9.7.2, Oxford instruments, UK) was used for image processing.

**Data Analysis:** Unless otherwise indicated, data were represented as mean of 3–6 individual experiments with error bars showing the standard deviation. One-way ANOVA followed by Tukey's multiple comparison test was used for statistical analysis.

## Supporting Information

Supporting Information is available from the Wiley Online Library or from the author.

## Acknowledgements

B.H and A.H contributed equally to this work. This project was funded by the German Federal Ministry of Education and Research (BMBF, Berlin, Germany), acronym ANTI-TB, under grant agreement FKZ: 16GW0167/GWANTA20. Further financial support in the DS lab was provided by the German Network for Bioinformatic Infrastructure (de.NBI, LIFS2, FKZ: 031L0108B). JPG acknowledges the funding by grants from the Spanish Ministry of Science, Universities and Innovation (RTI2018-094564-B-I00) and the Regional Government of Madrid (P2018/NMT-4389). The BioMaterialBank Nord is supported by the German Center for Lung Research (grant 82DZL001A1) and member of popgen 2.0 network (P2N). Some of the figures were created with BioRender.com.

## Conflict of Interest

The authors declare no conflict of interest.

## Author Contributions

B.H. designed the study, acquired data by performing most of the laboratory experiments, interpreted the data and drafted the manuscript. A.H. conceptualized and designed the study, acquired data by performing some of the laboratory experiments, interpreted all the data, drafted the manuscript and supervised the whole work. F.W. performed the lipidomics analysis. D.S. supervised the lipidomics analysis. K.I.G. processed and provided the BALs from donor patients; C.F. provided BTZ-NPs. P.C. assisted and designed some of the cellular studies. C.A. performed the protein analysis. J.P.G. provided porcine surfactant and supervised the

biophysical studies and protein analysis. K.S. provided the mucus samples from donor patients. X.M. assisted and established the purification and processing of surfactant from mucus. B.L. interpreted the data and supervised the work. And CML conceptualized the study and supervised the whole work. All authors critically revised the article for important intellectual content and finally approved the article in the present form. All authors agreed to be accountable for their contribution to the study ensuring accuracy and integrity of the presented work following rules of good scientific practice.

## Data Availability Statement

The data that support the findings of this study are available from the corresponding author upon reasonable request.

## Keywords

air–blood barrier, air–liquid interfaces, cellular lung models, drug delivery, lipidomics, nanotoxicities, particle corona, pulmonary surfactants

Received: June 15, 2021

Revised: September 2, 2021

Published online: October 23, 2021

- [1] A. Pietroiusti, H. Stockmann-Juvala, F. Lucaroni, K. Savolainen, *Wiley Interdiscip. Rev. Nanomed. Nanobiotechnol.* **2018**, *10*, 1513.
- [2] X. Murgia, B. Loretz, O. Hartwig, M. Hittinger, C.-M. Lehr, *Adv. Drug Delivery Rev.* **2018**, *124*, 82.
- [3] B. C. Huck, O. Hartwig, A. Biehl, K. Schwarzkopf, C. Wagner, B. Loretz, X. Murgia, C. M. Lehr, *Biomacromolecules* **2019**, *20*, 3504.
- [4] P. Gehr, S. Schürch, Y. Berthiaume, V. I. Hof, M. Geiser, *J. Aerosol. Med.* **1990**, *3*, 27.
- [5] D. E. Sims, M. M. Horne, *Am. J. Physiol.-Lung Cell. Mol. Physiol.* **1997**, *273*, L1036.
- [6] C. Garcia-Mouton, A. Hidalgo, A. Cruz, J. Pérez-Gil, *Eur. J. Pharmaceutics Biopharmaceutics* **2019**, *144*, 230.
- [7] O. Cañadas, B. Olmeda, A. Alonso, J. Pérez-Gil, *Int. J. Mol. Sci.* **2020**, *21*, 3708.
- [8] F. Mousseau, J.-F. Berret, *Soft Matter* **2018**, *14*, 5764.
- [9] O. Blanco, J. Pérez-Gil, *Eur. J. Pharmacol.* **2007**, *568*, 1.
- [10] J. Pérez-Gil, *Biochim. Biophys. Acta (BBA)-Biomembr.* **2008**, *1778*, 1676.
- [11] E. Parra, J. Pérez-Gil, *Chem. Phys. Lipids* **2015**, *185*, 153.
- [12] S. S. Raesch, S. Tenzer, W. Störck, A. Rurainski, D. Selzer, C. A. Ruge, J. Perez-Gil, U. F. Schaefer, C.-M. Lehr, *ACS Nano* **2015**, *9*, 11872.
- [13] I. Lynch, T. Cedervall, M. Lundqvist, C. Cabaleiro-Lago, S. Linse, K. A. Dawson, *Adv. Colloid Interface Sci.* **2007**, *134–135*, 167.
- [14] M. P. Monopoli, C. Aberg, A. Salvati, K. A. Dawson, *Nat. Nanotechnol.* **2012**, *7*, 779.
- [15] C. de Souza Carvalho, N. Daum, C. M. Lehr, *Adv. Drug Deliv. Rev.* **2014**, *75*, 129.
- [16] C. A. Ruge, J. Kirch, O. Cañadas, M. Schneider, J. Perez-Gil, U. F. Schaefer, C. Casals, C. M. Lehr, *Nanomed.: Nanotechnol. Biol. Med.* **2011**, *7*, 690.
- [17] M. Gasser, P. Wick, M. J. Clift, F. Blank, L. Diener, B. Yan, P. Gehr, H. F. Krug, B. Rothen-Rutishauser, *Particle Fibre Toxicol.* **2012**, *9*, 17.
- [18] J. Y. Kasper, L. Feiden, M. I. Hermanns, C. Bantz, M. Maskos, R. E. Unger, C. J. Kirkpatrick, *Beilstein J. Nanotechnol.* **2015**, *6*, 517.
- [19] M. Radiom, M. Sarkis, O. Brookes, E. K. Oikonomou, A. Baeza-Squiban, J. F. Berret, *Sci. Rep.* **2020**, *10*, 19436.

- [20] A. Kumar, W. Terakosolphan, M. Hassoun, K.-K. Vandera, A. Novicky, R. Harvey, P. G. Royall, E. M. Bicer, J. Eriksson, K. Edwards, *Pharm. Res.* **2017**, *34*, 2454.
- [21] J. W. Logan, F. R. Moya, *Therap. Clin. Risk Manage.* **2009**, *5*, 251.
- [22] C. Autilio, M. Echaide, S. Shankar-Aguilera, R. Bragado, D. Amidani, F. Salomone, J. Pérez-Gil, D. De Luca, *Am. J. Respir. Cell Mol. Biol.* **2020**, *63*, 327.
- [23] E. Lopez-Rodriguez, J. Pérez-Gil, *Biochim. Biophys. Acta* **2014**, *1838*, 1568.
- [24] J. Goerke, *Biochim. Biophys. Acta* **1998**, *1408*, 79.
- [25] A. Hidalgo, C. Garcia-Mouton, C. Autilio, P. Carravilla, G. Orellana, M. N. Islam, J. Bhattacharya, S. Bhattacharya, A. Cruz, J. Pérez-Gil, *J. Controlled Release* **2021**, *329*, 205.
- [26] W. Bernhard, H. P. Haagsman, T. Tschernig, C. F. Poets, A. D. Postle, M. E. Van Eijk, H. Von Der Hardt, *Am. J. Respir. Cell Mol. Biol.* **1997**, *17*, 41.
- [27] M. Q. Gaunsbaek, A. D. Kjeldsen, V. Svane-Knudsen, M. L. Henriksen, S. Hansen, *ORL* **2014**, *76*, 288.
- [28] S. Orgeig, P. S. Hiemstra, E. J. A. Veldhuizen, C. Casals, H. W. Clark, A. Haczku, L. Knudsen, F. Possmayer, *Respir. Physiol. Neurobiol.* **2010**, *173*, S43.
- [29] L. N. Suri, A. Cruz, R. A. Veldhuizen, J. F. Staples, F. Possmayer, S. Orgeig, J. Perez-Gil, *Biochim. Biophys. Acta* **2013**, *1828*, 1707.
- [30] G. Ma, H. C. Allen, *Langmuir* **2006**, *22*, 5341.
- [31] E. Lopez-Rodriguez, M. Echaide, A. Cruz, H. W. Tausch, J. Perez-Gil, *Biophys. J.* **2011**, *100*, 646.
- [32] E. Keating, Y. Y. Zuo, S. M. Tadayyon, N. O. Petersen, F. Possmayer, R. A. Veldhuizen, *Biochim. Biophys. Acta (BBA)-Biomembr.* **2012**, *1818*, 1225.
- [33] M. Beck-Broichsitter, *Langmuir* **2018**, *34*, 540.
- [34] M. Beck-Broichsitter, A. Bohr, *Nanotoxicology* **2019**, *13*, 964.
- [35] M. Beck-Broichsitter, C. Ruppert, T. Schmehl, A. Günther, W. Seeger, *Biochim. Biophys. Acta (BBA)-Biomembr.* **2014**, *1838*, 474.
- [36] W. Wohlleben, M. D. Driessen, S. Raesch, U. F. Schaefer, C. Schulze, B. V. Vacano, A. Vennemann, M. Wiemann, C. A. Ruge, H. Platsch, *Nanotoxicology* **2016**, *10*, 970.
- [37] R. F. Hamilton Jr, S. A. Thakur, A. Holian, *Free Radic. Biol. Med.* **2008**, *44*, 1246.
- [38] T. L. Moore, D. A. Urban, L. Rodriguez-Lorenzo, A. Milosevic, F. Crippa, M. Spuch-Calvar, S. Balog, B. Rothen-Rutishauser, M. Lattuada, A. Petri-Fink, *Sci. Rep.* **2019**, *9*, 900.
- [39] J. Li, H. Yang, S. Sha, J. Li, Z. Zhou, Y. Cao, *Ecotoxicology and environmental safety* **2019**, *186*, 109770, <https://doi.org/10.1016/j.ecoenv.2019.109770>.
- [40] H. W. Tausch, J. B. De La Serna, J. Perez-Gil, C. Alonso, J. A. Zasadzinski, *Biophys. J.* **2005**, *89*, 1769.
- [41] T. Curstedt, H. Jörnvall, B. Robertson, T. Bergman, P. Berggren, *Eur. J. Biochem.* **1987**, *168*, 255.
- [42] G. Rouser, A. N. Siakotos, S. Fleischer, *Lipids* **1966**, *1*, 85.
- [43] B. K. Rubin, O. Ramirez, J. G. Zayas, B. Finegan, M. King, *Am. Rev. Respir. Dis.* **1990**, *141*, 1040.
- [44] E. G. Bligh, W. J. Dyer, *Can. J. Biochem. Physiol.* **1959**, *37*, 911.
- [45] K. Haussinger, A. Ballin, H. D. Becker, P. Bölskei, R. Dierkesmann, I. Dittrich, W. Frank, L. Freitag, R. Gottschall, W. Guschall, W. Hartmann, R. Hauck, F. Herth, D. Kirsten, M. Kohlhäufel, A. Kreuzer, R. Loddenkemper, N. Macha, A. Markus, F. Stanzel, H. Steffen, M. Wagner, *Pneumologie* **2004**, *58*, 344.
- [46] J. Graessler, D. Schwudke, P. E. Schwarz, R. Herzog, A. Shevchenko, S. R. Bornstein, *PLoS one* **2009**, *4*, 6261.
- [47] L. F. Eggers, D. Schwudke, *Clinical Metabolomics*, Springer, Cham **2018**, pp. 163–174.
- [48] G. Liebisch, M. Binder, R. Schifferer, T. Langmann, B. Schulz, G. Schmitz, *Biochim. Biophys. Acta (BBA)—Mol. Cell Biol. Lipids* **2006**, *1761*, 121.
- [49] R. Herzog, D. Schwudke, K. Schuhmann, J. L. Sampaio, S. R. Bornstein, M. Schroeder, A. Shevchenko, *Genome Biol.* **2011**, *12*, R8.
- [50] D. Schwudke, A. Shevchenko, N. Hoffmann, R. Ahrends, *J. Biotechnol.* **2017**, *261*, 131.
- [51] A. Kuehn, S. Kletting, C. de Souza Carvalho-Wodarz, U. Repnik, G. Griffiths, U. Fischer, E. Meese, H. Huwer, D. Wirth, T. May, N. Schneider-Daum, C. M. Lehr, *Altex* **2016**, *33*, 251.
- [52] D. Thiyagarajan, B. Huck, B. Nothdurft, M. Koch, D. Rudolph, M. Rutschmann, C. Feldmann, C. Hozsa, M. Furch, K. F. W. Besecke, R. K. Gieseler, B. Loretz, C.-M. Lehr, *Drug Delivery Transl. Res.* **2021**, *11*, 1766.

## SUPPORTING INFORMATION

### Systematic Analysis of Composition, Interfacial Performance and Effects of Pulmonary Surfactant Preparations on Cellular Uptake and Cytotoxicity of Aerosolized Nanomaterials

*Benedikt Huck<sup>§</sup>, Alberto Hidalgo<sup>§\*</sup>, Franziska Waldow, Dominik Schwudke, Karoline I. Gaede, Claus Feldmann, Patrick Carius, Chiara Autilio, Jesus Perez-Gil, Konrad Schwarzkopf, Xabier Murgia, Brigitta Loretz and Claus-Michael Lehr\**

*<sup>§</sup>BH and AH equally contributed to the work.*

## SUPPLEMENTAL FIGURES

## FIGURE S1

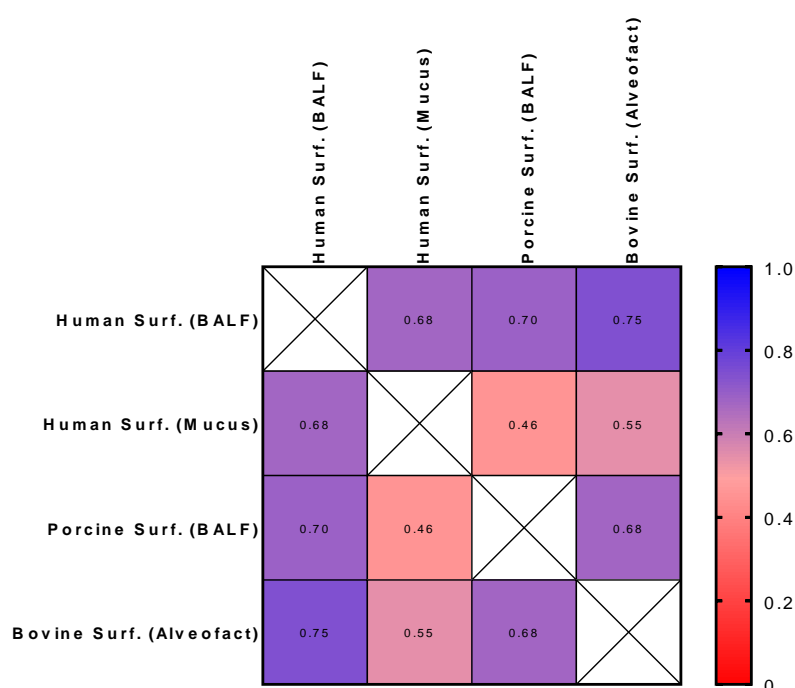


**Figure S1:** Spearman Rank's correlation analysis of lipid composition of pulmonary surfactant obtained from different sources (surfactant from human bronchoalveolar lavage fluid (BALF), human mucus and porcine BALF, and the clinical surfactant surfacant [Alveofact<sup>®</sup>]). Squares represent Spearman's rank correlation coefficients, where 1 correspond to the highest correlation (blue) and 0 the lowest (red). The analysis includes 48 lipid species that account for 95 mol% of the total lipid content.

## FIGURE S2

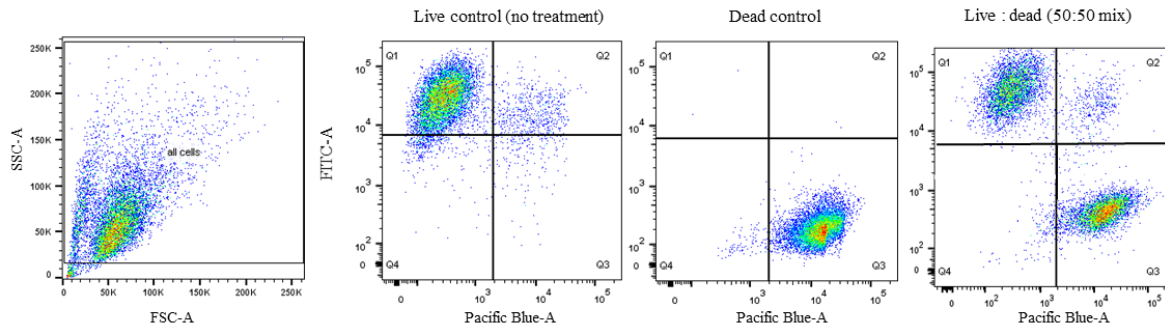


**Figure S2:** Gating strategy for flow cytometric live/dead staining.

**FIGURE S3**

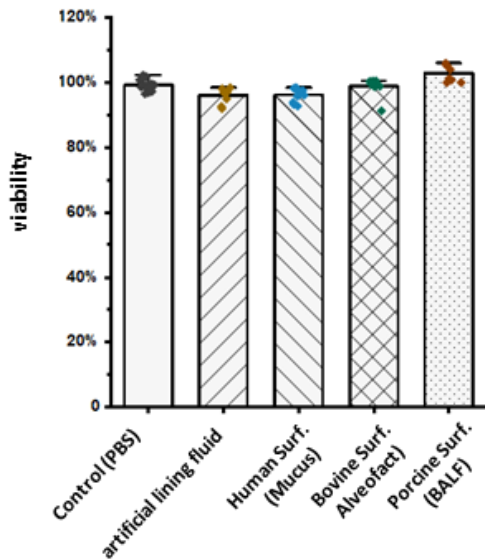


**Figure S3:** Viability of dTHP-1 cells incubated with 20 µL of various surfactant preparations at a concentration of 1 mg/mL for 4 hours at 37°C.

**SUPPLEMENTAL TABLES****Table S1:** Internal standards used for lipid quantification.

Substance	Amount added (pmol) <sup>a)</sup>
15:0-18:1(d7) PC	235.17
15:0-18:1(d7) PE	8.76
15:0-18:1(d7) PS	5.91
15:0-18:1(d7) PG	41.10
15:0-18:1(d7) PI	11.79
15:0-18:1(d7) PA	11.76
18:1(d7) LPC	52.95
18:1(d7) LPE	11.85
18:1(d7) Chol Ester	588.03
18:1(d7) MAG	5.82
15:0-18:1(d7) DAG	17.61
15:0-18:1(d7)-18:1 TAG	76.44
18:1(d9) SM	47.16
Cholesterold(d7)	293.01
Ceramide C17	113.07

a) IS amounts added in total to the samples prior shotgun lipidomics measurement

**Table S2:** Lipid standards and quantitation mode including quantitation ions for shotgun lipidomics.

Specie	Class	ESI Mode	Standard for	Quantitation mode	Quantitation Ion
LPE-IS	LPE	negative	LPE	MS2	Fatty acid fragment
PE-IS	PE		PE/PE-O	MS2	Fatty acid fragment
CL-IS	CL		CL	MS1	Precursor
PG-IS	PG		PG/LPG	MS2	Fatty acid fragment
PI-IS	PI		PI/LPI	MS2	Fatty acid fragment
PS-IS	PS		PS/LPS	MS2	Fatty acid fragment
Cer-IS	Cer	positive	Cer	MS2	LCB fragment
CE-IS	CE		CE	MS2	CE specific fragment
LPC-IS	LPC		LPC	MS2	PC (184) fragment
PC-IS	PC		PC/PC-O	MS2	PC (184) fragment
DAG-IS	DAG		DAG	MS2	Neutral loss + fragment
SM-IS	SM		SM	MS1	Precursor
TAG-IS	TAG		TAG	MS1	Precursor
<b>After acetylation</b>					
FC-IS	FC	FC	MS2	FC specific fragment	

**Table S3:** Characterization of specific acyl chains corresponding to PC 32:0, PC 34:1, PG 34:1 and PI 34:1 in the different surfactant samples using MS<sup>2</sup> in the negative ion mode. Contribution in % for each fatty acid species with respect to total amount.

		Human Surf. (BALF)	Human Surf. (Mucus)	Bovine Surf. (BALF)	Porcine Surf. (BALF)
PC 32:0	PC 14:0_18:0	0.50	0.26	1.29	0.77
	PC 16:0_16:0	99.50	99.74	98.71	99.23
PC 34:1	PC 16:1_18:0	2.82	2.78	3.72	3.64
	PC 16:0_18:1	97.18	97.22	96.28	96.36
PG 34:1	PG 16:1_18:0	4.46	5.05	0.97	4.64
	PG 16:0_18:1	95.54	94.95	99.03	95.36
PI 34:1	PI 16:0_18:1	100	100	100	100
	PI 16:1_18:0	n.d.	n.d.	n.d.	n.d.

**Table S4:** Particle size of plain silica and silica-NH<sub>2</sub> NPs in various surfactant preparations after incubation at a 1:1 ratio (w/w). Size was determined by dynamic light scattering (DLS) and nanoparticle tracking analysis (NTA).

Size [nm]								
Surfactant preparation	Human Surfactant (Mucus)		Porcine Surfactant (BALF)		Bovine Surfactant (BALF)		Artificial Lining Fluid	
	NTA	DLS	NTA	DLS	NTA	DLS	NTA	DLS
<b>Silica-NH<sub>2</sub> NPs</b>	154.2 ± 18.9	740.6 ± 21.8	432.2 ± 62.6	1663.0 ± 35.4	366.6 ± 26.9	2121.0 ± 239.3	207.7 ± 4.1	1251.0 ± 247.7
<b>Silica-NP (plain)</b>	235.7 ± 4.9	620.0 ± 31.2	329.0 ± 33.5	1031.0 ± 125.6	338.1 ± 13.6	1152.0 ± 76.2	231.1 ± 4.2	1031.0 ± 125.6

#### **5.4 Nano-in-Microparticles for Aerosol Delivery of Antibiotic-loaded, Fucose-derivatized and Macrophage-targeted Liposomes to Combat Mycobacterial Infections: *In Vitro* deposition, Pulmonary Barrier Interactions and Targeted Delivery**

**Benedikt C. Huck**, Durairaj Thiyagarajan, Aghiad Bali, Annette Boese, Karen F.W. Besecke, Constantin Hozsa, Robert K. Gieseler, Marcus Furch, Cristiane Carvalho-Wodarz, Franziska Waldow, Dominik Schwudke, Olga Metelkina, Alexander Titz, Hanno Huwer, Konrad Schwarzkopf, Jessica Hoppstädter, Alexandra K. Kiemer, Marcus Koch, Brigitta Loretz\*, Claus-Michael Lehr\*

Benedikt Huck, Aghiad Bali, Prof. Claus-Michael Lehr, Helmholtz Institute for Pharmaceutical Research Saarland, Department of Pharmacy, Saarland University, Campus E8 1, 66123 Saarbrücken, Germany, E-Mail: claus-michael.lehr@helmholtz-hips.de

Dr. Thiyagarajan Durairaj, Helmholtz Institute for Pharmaceutical Research Saarland, Department of anti-infective drug discovery, Campus E8 1, 66123 Saarbrücken, Germany

Dr. Annette Boese, Dr. Cristiane Carvalho-Wodarz, Dr. Brigitta Loretz, Helmholtz Institute for Pharmaceutical Research Saarland, Campus E8.1, 66123 Saarbrücken, Germany, E-Mail: brigitta.loretz@helmholtz-hips.de

Dr. Karen F.W. Besecke<sup>∇</sup>, Dr. Constantin Hozsa<sup>‡</sup>, Dr. Markus Furch<sup>†</sup>, Rodos Biotarget GmbH, 30625 Hannover, Germany

<sup>∇</sup>current address: Solmic BioTech GmbH, 40225 Düsseldorf, Germany

<sup>‡</sup>current address: Siegfried AG Hameln, 31789 Hameln, Germany

<sup>†</sup>current address: Biolife Holding AG, 69126 Heidelberg, Germany

Dr. Robert K. Gieseler, Laboratory of Immunology and Molecular Biology, and Department of Internal Medicine, University Hospital, Knappschaftskrankenhaus Bochum, Ruhr University Bochum, 44892 Bochum, Germany

Dr. Franziska Waldow, Research Center Borstel, Leibniz Lung Center, 23845 Borstel, Germany; German Center for Infection Research, Thematic Translational Unit Tuberculosis, Partner Site Hamburg-Lübeck-Borstel-Riems, Germany

Dr. Dominik Schwudke, Research Center Borstel, Leibniz Lung Center, 23845 Borstel, Germany, German Center for Infection Research, Thematic Translational Unit Tuberculosis, Partner Site Hamburg-Lübeck-Borstel-Riems, Germany; German Center for Lung Research (DZL), Airway Research Center North (ARC�), Kiel Nano, Surface and Interface Science KiNSIS, Kiel University, Germany

Olga Metelkina, Prof. Alexander Titz, Chemical Biology of Carbohydrates (CBCH), Helmholtz-Institute for Pharmaceutical Research Saarland (HIPS), Helmholtz Center for Infection Research, 66123 Saarbrücken, Germany; Department of Chemistry, Saarland University, 66123 Saarbrücken, Germany; Deutsches Zentrum für Infektionsforschung (DZIF), Hannover-Braunschweig site, Germany

Prof. Hanno Huwer, Cardiothoracic Surgery, Heart Center Voelklingen, 66333 Völklingen, Germany



Dr. Konrad Schwarzkopf, Department of Anaesthesia and Intensive Care, Klinikum Saarbrücken gGmbH, 66119 Saarbrücken, Germany

Dr. Jessica Hoppstädter, Prof. Alexandra Kiemer, Pharmaceutical Biology, Saarland University, Campus C2 3, 66123 Saarbrücken, Germany

Dr. Marcus Koch, INM – Leibniz Institute for New Materials, Campus D2 2, 66123 Saarbrücken,

*Advanced healthcare materials*, February 2022, <https://doi.org/10.1002/adhm.202102117>

# Nano-in-Microparticles for Aerosol Delivery of Antibiotic-Loaded, Fucose-Derivatized, and Macrophage-Targeted Liposomes to Combat Mycobacterial Infections: In Vitro Deposition, Pulmonary Barrier Interactions, and Targeted Delivery

Benedikt C. Huck, Durairaj Thiyagarajan, Aghiad Bali, Annette Boese, Karen F. W. Besecke, Constantin Hozsa, Robert K. Gieseler, Marcus Furch, Cristiane Carvalho-Wodarz, Franziska Waldow, Dominik Schwudke, Olga Metelkina, Alexander Titz, Hanno Huwer, Konrad Schwarzkopf, Jessica Hoppstädter, Alexandra K. Kiemer, Marcus Koch, Brigitta Loretz,\* and Claus-Michael Lehr\*

Nontuberculous mycobacterial infections rapidly emerge and demand potent medications to cope with resistance. In this context, targeted loco-regional delivery of aerosol medicines to the lungs is an advantage. However, sufficient antibiotic delivery requires engineered aerosols for optimized deposition. Here, the effect of bedaquiline-encapsulating fucosylated versus nonfucosylated liposomes on cellular uptake and delivery is investigated. Notably, this comparison includes critical parameters for pulmonary delivery, i.e., aerosol deposition and the noncellular barriers of pulmonary surfactant (PS) and mucus. Targeting increases liposomal uptake into THP-1 cells as well as peripheral blood monocyte- and lung-tissue derived macrophages. Aerosol deposition in the presence of PS, however, masks the effect of active targeting. PS alters antibiotic release that depends on the drug's hydrophobicity, while mucus reduces the mobility of nontargeted more than fucosylated liposomes. Dry-powder microparticles of spray-dried bedaquiline-loaded liposomes display a high fine particle fraction of >70%, as well as preserved liposomal integrity and targeting function. The antibiotic effect is maintained when deposited as powder aerosol on cultured *Mycobacterium abscessus*. When treating *M. abscessus* infected THP-1 cells, the fucosylated variant enabled enhanced bacterial killing, thus opening up a clear perspective for the improved treatment of nontuberculous mycobacterial infections.

## 1. Introduction

According to the WHO, mycobacterial infections are among the top ten causes of mortality worldwide with 7.1 million new infections and 1.4 million deaths in 2020.<sup>[1]</sup> Given the increase of antibiotic resistance, the treatment of such intracellular infections calls for improved medications and delivery approaches.<sup>[2,3]</sup> Poor drug permeability and systemic availability of orally administered antimycobacterial compounds including bedaquiline (BDQ) and levofloxacin (LVX) complicate the situation.<sup>[4]</sup> Therefore, therapeutic approaches that achieve high antibiotic concentrations at the target site are required. Targeted, local pulmonary delivery may complement conventional oral therapy, that is associated with high doses, long treatment periods, and severe side effects.<sup>[2,5]</sup> Here, the nature of the drug delivery system is essential as it must safely and efficiently encapsulate the antibiotic cargo, enable to reach the deeper lung, enter the target cells, and release the

 The ORCID identification number(s) for the author(s) of this article can be found under <https://doi.org/10.1002/adhm.202102117>

[+]Present address: Solmic BioTech GmbH, Düsseldorf 40225, Germany

[++]Present address: Siegfried AG Hameln, Hameln 31789, Germany

[+++]Present address: Biolife Holding AG, Heidelberg 69126, Germany

© 2022 The Authors. Advanced Healthcare Materials published by Wiley-VCH GmbH. This is an open access article under the terms of the Creative Commons Attribution License, which permits use, distribution and reproduction in any medium, provided the original work is properly cited.

DOI: 10.1002/adhm.202102117

B. C. Huck, A. Bali, A. Boese, C. Carvalho-Wodarz, B. Loretz, C.-M. Lehr  
Department of Drug Delivery  
Helmholtz Institute for Pharmaceutical Research Saarland  
Campus E8.1, Saarbrücken 66123, Germany  
E-mail: brigitta.loretz@helmholtz-hips.de  
claus-michael.lehr@helmholtz-hips.de

B. C. Huck, A. Bali, C.-M. Lehr  
Department of Pharmacy  
Helmholtz Institute for Pharmaceutical Research Saarland  
Saarland University  
Campus E8 1, Saarbrücken 66123, Germany  
D. Thiyagarajan  
Department of Anti-infective Drug Discovery  
Helmholtz Institute for Pharmaceutical Research Saarland

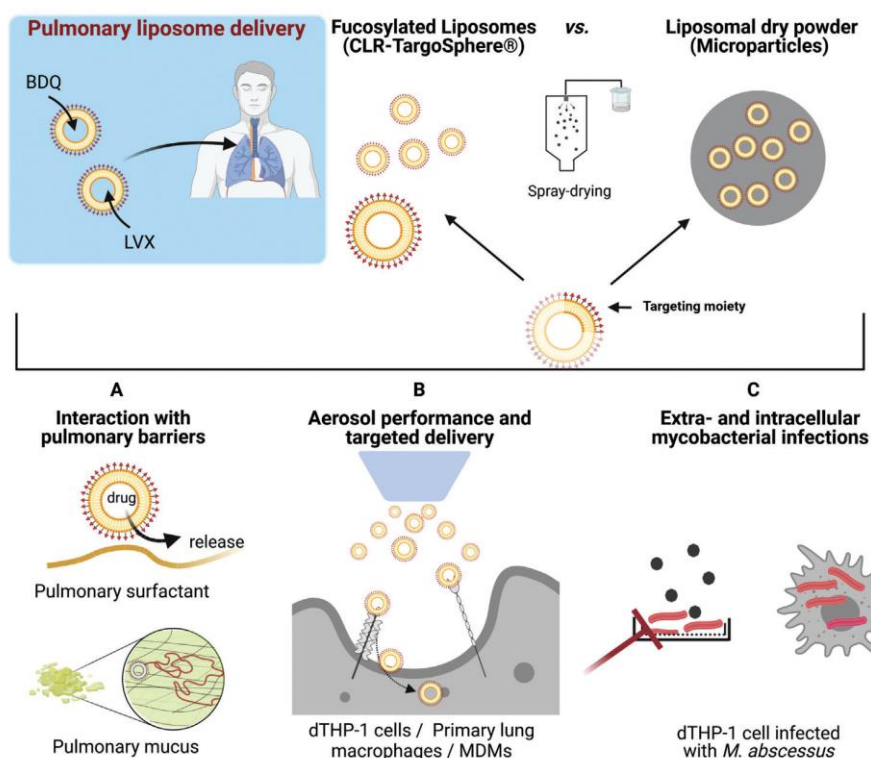
antibiotic into the appropriate intracellular compartments.<sup>[6]</sup> Further challenges result from interactions with the sophisticated pulmonary defense mechanisms, including renewable cellular (epithelial cells) and noncellular (pulmonary mucus and surfactant) barriers.<sup>[7]</sup> Liposomal drug carriers have evolved as potent delivery system by increasing both solubility and permeability of the active compound, particularly for intracellular infections.<sup>[8]</sup> The high cellular uptake rate of liposomes further benefits from controlled, targeted delivery to macrophages via receptor-mediated endocytosis in vitro and in vivo.<sup>[9]</sup> By specifically addressing the macrophage mannose receptor (CD206) using fucosylated TargoSphere liposomes, Duran et al. already demonstrated an increased cellular uptake and efficacy of such LVX-

loaded nanocarriers. Receptor-mediated endocytosis and intracellular routing thus direct the encapsulated antibiotics to acidic compartments where they can efficiently kill bacteria residing therein.<sup>[10]</sup>

There are, however, several obstacles when delivering liposomes to the deep lungs, i.e., first, the branching lung architecture and, second, the lungs' protective barrier mechanisms that challenge deep lung deposition of nanosized drug carriers.<sup>[11]</sup> The specific infection pathway of *Mycobacterium abscessus* is not fully understood but may include colonization of the respiratory mucosa and the resistance against intracellular killing within macrophages, in particular for patients with chronic lung diseases (COPD, bronchiectasis, cystic fibrosis) or in immunocompromised patients. The clinical manifestations of *M. avium* and *M. tuberculosis* infections show similarities and can lead to granuloma formation and/or colonization of the lung airways as biofilms as enduring, difficult-to-eradicate infections.<sup>[12]</sup> The main targets likely are the granulomas and/or mucus microaggregate biofilms located in the deep lung region and the respiratory bronchioles. Thus, characterizing the interaction of aerosolized liposomal dry powders with pulmonary mucus will help to predict their potential for lung applications.<sup>[13]</sup> In the distal airways at the alveolar air–blood epithelium, pulmonary surfactant (PS) lines the interface. This hydrophobic, lipid-rich material consists of four major surfactant proteins (SP), i.e., hydrophilic SP-A and SP-D and hydrophobic SP-B and SP-C.<sup>[14,15]</sup> Pulmonary absorption, clearance, and drug release are influenced by the bio–nano interactions with the PS that determine the fate of inhaled nanomaterials in the lungs. Depending on the type and surface properties of nanomaterials, contradicting observations range from increased uptake by opsonization through surfactant proteins to decreased uptake in case of silica nanoparticles.<sup>[16]</sup> Therefore, to evaluate possible effects of PS on the liposomes' integrity and uptake, a case-by-case study for newly developed liposomes or other nanomaterials is crucial. Broichsitter et al. demonstrated that the release of 5-carboxyfluorescein from liposomes upon contact with pulmonary surfactant (Alveofact) is altered both in vitro and in vivo.<sup>[17]</sup> Another aspect to be considered is the ability of fluoroquinolones including LVX to rapidly permeate the alveolar epithelium requiring formulation approaches to enhance lung residence time.<sup>[18]</sup>

A process often heeded only late in the development process is the demand for an inhalable dosage form with optimized aerodynamic properties and sufficient storage stability. The latter is particularly relevant for mycobacterial infections that mainly occur in low-income countries with inappropriate storage conditions. The intricacy of developing dry powders is to maintain the integrity of both the liposome and the cargo during production and storage.<sup>[19]</sup> Although liposomes are promising delivery systems, the removal of bulk water during a drying procedure may lead to the formation of their thermodynamically unstable multilamellar states when compared to solid or polymeric nanoparticles.<sup>[20]</sup> The removal of water, however, is crucial to maintain long-term colloidal and microbiological stability. Therefore, the optimization of methodical parameters is crucial to obtain dry powders with a high fine particle fraction, good flowability, and sufficient drug load while maintaining liposomal integrity.<sup>[21]</sup> Recent publications using lactose and leucine as excipients have described

Campus E8 1, Saarbrücken 66123, Germany  
K. F. W. Besecke<sup>[+]</sup>, C. Hozsa<sup>[++]</sup>, R. K. Gieseler, M. Furch<sup>[+++]</sup>  
Rodos Biotarget GmbH  
Hannover 30625, Germany  
R. K. Gieseler  
Laboratory of Immunology and Molecular Biology  
and Department of Internal Medicine  
University Hospital  
Knappschafts Krankenhaus Bochum  
Ruhr University Bochum  
Bochum 44892, Germany  
F. Waldow, D. Schwudke  
Research Center Borstel  
Leibniz Lung Center, Borstel 23845, Germany  
F. Waldow, D. Schwudke  
German Center for Infection Research  
Thematic Translational Unit Tuberculosis  
Partner Site Hamburg–Lübeck–Borstel–Riems  
Braunschweig 38124, Germany  
D. Schwudke  
German Center for Lung Research (DZL)  
Airway Research Center North (ARCN)  
Kiel Nano  
Surface and Interface Science KiNSIS  
Kiel University  
Kiel 24118, Germany  
O. Metelkina, A. Titz  
Chemical Biology of Carbohydrates (CBCH)  
Helmholtz-Institute for Pharmaceutical Research Saarland (HIPS)  
Helmholtz Center for Infection Research  
Saarbrücken 66123, Germany  
O. Metelkina, A. Titz  
Department of Chemistry  
Saarland University  
Saarbrücken 66123, Germany  
A. Titz  
Deutsches Zentrum für Infektionsforschung (DZIF)  
Hannover-Braunschweig site, Braunschweig 38124, Germany  
H. Huwer  
Cardiothoracic Surgery  
Heart Center Voelklingen, Völklingen 66333, Germany  
K. Schwarzkopf  
Department of Anaesthesia and Intensive Care  
Klinikum Saarbrücken gGmbH, Saarbrücken 66119, Germany  
J. Hoppstädter, A. K. Kiemer  
Pharmaceutical Biology  
Saarland University  
Campus C2 3, Saarbrücken 66123, Germany  
M. Koch  
INM – Leibniz Institute for New Materials  
Campus D2 2, Saarbrücken 66123, Germany



**Scheme 1.** Biological barriers in pulmonary drug delivery. Targeted liposomes and liposomal dry-powder formulations loaded with bedaquiline (BDQ) or levofloxacin (LVX), respectively, were developed to overcome such barriers. A) Interaction of liposomes with epithelial cells and pulmonary macrophages in the presence of mucus and surfactant. B) Receptor-mediated internalization of targeted liposomes into myeloid cells under submerged and air-liquid interface conditions and in the presence of pulmonary surfactant. C) Assessing antimycobacterial activity against extracellular and intracellular *Mycobacterium abscessus*. Abbreviations: MDMs: Peripheral blood monocyte-derived macrophages, dTHP-1: differentiated THP-1 cells.

the successful generation of liposomal dry powders loaded with dapson for inhalation against pulmonary infections.<sup>[22]</sup> However, these nanocarriers did not contain components for active targeting. The stability and interaction potential of a nanocarrier depends on its surface properties, which might be altered by the nature and amount of targeting ligand. Consequently, testing the targeted dry-powder formulation under relevant deposition conditions is required to evaluate the efficacy of the final product.

Here, we investigated whether the advantage of C-type lectin receptor (CLR-)TargoSphere liposomes for targeted delivery of BDQ to monocytes—the mycobacterial habitat—is maintained after their conversion into a respirable dry-powder aerosol formulation. The latter was obtained by spray-drying of liposomes, together with lactose and leucine, followed by a thorough characterization of the resulting microspheres as to their aerodynamic properties, liposomal integrity, drug load, and efficacy against *M. abscessus*. We further considered it as important to study the multiple interactions of such complex carrier systems with the lungs' biological barriers at different levels under controlled conditions in vitro. To investigate the interaction with macrophages in the presence of a lung lining fluid, we used different human cells (the differentiated THP-1 cell line, referred to as dTHP-1, as well as primary human peripheral blood-derived and pulmonary macrophages) and the commercially available phospholipid preparation, Alveofact, as suitable lung surfactant

substitute.<sup>[23]</sup> We further investigated the interaction of deposited aerosol particles with human tracheobronchial mucus. For release and permeability studies, LVX was included as a control, and to allow for some conclusions on the importance of drug properties in such interactions always by systematically comparing plain versus targeted liposomes before and after spray-drying. Finally, successful drug delivery and efficacy was assessed by the killing efficacy of *M. abscessus* in culture by powder aerosol deposition as well as by the killing of intracellular bacteria after infection of dTHP-1 cells. The overall concept of the study is summarized in Scheme 1.

## 2. Results

### 2.1. Characterization and Physicochemical Properties of Liposome Variants

Both LVX- and BDQ-loaded liposomes displayed homogenous size distributions with polydispersity index (PDI) values of <0.1 and a size range of 90–110 nm. Liposomes had a negative  $\zeta$ -potential with higher values for LVX- than for BDQ-loaded liposomes (–40 mV vs –14 mV). The aforementioned parameters remained unchanged regardless of the presence or absence of the fucose ligand for targeting of relevant macrophage CLRs such as CD206 and CD209. Table 1 summarizes the physicochemical

**Table 1.** Size, PDI,  $\zeta$ -potential, drug load and encapsulation efficacy of TargoSphere liposomes ( $n = 3$ –5 batches).

Sample	Targeting	Size [nm]	PDI	$\zeta$ -potential [mV]	Encapsulation efficacy [%]	Loading capacity [%]
TS_Levo	No	98.7 $\pm$ 3.0	0.1 $\pm$ 0.03	-39.6 $\pm$ 2.6	80.2 $\pm$ 6.9	17.2 $\pm$ 4.4
TS_Levo	Yes	110.2 $\pm$ 1.4	0.04 $\pm$ 0.01	-39.4 $\pm$ 3.5	66.0 $\pm$ 21.4	14.5 $\pm$ 5.1
TS_BDQ	No	97.6 $\pm$ 0.2	0.07 $\pm$ 0.01	-15.8 $\pm$ 1.3	98.2 $\pm$ 3.4	6.4 $\pm$ 1.3
TS_BDQ	Yes	89.2 $\pm$ 0.4	0.08 $\pm$ 0.01	-13.1 $\pm$ 1.2	98.0 $\pm$ 1.7	7.6 $\pm$ 2.5

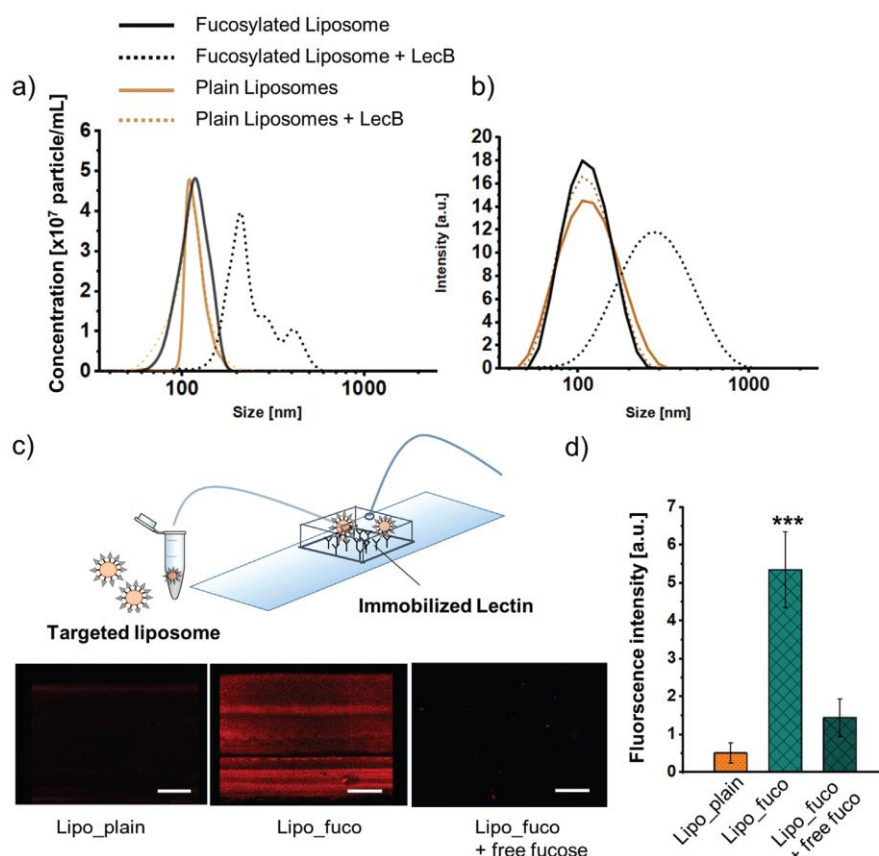


**Figure 1.** Size distribution of fucosylated liposomes in the presence of LecB after overnight incubation at a 2:1 molar ratio measured by a) particle tracking analysis and b) dynamic light scattering. c) Microfluidic assay with LecB covalently attached to the bottom of the flow chamber. Following a 10-min flush with TargoSphere liposomes and a 30-min rest, excess CLR-TargoSpheres were removed by flushing the chamber for 15 min with buffer. Images are representative for nontargeted liposomes (left), targeted liposomes (center), and targeted liposomes after an additional flushing step with competitive inhibitor (right). d) Quantification of fluorescence intensity. Error bars indicate means  $\pm$  SD ( $n = 12$ –15,  $N = 3$ ). Significance was defined as \*\*\* ( $p < 0.001$ ).

properties including the encapsulation efficiency and drug load of the respective formulations.

To verify the presence of the targeting ligands on the surface of liposomes, lectin binding assays were performed for BDQ-loaded liposomes. First, overnight incubation of liposomes with the fucose-specific *Pseudomonas aeruginosa* lectin, LecB, led to a significant shift of the size distribution to higher values as observed by nanoparticle tracking (Figure 1). This was only the case for fucosylated, but not plain liposomes, thus indicating

specific lectin-mediated liposome clustering. Next, the binding of perfused liposomes to LecB immobilized on the bottom of a microfluidic chamber was assessed.<sup>[24]</sup> Upon adding targeted liposomes for 30 min, liposomes tightly bound to the bottom of the glass slides were visualized by confocal microscopy. The resulting ten-fold difference in fluorescence intensity revealed the specific attachment of targeted liposomes to the immobilized lectin. Subsequent equilibration with buffer did not detach the TargoSphere liposomes, whereas the addition of a competitive

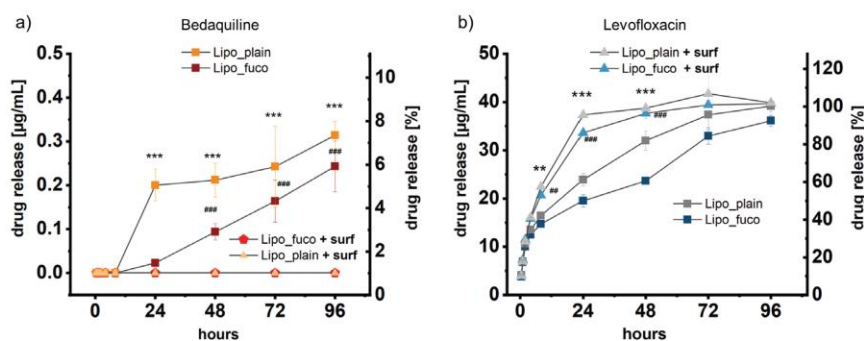


**Figure 2.** Release profiles of a) bedaquiline (BDQ) and b) levofloxacin (LVX) from fucosylated (Lipo\_fuco) and plain liposomes (Lipo\_plain) in the presence and absence of pulmonary surfactant Alveofact, respectively. LVX was released more rapidly in the presence of pulmonary surfactant (PS) and compared to BDQ. The release of BDQ did not exceed 10% after 96 h and was not detectable when PS was present in the donor medium. Error bars represent means  $\pm$  SD ( $n = 9$ ,  $N = 3$ ). Significance was defined as \*\*\*/### ( $p < 0.001$ ) and \*\*/## ( $p < 0.005$ ).

inhibitor (i.e.,  $250 \times 10^{-3}$  M L-fucose solution) removed most of them.

## 2.2. Drug Release and Permeability in Lung-Relevant Media and Cells

To determine the drug release from liposomes under lung-relevant conditions, the clinically used PS Alveofact was added to the respective release medium. **Figure 2a** shows that >80% of the more hydrophilic antibiotic, LVX, is released in the presence of PS already after 24 h, whereas in the absence of PS a similar amount was released after 72 h. In contrast, the concentration of the strongly hydrophobic and practically water-insoluble BDQ even after 96 h never exceeded 10% of the total drug load. (**Figure 2b**). After the same time, the BDQ amount in the acceptor compartment was strikingly below the detection limit when in the presence of PS. In spite of a slightly different lipid composition of the two formulations, the association of the drug within the hydrophilic core (for LVX) or the hydrophobic bilayered membrane (for BDQ) was comparable. Thus, release studies in lung-mimicking conditions revealed prominent differences depending on the nanomedical formulation (here: the liposomal composition and the biochemical nature of the encapsulated drug). Interestingly, liposomal encapsulation of LVX also reduced the membrane permeability when compared to the free drug, thereby potentially increasing the pulmonary residence time (**Figure S1a,b**, Supporting Information).

## 2.3. Cellular Liposome Uptake by Macrophages under Submerged and Air-Liquid Interface Conditions

The effect of fucose-functionalization on the cellular internalization was investigated on three different cell types, i.e., the differentiated human acute monocytic leukemia-derived cell line, dTHP-1, as well as human primary tissue-derived alveolar- and peripheral blood monocyte-derived macrophages (MDM). The selected cells, in particular the primary ones, express a high level of C-type lectin receptors, including the CD206 receptor, which facilitate mycobacterial internalization by myeloid lineage-

derived cells.<sup>[25]</sup> Similarly, the internalization of targeted liposomes by such cells is intended to shuttle the antibiotic cargo into their endosomal compartments. All types of macrophages showed an increase in uptake of PE-Texas red-labeled fucosylated liposomes after 2 h incubation at 37 °C under submerged conditions. Plain liposomes and cells pre-incubated with  $10 \times 10^{-3}$  M L-fucose solution displayed 20% lower uptake than fucosylated TargoSphere liposomes (**Figure 3** and **Figure S2**, Supporting Information). The same tendency was observed for both dTHP-1 and primary cells, although the latter showed a higher CD206 expression (**Figure S3**, Supporting Information).

To demonstrate active phagocytosis, dTHP-1 cells were additionally incubated at 4 °C, whereupon <5% of the cells showed uptake/association. This proportion of cells might indicate the extent of liposomal binding to the cell surface.

Aerosolization of liposomes on cells that were transferred to air-liquid interface allows for a simulation of pulmonary deposition in the presence or absence of pulmonary surfactant (**Figure 4**). When depositing the same dose using a vibrating mesh nebulizer, the number of positive cells generally increased when compared to submerged conditions. As the overall liposome uptake under air-liquid interface conditions was high, no surplus uptake of fucose-targeted liposomes was observed. The addition of PS to the interface did alter the uptake behavior in the case of dTHP-1 cells, attributable to a lower fluctuation in uptake compared to primary cells, preventing to assess such deviations in the latter.

## 2.4. Development of BDQ-Loaded Microparticles by Spray-Drying

To produce a nano-in-micro system for aerosol delivery to the lung, lactose-leucine-based microparticles containing plain or fucosylated liposomes were produced by spray-drying. Lactose and leucine were selected as well-established excipients for dry-powder formulations.<sup>[26]</sup> When the concentrations of lactose and leucine were optimized to 2.5% or 1% w/v, respectively, stable microparticles with a high fine-particle fraction were achieved. To determine its aerodynamic properties after adding BDQ-loaded liposomes, the microparticles were investigated using a next-generation impactor. At a flow rate of 60

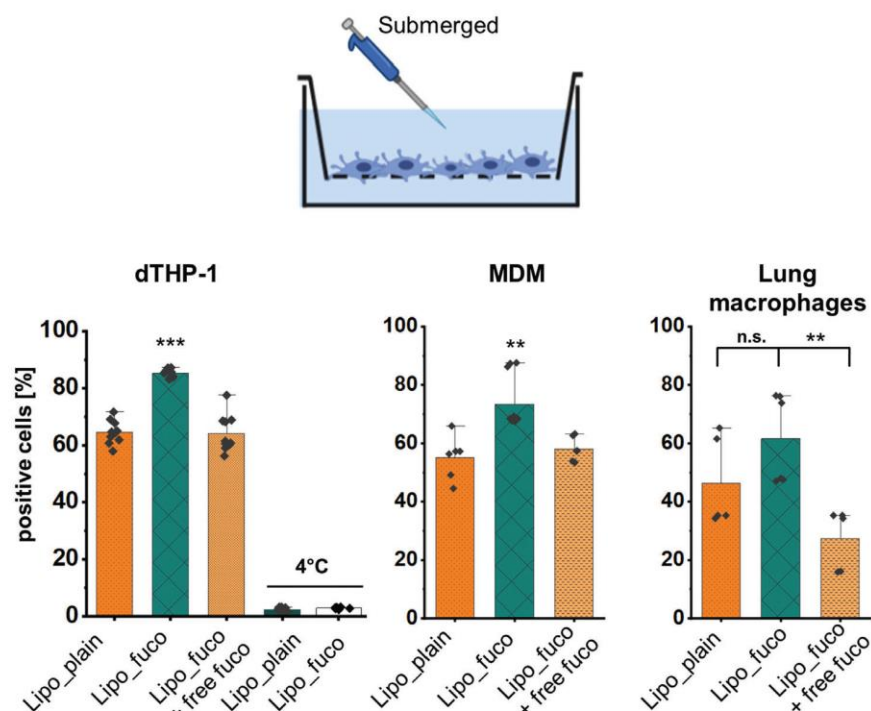


**Figure 3.** Quantification of liposome uptake by flow cytometry under submerged conditions at a concentration of  $50 \mu\text{g mL}^{-1}$  after 2 h incubation at  $37^\circ\text{C}$  in volumes of  $300 \mu\text{L}$  per condition. Fucosylated liposomes showed a higher uptake than plain liposomes. Increased uptake into human dTHP-1 cells, peripheral blood monocyte-derived macrophages (MDM) and lung tissue macrophages was reduced in the presence of free L-fucose ( $10 \times 10^{-3} \text{ M}$ ) as a competitive inhibitor. At  $4^\circ\text{C}$ , the internalization was drastically reduced due to the inhibition of active uptake, thus indicating the proportion of cell-associated liposomes in this specific case. Data represent means  $\pm$  SD ( $n = 6-9$ ,  $N = 3$  for dTHP-1 and MDM, and  $n = 3-5$  with  $N = 2$  for lung macrophages). Significance was defined as \*\*\* ( $p < 0.001$ ), \*\* ( $p < 0.005$ ), and \* ( $p < 0.05$ ).

$\text{L min}^{-1}$ , all investigated microparticles preferably deposited in stages 2–5 of the inertial impactor, which is equivalent to the fraction with a mass median aerodynamic diameter (MMAD) suitable to reach the deeper lungs. The amount of powder left in the capsule was  $<10\%$ . However, there was a portion of 15%–20% deposited in the L-shaped induction port that reflects the amount deposited in the throat (Figure 5a). Yet, the fine-particle fraction (equivalent to stages 2–5) was  $>70\%$ , and it was preserved when adding either fucosylated or plain liposomes to the microparticles. Their volume mean diameter determined by static light scattering was determined as  $2.6-3.0 \mu\text{m}$ , and all microparticles exhibited a spherical appearance and smooth surface morphology (Figure 5b and Figure S5, Supporting Information).

Maintaining the integrity of the spray-dried liposomes was essential to exert a proper functionality. This includes the liposomes' size, shape, drug load, and active targeting. Immediately after spray-drying, a 20-nm size increase was observed for both plain and fucosylated liposomes; this size did not change over a test period of six weeks (Figure 6a). The negative  $\zeta$ -potential of  $-14 \text{ mV}$  only slightly increased after spray-drying, which may contribute to stabilizing the liposomes at higher concentrations. The amount of BDQ retained in the microparticles determined by LC-MS/MS was  $1.03 \pm 0.16 \mu\text{g mg}^{-1}$  of microparticles (dry powder) for plain and  $1.00 \pm 0.19 \mu\text{g mg}^{-1}$  microparticles for fucose-targeted liposomes.

For more close inspection, cryogenic transmission microscopy images of TargoSphere liposomes from the initial batch (not spray-dried), in lactose-leucine solution (not spray-dried) and after spray-drying and redispersion were obtained (Figure 6b). Before and after spray-drying, spherical liposomes with visibly intact membranes in a size range of  $<200 \text{ nm}$  were observed. Liposome numbers were highest for those made from the initial batch with no additional dilution. The distribution of PE-Texas red-labeled liposomes within microparticles was further evaluated by confocal microscopy (Figure S6, Supporting Information).

### 2.5. Assessment of Targeting Function and Mucus Interaction after Spray-Drying

After successful spray-drying of BDQ-loaded liposomes, the functionality of fucose-targeting was explored. By applying the LecB binding assays already described in context with nonspray-dried liposomes, a LecB-mediated size increase and specific binding of fucosylated liposomes to immobilized LecB was observed (Figure 7a,b). In addition, the percentage of PE-Texas red positive dTHP-1 cells treated with microparticles consisting of fucosylated liposomes was higher compared to their plain counterparts as assessed by flow cytometry (Figure 7c), thus indicating that the targeting function is preserved after spray-drying. Next, confocal microscopy was applied to validate the efficiency of liposome

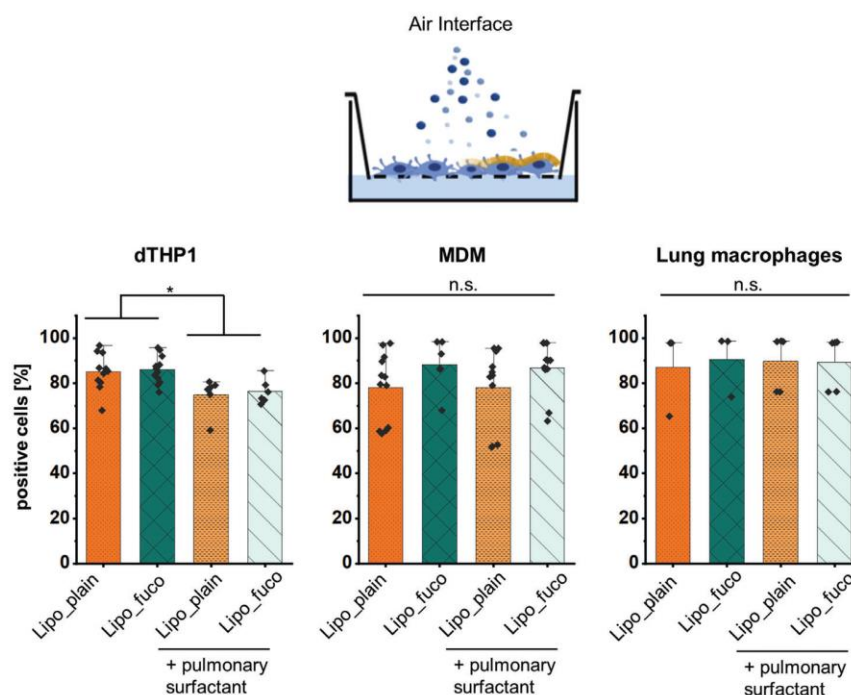


**Figure 4.** Quantification of liposome uptake by flow cytometry after aerosol deposition at a dose of 15  $\mu\text{g}/\text{well}$  after 2-h incubation at 37  $^{\circ}\text{C}$  in the presence or absence of pulmonary surfactant, Alveofact, respectively. When pulmonary surfactant was present in the interface, the uptake into dTHP-1 cells was reduced, which was not observed for blood-monocyte derived macrophages (MDM) and macrophages from human lung tissue. Data represent mean  $\pm$  SD ( $n = 6-9$ ,  $N = 3$  for dTHP-1 and MDM and  $n = 3-5$  with  $N = 2$  for lung macrophages). Significance was defined as \* ( $p < 0.05$ ).

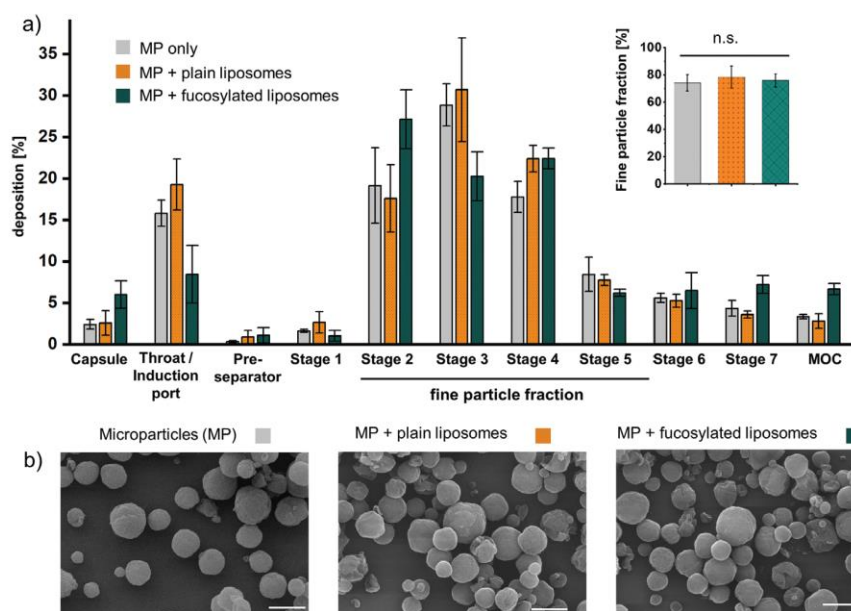


**Figure 5.** a) Aerodynamic properties of microparticles and their deposition in different stages of the next-generation impactor and b) scanning electron microscopy images of empty lactose-leucine microparticles (MP) and of MP containing fucosylated or plain liposomes, respectively. No differences in the fine-particle fraction were found between the different MP variants. Scale bars: 2  $\mu\text{m}$ . Data represent means  $\pm$  SD from three independent replicates ( $n = 9$ ,  $N = 3$ ). Cut-off sizes for the Next Generation Impactor at a flow rate of 60  $\text{L min}^{-1}$  are 8.06, 4.46, 2.82, 1.66, 0.94, 0.55, and 0.34  $\mu\text{m}$  for stages 1–7, and MOC for micro-orifice collector, respectively.<sup>[27]</sup>



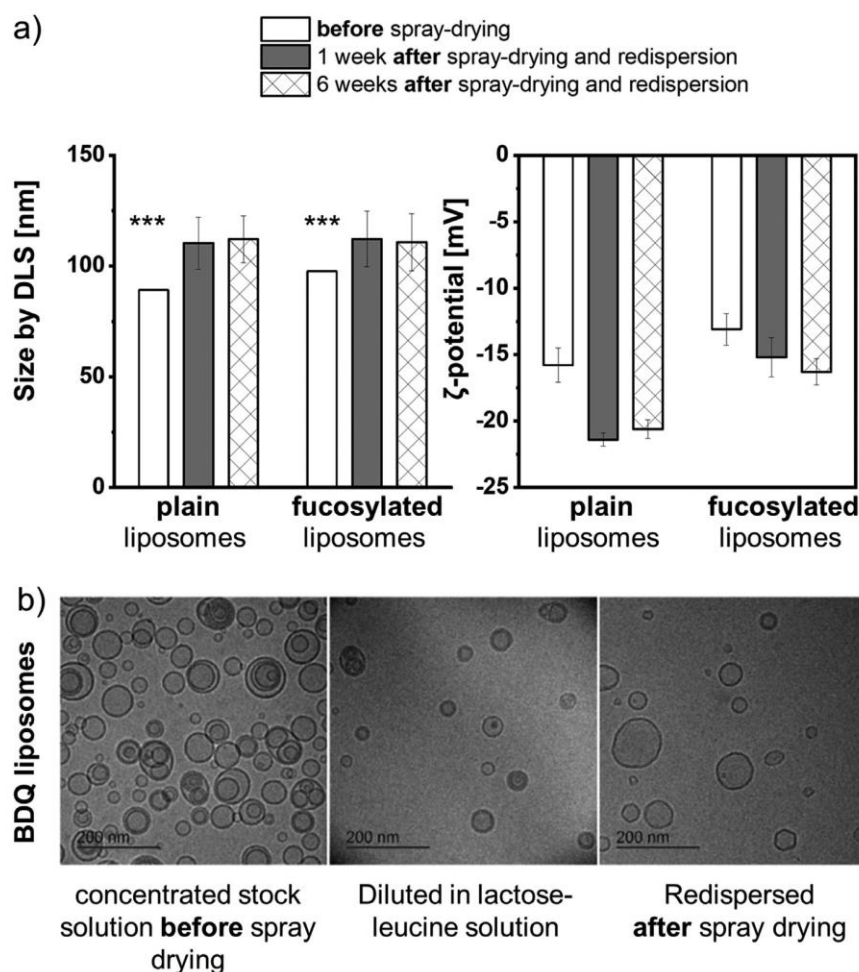


**Figure 6.** a) The initial size of the liposomes increases during spray-drying and remains constant upon six weeks of storage. b) BDQ-loaded liposomes before and after spray-drying (and redispersion) have similar sizes with intact lipid bilayers as observed by cryo-transmission electron microscopy. Data represent means  $\pm$  SD ( $n = 6-8$ ,  $N = 3$ ) with significance defined as \*\*\* ( $p < 0.001$ ).

internalization (Figure 7d). The images obtained for microparticles of fucosylated liposomes clearly depict their presence within the cells that are framed by the phalloidin-stained actin-rich filaments of the cell membrane (green, Figure 7d).

As considerable amounts of dry powder are lost in the small airways due to its interaction with pulmonary mucus, multiple particle tracking of liposomal dry powders was applied to assess the extent of liposomes that bind to the mucus layer. Therefore, microparticles were deposited on a glass slide that was covered with a small volume of human pulmonary mucus and placed into stages 2 and 3 (according to a preferential deposition of the microparticles in these stages, see Figure 5) of the next-generation impactor (Figure 8a and Figure S7, Supporting Information). Individual trajectories and mean squared displacements (MSD) of liposomes released from microparticles are represented in Figure 8b. The number of individual MSD curves with a slope  $> 0.5$  (black line)—classifying diffusive or mobile particles—was 28.6% for plain liposomes and 33.5% for fucosylated liposomes, while a slope  $< 0.5$  (red line) represents immobile particles (Fig-

ure 8b). The shift of the log (MSD) distribution to higher values highlights the interesting fact that mobile, fucosylated liposomes move more rapidly than plain ones (Figure 8c). However, as most liposomes are immobilized in the mucus meshwork, it is crucial to tune aerodynamic properties to avoid mucus interaction for maximizing the delivery into the respiratory bronchioles.

## 2.6. In Vitro Antimycobacterial Activity against *M. abscessus*

To assess the antimycobacterial activity of the dry powders and liposomes, in vitro killing assays with extracellular *M. abscessus* were performed. As the killing of extracellular bacteria does not benefit from the active targeting of macrophages, the respective experiments were performed with nontargeted formulations only. In a first step, the activity of BDQ-loaded liposomes and microparticles was assessed at different BDQ concentrations of 50, 150, and 300 ng mL<sup>-1</sup>, respectively (Figure 9a). At a concentration of only 300 ng mL<sup>-1</sup>, an almost 4-log reduc-

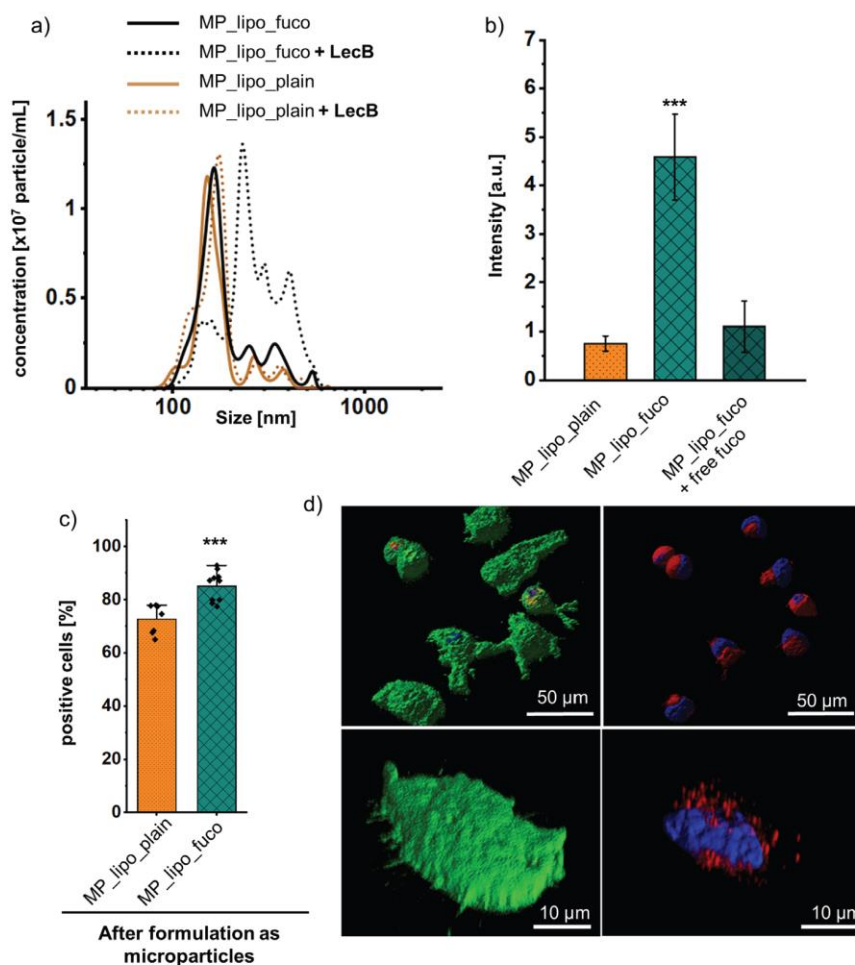


**Figure 7.** Targeting function of liposomes is preserved after spray-drying as demonstrated by the a) LecB binding assay and b) in microfluidic chambers. c) Uptake of plain (MP\_lipo\_plain) and fucosylated (MP\_lipo\_fuco) BDQ-loaded nano-in-microparticles following redispersion. Uptake after 2-h incubation at 37 °C by dTHP-1 cells evidenced by flow cytometry confirmed that active targeting was preserved. d) Representative confocal images analyzed for dissolved dry powders containing fucosylated liposomes show the intracellular localization of liposomes. Nuclei were stained with DAPI (blue), actin with phalloidin (green), and liposomes with PE-Texas red. Data represent means  $\pm$  SD ( $n = 9$ ,  $N = 3$ ) with significance defined as \*\*\* ( $p < 0.001$ ).

tion was observed for all formulations. A similar colony forming unit (CFU) reduction was achieved when microparticles were deposited as dry-powder aerosols from the air interface using the PADOCC systems (cf. the Experimental Section)<sup>[28]</sup> (Figure 9b), reflecting the deposition scenario relevant for lung applications. Noteworthy, due to a higher variation of the dose after aerosol deposition compared to submerged conditions—as reflected by a higher standard deviation—the amount of BDQ used in this experiment was increased to ensure sufficient deposition.

Finally, the effect of macrophage targeting on the reduction of intracellular bacteria was investigated on dTHP-1 cells infected with *M. abscessus*. After 24 h, all formulations (except for free BDQ) significantly reduced CFU numbers (Figure 9c). Although the killing is more pronounced for liposomes before spray-drying when compared to dry powders at the same BDQ dose, both of the targeted formulations showed improved killing compared to

the nontargeted ones after 72 h (Figure 9d). In line with this finding, only when treated with BDQ, the cell viability was similar to that of noninfected cells (Figure S8, Supporting Information). After 24 h, fucosylated liposomes (Lipo\_fuco) inhibited bacterial growth almost completely.

### 3. Discussion

We investigated the potential of fucosylated liposomes loaded with the second-line antibiotic, bedaquiline, for targeting macrophages in order to improve the killing of intracellular mycobacteria. Aiming at pulmonary administration as an aerosolized medication, we further investigated the roles of tracheobronchial mucus and pulmonary surfactant in this context. A dry-powder aerosol formulation of BDQ-liposomes was developed by spray-drying, yielding aerodynamic properties suitable

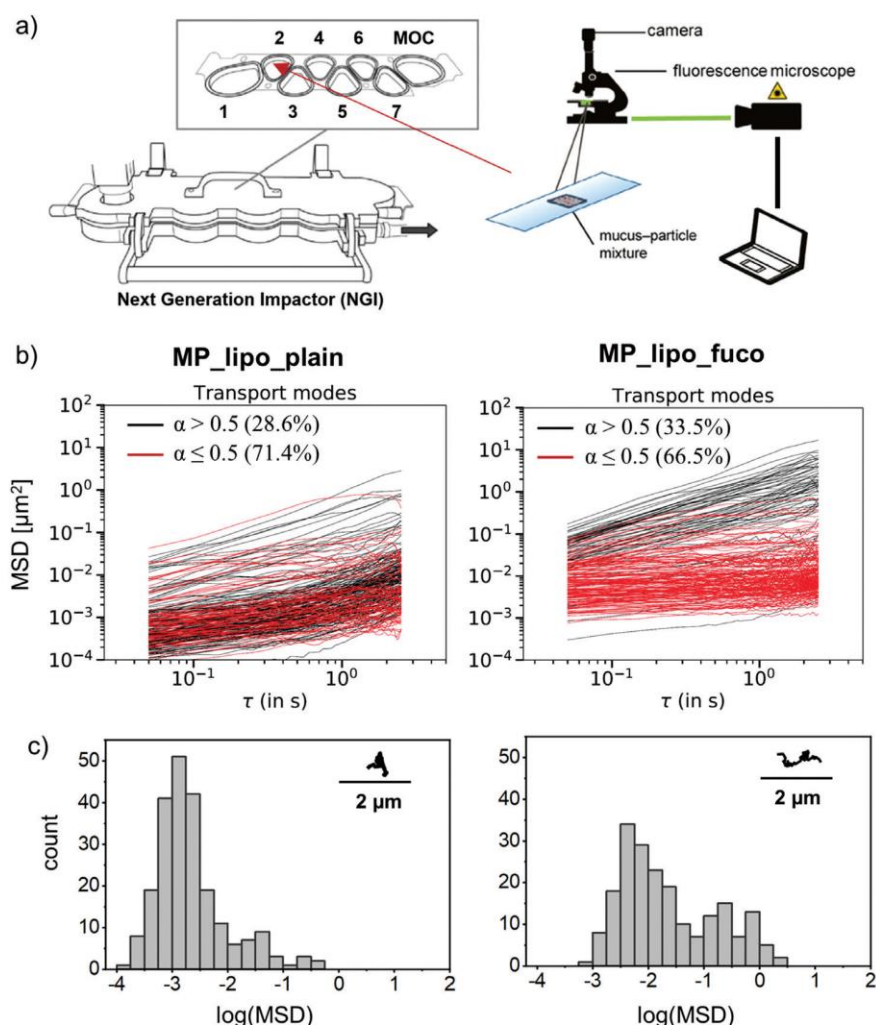


**Figure 8.** a) A slide with deposited tracheobronchial mucus was placed into stage 2 of the next generation impactor and analyzed by video microscopy after deposition of the dry powder to study the mobility of plain (MP\_lipo\_plain) and fucosylated (MP\_lipo\_fuco) liposomes released from microparticles. b) The slope of individual mean squared displacement (MSD) curves discriminates between mobile (black line,  $\alpha > 0.5$ ) and immobile (red line,  $\alpha \leq 0.5$ ) particles. Percentages indicate the mobile/immobile fraction of all tracked particles. c) The distribution of  $\log(\text{MSD})$  values at a timescale of  $t = 0.5$  s indicates a higher mobility of fucosylated liposomes, as also signified in the representative trajectory. Three independent experiments were performed with at least  $> 150$  particles/frame.

for pulmonary delivery. While maintaining the liposomal structure and targeting ability, this formulation showed promising activity against both extra- and intracellular *M. abscessus*.

The delivery of liposomes to the lungs is an appealing route for noninvasive, local therapy of infectious lung diseases.<sup>[29]</sup> Liposomes are versatile carrier systems that can be tuned in size, hydrophobicity, and release profile—and they can encapsulate a variety of drugs with different physicochemical properties, while surface engineering allows to specifically address alveolar macrophages, the cellular niche of mycobacterial infections.<sup>[30,31]</sup> Moreover, for hydrophobic (such as LVX) and poorly water soluble drugs (such as BDQ), liposomal encapsulation can solve solubility issues while reducing potential side effects including cardiotoxicity.<sup>[32]</sup>

Given a successful aerosol deposition in the alveolar region, the release and dissolution kinetics of liposomally encapsulated drugs are affected by the extremely small volumes and highly lipid-rich content of the airways' lining fluid.<sup>[33]</sup> The addition of  $1 \text{ mg mL}^{-1}$  pulmonary surfactant (here applied in the form of Alveofact) to the release medium increased the amount of LVX released after 24 h by twofold until a complete release was achieved at 48 h. This is in line with a recent study with LVX-loaded liposomes where the entire amount of drug was also released after 48 h, even though in a simple buffer (PBS, pH 7.4) only.<sup>[34]</sup> In contrast, BDQ liposomes showed literally no release when Alveofact was present in the donor medium. Also in its absence, the release did not exceed 10% even after a 96-h period. The more rapid release of LVX when compared to BDQ is likely

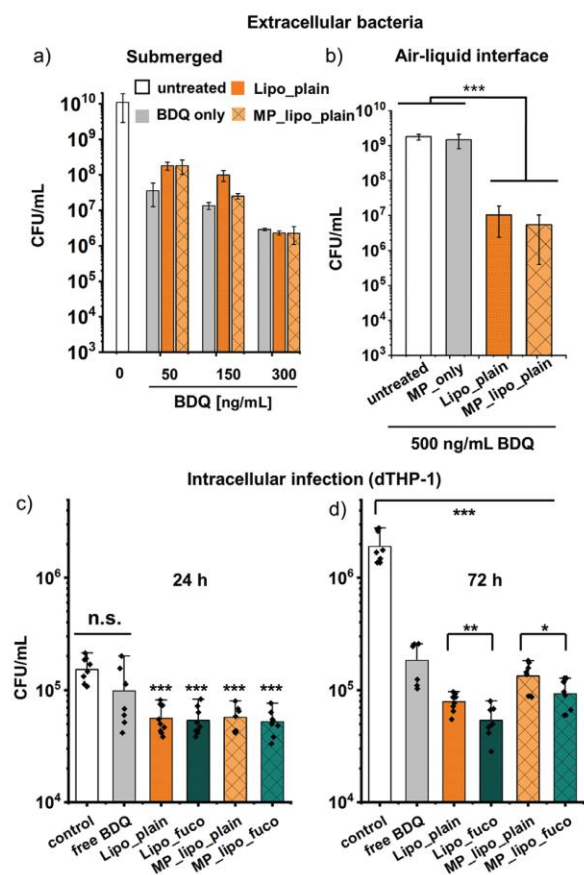


**Figure 9.** Antimycobacterial activity of free bedaquiline (BDQ), BDQ-loaded liposomes and dry powders of BDQ-loaded liposomes on extra- and intracellular *M. abscessus* under submerged and air-liquid interface conditions. a) Efficacy of the formulations against extracellular bacteria at different BDQ concentrations at submerged conditions and b) at a fixed concentration of 500 ng mL<sup>-1</sup> after dry powder aerosol deposition at air-interface conditions. Intracellular infection of dTHP-1 cells treated with free BDQ, BDQ liposomes, and the respective powders with and without fucose targeting after c) 24 h and d) 72 h. Data represent means  $\pm$  SD ( $n = 9$ ,  $N = 3$ ) with significance defined as \*\*\* ( $p < 0.001$ ), \*\* ( $p < 0.01$ ), and \* ( $p < 0.05$ ).

due to the drugs' divergent localizations within the aqueous core (LVX) as opposed to the liposomal bilayer (BDQ), respectively, thus effecting their different release profiles upon contacting a simulated pulmonary release medium.<sup>[35]</sup> However, drug release upon contact with pulmonary surfactant should not necessarily be considered a constraint, since both released and encapsulated drug can act on mycobacteria that are present both intra- and extracellularly.<sup>[36]</sup> Against this background, certain combinatorial ratios of LVX- and BDQ-loaded nano-in-micro systems might indeed offer a "best-of-both-worlds" approach as to the intra- and extracellular antimycobacterial eradication efficacy.

Some drug compounds, including fluoroquinolone antibiotics, can be cleared from the lungs by rapid transition across the pulmonary epithelium, which limits their pulmonary bioavailability, but increases their systemic exposure and the risk of as-

sociated adverse effects.<sup>[37,18]</sup> On the example of Calu-3 cells, we demonstrated that LVX liposomal encapsulation can reduce the degree of permeation through the lung epithelium.

To improve specific liposomal uptake and intracellular routing, the addition of fucose-derived targeting ligands is appealing because of their ability to bind to CLR expressed on the surface of myeloid antigen-presenting cells.<sup>[30,38,18]</sup> Such receptors include the macrophage mannose (CD206) and DC-SIGN (CD209) receptors present on alveolar macrophages that serve as entry ports and reservoirs of mycobacteria.<sup>[39,40]</sup> Following this pathway, Duran et al. demonstrated that addressing the CD206 receptor will direct fucosylated liposomes and associated antibiotics to early and late endosomes where mycobacteria typically persist. Knockout of the CD206 receptor and fucose inhibition experiments confirmed the specificity and validity of such a strategy for intracellular targeting.<sup>[10]</sup> Although macrophages have a high basal phagocytic activity, the uptake into both dTHP-1 cells and primary blood monocyte- and lung tissue-derived macrophages (all of which of human origin) clearly benefitted from active targeting. Noteworthy, to observe such elevated uptake more clearly, monocytic cells were costimulated with IL-4 to increase CD206 expression.<sup>[41]</sup> Reduced uptake of fucosylated liposomes in the presence of soluble  $\alpha$ -fucose—i.e., a direct competitive inhibitor for receptor binding—to the level of plain liposomes confirmed the involvement of this receptor-mediated mechanism. In addition, this pathway shuttles encapsulated drugs into compartments different from those addressed when being internalized via the phagocytic pathway. As reported recently, liposomes preferentially colocalize in endosomal compartments only after receptor-mediated endocytosis, where they could contribute to enhanced antibiotic efficacy.<sup>[10,42,43]</sup>

None of those studies, however, have taken into account the exposure of the targeted cells to aerosolized liposomes while introducing pulmonary surfactant as an inevitable barrier to drug delivery at the alveolar interface.<sup>[14]</sup> Surprisingly, when liposomes were deposited at the air-interface (in the absence of medium), the number of cells that showed liposome uptake was higher compared to submerged conditions, while an increase in uptake of targeted liposomes was not observed. This may be related to the absence of cell culture medium, allowing a direct particle-cell contact while neglecting sedimentation effects and the particle corona formation. Sophisticated in vitro models that include relevant lung lining fluids such as Alveofact, can therefore help to elicit cell-particle interactions more closely reflecting the real-life scenario.<sup>[44]</sup> Particle-corona formation upon contact with Alveofact may influence cellular uptake, as shown in previous studies.<sup>[45]</sup> In primary cells, however, a mitigated uptake in the presence of surfactant was not observed. Noteworthy, clinical surfactants including Alveofact do not contain hydrophilic SP-A and SP-D that are involved in host defense mechanisms and macrophage uptake while possibly underestimating the observed effects.<sup>[46]</sup>

When considering liposome administration via the pulmonary route, efficient deep lung deposition requires adequate aerodynamic properties. We therefore developed liposomal dry powders that coalesce high stability, propellant-free nature, and high patient compliance.<sup>[47]</sup> Spray-drying of liposomes in the presence of the biocompatible excipients lactose and leucine yielded spherical microparticles with a homogenous surface morphology and

a fine-particle fraction of >70%, thus meeting the criteria for deep-lung deposition.<sup>[48]</sup> Whereas an aerodynamic diameter of the dry-powder microparticles within a range of 2–5 μm is optimal for such a deposition, the size of the incorporated liposomes has to be significantly smaller. In contrast, liposomes in the size range of 100–200 nm, however, may not be optimal for efficient macrophage uptake.<sup>[49]</sup> After dissolving the microparticles, the released liposomes showed a slight size increase when compared to liposomes before spray-drying. This has been linked to structural rearrangements due to dehydration during the spray-drying process and the subsequent rehydration.<sup>[50]</sup> However, we could demonstrate that the size remained stable upon storage, and cryogenic transmission electron microscopy (cryo-TEM) images indicated that the liposomes' structural integrity is maintained during spray-drying as is mandatory for retaining their targeting function.

It is assumed that a considerable portion of inhaled dry powders is trapped by steric obstruction and adhesion to pulmonary mucus covering the airway epithelium. Via mucociliary clearance, the inhaled material is expelled from the lungs, which drastically limits the retention time and local action of therapeutic aerosols.<sup>[51]</sup> When placing human tracheobronchial mucus into stages 2 and 3 of the next generation impactor, we found that liposomes released from the deposited dry-powders are sterically trapped in the viscoelastic mucus meshwork. Besides physical and hydrophobic interactions, the fact that fucosylated liposomes moved more rapidly when compared to plain ones might be due to different surface properties because of the attachment of targeting ligands via polyethylene glycol spacers. Similar observations were made by Chai et al.—i.e., one of the few studies that investigated interactions of dry powders.<sup>[52]</sup> Hence, when engineered appropriately, biocompatible nano-in-micro formulations of BDQ-loaded liposomes can combine both the aerodynamic advantages of microparticles and the advantages of liposomes at the cellular level while coping with the cellular and noncellular pulmonary barriers.<sup>[53]</sup>

A formulation optimized to reach the target site further has to prove its antibacterial activity. Thus, the antibiotic activity was first tested against extracellular *M. abscessus*—an emerging respiratory pathogen<sup>[54]</sup>—in the absence of macrophages. When deposited as an aerosol, microparticles showed the same activity against *M. abscessus* compared to a mere liposomal suspension. Subsequently, dTHP-1 macrophages infected with *M. abscessus* were used as a model to evaluate the intracellular activity of the macrophage-targeted formulations.<sup>[55]</sup> At the early stage of mycobacterial infections, macrophages typically favor M1 polarization. However, these may develop into anti-inflammatory M2-like phenotypes during disease progression.<sup>[40]</sup> For this reason, intracellular killing studies were performed without the addition of IL-4.

Both liposomes alone as well as the liposomal dry powders exhibited an improved reduction in CFUs after 24 h compared to the free drug. When using TargoSphere liposomes surface-modified with fucose-derived targeting ligands, intracellular bacteria were killed more efficiently, most likely as a consequence of increased uptake and intracellular routing.<sup>[10,39,42]</sup> The fucosylated liposomal antibiotic formulation essentially inhibited mycobacterial growth when comparing the CFU numbers at 24 and 72 h, which can in part be explained by the relatively slow growth

of *M. abscessus* compared to other bacteria.<sup>[56]</sup> Thus, although the uptake rate of nonfucosylated versus fucosylated liposomes is already evidently higher for the latter after 2-h incubation, significant growth inhibition was only observed 72 h after treatment.

The slightly higher CFU count observed for liposomal dry powders might be related to the presence of lactose in the dry-powder formulation; lactose was earlier demonstrated to alter mycobacterial growth and metabolism because it can serve as an alternative source for carbohydrates.<sup>[57]</sup> Alternatively, a considerable fraction of extracellular bacteria present in this setup might obscure the benefit of receptor-mediated BDQ delivery to macrophages. Finally, the effect might also result from both the presence of lactose and extracellular bacteria. The actual underlying mechanism may be clarified in future studies by using more complex models.

#### 4. Conclusion

Liposomes whose surface is fucose-decorated for CLR-mediated macrophage targeting/uptake and loaded with the second-line antimycobacterial drug, bedaquiline, were developed for treating pulmonary infections by intracellular mycobacteria. Spray-drying enabled improved stability and aerodynamic properties as needed for pulmonary administration while preserving liposome size, drug load, and targeting function. Enhanced killing of intracellular *M. abscessus* was indeed observed for fucosylated as opposed to plain liposomes, suggesting that such dry-powder formulations can combine both the aerodynamic advantages of microparticles with the fucose-dependent targeting of nanocarriers to alveolar macrophages. Besides, the interaction with noncellular barriers such as mucus and surfactant were demonstrated as key factors that eventually could limit therapeutic outcomes. By improving the delivery to intracellular bacteria and reducing systemic drug exposure, targeted aerosolizable nano-in-micro delivery systems may help to cope with the ever-increasing challenge of mycobacterial resistance.

#### 5. Experimental Section

**Materials:** Lactose, L-fucose, leucine, and sodium-fluorescein were purchased from Sigma-Aldrich (Darmstadt, Germany). 1-Octanol was purchased from Honeywell (Charlotte, NC). BDQ- and LVX were obtained from Selleckchem (Munich, Germany). BDQ- and LVX-loaded liposomes (TargoSphere) were formulated by Rodos Biotarget GmbH (Hannover, Germany).

**Preparation and Characterization of Fucosylated Liposomes:** Fucosylated nanocarriers used herein were CLR-TargoSphere liposomes—i.e., one of several different lipid-based TargoSphere nanocarriers, in this case named due to their CLR specificity<sup>[30]</sup>—that were loaded with either LVX or BDQ. These formulations were prepared via the thin-film hydration method followed by extrusion as described before.<sup>[10]</sup>

Encapsulation efficiency and loading capacity were calculated as follows

$$\text{Encapsulation efficiency [\%]} = \frac{c_{\text{total}} - c_{\text{out}}}{c_{\text{total}}} \times 100 \quad (1)$$

$$\text{Loading capacity [\%]} = \frac{c_{\text{total}}}{c_{\text{lipids+targeting ligand}}} \quad (2)$$

where  $c_{\text{out}}$  is the concentration of the active pharmaceutical ingredient (API) in the supernatant after removing liposomes from the surrounding

medium via ultrafiltration using Centriscart, and where  $c_{\text{total}}$  is the whole API concentration determined after the disruption of liposomes to release the encapsulated drugs into the solvent. To calculate the loading capacity, the total drug amount ( $c_{\text{total}}$ ) is referred to that of the carrier system ( $c_{\text{lipids}} + \text{targeting ligand}$ ).

Size, PDI, and  $\zeta$ -potential of the final formulations were determined by dynamic light scattering (DLS) using a Zetasizer ZS Series (Malvern Instruments Limited, Malvern, UK). Results are summarized in Table 1.

**Drug Quantifications:** LVX- or BDQ-loaded TargoSphere batches were quantified routinely for their drug loads at the Research Center Borstel according to the following method (see also the Supporting Information):

**Drug Quantifications—Quantification of LVX and BDQ via LC-MS/MS:** Liquid chromatography was performed on an Agilent 1100 Series HPLC (Agilent Technologies, Santa Clara, CA) using a SeQuant ZIC-HILIC column (Merck Millipore SeQuant, 2.1 inner diameter  $\times$  150 mm length with 5  $\mu\text{m}$  particle size, pore size 200 Å) at a column temperature of 30 °C. The mobile phase consisted of 1% formic acid (FA, solvent A) and acetonitrile (ACN, solvent B).

**Drug Quantifications—Extraction of LVX and BDQ for LC-MS/MS:** 20  $\mu\text{L}$  of BDQ- or LVX-loaded fucosylated liposomes were diluted in 800  $\mu\text{L}$  ACN and 180  $\mu\text{L}$  1% FA, followed by thorough vortexing. Afterward, 20  $\mu\text{L}$  of this mixture was further diluted in 800  $\mu\text{L}$  ACN and 180  $\mu\text{L}$  1% FA. The solution was vortexed again and then centrifuged for 10 min at 15,000 $\times$  g at RT.  $\approx$ 500  $\mu\text{L}$  of the resulting supernatant were transferred to a 1.5 mL Eppendorf tube and recentrifuged under the same conditions. Next, 60  $\mu\text{L}$  supernatant were transferred to a vial (three aliquots per sample); the injection volume was 5  $\mu\text{L}$  for LC-MS/MS analysis.

Quantifications of BDQ and LVX in dry-powder formulations were performed as described below:

**Drug Quantifications—LVX Quantification by HPLC:** LVX was quantified using a Dionex Ultimate 3000 U-HPLC equipped with a Synchronis C18 50  $\times$  2.1 mm, 1.7  $\mu\text{m}$  column, and a UV-vis detector (all from Thermo Fischer, Dreieich, Germany). The system was operated at a flow of 0.3 mL  $\text{min}^{-1}$  with 18% of mobile phase A (acetonitrile, Sigma, Germany) and 72% of mobile phase B (0.5% trimethylamine buffer at pH 2.5). Data analysis was performed with Chromeleon 7 software (Thermo Fischer, Germany).

**Drug Quantifications—BDQ Quantification by LC/MS:** Analysis was performed using an Accela UHPLC system coupled with a TSQ Quantum Access Max tandem quadrupole mass spectrometer (both from Thermo Fisher Scientific, Waltham, USA). An Accucore RP-MS column (150  $\times$  2.1 mm, 1.7  $\mu\text{m}$ ; Thermo Fisher Scientific) was eluted with mobile phase A consisting of acetonitrile + 0.1% formic acid and mobile phase B consisting of  $\text{H}_2\text{O}$  + 0.1% formic acid. The gradient elution was applied as follows: 2 min elution at 10% A and a subsequent increase to 99% A until minute 8, which was then maintained for 3 min follow by a return to initial conditions. The system was operated at a flow rate of 0.3 mL  $\text{min}^{-1}$ , with the column oven set at 40 °C. The transitions were monitored using selected reaction monitoring of BDQ (parent mass 557.15 m/z) with fragments A (58.2 m/z) and B (330.06 m/z) using heated electrospray ionization (H-ESI) in the positive ion mode. The entire system was operated via the standard software Xcalibur (Thermo Fisher Scientific).

**Verification of the Targeting Function of Fucosylated Liposomes—LecB Binding Assay:** To verify the presence of targeting ligands on the liposomes' surface, fucosylated and nonfucosylated (control) liposomes were incubated overnight in the presence of the *Pseudomonas aeruginosa* fucose-binding lectin, LecB.<sup>[58]</sup> In brief, BDQ-loaded liposomes were incubated overnight in PBS- $\text{Ca}^{2+}$  buffer (pH 7.4, 50  $\times$  10<sup>-6</sup> M  $\text{Ca}^{2+}$ ) at a 2:1 molar ratio of LecB/fucose-ligand. The next day, the size of the liposomes was measured by dynamic light scattering using a Zetasizer ZS Series (Malvern Instruments Limited) and by Nanoparticle Tracking Analysis (NTA LM-10, Malvern).

**Verification of the Targeting Function of Fucosylated Liposomes—Flow-Chamber Experiments:** To demonstrate the ability of fucose-decorated liposomes to interact with LecB, a fluorescence intensity-based microfluidic assay was applied.<sup>[59]</sup> Plain or fucosylated liposomes (300  $\mu\text{g mL}^{-1}$ ) in PBS/ $\text{Ca}^{2+}$  were injected into a flow chamber containing immobilized LecB for 10 min at a rate of 0.5 mL  $\text{min}^{-1}$  followed by a 30 min incuba-

tion period. Finally, to detach lectin-bound liposomes, the chamber was equilibrated for 10 min with a L-fucose solution (250  $\times$  10<sup>-3</sup> M). Images were acquired with a Leica DMI8 confocal microscope (Leica Microsystems, Wetzlar, Germany) equipped with a 25 $\times$  water immersion objective after each equilibration step. Image processing and quantification was performed using ImageJ, version 1.52 (NIH, Bethesda, MD).

**Pulmonary Interaction Studies—Drug Release in the Presence of Pulmonary Surfactant:** Prior to the experiment, LVX- and BDQ-loaded liposomes were ultrafiltrated using Centriscart I 300000 MWCO (Sartorius, Göttingen, Germany) for 30 min at 2000 g to remove nonencapsulated drug. The release system consisted of a Slide-A-Lyzer MINI Dialysis Device with 10000 Dalton MWCO (Thermo Fisher, Karlsruhe, Germany) placed into a 12-well plate (Greiner bio-one, Frickenhausen, Germany) and filled with 3.5 mL PBS in case of LVX and PBS + Moviol 4-88 (3% w/v) (Sigma-Aldrich, Darmstadt, Germany) in case of BDQ. The plate was covered and placed on an orbital shaker operating at 300 rpm at RT. A volume of 150  $\mu\text{L}$  of liposomes (250 and 25  $\mu\text{g mL}^{-1}$  final concentration of LVX or BDQ, respectively) was added to the apical side of the dialysis device, and 200- $\mu\text{L}$  volumes were sampled at the respective time intervals from the acceptor compartment. Removed medium was replaced with fresh buffer, and the cumulative permeated mass was calculated. To study to the impact of pulmonary surfactant on the release kinetics, experiments were performed in the presence of Alveofact (Lyomark Pharma, Oberhaching, Germany) added to the donor compartment at a final concentration of 1 mg  $\text{mL}^{-1}$ .

**Pulmonary Interaction Studies—Pulmonary Mucus Extraction:** Mucus was collected from endotracheal tubes of patients undergoing elective surgery at the Klinikum Saarbrücken gGmbH (Saarbrücken, Saarland, Germany) according to the protocol approved by the Ethics Committee of the Saarland Medical Chamber (file number 19/15), and in line with the 2013 Declaration of Helsinki, as previously described. All patients provided written informed consent before enrollment. Only nonsmokers and patients without lung disease were included in this study. Briefly, endotracheal tubes obtained from mechanically ventilated patients were cut down to 10–15 cm pieces and centrifuged twice at 1000 rpm at 4 °C for 30 s, each, to spin down the mucus. Samples were stored at -20 °C and gradually thawed overnight prior to experimental use.<sup>[60]</sup>

**Pulmonary Interaction Studies—Multiple Particle Tracking in Pulmonary Mucus:** A glass slide with a 10  $\times$  10 mm gene frame chamber (Thermo Fisher Scientific) attached to the surface was placed into stages 2 or 3 of the NGL. After dry-powder deposition, the chamber was sealed with a cover slip and imaged immediately. Measurements were performed with a Nikon Eclipse Ti-S inverted fluorescence microscope equipped with a Nikon Intensilight 130 W mercury lamp and 40 $\times$  S-plan Fluor Nikon objective with a numerical aperture of 0.6 (all from Nikon, Tokyo, Japan). Short tracking videos of  $\geq$ 20 s length were recorded at a frame rate of 20 frames per second (fps) with an Orca R2 monochrome 1.3 MP CCD camera (Hamamatsu) at a resolution of 0.135  $\mu\text{m pixel}^{-1}$ . 2D displacement in the X and Y directions was obtained using a ParticleTracker from MOSAIC ToolSuite (Plugin for ImageJ) developed by Sbalzarini and Koumoutsakos for each individual frame.<sup>[61]</sup> A custom-made Python script calculated the averaged mean squared displacement (MSD or  $\Delta r^2(\tau)$ )

$$(\Delta r^2(\tau)) = (\Delta x^2 + \Delta y^2) \quad (3)$$

The slope (defined as  $\alpha$ ) of the resulting MSD allows to calculate the extent of particle diffusion within the mucus samples. We defined an arbitrary cut-off at  $\Omega = 0.5$ , thus considering particles with  $\alpha < 0.5$  as immobile and such with a slope  $> 0.5$  as mobile within the tested mucus sample.

**Cell Culture, Isolation, and Differentiation—THP-1 Cells:** The THP-1 human monocytic leukemia cell line (DSMZ, Braunschweig, Germany) was cultured in medium RPMI 1640 supplemented with 10% FCS during passages 8–20 at a density not exceeding 1  $\times$  10<sup>6</sup> cells  $\text{mL}^{-1}$ . In a 24-well plate (Greiner bio-one, Frickenhausen, Germany), 200 000 cells/well at 0.5 mL were differentiated for 48 h in the presence of 25 ng  $\text{mL}^{-1}$  of phorbol-12-myristate-13-acetate (PMA, Sigma Aldrich, Darmstadt, Germany) and interleukin 4 (IL-4, Sigma Aldrich, Darmstadt, Germany) and kept in cul-

ture for an additional 24-h period. Differentiated THP-1 cells are referred to as dTHP-1 cells.

**Cell Culture, Isolation, and Differentiation—Blood MDM:** Buffy coats were obtained from healthy adult blood donors (Blood Donation Center, Saarbrücken Germany) and approved by the local ethics committee (State Medical Board of Registration, Saarbrücken, Germany, permission no. 173/18). In a first step, blood mononuclear cells were separated by gradient centrifugation using Leucosep falcon tubes (Greiner, Bio-One, Frickenhausen, Germany) in lymphocyte separation medium (Sigma, Germany). Subsequently, cells were washed twice with PBS without  $\text{Ca}^{2+}/\text{Mg}^{2+}$  (Sigma Aldrich, Darmstadt, Germany) containing EDTA ( $2 \times 10^{-3}$  M, Sigma, Germany). Monocytes were enriched by positive selection using anti-CD14 microbeads (Miltenyi Biotec, USA) according to the manufacturer's protocol, and seeded at a density of  $2 \times 10^5$  cells/200- $\mu\text{L}$  well, and cultured in medium RPMI 1640 supplemented with 10% (v/v) FCS, 1% (v/v) glutamine and 1% (v/v) penicillin/streptomycin (P/S) for 6 d at  $37^\circ\text{C}$  and 5%  $\text{CO}_2$ . Throughout this period, cells were supplemented with  $10 \text{ ng mL}^{-1}$  human recombinant macrophage colony-stimulating factor (M-CSF, Miltenyi, Germany) and  $20 \text{ ng mL}^{-1}$  IL-4 (Sigma Aldrich, Darmstadt, Germany). Medium and supplements were renewed every second day.

**Cell Culture, Isolation, and Differentiation—Alveolar Macrophages:** Lung tissue was obtained from patients undergoing lung resection at the SHG Kliniken Völklingen with the consent of the Local Ethics Committee (State Medical Board of Registration, Saarland, Germany) and in line with the 2013 Declaration of Helsinki, as previously described. All patients provided written informed consent before enrollment. Only nonsmokers and patients without lung disease were included in this study. In brief, lung tissue was chopped into small pieces of  $\approx 5 \mu\text{m}$  and washed with balanced salt solution (BSS,  $137 \times 10^{-3}$  M NaCl,  $5 \times 10^{-3}$  M KCl,  $0.7 \times 10^{-3}$  M  $\text{Na}_2\text{HPO}_4$ ,  $10 \times 10^{-3}$  M HEPES,  $5.5 \times 10^{-3}$  M glucose, pH 7.4) with a  $100\text{-}\mu\text{m}$  pore size cell strainer (BD, Heidelberg, Germany). This filtrate mainly comprising erythrocytes and alveolar macrophages was washed again with medium RPMI 1640 (Gibco, Darmstadt, Germany) containing 5% v/v FCS and 1% v/v P/S. Next, cells were added to three Petri dishes and incubated for 1 h ( $37^\circ\text{C}$ , 5%  $\text{CO}_2$  and 95% humidity). Nonadherent erythrocytes were removed from the adherent alveolar macrophages by three washes with BSS. Cells were then cultured in medium RPMI 1640 with medium exchange after 24 h. On day 3, cells were detached with trypsin (Sigma, Germany) and counted in a Neubauer hemocytometer (Sigma Aldrich, Darmstadt, Germany) containing trypan blue for dead-cell exclusion. A total number of 200 000 cells/200- $\mu\text{L}$  well were seeded in either 12-well Transwell permeable supports ( $0.4 \mu\text{m}$  pore size, Corning Costar, Bodenheim, Germany) or 24-well plates (Greiner Bio-One), respectively.

**Uptake Studies—Particle Uptake:** The respective macrophage variants were seeded at a density of 200 000 cells/well in 24-well plates for submerged conditions or 12-well Transwell plates for air–liquid interface conditions. Prior to the experiment, cells were washed with PBS without  $\text{Ca}^{2+}/\text{Mg}^{2+}$ , 300  $\mu\text{L}$  of BDQ-loaded liposomes ( $50 \mu\text{g mL}^{-1}$  in medium RPMI 1640) were added, and the cells were incubated for 2 h at  $37^\circ\text{C}$ . Alternatively, medium was removed from the apical side of the Transwell, and the same liposomes were deposited with a Vitrocell cloud system (Vitrocell, Waldkirch, Germany) at a final dose of 15  $\mu\text{g}$  liposomes/well in the presence or absence of 20  $\mu\text{L}$  of pulmonary surfactant (Alveofact at  $5 \text{ mg mL}^{-1}$ ). After 2-h incubation, cells were washed twice with PBS without  $\text{Ca}^{2+}/\text{Mg}^{2+}$ , and 100  $\mu\text{L}$  accutase solution (Sigma) was added for 25–30 min for cell detachment.

**Uptake Studies—Flow Cytometry:** Cells were transferred to FACS tubes (Greiner, Frickenhausen, Germany) centrifuged at  $300 \times g$  for 5 min, and resuspended in PBS containing 4% FCS. Cells were measured at  $>10\,000$  cells/sample with a BD LSRFortessa flow cytometer (BD Bioscience, San Jose, CA) and analyzed with FlowJo software, version 10.7.1 (FlowJo, Ashland, OR).

**Microparticle Production and Characterization: Production of Dry Powders:** 2.5% (w/v) of lactose solution was prepared by dissolving the lactose in Milli-Q water by overnight stirring at 650 rpm. Leucine was added to meet a final concentration of 1% (w/v) and stirred until complete dissolution. This solution was filtered using a  $0.45\text{-}\mu\text{m}$  filter. 120  $\mu\text{L}$  of BDQ-loaded

plain or fucosylated liposomes were added to the solution and gently dispersed for 5 min. The lactose microparticles used for confocal microscopy and NGI experiments were additionally stained with sodium-fluorescein at a final concentration of 1% (w/v). The solution containing lactose, leucine, liposomes, and sodium-fluorescein was spray-dried using a Büchi-90 nano spray-dryer (Büchi, Flawel, Switzerland) under the following conditions (gas flow:  $112 \text{ L min}^{-1}$ ; frequency: 122 kHz, inlet temperature:  $87^\circ\text{C}$ , outlet temperature:  $35^\circ\text{C}$ , pump: 30%, spray: 80%, pressure: 37–38 mbar, and room humidity: 20%–30%). Produced microparticles were collected using a clean plastic scraper and stored in a desiccator at RT in the dark.

**Microparticle Production and Characterization—Scanning Electron Microscopy:** Powder formulations obtained by spray-drying were deposited on a carbon tape while applying mild airflow to remove loosely bound particles from the surface. The samples were gold-coated (Quorum Q150R ES) and examined in a Zeiss EVO MA15 LaB<sub>6</sub> field emission scanning electron microscope (Zeiss, Oberkochen, Germany) at 5.0 kV and 20 000 $\times$  magnification.

**Microparticle Production and Characterization—Aerodynamic Properties of Dry-Powder Formulations:** A next-generation impactor (NGI, model 170, Copley Scientific, Nottingham, UK) equipped with an Akita airflow unit was used to study the aerodynamic properties of the dry-powder formulations. In brief, 10 mg of each powder sample was weighed into a clear gelatin capsule. NGI plates were coated with a 1% (w/v) polyalkylene glycol ether (Brij35) and glycerol coating solution to ensure proper particle binding to the surface of the plate upon air circulation. The capsule was placed inside a HandiHaler (Boehringer Ingelheim, Ingelheim, Germany), and the capsule was pierced once to release the dry powders. The HandiHaler was connected to a mouth piece adaptor, and pressurized air was applied for 4 s at a rate of  $60 \text{ L min}^{-1}$ . Samples from all eight stages, tube, pre-separator, and empty capsule were collected by redispersion in Milli-Q water. The fluorescence intensity of the labeled dry powders was analyzed on a M200 plate reader (Tecan, Crailsheim, Germany) at  $\lambda_{\text{ex}} = 460 \text{ nm}$  and  $\lambda_{\text{em}} = 515 \text{ nm}$ . Particles in stages 2–5 were considered as a respirable portion based on their MMAD of 1–5  $\mu\text{m}$ .

**Microparticle Production and Characterization—Cryogenic Transmission Electron Microscopy:** Cryo-TEM was performed on liposomes in PBS, liposomes in lactose–leucine solution, and on redispersed spray-dried microparticles pelleted after ultracentrifugation. Briefly, 3  $\mu\text{L}$  of sample was dropped onto a holey carbon grid (type S147-4, Plano, Wetzlar, Germany) and blotted for 2 s before plunging into liquid ethane using a Cp3 cryo plunger (Gatan, Pleasanton, CA) operating at  $T = -165^\circ\text{C}$ . The sample was immersed in liquid nitrogen, transferred to a cryo-TEM sample holder (Gatan model 914), and investigated at  $T = -173^\circ\text{C}$  by low-dose TEM bright-field imaging using a JEOL (Tokyo, Japan) JEM-2100 LaB<sub>6</sub> at an accelerating voltage of 200 kV.

**Microparticle Production and Characterization—Size and  $\zeta$ -Potential:** Hydrodynamic diameter and  $\zeta$ -potential of liposomal dry powders were determined by dynamic light scattering (Zetasizer Nano-ZS, Malvern Instruments) in PBS without  $\text{Ca}^{2+}/\text{Mg}^{2+}$ . 10 mg of the respective dry powders were dispersed in 1 mL of PBS and vortexed for 5 min, followed by 15 min ultrasound, and measured immediately. Measures were taken before dry-powder production as well as after one or six weeks, respectively.

**Antimycobacterial Activity—Bacterial Culture:** The *M. abscessus* smooth variant isolated from the sputum of patients with cystic fibrosis was grown for 72 h at  $37^\circ\text{C}$  in 7H11 agar medium supplemented with 10% Middlebrook OADC (both from Sigma, Germany). Single colonies were inoculated into 50 mL 7H9 medium + 10% OADC and incubated for 72 h at  $37^\circ\text{C}$ . Overnight cultures of *M. abscessus* were diluted (final OD 0.001) to a final volume of 100  $\mu\text{L}$  in 7H9 medium and placed onto Corning Costar Snapwell permeable supports ( $0.4 \mu\text{m}$  pore size, Corning Costar, NY). After dry-powder aerosol deposition (see below), inserts were placed into 12-well plates with some plates filled with PBS to prevent evaporation. Bacteria were grown for 72 h ( $37^\circ\text{C}$ , 5%  $\text{CO}_2$ , 95% RH) followed by CFU determination by dilution plating on 7H11 agar plates.

**Antimycobacterial Activity—Dry-Powder Deposition on Cell Culture:** Dry-powder formulations were deposited using the dry-powder deposition device on cell culture (PADDCCC) as described previously.<sup>[28]</sup> In brief, 100 mg of dry powder was filled into a gelatin capsule, which then was

inserted into a HandiHaler (Boehringer Ingelheim). The airstream generated by the Akita Jet System (OxyCare GmbH, Bremen, Germany) creates a pressure that releases the content of the capsule. Large particles are impacted, and the remaining smaller particles were allowed to settle for 10 min. The exposure was repeated three times to ensure a complete release of the dry powder from the capsule. The deposited amount of dry powder, as determined by measuring the fluorescence of the fluorescein labeled microparticles in the acceptor compartment, is 0.5% of the initial powder mass.

**Antimycobacterial Activity—Intracellular Infection:** dTHP-1 cells were generated as described above and infected with *M. abscessus* at a multiplicity of infection of 1:1. After 3 h, infected cells were washed carefully with HBSS (Sigma, Germany) to remove extracellular bacteria. Cells were treated with medium containing Lipo\_plain, Lipo\_fuco, MP\_lipo\_plain, MP\_lipo\_fuco, or nonencapsulated BDQ, at equal BDQ concentrations for 24 or 72 h, respectively. Infected but untreated cells in medium RPMI 1640 served as a control. After each time point, the cells were washed with PBS without  $\text{Ca}^{2+}/\text{Mg}^{2+}$ , and incubated in sterile deionized  $\text{H}_2\text{O}$  for 30 min to lyse the cells and release the intracellular bacteria. Serial dilutions of 1:10 on 7H11 agar plates were performed for CFU determination.

**Statistical Analysis:** Results were provided as means  $\pm$  SD and sample sizes provided as  $N =$  independent experiments, and  $n =$  number of total measurements for all experiments with statistical analysis. One-way ANOVA followed by Tukey's multiple comparison test was used for statistical analysis using OriginPro 2021, version 9.8.0.200. Significance was defined as \*\*\*/### ( $p < 0.001$ ) and \*\*/## ( $p < 0.005$ ), unless otherwise specified.

## Supporting Information

Supporting Information is available from the Wiley Online Library or from the author.

## Acknowledgements

This project (acronymized ANTI-TB) was funded by the German Federal Ministry of Education and Research (*Bundesministerium für Bildung und Forschung* [BMBF], Berlin, Germany), under grant agreement FKZ: 16GW0167/GWANTA20. A.T. acknowledges support from the European Research Council for an ERC Starting Grant (Sweetbullets, grant no. 716311). The authors would like to thank Prof. John Pery (Microbiology Department, Freeman Hospital, The Newcastle upon Tyne Hospitals NHS Foundation Trust, Newcastle upon Tyne, UK) for providing the *Mycobacterium abscessus* smooth variant; Pascal Paul for his kind support in LCMS analysis; and Jonathan O'Connor and Andreas Manz for providing PDMS flow chambers. The BioRender program (Toronto, ON, Canada) was used to create some of the figures used in this paper.

Open access funding enabled and organized by Projekt DEAL.

## Conflict of Interest

The authors declare no conflict of interest.

## Author Contributions

B.C.H. designed the study, performed most of the laboratory experiments, interpreted the data, and drafted the manuscript. D.T. helped in the design of the study, performed spray-drying experiments, and interpreted the data. A.B. and A.B. performed in vitro experiments with *Mycobacterium abscessus* and reviewed the manuscript. C.C.-W. supervised these experiments. K.F.W.B. and C.H. produced and provided fucosylated liposomes (a.k.a. TargoSphere). R.K.G. and M.F. were involved in the data interpretation and reviewed the manuscript. F.W. and D.S. performed quantitative

analysis of antibiotics. O.M. provided LecB and lectin-immobilized flow chambers and helped in performing lectin binding assays, and A.T. supervised this work. H.H. provided lung tissue, K.S. provided pulmonary mucus, and J.H. provided buffy coats. M.K. and D.T. performed cryo-TEM imaging. B.L. and C.M.L. interpreted data, drafted the manuscript, as well as conceptualized and supervised the work. All authors critically revised the paper for important intellectual content and finally approved the paper in the present form. All authors agreed to be accountable for their respective contribution of the work in ensuring that questions related to the accuracy or integrity of the work were appropriately investigated and resolved.

## Data Availability Statement

The data that support the findings of this study are available from the corresponding author upon reasonable request.

## Keywords

air–liquid interfaces, bedaquiline, liposomal dry powders, particle tracking, pulmonary surfactants

Received: October 4, 2021

Revised: January 14, 2022

Published online:

- [1] J. Chakaya, M. Khan, F. Ntoumi, E. Aklillu, R. Fatima, P. Mwaba, N. Kapata, S. Mfinanga, S. E. Hasnain, P. D. M. C. Katoto, A. N. H. Bulabula, N. A. Sam-Agudu, J. B. Nachega, S. Tiberi, T. D. McHugh, I. Abubakar, A. Zumla, *Int. J. Infect. Dis.* **2021**.
- [2] B. Nabi, S. Rehman, S. Aggarwal, S. Baboota, J. Ali, *Drug Delivery Transl. Res.* **2020**, *10*, 1111.
- [3] S. Menina, J. Eisenbeis, M. A. M. Kamal, M. Koch, M. Bischoff, S. Gordon, B. Loretz, C.-M. Lehr, *Adv. Healthcare Mater.* **2019**, *8*, 1900564.
- [4] M. Laudon, B. Romanowicz, 11th Annual TechConnect World Innovation Conference & Expo, May 14–17, **2017**.
- [5] P. Muttill, C. Wang, A. J. Hickey, *Pharm. Res.* **2009**, *26*, 2401.
- [6] S. P. Newman, *Ther. Delivery* **2017**, *8*, 647.
- [7] D.-K. Ho, B. L. B. Nichols, K. J. Edgar, X. Murgia, B. Loretz, C.-M. Lehr, *Eur. J. Pharm. Biopharm.* **2019**, *144*, 110.
- [8] a) S. J. Rose, M. E. Neville, R. Gupta, L. E. Bermudez, *PLoS One* **2014**, *9*, e108703; b) J. Zhang, F. Leifer, S. Rose, D. Y. Chun, J. Thaisz, T. Herr, M. Nashed, J. Joseph, W. R. Perkins, K. DiPettillo, *Front. Microbiol.* **2018**, *9*, 915.
- [9] a) W. Wijagkanalan, S. Kawakami, M. Takenaga, R. Igarashi, F. Yamashita, M. Hashida, *J. Controlled Release* **2008**, *125*, 121; b) C. Kelly, C. Jefferies, S.-A. Cryan, *J. Drug Delivery* **2011**, *2011*, 727241.
- [10] V. Durán, E. Grabski, C. Hozsa, J. Becker, H. Yasar, J. T. Monteiro, B. Costa, N. Koller, Y. Lueder, B. Wiegmann, G. Brandes, V. Kaever, C.-M. Lehr, B. Lepenies, R. Tampé, R. Förster, B. Bošnjak, M. Furch, T. Graalman, U. Kalinke, *J. Controlled Release* **2021**.
- [11] X. Murgia, C. de Souza Carvalho, C.-M. Lehr, *Eur. J. Nanomed.* **2014**, *6*.
- [12] K. To, R. Cao, A. Yegiazaryan, J. Owens, V. Venketaraman, *J. Clin. Med.* **2020**, *9*.
- [13] a) Y. Li, E. Arranz, A. Guri, M. Corredig, *Food Res. Int.* **2017**, *92*, 128; b) D. Chen, D. Xia, X. Li, Q. Zhu, H. Yu, C. Zhu, Y. Gan, *Int. J. Pharm.* **2013**, *449*, 1.
- [14] A. Hidalgo, A. Cruz, J. Pérez-Gil, *Eur. J. Pharm. Biopharm.* **2015**, *95*, 117.
- [15] A. Hidalgo, A. Cruz, J. Pérez-Gil, *Biochim. Biophys. Acta, Biomembr.* **2017**, *1859*, 1740.



- [16] a) C. A. Ruge, J. Kirch, O. Cañadas, M. Schneider, J. Perez-Gil, U. F. Schaefer, C. Casals, C.-M. Lehr, *Nanomedicine* **2011**, *7*, 690; b) M. Radiom, M. Sarkis, O. Brookes, E. K. Oikonomou, A. Baeza-Squiban, J.-F. Berret, *Sci. Rep.* **2020**, *10*, 19436.
- [17] M. Beck-Broichsitter, F. Waldow, D. Schwudke, K. I. Gaede, C. Feldmann, P. Carius, C. Autilio, J. Perez-Gil, K. Schwarzkopf, X. Murgia, B. Loretz, C.-M. Lehr, *Small Sci.* **2021**, *1*, 2100067.
- [18] J. Brillault, F. Tewes, *Pharmaceutics* **2020**, *12*.
- [19] P. Goldbach, H. Brochart, A. A. Stamm, *Drug Dev. Ind. Pharm.* **1993**, *19*, 2611.
- [20] L. Willis, D. Hayes, H. M. Mansour, *Lung* **2012**, *190*, 251.
- [21] G. P. Alves, M. H. A. Santana, *Powder Technol.* **2004**, *145*, 139.
- [22] M. Chougule, B. Padhi, A. Misra, *AAPS PharmSciTech* **2008**, *9*, 47.
- [23] B. Huck, A. Hidalgo, F. Waldow, D. Schwudke, K. I. Gaede, C. Feldmann, P. Carius, C. Autilio, J. Perez-Gil, K. Schwarzkopf, X. Murgia, B. Loretz, C.-M. Lehr, *Small Sci.* **2021**, *1*, 2100067.
- [24] a) R. Sommer, S. Wagner, A. Varrot, C. M. Nycholat, A. Khaledi, S. Häussler, J. C. Paulson, A. Imberty, A. Titz, *Chem. Sci.* **2016**, *7*, 4990; b) O. Metelkina, B. Huck, J. S. O'Connor, M. Koch, A. Manz, C.-M. Lehr, A. Titz, *J. Mater. Chem. B* **2022**, *10*, 537.
- [25] A. K. Azad, M. V. S. Rajaram, L. S. Schlesinger, *J. Cytol. Mol. Biol.* **2014**, *1*, 1000003.
- [26] D. Thiagarajan, B. Huck, B. Nothdurft, M. Koch, D. Rudolph, M. Rutschmann, C. Feldmann, C. Hozsa, M. Furch, K. F. W. Besecke, R. K. Gieseler, B. Loretz, C.-M. Lehr, *Drug Delivery Transl. Res.* **2021**.
- [27] V. A. Marple, D. L. Roberts, F. J. Romay, N. C. Miller, K. G. Truman, M. van Oort, B. Olsson, M. J. Holroyd, J. P. Mitchell, D. Hochrainer, *J. Aerosol Med.* **2003**, *16*, 283.
- [28] S. Hein, M. Bur, U. F. Schaefer, C.-M. Lehr, *Eur. J. Pharm. Biopharm.* **2011**, *77*, 132.
- [29] D. Cipolla, J. Blanchard, I. Gonda, *Pharmaceutics* **2016**, *8*.
- [30] T. Frenz, E. Grabski, V. Durán, C. Hozsa, A. Stepczyńska, M. Furch, R. K. Gieseler, U. Kalinke, *Eur. J. Pharm. Biopharm.* **2015**, *95*, 13.
- [31] a) S. P. Vyas, M. E. Kannan, S. Jain, V. Mishra, P. Singh, *Int. J. Pharm.* **2004**, *269*, 37; b) S. Chono, T. Tanino, T. Seki, K. Morimoto, *J. Drug Targeting* **2006**, *14*, 557.
- [32] K. I. Kuok, P. C. in Ng, X. Ji, C. Wang, W. W. Yew, D. P. C. Chan, J. Zheng, S. M. Y. Lee, R. Wang, *Food Chem. Toxicol.* **2018**, *119*, 425.
- [33] B. Forbes, P. Bäckman, D. Christopher, M. Dolovich, B. V. Li, B. Morgan, *AAPS J.* **2015**, *17*, 837.
- [34] R. M. Derbali, V. Aoun, G. Moussa, G. Frei, S. F. Tehrani, J. C. Del'Orto, P. Hildgen, V. G. Roullin, J. L. Chain, *Mol. Pharm.* **2019**, *16*, 1906.
- [35] a) L. de Matteis, D. Jary, A. Lucía, S. García-Embid, I. Serrano-Sevilla, D. Pérez, J. A. Ainsa, F. P. Navarro, J. La, M. de Fuente, *Chem. Eng. J.* **2018**, *340*, 181; b) R. Nisini, N. Poerio, S. Mariotti, F. de Santis, M. Fraziano, *Front. Immunol.* **2018**, *9*, 155.
- [36] A. Viljoen, J.-L. Herrmann, O. K. Onajole, J. Stec, A. P. Kozikowski, L. Kremer, *Front. Cell. Infect. Microbiol.* **2017**, *7*, 388.
- [37] a) J. P. Wong, H. Yang, K. L. Blasetti, G. Schnell, J. Conley, L. N. Schofield, *J. Controlled Release* **2003**, *92*, 265; b) B. Lamy, F. Tewes, D. R. Serrano, I. Lamarche, P. Gobin, W. Couet, A. M. Healy, S. Marchand, *J. Controlled Release* **2018**, *271*, 118.
- [38] a) Y. Suzuki, M. Shirai, K. Asada, H. Yasui, M. Karayama, H. Hozumi, K. Furuhashi, N. Enomoto, T. Fujisawa, Y. Nakamura, N. Inui, T. Shirai, H. Hayakawa, T. Suda, *Sci. Rep.* **2018**, *8*, 13129; b) S. T. T. Scheters, L. J. W. Kruijssen, M. H. W. Crommentuijn, H. Kalay, J. Ochando, J. M. M. den Haan, J. J. Garcia-Vallejo, Y. van Kooyk, *Front. Immunol.* **2018**, *9*, 990.
- [39] M. Woo, C. Wood, D. Kwon, K.-H. P. Park, G. Fejer, V. Delorme, *Front. Immunol.* **2018**, *9*, 438.
- [40] G. Lugo-Villarino, D. Hudrisier, A. Tanne, O. Neyrolles, *Eur. J. Microbiol. Immunol.* **2011**, *1*, 25.
- [41] C. Berges, C. Naujokat, S. Tinapp, H. Wiczorek, A. Höh, M. Sadeghi, G. Opelz, V. Daniel, *Biochem. Biophys. Res. Commun.* **2005**, *333*, 896.
- [42] I. Vergne, M. Gilleron, J. Nigou, *Front. Cell. Infect. Microbiol.* **2014**, *4*, 187.
- [43] C. Bussi, M. G. Gutierrez, *FEMS Microbiol. Rev.* **2019**, *43*, 341.
- [44] a) A.-G. Lenz, E. Karg, E. Brendel, H. Hinze-Heyn, K. L. Maier, O. Eickelberg, T. Stoeger, O. Schmid, *BioMed. Res. Int.* **2013**, *2013*, 652632; b) L. K. Limbach, Y. Li, R. N. Grass, T. J. Brunner, M. A. Hintermann, M. Muller, D. Gunther, W. J. Stark, *Environ. Sci. Technol.* **2005**, *39*, 9370; c) S. Upadhyay, L. Palmberg, *Toxicol. Sci.* **2018**, *164*, 21.
- [45] a) K. L. Hartshorn, E. Crouch, M. R. White, M. L. Colamussi, A. Kakkannatt, B. Tauber, V. Shepherd, K. N. Sastry, *Am. J. Physiol.* **1998**, *274*, L958; b) T. L. Schagat, J. A. Wofford, J. R. Wright, *J. Immunol.* **2001**, *166*, 2727.
- [46] a) C. D. Gaynor, F. X. McCormack, D. R. Voelker, S. E. McGowan, L. S. Schlesinger, *J. Immunol.* **1995**, *155*, 5343; b) J. S. Ferguson, D. R. Voelker, J. A. Ufnar, A. J. Dawson, L. S. Schlesinger, *J. Immunol.* **2002**, *168*, 1309.
- [47] A. Misra, K. Jinturkar, D. Patel, J. Lalani, M. Chougule, *Expert Opin. Drug Delivery* **2009**, *6*, 71.
- [48] P. Mehta, *J. Drug Delivery* **2018**, *2018*, 5635010.
- [49] Y. Pei, Y. Yeo, *J. Controlled Release* **2016**, *240*, 202.
- [50] P. Wessman, K. Edwards, D. Mahlin, *J. Pharm. Sci.* **2010**, *99*, 2032.
- [51] X. Murgia, B. Loretz, O. Hartwig, M. Hittinger, C.-M. Lehr, *Adv. Drug Delivery Rev.* **2018**, *124*, 82.
- [52] G. Chai, A. Hassan, T. Meng, L. Lou, J. Ma, R. Simmers, L. Zhou, B. K. Rubin, Q. T. Zhou, P. W. Longest, M. Hindle, Q. Xu, *Nanomedicine* **2020**, *29*, 102262.
- [53] M. A. M. Momin, B. Rangnekar, S. Sinha, C.-Y. Cheung, G. M. Cook, S. C. Das, *Pharmaceutics* **2019**, *11*.
- [54] a) M.-R. Lee, W.-H. Sheng, C.-C. Hung, C.-J. Yu, L.-N. Lee, P.-R. Hsueh, *Emerging Infect. Dis.* **2015**, *21*, 1638; b) M. D. Johansen, J.-L. Herrmann, L. Kremer, *Nat. Rev. Microbiol.* **2020**, *18*, 392.
- [55] C. A. Molina-Torres, L. Tamez-Peña, J. Castro-Garza, J. Ocampo-Candiani, L. Vera-Cabrera, *J. Microbiol. Methods* **2018**, *148*, 29.
- [56] R. Nessar, E. Cambau, J. M. Reyat, A. Murray, B. Gicquel, *J. Antimicrob. Chemother.* **2012**, *67*, 810.
- [57] M. Korycka-Machała, J. Pawełczyk, P. Borówka, B. Dziadek, A. Brzostek, M. Kawka, A. Bekier, S. Rykowski, A. B. Olejniczak, D. Strapiel, Z. Witczak, J. Dziadek, *Cells* **2020**, *9*.
- [58] D. Hauck, I. Joachim, B. Frommeyer, A. Varrot, B. Philipp, H. M. Möller, A. Imberty, T. E. Exner, A. Titz, *ACS Chem. Biol.* **2013**, *8*, 1775.
- [59] O. Metelkina, B. Huck, J. O'Connor, M. Koch, A. Manz, C.-M. Lehr, A. Titz, *Journal of Materials Chemistry B* **2022**, *10*, 537.
- [60] a) X. Murgia, H. Yasar, C. Carvalho-Wodarz, B. Loretz, S. Gordon, K. Schwarzkopf, U. Schaefer, C.-M. Lehr, *Eur. J. Pharm. Biopharm.* **2017**, *118*, 79; b) D.-K. Ho, S. Frisch, A. Biehl, E. Terriac, C. de Rossi, K. Schwarzkopf, F. Lautenschläger, B. Loretz, X. Murgia, C.-M. Lehr, *Biomacromolecules* **2018**, *19*, 3489.
- [61] I. F. Sbalzarini, P. Koumoutsakos, *J. Struct. Biol.* **2005**, *151*, 182.

# ADVANCED HEALTHCARE MATERIALS

## Supporting Information

for *Adv. Healthcare Mater.*, DOI 10.1002/adhm.202102117

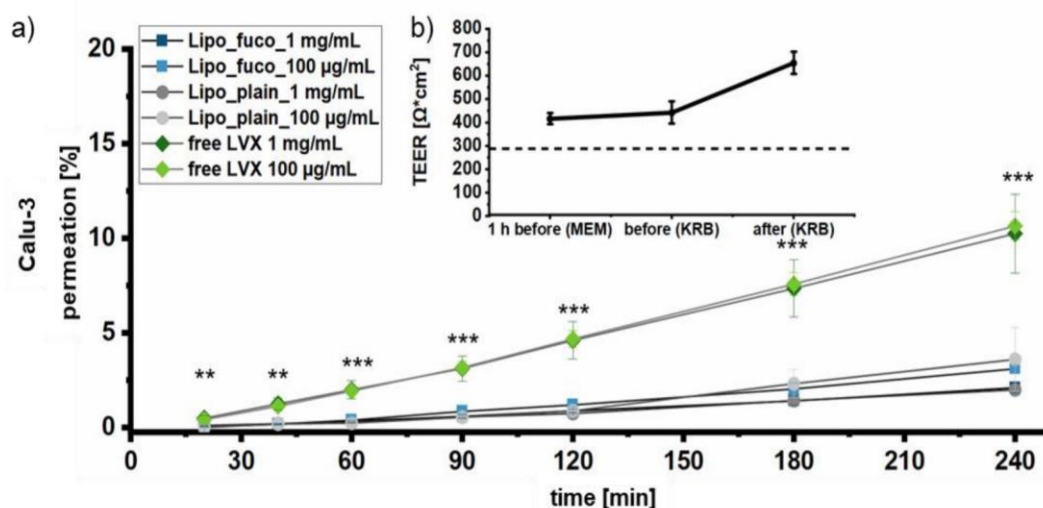
Nano-in-Microparticles for Aerosol Delivery of Antibiotic-Loaded, Fucose-Derivatized, and Macrophage-Targeted Liposomes to Combat Mycobacterial Infections: In Vitro Deposition, Pulmonary Barrier Interactions, and Targeted Delivery

*Benedikt C. Huck, Durairaj Thiyagarajan, Aghiad Bali, Annette Boese, Karen F. W. Besecke, Constantin Hozsa, Robert K. Gieseler, Marcus Furch, Cristiane Carvalho-Wodarz, Franziska Waldow, Dominik Schwudke, Olga Metelkina, Alexander Titz, Hanno Huwer, Konrad Schwarzkopf, Jessica Hoppstädter, Alexandra K. Kiemer, Marcus Koch, Brigitta Loretz\* and Claus-Michael Lehr\**

Supporting Information to the manuscript:

### Nano-in-Microparticles for Aerosol Delivery of Antibiotic-loaded, Fucose-derivatized and Macrophage-targeted Liposomes to Combat Mycobacterial Infections: *In-Vitro* deposition, Pulmonary Barrier Interactions and Targeted Delivery

*Benedikt C. Huck, Durairaj Thiyagarajan, Aghiad Bali, Annette Boese, Karen F.W. Besecke, Constantin Hozsa, Robert K. Gieseler, Marcus Furch, Cristiane Carvalho-Wodarz, Franziska Waldow, Dominik Schwudke, Olga Metelkina, Alexander Titz, Hanno Huwer, Konrad Schwarzkopf, Jessica Hoppstädter, Alexandra K. Kiemer, Markus Koch, Brigitta Loretz\*, Claus-Michael Lehr\**



**Supplementary Figure 1)** a) Permeability of free and encapsulated LVX through Calu-3 cells forming a tight barrier with TEER values  $>400 \Omega \times \text{cm}^2$  (b). LVX encapsulated in liposomes shows a reduced permeability and is retained by Calu-3 cells. Error bars represent mean  $\pm$  SD (n = 9, N = 3)

Due to technical limitations in sufficiently solubilizing and detecting BDQ in the cell culture medium, transport experiments through Calu-3 cells (a human epithelial lung cancer cell line) were only performed with LVX-loaded liposomes *vs.* free LVX. A concentration-independent permeability of LVX through a tight epithelium (TEER  $> 400 \Omega \text{ cm}^2$ ) was observed (**Figures S1a** and **S1b**). However, liposomal encapsulation of LVX significantly reduced its permeability. This is reflected in the apparent permeability coefficient ( $P_{\text{app}}$ ), which was

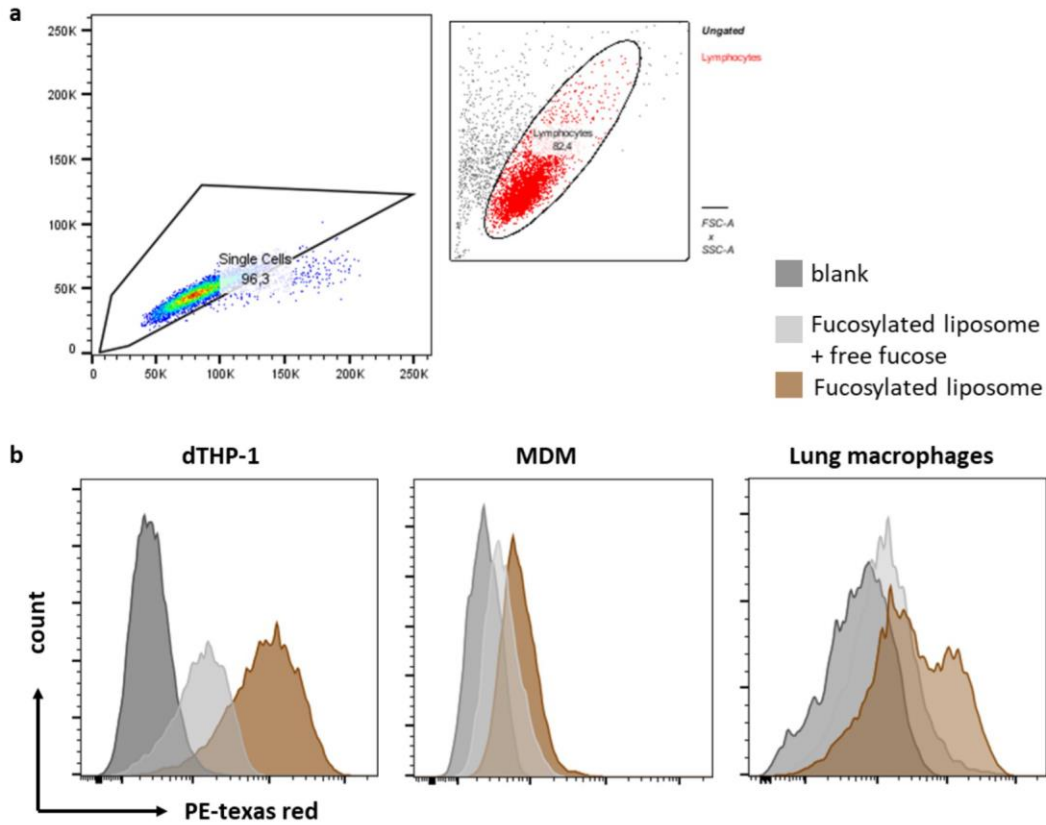
$0.71 \times 10^{-6}$ , and  $0.72 \times 10^{-6}$  for targeted and plain liposomes, respectively, and  $3.5 \times 10^{-6} \text{ cm s}^{-1}$  for free LVX at an initial concentration of 1 mg/mL. No differences were measured for targeted vs. plain liposomes. LVX was solely used for comparative purposes, so that the following sections will report on BDQ-loaded liposomes only.

**M&M:** The Calu-3 (HTB-55) human lung epithelial carcinoma cell line (ATCC, Manassas, VA, USA) was cultured in minimum essential medium (MEM; Thermo Fisher, Kandel, Germany) supplemented with 10% fetal calf serum (FCS), 1% non-essential amino acids and 1% sodium pyruvate (all from Sigma, Germany) during passages 48–53. Totals of 10,000 cells were seeded onto Transwell permeable supports ( $A = 1.12 \text{ cm}^2$ ) (Greiner, Frickenhausen, Germany) and grown for 12–14 days with medium replacement every second day. Experiments were performed when the transepithelial electrical resistance (TEER) values were  $> 400 \Omega \text{ cm}^2$  using an EVOM2 (World Precision instruments, Sarasota, FL, USA). TEER values are determined according to:

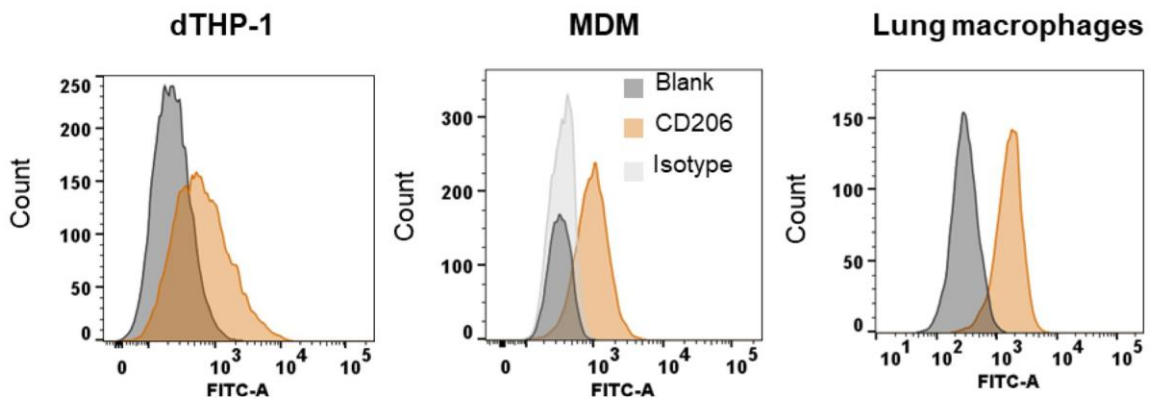
$$\text{TEER} [\Omega \times \text{cm}^2] = R_{\text{cells}} (\Omega) \times A_{\text{epith}} (\text{cm}^2) \quad (1),$$

where  $R_{\text{cells}}$  is the cell layer-specific resistance, and  $A_{\text{epith}}$  is the area of the epithelial layer.

Prior to and after the experiments, TEER values were measured again to confirm integrity of the barrier. LVX-loaded liposomes and free LVX were suspended in Krebs-Ringer buffer at a final concentration of 1 mg/mL or 100  $\mu\text{g/mL}$ , respectively, and 500  $\mu\text{L}$  volumes were added to the donor compartment. At each time interval, 200  $\mu\text{L}$  medium were withdrawn from the acceptor compartment and replaced with 200  $\mu\text{L}$  fresh medium.

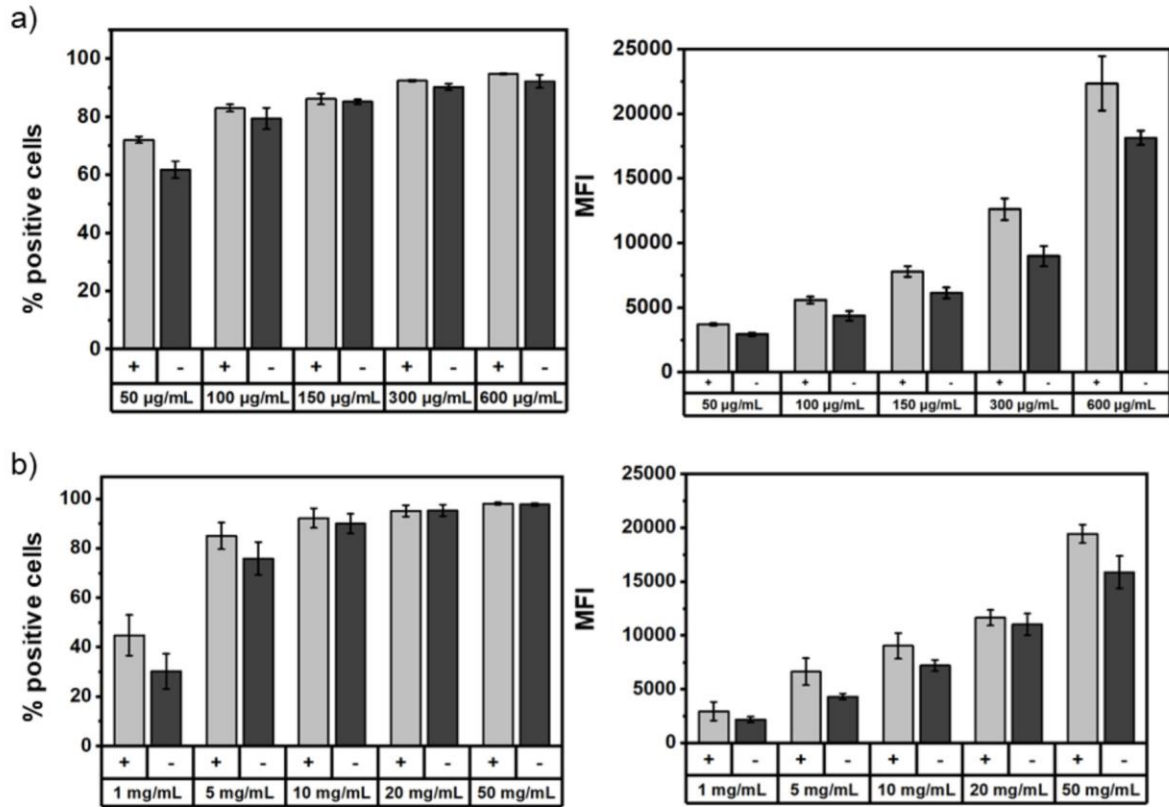


**Supplementary Figure 2)** a) Gating strategy for flow cytometric analysis and b) representative cytometer plots (histograms) of phagocytic cells after 2 h at 37°C (submerged conditions) of incubation with fucosylated liposomes and in the presence of soluble L-fucose as a competitive inhibitor.

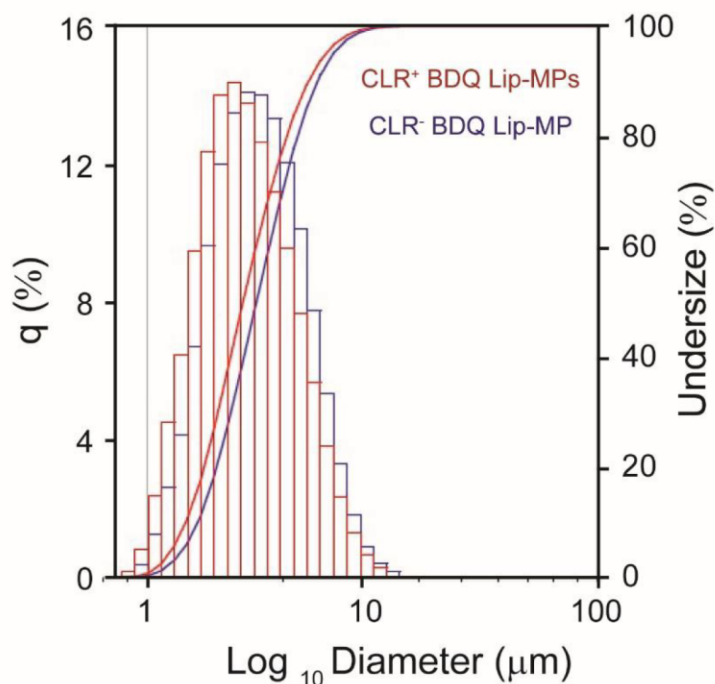


**Supplementary Figure 3)** Macrophage mannose receptor (CD206) expression of dTHP-1 cells, blood monocyte derived macrophages (MDM), and lung tissue-derived macrophages determined by flow cytometry.

Heidelberg, Germany). Subsequently, cells were incubated with anti-CD206 antibody (Abcam, Cambridge, UK) or isotype-matched monoclonal control antibody (Abcam, Cambridge, UK) for 2 h at 4°C in PBS containing 1% (v/v) bovine serum albumin (BSA, Sigma, Germany) and 10% FCS.

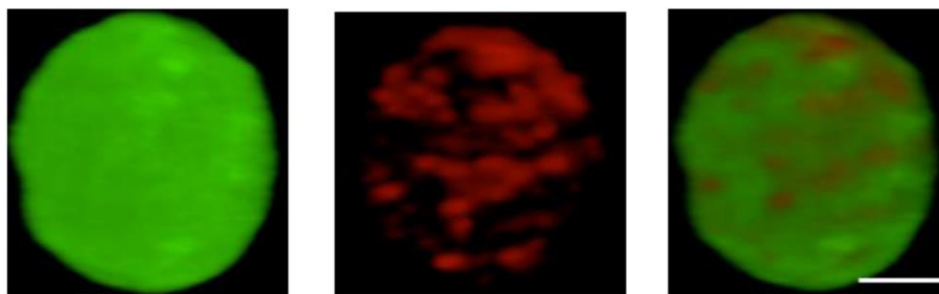


**Supplementary Figure 4** a) Uptake of fucosylated liposomes (+) vs. plain liposomes (-) and b) the respective liposomal dry powders at increasing concentrations denoted as µg/mL liposome or mg/mL dissolved dry powder. THP-1 cells were incubated for 2 h at 37°C and analyzed by flow cytometry.



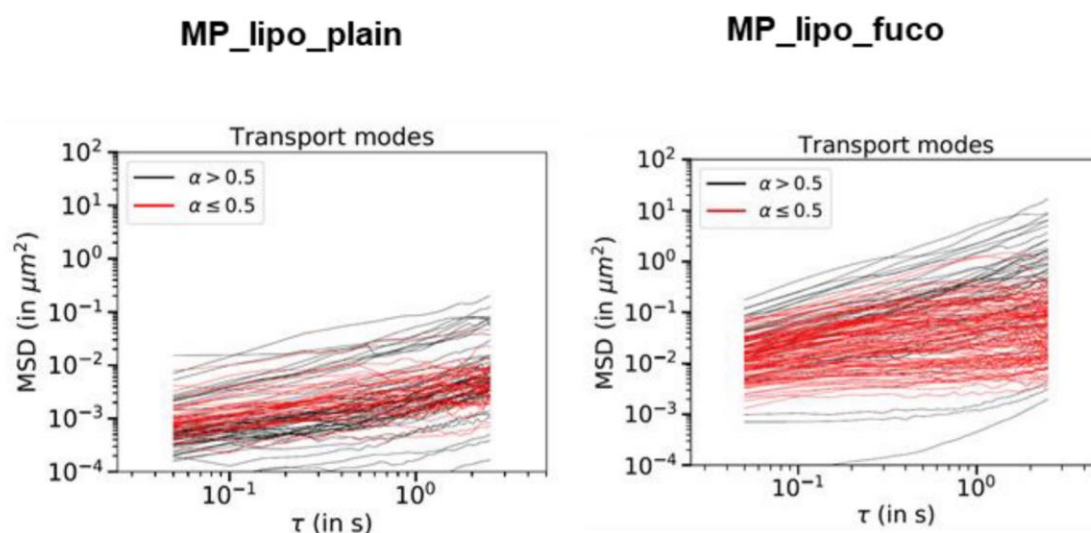
**Supplementary Figure 5)** Static light scattering of microparticles containing CLR-targeted (red) or plain liposomes (blue) with median sizes of 2.65  $\mu\text{m}$  or 3.04  $\mu\text{m}$ , respectively.

**M&M:** *Static Light Scattering:* For static light scattering of the particles, 15 mL of 1-octanol in a quartz cuvette served as a blank in the laser diffraction particle size distribution analyzer (Partica LA-960, Horiba). Ten mg of the powders were dispersed in 15 mL octanol, sonicated for 1 min and gradually added to the cuvette under gentle stirring. The particle size distribution was calculated as based on the reduction in transparency and scattering values. The median value of each sample was plotted.



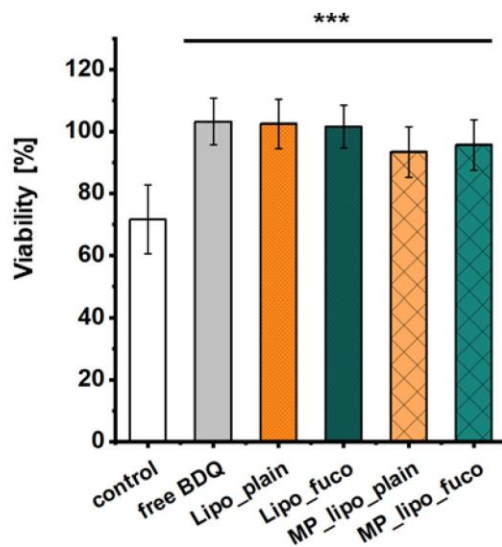
**Supplementary Figure 6)** Confocal microscopic micrographs of fluorescein-labeled (green) microparticles containing CLR-targeted or plain liposomes (red). Scale bar: 2  $\mu\text{m}$ .

**M&M:** *Confocal microscopy:* One mg of the powder was admixed with 50  $\mu\text{L}$  of 1-octanol and sonicated for 1 min to disperse. One microliter from the above solution was placed on a microscopic slide and sealed with a coverslip. Images were taken with a confocal microscope (Leica DMI8) equipped with a  $\times 63$  water immersion objective (HC APO CS2 63 $\times$ /1.20) and image analysis was performed with LAS X software (Leica Application Suite X).



**Supplementary Figure 7)** Transport modes of liposomes deposited in stage 3 of the next generation impactor.





**Supplementary Figure 8)** Viability of dTHP-1 cells determined by LDH assay 72 h after infection. Data represent means  $\pm$  SD (n=9, N=3).

**M&M:** *LDH assay:* The release of intracellular LDH of dTHP-1 cells infected with *M. abscessus* and subsequently treated, was measured 72 h after infection. One-hundred  $\mu$ L from LDH secreted to the cell culture medium (centrifuge) were transferred to a 96-well plate, and 100  $\mu$ L of a mixture of 11.25 mL solution A and 250  $\mu$ L solution B from LDH Cytotoxicity Detection KIT (Roche, Basel, CH) was added to the well according to the manufacturer's instructions. Untreated cells were used as a negative control; cells treated with 0.1% Triton X-100 (Sigma, Darmstadt, Germany) as a positive control; and cell-free medium served as a blank.

Cytotoxicity (LDH release) was calculated after subtracting the blank as:

$$\text{Cytotoxicity (\%)} = \frac{\text{exp.value} - \text{low control}}{\text{high control} - \text{low control}} * 100$$

**Supplementary Table 1)** Conditions of the hydrophilic interaction chromatography. Solvent A: 1% formic acid. Solvent B: acetonitrile.

Time [min]	Solvent B [%]	Flow [mL/min]
0.0	90.0	0.5
1.0	90.0	0.5
4.0	2.0	0.5
4.1	2.0	0.8
10.0	2.0	0.8
15.0	90.0	0.8
19.0	90.0	0.8
20.0	90.0	0.5

**Supplementary Table 2)** Mass spectrometry conditions including transitions of BDQ, LVX and reserpine (used as an internal standard).

Analyte	Parent [m/z]	Daughter [m/z]	Cone Voltage [EV]	Collision Energy [EV]	Dwell [s]
Bedaquiline	555.14	58.16	30	35	0.05
Levofloxacin	361.82	261.17	40	30	0.05
Internal standard					
Reserpine	608.55	194.91	30	35	0.05

**M&M LC-MS/MS:**

*Gradient:* The gradient started at 90% B at a flowrate of 0.5 mL/min. After 1 min of isocratic conditions, the percentage of ACN was decreased to 2% B until minute four. At minute four, the flow-rate was increased to 0.8 mL/min. The gradient was kept isocratic at 2% B with a flowrate of 0.8 mL/min for 6 min until minute 10. Afterwards, the percentage of ACN was re-increased to 90% B until minute 15, and the flow-rate was again decreased to 0.5 mL/min until minute 19. These conditions were maintained for 1 min, so that the total run-time was 20

min (**Table S1**). The autosampler temperature was set to 4 °C, and the sample injection volume was 5 µL for LC-MS/MS analysis.

The Waters Micromass Quattro Premier XE Triple Quadrupole Mass Spectrometer (Waters Corporation, Milford, Massachusetts, USA) using electrospray ionization (ESI) was operated in the positive ion mode using multiple reaction monitoring (MRM). Parent and daughter transition was used to quantify the analytes (**Table S2**). In the mass spectrometer, BDQ, LVX, and reserpine (internal standard) were ionized through electrospray ionization source under the positive ion mode with the following source parameters: The cone gas- and desolvation gas flow were set to 100 L/h and 800 L/h, respectively. The extractor voltage was 3.0 V. We optimized the capillary voltage, the source temperature, and the desolvation gas temperature and selected 3.0 kV, 450 °C, and 90 °C. MassLynx 4.1 and TargetLynx (Waters Corporation, Milford, Massachusetts, USA) were used for operating the platform and quantifying the samples, respectively. Quantification was based on external calibration using an API-free reference as background. Stock solutions of BDQ and LVX at 0.5 mg/mL, each, were prepared in ACN. Reserpine was used as an internal standard (12.5 ng/mL in ACN) for sample processing. Calibration standards were prepared by diluting stock solutions with individual standard curves ranging from 0.00–0.005 µg/mL for BDQ and 0.001–0.25 µg/mL for LVX.

*Extraction of LVX and BDQ for LC-MS/MS:* Twenty µL of BDQ- or LVX-loaded fucosylated liposomes were diluted in 800 µL ACN and 180 µL 1% formic acid, and the mixture was thoroughly vortexed. Afterwards, 20 µL of this mixture was further diluted in 800 µL ACN and 180 µL 1% FA. The solution was vortexed and then centrifuged for 10 min at  $15.000 \times g$  at RT. Approximately 500 µL of the resulting supernatant were transferred in a 1.5 mL Eppendorf tube and re-centrifuged under the same conditions. Afterwards, 60 µL of the supernatant was transferred to a vial (three aliquots per sample), and the injection volume was 5 µL for LC-MS/MS analysis.

## 6 References

- [1] A. Natarajan, H.-W. Su, C. Heneghan, L. Blunt, C. O'Connor, L. Niehaus, Measurement of respiratory rate using wearable devices and applications to COVID-19 detection, *NPJ Digit. Med.* 4 (2021) 136. <https://doi.org/10.1038/s41746-021-00493-6>.
- [2] A. Person, M.L. Mintz, Anatomy and Physiology of the Respiratory Tract, in: M.L. Mintz (Ed.), *Disorders of the Respiratory Tract: Common Challenges in Primary Care*, Humana Press, Totowa, NJ, 2006, pp. 11–15.
- [3] J.S. Patton, C.S. Fishburn, J.G. Weers, The lungs as a portal of entry for systemic drug delivery, *Proc. Am. Thorac. Soc.* 1 (2004). <https://doi.org/10.1513/pats.200409-049TA>.
- [4] J.S. Patton, Mechanisms of macromolecule absorption by the lungs, *Adv. Drug Deliv. Rev.* 19 (1996) 3–36. [https://doi.org/10.1016/0169-409X\(95\)00113-L](https://doi.org/10.1016/0169-409X(95)00113-L).
- [5] J. Perez-Gil, T.E. Weaver, Pulmonary surfactant pathophysiology: current models and open questions, *Physiology (Bethesda)* 25 (2010) 132–141. <https://doi.org/10.1152/physiol.00006.2010>.
- [6] A. Kuehn, S. Kletting, C. Carvalho-Wodarz, Urska Repnik, G. Griffiths, U. Fischer, E. Meese, H. Huwer, D. Wirth, T. May, N. Schneider-Daum, C.-M. Lehr, Human alveolar epithelial cells expressing tight junctions to model the air-blood barrier, *ALTEX* 33 (2016) 251–260. <https://doi.org/10.14573/altex.1511131>.
- [7] Lars Knudsen, Matthias Ochs, The micromechanics of lung alveoli: structure and function of surfactant and tissue components, *Histochem. Cell Biol.* 150 (2018) 661–676. <https://doi.org/10.1007/s00418-018-1747-9>.
- [8] B.C. Huck, O. Hartwig, A. Biehl, K. Schwarzkopf, C. Wagner, B. Loretz, X. Murgia, C.-M. Lehr, Macro- and Microrheological Properties of Mucus Surrogates in Comparison to Native Intestinal and Pulmonary Mucus, *Biomacromolecules* 20 (2019) 3504–3512. <https://doi.org/10.1021/acs.biomac.9b00780>.
- [9] X. Murgia, B. Loretz, O. Hartwig, M. Hittinger, C.-M. Lehr, The role of mucus on drug transport and its potential to affect therapeutic outcomes, *Adv. Drug Deliv. Rev.* 124 (2018) 82–97. <https://doi.org/10.1016/j.addr.2017.10.009>.
- [10] B. Huck, X. Murgia, S. Frisch, M. Hittinger, A. Hidalgo, B. Loretz, C.-M. Lehr, Models using native tracheobronchial mucus in the context of pulmonary drug delivery research: Composition, structure and barrier properties, *Adv. Drug Deliv. Rev.* (2022) 114141. <https://doi.org/10.1016/j.addr.2022.114141>.
- [11] D.A. Groneberg, P.R. Eynott, T. Oates, S. Lim, R. Wu, I. Carlstedt, A.G. Nicholson, K.F. Chung, Expression of MUC5AC and MUC5B mucins in normal and cystic fibrosis lung, *Respir. Med.* 96 (2002) 81–86. <https://doi.org/10.1053/rmed.2001.1221>.
- [12] E.R. Lillehoj, K.C. Kim, Airway mucus: its components and function, *Arch. Pharm. Res.* 25 (2002) 770–780. <https://doi.org/10.1007/BF02976990>.
- [13] J. Perez-Vilar, R.L. Hill, The structure and assembly of secreted mucins, *J. Biol. Chem.* 274 (1999) 31751–31754. <https://doi.org/10.1074/jbc.274.45.31751>.
- [14] B. Huck, A. Hidalgo, F. Waldow, D. Schwudke, K.I. Gaede, C. Feldmann, P. Carius, C. Autilio, J. Pérez-Gil, K. Schwarzkopf, X. Murgia, B. Loretz, C.-M. Lehr, Systematic Analysis of Composition,

- Interfacial Performance and Effects of Pulmonary Surfactant Preparations on Cellular Uptake and Cytotoxicity of Aerosolized Nanomaterials, *Small Science* 1 (2021) 2100067. <https://doi.org/10.1002/smsc.202100067>.
- [15] N.S. Joo, I.A.T. Evans, H.-J. Cho, I.-H. Park, J.F. Engelhardt, J.J. Wine, Proteomic analysis of pure human airway gland mucus reveals a large component of protective proteins, *PLoS ONE* 10 (2015) e0116756. <https://doi.org/10.1371/journal.pone.0116756>.
- [16] J.G. Widdicombe, Rôle of lipids in airway function, *Eur. J. Respir. Dis. Suppl.* 153 (1987) 197–204.
- [17] S. Girod, J.M. Zahm, C. Plotkowski, G. Beck, E. Puchelle, Role of the physicochemical properties of mucus in the protection of the respiratory epithelium, *Eur. Respir. J.* 5 (1992) 477–487.
- [18] F. Lecaille, G. Lalmanach, P.M. Andrault, Antimicrobial proteins and peptides in human lung diseases: A friend and foe partnership with host proteases, *Biochimie* 122 (2016). <https://doi.org/10.1016/j.biochi.2015.08.014>.
- [19] B.S. Schuster, J.S. Suk, G.F. Woodworth, J. Hanes, Nanoparticle diffusion in respiratory mucus from humans without lung disease, *Biomaterials* 34 (2013) 3439–3446. <https://doi.org/10.1016/j.biomaterials.2013.01.064>.
- [20] E. Parra, J. Pérez-Gil, Composition, structure and mechanical properties define performance of pulmonary surfactant membranes and films, *Chem. Phys. Lipids* 185 (2015) 153–175. <https://doi.org/10.1016/j.chemphyslip.2014.09.002>.
- [21] J. Pérez-Gil, Structure of pulmonary surfactant membranes and films: The role of proteins and lipid–protein interactions, *Biochim. Biophys. Acta* 1778 (2008) 1676–1695. <https://doi.org/10.1016/j.bbamem.2008.05.003>.
- [22] M. Radiom, M. Sarkis, O. Brookes, E.K. Oikonomou, A. Baeza-Squiban, J.-F. Berret, Pulmonary surfactant inhibition of nanoparticle uptake by alveolar epithelial cells, *Sci. Rep.* 10 (2020) 19436. <https://doi.org/10.1038/s41598-020-76332-7>.
- [23] R. Veldhuizen, K. Nag, S. Orgeig, F. Possmayer, The role of lipids in pulmonary surfactant, *Biochim. Biophys. Acta* 1408 (1998) 90–108. [https://doi.org/10.1016/S0925-4439\(98\)00061-1](https://doi.org/10.1016/S0925-4439(98)00061-1).
- [24] E. Lopez-Rodriguez, J. Pérez-Gil, Structure-function relationships in pulmonary surfactant membranes: from biophysics to therapy, *Biochim. Biophys. Acta* 1838 (2014) 1568–1585. <https://doi.org/10.1016/j.bbamem.2014.01.028>.
- [25] O. Cañadas, B. Olmeda, A. Alonso, J. Pérez-Gil, Lipid-Protein and Protein-Protein Interactions in the Pulmonary Surfactant System and Their Role in Lung Homeostasis, *Int. J. Mol. Sci.* 21 (2020). <https://doi.org/10.3390/ijms21103708>.
- [26] C. Autilio, J. Pérez-Gil, Understanding the principle biophysics concepts of pulmonary surfactant in health and disease, *Arch. Dis. Child. Fetal Neonatal Ed.* 104 (2019) F443-F451. <https://doi.org/10.1136/archdischild-2018-315413>.
- [27] T.L. Moore, D.A. Urban, L. Rodriguez-Lorenzo, A. Milosevic, F. Crippa, M. Spuch-Calvar, S. Balog, B. Rothen-Rutishauser, M. Lattuada, A. Petri-Fink, Nanoparticle administration method in cell culture alters particle-cell interaction, *Sci. Rep.* 9 (2019) 900. <https://doi.org/10.1038/s41598-018-36954-4>.
- [28] M. Gasser, P. Wick, M.J.D. Clift, F. Blank, L. Diener, B. Yan, P. Gehr, H.F. Krug, B. Rothen-Rutishauser, Pulmonary surfactant coating of multi-walled carbon nanotubes (MWCNTs)

- influences their oxidative and pro-inflammatory potential in vitro, *Part. Fibre Toxicol.* 9 (2012) 17. <https://doi.org/10.1186/1743-8977-9-17>.
- [29] A. Hidalgo, A. Cruz, J. Pérez-Gil, Pulmonary surfactant and nanocarriers: Toxicity versus combined nanomedical applications, *Biochim. Biophys. Acta* 1859 (2017) 1740–1748. <https://doi.org/10.1016/j.bbamem.2017.04.019>.
- [30] World Health Organization, *World Health Statistics 2021: Monitoring Health for the SDGs*, <http://www.who.int/>, 2021.
- [31] N. Woodford, D.M. Livermore, Infections caused by Gram-positive bacteria: a review of the global challenge, *J. Infect.* 59 (2009) S4-S16. [https://doi.org/10.1016/S0163-4453\(09\)60003-7](https://doi.org/10.1016/S0163-4453(09)60003-7).
- [32] F. Boldrin, R. Provvedi, L. Cioetto Mazzabò, G. Segafreddo, R. Manganelli, Tolerance and Persistence to Drugs: A Main Challenge in the Fight Against *Mycobacterium tuberculosis*, *Front. Microbiol.* 11 (2020) 1924. <https://doi.org/10.3389/fmicb.2020.01924>.
- [33] M.R. Delghandi, M. El-Matbouli, S. Menanteau-Ledouble, *Mycobacteriosis and Infections with Non-tuberculous Mycobacteria in Aquatic Organisms: A Review*, *Microorganisms* 8 (2020) 1368. <https://doi.org/10.3390/microorganisms8091368>.
- [34] C.J.L. Murray, K.S. Ikuta, F. Sharara, L. Swetschinski, G. Robles Aguilar, A. Gray, C. Han, C. Bisignano, P. Rao, E. Wool, S.C. Johnson, A.J. Browne, M.G. Chipeta, F. Fell, S. Hackett, G. Haines-Woodhouse, B.H. Kashef Hamadani, E.A.P. Kumaran, B. McManigal, R. Agarwal, S. Akech, S. Albertson, J. Amuasi, J. Andrews, A. Aravkin, E. Ashley, F. Bailey, S. Baker, B. Basnyat, A. Bekker, R. Bender, A. Bethou, J. Bielicki, S. Boonkasidecha, J. Bukosia, C. Carvalho, C. Castañeda-Orjuela, V. Chansamouth, S. Chaurasia, S. Chiurchiù, F. Chowdhury, A.J. Cook, B. Cooper, T.R. Cressey, E. Criollo-Mora, M. Cunningham, S. Darboe, N.P.J. Day, M. de Luca, K. Dokova, A. Dramowski, S.J. Dunachie, T. Eckmanns, D. Eibach, A. Emami, N. Feasey, N. Fisher-Pearson, K. Forrest, D. Garrett, P. Gastmeier, A.Z. Giref, R.C. Greer, V. Gupta, S. Haller, A. Haselbeck, S.I. Hay, M. Holm, S. Hopkins, K.C. Iregbu, J. Jacobs, D. Jarovsky, F. Javanmardi, M. Khorana, N. Kisoona, E. Kobeissi, T. Kostyanov, F. Krapp, R. Krumkamp, A. Kumar, H.H. Kyu, C. Lim, D. Limmathurotsakul, M.J. Loftus, M. Lunn, J. Ma, N. Mturi, T. Munera-Huertas, P. Musicha, M.M. Mussi-Pinhata, T. Nakamura, R. Nanavati, S. Nangia, P. Newton, C. Ngoun, A. Novotney, D. Nwakanma, C.W. Obiero, A. Olivas-Martinez, P. Olliaro, E. Ooko, E. Ortiz-Brizuela, A.Y. Peleg, C. Perrone, N. Plakkal, A. Ponce-de-Leon, M. Raad, T. Ramdin, A. Riddell, T. Roberts, J.V. Robotham, A. Roca, K.E. Rudd, N. Russell, J. Schnall, J.A.G. Scott, M. Shivamallappa, J. Sifuentes-Osornio, N. Steenkeste, A.J. Stewardson, T. Stoeva, N. Tasak, A. Thaiprakong, G. Thwaites, C. Turner, P. Turner, H.R. van Doorn, S. Velaphi, A. Vongpradith, H. Vu, T. Walsh, S. Waner, T. Wangrangsimakul, T. Wozniak, P. Zheng, B. Sartorius, A.D. Lopez, A. Stergachis, C. Moore, C. Dolecek, M. Naghavi, *Global burden of bacterial antimicrobial resistance in 2019: a systematic analysis*, *The Lancet* (2022). [https://doi.org/10.1016/S0140-6736\(21\)02724-0](https://doi.org/10.1016/S0140-6736(21)02724-0).
- [35] O. Boucherat, J. Boczkowski, L. Jeannotte, C. Delacourt, Cellular and molecular mechanisms of goblet cell metaplasia in the respiratory airways, *Exp. Lung Res.* 39 (2013) 207–216. <https://doi.org/10.3109/01902148.2013.791733>.
- [36] M.B. Antunes, N.A. Cohen, Mucociliary clearance--a critical upper airway host defense mechanism and methods of assessment, *Curr. Opin. Allergy Clin. Immunol.* 7 (2007) 5–10. <https://doi.org/10.1097/ACI.0b013e3280114eef>.
- [37] M. Zanin, P. Baviskar, R. Webster, R. Webby, The Interaction between Respiratory Pathogens and Mucus, *Cell Host Microbe* 19 (2016) 159–168. <https://doi.org/10.1016/j.chom.2016.01.001>.

- [38] J.S. Elborn, Cystic fibrosis, *The Lancet* 388 (2016) 2519–2531. [https://doi.org/10.1016/S0140-6736\(16\)00576-6](https://doi.org/10.1016/S0140-6736(16)00576-6).
- [39] N. Acosta, B. Waddell, A. Heirali, R. Somayaji, M.G. Surette, M.L. Workentine, H.R. Rabin, M.D. Parkins, Cystic Fibrosis Patients Infected With Epidemic *Pseudomonas aeruginosa* Strains Have Unique Microbial Communities, *Front. Cell. Infect. Microbiol.* 10 (2020) 173. <https://doi.org/10.3389/fcimb.2020.00173>.
- [40] J. Chakaya, M. Khan, F. Ntoumi, E. Aklillu, R. Fatima, P. Mwaba, N. Kapata, S. Mfinanga, S.E. Hasnain, P.D.M.C. Katoto, A.N.H. Bulubula, N.A. Sam-Agudu, J.B. Nachega, S. Tiberi, T.D. McHugh, I. Abubakar, A. Zumla, Global Tuberculosis Report 2020 - Reflections on the Global TB burden, treatment and prevention efforts, *Int. J. Infect. Dis.* (2021). <https://doi.org/10.1016/j.ijid.2021.02.107>.
- [41] C. Bussi, M.G. Gutierrez, Mycobacterium tuberculosis infection of host cells in space and time, *FEMS Microbiol. Rev.* 43 (2019) 341–361. <https://doi.org/10.1093/femsre/fuz006>.
- [42] Y. Suzuki, M. Shirai, K. Asada, H. Yasui, M. Karayama, H. Hozumi, K. Furuhashi, N. Enomoto, T. Fujisawa, Y. Nakamura, N. Inui, T. Shirai, H. Hayakawa, T. Suda, Macrophage mannose receptor, CD206, predict prognosis in patients with pulmonary tuberculosis, *Sci. Rep.* 8 (2018) 13129. <https://doi.org/10.1038/s41598-018-31565-5>.
- [43] V. Durán, E. Grabski, C. Hozsa, J. Becker, H. Yasar, J.T. Monteiro, B. Costa, N. Koller, Y. Lueder, B. Wiegmann, G. Brandes, V. Kaefer, C.-M. Lehr, B. Lepenies, R. Tampé, R. Förster, B. Bošnjak, M. Furch, T. Graalman, U. Kalinke, Fucosylated lipid nanocarriers loaded with antibiotics efficiently inhibit mycobacterial propagation in human myeloid cells, *J. Control. Release* (2021). <https://doi.org/10.1016/j.jconrel.2021.04.012>.
- [44] S. Ehlers, U.E. Schaible, The granuloma in tuberculosis: dynamics of a host-pathogen collusion, *Front. Immunol.* 3 (2012) 411. <https://doi.org/10.3389/fimmu.2012.00411>.
- [45] C.N. Ratnatunga, V.P. Lutzky, A. Kupz, D.L. Doolan, D.W. Reid, M. Field, S.C. Bell, R.M. Thomson, J.J. Miles, The Rise of Non-Tuberculosis Mycobacterial Lung Disease, *Front. Immunol.* 11 (2020) 303. <https://doi.org/10.3389/fimmu.2020.00303>.
- [46] Susmita Sarkar, Advaita Ganguly, Current Overview of Anti-Tuberculosis Drugs: Metabolism and Toxicities, *Mycobacterial Diseases* 6 (2016). <https://doi.org/10.4172/2161-1068.1000209>.
- [47] A. Koul, E. Arnoult, N. Lounis, J. Guillemont, K. Andries, The challenge of new drug discovery for tuberculosis, *Nature* 469 (2011) 483–490. <https://doi.org/10.1038/nature09657>.
- [48] M. Miethke, M. Pieroni, T. Weber, M. Brönstrup, P. Hammann, L. Halby, P.B. Arimondo, P. Glaser, B. Aigle, H.B. Bode, R. Moreira, Y. Li, A. Luzhetskyy, M.H. Medema, J.-L. Pernodet, M. Stadler, J.R. Tormo, O. Genilloud, A.W. Truman, K.J. Weissman, E. Takano, S. Sabatini, E. Stegmann, H. Brötz-Oesterhelt, W. Wohlleben, M. Seemann, M. Empting, A.K.H. Hirsch, B. Loretz, C.-M. Lehr, A. Titz, J. Herrmann, T. Jaeger, S. Alt, T. Hestekamp, M. Winterhalter, A. Schiefer, K. Pfarr, A. Hoerauf, H. Graz, M. Lindvall, S. Ramurthy, A. Karlén, M. van Dongen, H. Petkovic, A. Keller, F. Peyrane, S. Donadio, L. Fraisse, L.J.V. Piddock, I.H. Gilbert, H.E. Moser, R. Müller, Towards the sustainable discovery and development of new antibiotics, *Nat. Rev. Chem.* (2021) 1–24. <https://doi.org/10.1038/s41570-021-00313-1>.
- [49] D.-K. Ho, B.L.B. Nichols, K.J. Edgar, X. Murgia, B. Loretz, C.-M. Lehr, Challenges and strategies in drug delivery systems for treatment of pulmonary infections, *Eur. J. Pharm. Biopharm.* 144 (2019) 110–124. <https://doi.org/10.1016/j.ejpb.2019.09.002>.

- [50] Q.T. Zhou, S.S.Y. Leung, P. Tang, T. Parumasivam, Z.H. Loh, H.-K. Chan, Inhaled formulations and pulmonary drug delivery systems for respiratory infections, *Adv. Drug. Deliv. Rev.* 85 (2015) 83–99. <https://doi.org/10.1016/j.addr.2014.10.022>.
- [51] D.S. Pelloso, I. d'Angelo, S. Maiolino, E. Mitidieri, R. Di d'Emmanuele Villa Bianca, R. Sorrentino, F. Quaglia, F. Ungaro, In vitro/in vivo investigation on the potential of Pluronic® mixed micelles for pulmonary drug delivery, *Eur. J. Pharm. Biopharm.* 130 (2018) 30–38. <https://doi.org/10.1016/j.ejpb.2018.06.006>.
- [52] X. Murgia, C. de Souza Carvalho, C.-M. Lehr, Overcoming the pulmonary barrier: new insights to improve the efficiency of inhaled therapeutics, *Eur. J. Nanomed.* 6 (2014). <https://doi.org/10.1515/ejnm-2014-0019>.
- [53] C. Darquenne, Deposition Mechanisms, *J. Aerosol Med. Pulm. Drug Deliv.* 33 (2020) 181–185. <https://doi.org/10.1089/jamp.2020.29029.cd>.
- [54] J. Heyder, Deposition of inhaled particles in the human respiratory tract and consequences for regional targeting in respiratory drug delivery, *Proc. Am. Thorac. Soc.* 1 (2004) 315–320. <https://doi.org/10.1513/pats.200409-046TA>.
- [55] C. Darquenne, Aerosol deposition in health and disease, *J. Aerosol Med. Pulm. Drug Deliv.* 25 (2012) 140–147. <https://doi.org/10.1089/jamp.2011.0916>.
- [56] S.P. Newman, Drug delivery to the lungs: challenges and opportunities, *Ther. Deliv.* 8 (2017) 647–661. <https://doi.org/10.4155/tde-2017-0037>.
- [57] M.B. Dolovich, R. Dhand, Aerosol drug delivery: developments in device design and clinical use, *The Lancet* 377 (2011) 1032–1045. [https://doi.org/10.1016/S0140-6736\(10\)60926-9](https://doi.org/10.1016/S0140-6736(10)60926-9).
- [58] A.A. Matthews, P.L.R. Ee, R. Ge, Developing inhaled protein therapeutics for lung diseases, *Mol. Biomed.* 1 (2020) 11. <https://doi.org/10.1186/s43556-020-00014-z>.
- [59] J. Kirch, M. Guenther, N. Doshi, U.F. Schaefer, M. Schneider, S. Mitragotri, C.-M. Lehr, Mucociliary clearance of micro- and nanoparticles is independent of size, shape and charge--an ex vivo and in silico approach, *J. Control. Release* 159 (2012) 128–134. <https://doi.org/10.1016/j.jconrel.2011.12.015>.
- [60] M. Ahmad, C. Ritzoulis, W. Pan, J. Chen, Biologically-relevant interactions, phase separations and thermodynamics of chitosan–mucin binary systems, *Process Biochem.* 94 (2020) 152–163. <https://doi.org/10.1016/j.procbio.2020.04.003>.
- [61] J.F. Chisholm, S.K. Shenoy, J.K. Shade, V. Kim, N. Putcha, K.A. Carson, R. Wise, N.N. Hansel, J.S. Hanes, J.S. Suk, E. Neptune, Nanoparticle diffusion in spontaneously expectorated sputum as a biophysical tool to probe disease severity in COPD, *Eur. Respir. J.* 54 (2019). <https://doi.org/10.1183/13993003.00088-2019>.
- [62] T.-T. Tran, K. Hadinoto, Ternary nanoparticle complex of antibiotic, polyelectrolyte, and mucolytic enzyme as a potential antibiotic delivery system in bronchiectasis therapy, *Colloids Surf. B Biointerfaces* 193 (2020) 111095. <https://doi.org/10.1016/j.colsurfb.2020.111095>.
- [63] W. Yin, Y. Wang, L. Liu, J. He, Biofilms: The Microbial “Protective Clothing” in Extreme Environments, *Int. J. Mol. Sci.* 20 (2019) 3423. <https://doi.org/10.3390/ijms20143423>.
- [64] C. Schütz, D.-K. Ho, M.M. Hamed, A.S. Abdelsamie, T. Röhrig, C. Herr, A.M. Kany, K. Rox, S. Schmelz, L. Siebenbürger, M. Wirth, C. Börger, S. Yahiaoui, R. Bals, A. Scrima, W. Blankenfeldt,



- J.C. Horstmann, R. Christmann, X. Murgia, M. Koch, A. Berwanger, B. Loretz, A.K.H. Hirsch, R.W. Hartmann, C.-M. Lehr, M. Empting, A New PqsR Inverse Agonist Potentiates Tobramycin Efficacy to Eradicate *Pseudomonas aeruginosa* Biofilms, *Adv. Sci. (Weinh)* 8 (2021) e2004369. <https://doi.org/10.1002/adv.202004369>.
- [65] O. Metelkina, B. Huck, J.S. O'Connor, M. Koch, A. Manz, C.-M. Lehr, A. Titz, Targeting extracellular lectins of *Pseudomonas aeruginosa* with glycomimetic liposomes, *J. Mater. Chem. B* 10 (2022) 537–548. <https://doi.org/10.1039/d1tb02086b>.
- [66] A. Lesniak, F. Fenaroli, M.P. Monopoli, C. Åberg, K.A. Dawson, A. Salvati, Effects of the presence or absence of a protein corona on silica nanoparticle uptake and impact on cells, *ACS Nano* 6 (2012) 5845–5857. <https://doi.org/10.1021/nn300223w>.
- [67] D. Docter, D. Westmeier, M. Markiewicz, S. Stolte, S.K. Knauer, R.H. Stauber, The nanoparticle biomolecule corona: lessons learned – challenge accepted?, *Chem. Soc. Rev.* 44 (2015) 6094–6121. <https://doi.org/10.1039/C5CS00217F>.
- [68] S. Tenzer, D. Docter, S. Rosfa, A. Wlodarski, J. Kuharev, A. Reik, S.K. Knauer, C. Bantz, T. Nawroth, C. Bier, J. Sirirattanapan, W. Mann, L. Treuel, R. Zellner, M. Maskos, H. Schild, R.H. Stauber, Nanoparticle size is a critical physicochemical determinant of the human blood plasma corona: a comprehensive quantitative proteomic analysis, *ACS Nano* 5 (2011) 7155–7167. <https://doi.org/10.1021/nn201950e>.
- [69] M.P. Monopoli, D. Walczyk, A. Campbell, G. Elia, I. Lynch, F.B. Bombelli, K.A. Dawson, Physical-chemical aspects of protein corona: relevance to in vitro and in vivo biological impacts of nanoparticles, *J. Am. Chem. Soc.* 133 (2011) 2525–2534. <https://doi.org/10.1021/ja107583h>.
- [70] S.S. Raesch, S. Tenzer, W. Storck, A. Rurainski, D. Selzer, C.A. Ruge, J. Perez-Gil, U.F. Schaefer, C.-M. Lehr, Proteomic and Lipidomic Analysis of Nanoparticle Corona upon Contact with Lung Surfactant Reveals Differences in Protein, but Not Lipid Composition, *ACS Nano* 9 (2015) 11872–11885. <https://doi.org/10.1021/acs.nano.5b04215>.
- [71] C. Schulze, U.F. Schaefer, C.A. Ruge, W. Wohlleben, C.-M. Lehr, Interaction of metal oxide nanoparticles with lung surfactant protein A, *Eur. J. Pharm. Biopharm.* 77 (2011) 376–383. <https://doi.org/10.1016/j.ejpb.2010.10.013>.
- [72] C.A. Ruge, J. Kirch, O. Cañadas, M. Schneider, J. Perez-Gil, U.F. Schaefer, C. Casals, C.-M. Lehr, Uptake of nanoparticles by alveolar macrophages is triggered by surfactant protein A, *Nanomedicine nanotechnology, biology, and medicine* 7 (2011) 690–693. <https://doi.org/10.1016/j.nano.2011.07.009>.
- [73] C. García-Mouton, A. Hidalgo, R. Arroyo, M. Echaide, A. Cruz, J. Pérez-Gil, Pulmonary Surfactant and Drug Delivery: An Interface-Assisted Carrier to Deliver Surfactant Protein SP-D Into the Airways, *Front. Bioeng. Biotechnol.* 8 (2020) 613276. <https://doi.org/10.3389/fbioe.2020.613276>.
- [74] G. Lugo-Villarino, D. Hudrisier, A. Tanne, Olivier Neyrolles, C-type lectins with a sweet spot for *Mycobacterium tuberculosis*, *Eur. J. Microbiol. Immunol.* 1 (2011) 25–40. <https://doi.org/10.1556/eujmi.1.2011.1.6>.
- [75] C.D. Gaynor, F.X. McCormack, D.R. Voelker, S.E. McGowan, L.S. Schlesinger, Pulmonary surfactant protein A mediates enhanced phagocytosis of *Mycobacterium tuberculosis* by a direct interaction with human macrophages, *J. Immunol.* 155 (1995) 5343–5351.

- [76] W. Xiao, H. Gao, The impact of protein corona on the behavior and targeting capability of nanoparticle-based delivery system, *Int. J. Pharm.* 552 (2018) 328–339. <https://doi.org/10.1016/j.ijpharm.2018.10.011>.
- [77] E. Parra, L.H. Moleiro, I. López-Montero, A. Cruz, F. Monroy, J. Pérez-Gil, A combined action of pulmonary surfactant proteins SP-B and SP-C modulates permeability and dynamics of phospholipid membranes, *Biochem J* 438 (2011) 555–564. <https://doi.org/10.1042/BJ20110681>.
- [78] A. Hidalgo, C. Garcia-Mouton, C. Autilio, P. Carravilla, G. Orellana, M.N. Islam, J. Bhattacharya, S. Bhattacharya, A. Cruz, J. Pérez-Gil, Pulmonary surfactant and drug delivery: Vehiculization, release and targeting of surfactant/tacrolimus formulations, *J. Control. Release* 329 (2021) 205–222. <https://doi.org/10.1016/j.jconrel.2020.11.042>.
- [79] A. Hidalgo, F. Salomone, N. Fresno, G. Orellana, A. Cruz, J. Perez-Gil, Efficient Interfacially Driven Vehiculization of Corticosteroids by Pulmonary Surfactant, *Langmuir* 33 (2017) 7929–7939. <https://doi.org/10.1021/acs.langmuir.7b01177>.
- [80] F. Wang, J. Liu, H. Zeng, Interactions of particulate matter and pulmonary surfactant: Implications for human health, *Adv. Colloid Interface Sci.* 284 (2020) 102244. <https://doi.org/10.1016/j.cis.2020.102244>.
- [81] O. Blanco, J. Pérez-Gil, Biochemical and pharmacological differences between preparations of exogenous natural surfactant used to treat Respiratory Distress Syndrome: role of the different components in an efficient pulmonary surfactant, *Eur. J. Pharmacol.* 568 (2007) 1–15. <https://doi.org/10.1016/j.ejphar.2007.04.035>.
- [82] J. Li, H. Yang, S. Sha, J. Li, Z. Zhou, Y. Cao, Evaluation of in vitro toxicity of silica nanoparticles (NPs) to lung cells: Influence of cell types and pulmonary surfactant component DPPC, *Ecotoxicol. Environ. Saf.* 186 (2019) 109770. <https://doi.org/10.1016/j.ecoenv.2019.109770>.
- [83] M. Beck-Broichsitter, C. Ruppert, T. Schmehl, A. Günther, W. Seeger, Biophysical inhibition of synthetic vs. naturally-derived pulmonary surfactant preparations by polymeric nanoparticles, *Biochim. Biophys. Acta* 1838 (2014) 474–481. <https://doi.org/10.1016/j.bbamem.2013.10.016>.
- [84] M. Beck-Broichsitter, A. Bohr, Bioinspired polymer nanoparticles omit biophysical interactions with natural lung surfactant, *Nanotoxicology* 13 (2019) 964–976. <https://doi.org/10.1080/17435390.2019.1621400>.
- [85] C.A. Ruge, U.F. Schaefer, J. Herrmann, J. Kirch, O. Cañadas, M. Echaide, J. Pérez-Gil, C. Casals, R. Müller, C.-M. Lehr, The interplay of lung surfactant proteins and lipids assimilates the macrophage clearance of nanoparticles, *PLoS ONE* 7 (2012) e40775. <https://doi.org/10.1371/journal.pone.0040775>.
- [86] M. Beck-Broichsitter, Compatibility of PEGylated Polymer Nanoparticles with the Biophysical Function of Lung Surfactant, *Langmuir* 34 (2018) 540–545. <https://doi.org/10.1021/acs.langmuir.7b03818>.
- [87] J.T. Huckaby, S.K. Lai, PEGylation for enhancing nanoparticle diffusion in mucus, *Adv. Drug Deliv. Rev.* 124 (2018) 125–139. <https://doi.org/10.1016/j.addr.2017.08.010>.
- [88] R. Mathaes, G. Winter, A. Besheer, J. Engert, Influence of particle geometry and PEGylation on phagocytosis of particulate carriers, *Int. J. Pharm.* 465 (2014) 159–164. <https://doi.org/10.1016/j.ijpharm.2014.02.037>.

- [89] P. Muttli, C. Wang, A.J. Hickey, Inhaled drug delivery for tuberculosis therapy, *Pharm. Res.* 26 (2009) 2401–2416. <https://doi.org/10.1007/s11095-009-9957-4>.
- [90] H.-K. Ropponen, R. Richter, A.K.H. Hirsch, C.-M. Lehr, Mastering the Gram-negative bacterial barrier – Chemical approaches to increase bacterial bioavailability of antibiotics, *Adv. Drug Deliv. Rev.* 172 (2021) 339–360. <https://doi.org/10.1016/j.addr.2021.02.014>.
- [91] E. Fröhlich, A. Mercuri, S. Wu, S. Salar-Behzadi, Measurements of Deposition, Lung Surface Area and Lung Fluid for Simulation of Inhaled Compounds, *Front. Pharmacol.* 7 (2016) 181. <https://doi.org/10.3389/fphar.2016.00181>.
- [92] M.A.M. Momin, B. Rangnekar, S. Sinha, C.-Y. Cheung, G.M. Cook, S.C. Das, Inhalable Dry Powder of Bedaquiline for Pulmonary Tuberculosis: In Vitro Physicochemical Characterization, Antimicrobial Activity and Safety Studies, *Pharmaceutics* 11 (2019). <https://doi.org/10.3390/pharmaceutics11100502>.
- [93] D. Rudolph, N. Redinger, U.E. Schaible, C. Feldmann, Transport of Lipophilic Anti-Tuberculosis Drug Benzothiazone-043 in Ca<sub>3</sub>(PO<sub>4</sub>)<sub>2</sub> Nanocontainers, *ChemNanoMat* 7 (2021) 7–16. <https://doi.org/10.1002/cnma.202000421>.
- [94] D. Thiyagarajan, B. Huck, B. Nothdurft, M. Koch, D. Rudolph, M. Rutschmann, C. Feldmann, C. Hozsa, M. Furch, K.F.W. Besecke, R.K. Gieseler, B. Loretz, C.-M. Lehr, Spray-dried lactose-leucine microparticles for pulmonary delivery of antimycobacterial nanopharmaceuticals, *Drug Deliv. Transl. Res.* 11 (2021) 1766–1778. <https://doi.org/10.1007/s13346-021-01011-7>.
- [95] J.E. Hastedt, P. Bäckman, A.R. Clark, W. Doub, A. Hickey, G. Hochhaus, P.J. Kuehl, C.-M. Lehr, P. Mauser, J. McConville, R. Niven, M. Sakagimi, J.G. Weers, Scope and relevance of a pulmonary biopharmaceutical classification system AAPS/FDA/USP Workshop March 16-17th, 2015 in Baltimore, MD, *AAPS Open* 2 (2016). <https://doi.org/10.1186/s41120-015-0002-x>.
- [96] A. Floroiu, M. Klein, J. Krämer, C.-M. Lehr, Towards Standardized Dissolution Techniques for In Vitro Performance Testing of Dry Powder Inhalers, *Dissolution Technol.* 25 (2018) 6–18. <https://doi.org/10.14227/DT250318P6>.
- [97] B.K. Rubin, O. Ramirez, J.G. Zayas, B. Finegan, M. King, Collection and analysis of respiratory mucus from subjects without lung disease, *Am. Rev. Respir. Dis.* 141 (1990) 1040–1043. [https://doi.org/10.1164/ajrccm/141.4\\_Pt\\_1.1040](https://doi.org/10.1164/ajrccm/141.4_Pt_1.1040).
- [98] T. Curstedt, H. Jörnvall, B. Robertson, T. Bergman, P. Berggren, Two hydrophobic low-molecular-mass protein fractions of pulmonary surfactant. Characterization and biophysical activity, *Eur. J. Biochem.* 168 (1987). <https://doi.org/10.1111/j.1432-1033.1987.tb13414.x>.
- [99] O.W. Meldrum, G.E. Yakubov, M.R. Bonilla, O. Deshmukh, M.A. McGuckin, M.J. Gidley, Mucin gel assembly is controlled by a collective action of non-mucin proteins, disulfide bridges, Ca<sup>2+</sup>-mediated links, and hydrogen bonding, *Sci. Rep.* 8 (2018) 5802. <https://doi.org/10.1038/s41598-018-24223-3>.
- [100] A.L. Innes, S.D. Carrington, D.J. THORNTON, S. KIRKHAM, K. Rousseau, R.H. Dougherty, W.W. Raymond, G.H. Caughey, S.J. Muller, J.V. Fahy, Ex vivo sputum analysis reveals impairment of protease-dependent mucus degradation by plasma proteins in acute asthma, *Am. J. Respir. Crit. Care Med.* 180 (2009) 203–210. <https://doi.org/10.1164/rccm.200807-1056OC>.
- [101] F. Fasquelle, R. Carpentier, B. Demouveau, J.-L. Desseyn, D. Betbeder, Importance of the Phospholipid Core for Mucin Hydrogel Penetration and Mucosal Cell Uptake of Maltodextrin

- Nanoparticles, *ACS Appl. Bio Mater.* 3 (2020) 5741–5749.  
<https://doi.org/10.1021/acsabm.0c00521>.
- [102] C.A. Silva, T.M. Nobre, F.J. Pavinatto, O.N. Oliveira, Interaction of chitosan and mucin in a biomembrane model environment, *J. Colloid Interface Sci.* 376 (2012) 289–295.  
<https://doi.org/10.1016/j.jcis.2012.03.027>.
- [103] M. Boegh, S.G. Baldursdóttir, A. Müllertz, H.M. Nielsen, Property profiling of biosimilar mucus in a novel mucus-containing in vitro model for assessment of intestinal drug absorption, *Eur. J. Pharm. Biopharm.* 87 (2014) 227–235. <https://doi.org/10.1016/j.ejpb.2014.01.001>.
- [104] M. Tan, Y. Mao, T.W. Walker, Rheological Enhancement of Artificial Sputum Medium, *Applied Rheology* 30 (2020) 27–38. <https://doi.org/10.1515/arh-2020-0100>.
- [105] R. Hamed, J. Fiegel, Synthetic tracheal mucus with native rheological and surface tension properties, *J. Biomed. Mater. Res. Part A* 102 (2014) 1788–1798.  
<https://doi.org/10.1002/jbm.a.34851>.
- [106] J. Ernst, M. Klinger-Strobel, K. Arnold, J. Thamm, A. Hartung, M.W. Pletz, O. Makarewicz, D. Fischer, Polyester-based particles to overcome the obstacles of mucus and biofilms in the lung for tobramycin application under static and dynamic fluidic conditions, *Eur. J. Pharm. Biopharm.* 131 (2018) 120–129. <https://doi.org/10.1016/j.ejpb.2018.07.025>.
- [107] C. Cristallini, N. Barbani, L. Ventrelli, C. Summa, S. Filippi, T. Capelôa, E. Vitale, C. Albera, B. Messore, C. Giachino, Biodegradable microparticles designed to efficiently reach and act on cystic fibrosis mucus barrier, *Mater. Sci. Eng., C* 95 (2019) 19–28.  
<https://doi.org/10.1016/j.msec.2018.10.064>.
- [108] I.A. Sogias, A.C. Williams, V.V. Khutoryanskiy, Why is chitosan mucoadhesive?, *Biomacromolecules* 9 (2008) 1837–1842. <https://doi.org/10.1021/bm800276d>.
- [109] G. Alp, N. Aydogan, Lipid-based mucus penetrating nanoparticles and their biophysical interactions with pulmonary mucus layer, *Eur. J. Pharm. Biopharm.* 149 (2020) 45–57.  
<https://doi.org/10.1016/j.ejpb.2020.01.017>.
- [110] S.K. Lai, D.E. O'Hanlon, S. Harrold, S.T. Man, Y.-Y. Wang, R. Cone, J. Hanes, Rapid transport of large polymeric nanoparticles in fresh undiluted human mucus, *PNAS* 104 (2007) 1482–1487.  
<https://doi.org/10.1073/pnas.0608611104>.
- [111] X. Murgia, P. Pawelzyk, U.F. Schaefer, C. Wagner, N. Willenbacher, C.-M. Lehr, Size-Limited Penetration of Nanoparticles into Porcine Respiratory Mucus after Aerosol Deposition, *Biomacromolecules* 17 (2016) 1536–1542. <https://doi.org/10.1021/acs.biomac.6b00164>.
- [112] X. Li, D. Chen, C. Le, C. Zhu, Y. Gan, L. Hovgaard, M. Yang, Novel mucus-penetrating liposomes as a potential oral drug delivery system: preparation, in vitro characterization, and enhanced cellular uptake, *Int. J. Nanomedicine* 6 (2011) 3151–3162.  
<https://doi.org/10.2147/IJN.S25741>.
- [113] V. Zabaleta, G. Ponchel, H. Salman, M. Agüeros, C. Vauthier, J.M. Irache, Oral administration of paclitaxel with pegylated poly(anhydride) nanoparticles: permeability and pharmacokinetic study, *Eur. J. Pharm. Biopharm.* 81 (2012) 514–523. <https://doi.org/10.1016/j.ejpb.2012.04.001>.
- [114] A. Torge, S. Wagner, P.S. Chaves, E.G. Oliveira, S.S. Guterres, A.R. Pohlmann, A. Titz, M. Schneider, R.C.R. Beck, Ciprofloxacin-loaded lipid-core nanocapsules as mucus penetrating drug

- delivery system intended for the treatment of bacterial infections in cystic fibrosis, *Int. J. Pharm.* 527 (2017) 92–102. <https://doi.org/10.1016/j.ijpharm.2017.05.013>.
- [115] A.K.M. Shamsuddin, P.M. Quinton, Concurrent absorption and secretion of airway surface liquids and bicarbonate secretion in human bronchioles, *Am. J. Physiol. Lung Cell. Mol. Physiol.* 316 (2019) L953-L960. <https://doi.org/10.1152/ajplung.00545.2018>.
- [116] E. Cingolani, S. Alqahtani, R.C. Sadler, D. Prime, S. Stolnik, C. Bosquillon, In vitro investigation on the impact of airway mucus on drug dissolution and absorption at the air-epithelium interface in the lungs, *Eur. J. Pharm. Biopharm.* 141 (2019) 210–220. <https://doi.org/10.1016/j.ejpb.2019.05.022>.
- [117] S. Alqahtani, C.J. Roberts, S. Stolnik, C. Bosquillon, Development of an In Vitro System to Study the Interactions of Aerosolized Drugs with Pulmonary Mucus, *Pharmaceutics* 12 (2020). <https://doi.org/10.3390/pharmaceutics12020145>.
- [118] S. Hein, M. Bur, U.F. Schaefer, C.-M. Lehr, A new Pharmaceutical Aerosol Deposition Device on Cell Cultures (PADD OCC) to evaluate pulmonary drug absorption for metered dose dry powder formulations, *Eur. J. Pharm. Biopharm.* 77 (2011) 132–138. <https://doi.org/10.1016/j.ejpb.2010.10.003>.
- [119] T. Samad, J.Y. Co, J. Witten, K. Ribbeck, Mucus and Mucin Environments Reduce the Efficacy of Polymyxin and Fluoroquinolone Antibiotics against *Pseudomonas aeruginosa*, *ACS Biomater. Sci. Eng.* 5 (2019) 1189–1194. <https://doi.org/10.1021/acsbiomaterials.8b01054>.
- [120] P. Drevinek, M.T.G. Holden, Z. Ge, A.M. Jones, I. Ketchell, R.T. Gill, E. Mahenthiralingam, Gene expression changes linked to antimicrobial resistance, oxidative stress, iron depletion and retained motility are observed when *Burkholderia cenocepacia* grows in cystic fibrosis sputum, *BMC Infect. Dis.* 8 (2008) 121. <https://doi.org/10.1186/1471-2334-8-121>.
- [121] S. Diraviam Dinesh, Artificial Sputum Medium, *Nat. Protoc.* (2010). <https://doi.org/10.1038/protex.2010.212>.
- [122] P.G. Bhat, D.R. Flanagan, M.D. Donovan, Drug diffusion through cystic fibrotic mucus: steady-state permeation, rheologic properties, and glycoprotein morphology, *J. Pharm. Sci.* 85 (1996) 624–630. <https://doi.org/10.1021/js950381s>.
- [123] H. Friedl, S. Dünnhaupt, F. Hintzen, C. Waldner, S. Parikh, J.P. Pearson, M.D. Wilcox, A. Bernkop-Schnürch, Development and evaluation of a novel mucus diffusion test system approved by self-nanoemulsifying drug delivery systems, *J. Pharm. Sci.* 102 (2013) 4406–4413. <https://doi.org/10.1002/jps.23757>.
- [124] M.R. Markovetz, D.B. Subramani, W.J. Kissner, C.B. Morrison, I.C. Garbarine, A. Ghio, K.A. Ramsey, H. Arora, P. Kumar, D.B. Nix, T. Kumagai, T.M. Krunkosky, D.C. Krause, G. Radicioni, N.E. Alexis, M. Kesimer, M. Tiemeyer, R.C. Boucher, C. Ehre, D.B. Hill, Endotracheal tube mucus as a source of airway mucus for rheological study, *Am. J. Physiol. Lung Cell. Mol. Physiol.* 317 (2019) L498-L509. <https://doi.org/10.1152/ajplung.00238.2019>.
- [125] C.D.M. Wijers, R. Vagedes, C. Weingart, A novel method for investigating *Burkholderia cenocepacia* infections in patients with cystic fibrosis and other chronic diseases of the airways, *BMC Microbiol.* 16 (2016) 200. <https://doi.org/10.1186/s12866-016-0811-7>.
- [126] J.C. Horstmann, A. Laric, A. Boese, D. Yildiz, T. Röhrig, M. Empting, N. Frank, D. Krug, R. Müller, N. Schneider-Daum, C. de Souza Carvalho-Wodarz, C.-M. Lehr, Transferring

- Microclusters of *P. aeruginosa* Biofilms to the Air-Liquid Interface of Bronchial Epithelial Cells for Repeated Deposition of Aerosolized Tobramycin, *ACS Infect. Dis.* (2021). <https://doi.org/10.1021/acsinfecdis.1c00444>.
- [127] F. Anversa Dimer, C. de Souza Carvalho-Wodarz, A. Goes, K. Cirnski, J. Herrmann, V. Schmitt, L. Pätzold, N. Abed, C. de Rossi, M. Bischoff, P. Couvreur, R. Müller, C.-M. Lehr, PLGA nanocapsules improve the delivery of clarithromycin to kill intracellular *Staphylococcus aureus* and *Mycobacterium abscessus*, *Nanomedicine nanotechnology, biology, and medicine* 24 (2020) 102125. <https://doi.org/10.1016/j.nano.2019.102125>.
- [128] H.X. Ong, D. Traini, P.M. Young, Pharmaceutical applications of the Calu-3 lung epithelia cell line, *Expert Opin. Drug Deliv.* 10 (2013) 1287–1302. <https://doi.org/10.1517/17425247.2013.805743>.
- [129] J.J. Schüer, A. Arndt, C. Wölk, Pinnapireddy SR, U. Bakowsky, Establishment of a Synthetic In Vitro Lung Surfactant Model for Particle Interaction Studies on a Langmuir Film Balance, *Langmuir* 36 (2020). <https://doi.org/10.1021/acs.langmuir.9b03712>.
- [130] J.J. Schüer, C. Wölk, U. Bakowsky, S.R. Pinnapireddy, Comparison of Tanaka lipid mixture with natural surfactant Alveofact to study nanoparticle interactions on Langmuir film balance, *Colloids Surf. B Biointerfaces* 188 (2020) 110750. <https://doi.org/10.1016/j.colsurfb.2019.110750>.
- [131] A. Kumar, W. Terakosolphan, M. Hassoun, K.-K. Vandera, A. Novicky, R. Harvey, P.G. Royall, E.M. Bicer, J. Eriksson, K. Edwards, D. Valkenborg, I. Nelissen, D. Hassall, I.S. Mudway, B. Forbes, A Biocompatible Synthetic Lung Fluid Based on Human Respiratory Tract Lining Fluid Composition, *Pharm. Res.* 34 (2017) 2454–2465. <https://doi.org/10.1007/s11095-017-2169-4>.
- [132] A. Tridente, L. de Martino, D. de Luca, Porcine vs bovine surfactant therapy for preterm neonates with RDS: systematic review with biological plausibility and pragmatic meta-analysis of respiratory outcomes, *Respir. Res.* 20 (2019) 1–13. <https://doi.org/10.1186/s12931-019-0979-0>.
- [133] C. Garcia-Mouton, A. Hidalgo, A. Cruz, J. Pérez-Gil, The Lord of the Lungs: The essential role of pulmonary surfactant upon inhalation of nanoparticles, *Eur. J. Pharm. Biopharm.* 144 (2019) 230–243. <https://doi.org/10.1016/j.ejpb.2019.09.020>.
- [134] A. Hidalgo, A. Cruz, J. Pérez-Gil, Barrier or carrier? Pulmonary surfactant and drug delivery, *Eur. J. Pharm. Biopharm.* 95 (2015) 117–127. <https://doi.org/10.1016/j.ejpb.2015.02.014>.
- [135] J. Goerke, Pulmonary surfactant: functions and molecular composition, *Biochim. Biophys. Acta* 1408 (1998) 79–89. [https://doi.org/10.1016/S0925-4439\(98\)00060-X](https://doi.org/10.1016/S0925-4439(98)00060-X).
- [136] A.T. Kodama, C.-C. Kuo, T. Boatwright, M. Dennin, Investigating the effect of particle size on pulmonary surfactant phase behavior, *Biophys. J.* 107 (2014) 1573–1581. <https://doi.org/10.1016/j.bpj.2014.08.010>.
- [137] M. Beck-Broichsitter, Biophysical Activity of Impaired Lung Surfactant upon Exposure to Polymer Nanoparticles, *Langmuir* 32 (2016) 10422–10429. <https://doi.org/10.1021/acs.langmuir.6b02893>.
- [138] M. Rojewska, W. Smułek, E. Kaczorek, K. Prochaska, Langmuir Monolayer Techniques for the Investigation of Model Bacterial Membranes and Antibiotic Biodegradation Mechanisms, *Membranes (Basel)* 11 (2021). <https://doi.org/10.3390/membranes11090707>.

- [139] M.P. Monopoli, C. Åberg, A. Salvati, K.A. Dawson, Biomolecular coronas provide the biological identity of nanosized materials, *Nature Nanotech.* 7 (2012) 779–786. <https://doi.org/10.1038/nnano.2012.207>.
- [140] Y.E. Silina, J. Welck, A. Kraegeloh, M. Koch, C. Fink-Straube, Interactions between DPPC as a component of lung surfactant and amorphous silica nanoparticles investigated by HILIC-ESI-MS, *J. Chromatogr. B Analyt. Technol. Biomed. Life Sci.* 1029-1030 (2016) 222–229. <https://doi.org/10.1016/j.jchromb.2016.07.014>.
- [141] I.G. Theodorou, P. Ruenraroengsak, A. Gow, S. Schwander, J.J. Zhang, K.F. Chung, T.D. Tetley, M.P. Ryan, A.E. Porter, Effect of pulmonary surfactant on the dissolution, stability and uptake of zinc oxide nanowires by human respiratory epithelial cells, *Nanotoxicology* 10 (2016) 1351–1362. <https://doi.org/10.1080/17435390.2016.1214762>.
- [142] J.Y. Kasper, M.I. Hermanns, R.E. Unger, C.J. Kirkpatrick, A responsive human triple-culture model of the air-blood barrier: incorporation of different macrophage phenotypes, *J. Tissue Eng. Regen. Med.* 11 (2017) 1285–1297. <https://doi.org/10.1002/term.2032>.
- [143] B.M. Rothen-Rutishauser, S.G. Kiama, P. Gehr, A three-dimensional cellular model of the human respiratory tract to study the interaction with particles, *Am. J. Respir. Cell Mol. Biol.* 32 (2005) 281–289. <https://doi.org/10.1165/rcmb.2004-0187OC>.
- [144] S. Azarmi, W.H. Roa, R. Löbenberg, Targeted delivery of nanoparticles for the treatment of lung diseases, *Adv. Drug. Deliv. Rev.* 60 (2008) 863–875. <https://doi.org/10.1016/j.addr.2007.11.006>.
- [145] M.A. Desai, M. Mutlu, P. Vadgama, A study of macromolecular diffusion through native porcine mucus, *Experientia* 48 (1992) 22–26.
- [146] A.W. Larhed, P. Artursson, J. Gråsjö, E. Björk, Diffusion of drugs in native and purified gastrointestinal mucus, *J. Pharm. Sci.* 86 (1997) 660–665. <https://doi.org/10.1021/js960503w>.
- [147] Y.-Y. Wang, S.K. Lai, J.S. Suk, A. Pace, R. Cone, J. Hanes, Addressing the PEG mucoadhesivity paradox to engineer nanoparticles that "slip" through the human mucus barrier, *Angew. Chem. Int. Ed Engl.* 47 (2008) 9726–9729. <https://doi.org/10.1002/anie.200803526>.
- [148] J.S. Suk, Q. Xu, N. Kim, J. Hanes, L.M. Ensign, PEGylation as a strategy for improving nanoparticle-based drug and gene delivery, *Adv. Drug Deliv. Rev.* 99 (2016) 28–51. <https://doi.org/10.1016/j.addr.2015.09.012>.
- [149] S. Köllner, S. Dünnhaupt, C. Waldner, S. Hauptstein, I. Pereira de Sousa, A. Bernkop-Schnürch, Mucus permeating thiomers nanoparticles, *Eur. J. Pharm. Biopharm.* 97 (2015) 265–272. <https://doi.org/10.1016/j.ejpb.2015.01.004>.
- [150] G.A. Duncan, N. Kim, Y. Colon-Cortes, J. Rodriguez, M. Mazur, S.E. Birket, S.M. Rowe, N.E. West, A. Livraghi-Butrico, R.C. Boucher, J. Hanes, G. Aslanidi, J.S. Suk, An Adeno-Associated Viral Vector Capable of Penetrating the Mucus Barrier to Inhaled Gene Therapy, *Mol. Ther. Methods Clin. Dev.* 9 (2018) 296–304. <https://doi.org/10.1016/j.omtm.2018.03.006>.
- [151] J. Leal, T. Dong, A. Taylor, E. Siegrist, F. Gao, H.D.C. Smyth, D. Ghosh, Mucus-penetrating phage-displayed peptides for improved transport across a mucus-like model, *Int. J. Pharm.* 553 (2018) 57–64. <https://doi.org/10.1016/j.ijpharm.2018.09.055>.
- [152] J. Leal, X. Peng, X. Liu, D. Arasappan, D.C. Wylie, S.H. Schwartz, J.J. Fullmer, B.C. McWilliams, H.D.C. Smyth, D. Ghosh, Peptides as surface coatings of nanoparticles that penetrate human

- cystic fibrosis sputum and uniformly distribute in vivo following pulmonary delivery, *J. Control. Release* 322 (2020) 457–469. <https://doi.org/10.1016/j.jconrel.2020.03.032>.
- [153] G. Alp, N. Aydogan, Enhancing the Spreading Behavior on Pulmonary Mucus Mimicking Subphase via Catanionic Surfactant Solutions: Toward Effective Drug Delivery through the Lungs, *Mol. Pharm.* 15 (2018) 1361–1370. <https://doi.org/10.1021/acs.molpharmaceut.8b00086>.
- [154] H. Douafer, V. Andrieu, J.M. Brunel, Scope and limitations on aerosol drug delivery for the treatment of infectious respiratory diseases, *J. Control. Release* 325 (2020) 276–292. <https://doi.org/10.1016/j.jconrel.2020.07.002>.
- [155] D.E. Geller, M.W. Konstan, J. Smith, S.B. Noonberg, C. Conrad, Novel tobramycin inhalation powder in cystic fibrosis subjects: pharmacokinetics and safety, *Pediatr. Pulmonol.* 42 (2007) 307–313. <https://doi.org/10.1002/ppul.20594>.
- [156] T. Jensen, S.S. Pedersen, S. Garne, C. Heilmann, N. Højby, C. Koch, Colistin inhalation therapy in cystic fibrosis patients with chronic *Pseudomonas aeruginosa* lung infection, *J. Antimicrob. Chemother.* 19 (1987). <https://doi.org/10.1093/jac/19.6.831>.
- [157] R.L. Gibson, G.Z. Retsch-Bogart, C. Oermann, C. Milla, J. Pilewski, C. Daines, R. Ahrens, K. Leon, M. Cohen, S. McNamara, T.L. Callahan, R. Markus, J.L. Burns, Microbiology, safety, and pharmacokinetics of aztreonam lysinate for inhalation in patients with cystic fibrosis, *Pediatr. Pulmonol.* 41 (2006) 656–665. <https://doi.org/10.1002/ppul.20429>.
- [158] O. Khan, N. Chaudary, The Use of Amikacin Liposome Inhalation Suspension (Arikayce) in the Treatment of Refractory Nontuberculous Mycobacterial Lung Disease in Adults, *Drug Des. Devel. Ther.* 14 (2020) 2287–2294. <https://doi.org/10.2147/DDDT.S146111>.
- [159] A. Misra, A.J. Hickey, C. Rossi, G. Borchard, H. Terada, K. Makino, P.B. Fourie, P. Colombo, Inhaled drug therapy for treatment of tuberculosis, *Tuberculosis (Edinb)* 91 (2011) 71–81. <https://doi.org/10.1016/j.tube.2010.08.009>.
- [160] S.P. Vyas, M.E. Kannan, S. Jain, V. Mishra, P. Singh, Design of liposomal aerosols for improved delivery of rifampicin to alveolar macrophages, *Int. J. Pharm.* 269 (2004) 37–49. <https://doi.org/10.1016/j.ijpharm.2003.08.017>.
- [161] G. Chimote, R. Banerjee, Effect of mycobacterial lipids on surface properties of Curosurf: implications for lung surfactant dysfunction in tuberculosis, *Respir. Physiol. Neurobiol.* 162 (2008) 73–79. <https://doi.org/10.1016/j.resp.2008.04.004>.
- [162] G. Chimote, R. Banerjee, Evaluation of antitubercular drug-loaded surfactants as inhalable drug-delivery systems for pulmonary tuberculosis, *J. Biomed. Mater. Res. A* 89 (2009) 281–292. <https://doi.org/10.1002/jbm.a.31959>.
- [163] G. Chimote, R. Banerjee, In vitro evaluation of inhalable isoniazid-loaded surfactant liposomes as an adjunct therapy in pulmonary tuberculosis, *J. Biomed. Mater. Res. B Appl. Biomater.* 94 (2010) 1–10. <https://doi.org/10.1002/jbm.b.31608>.
- [164] L. Sercombe, T. Veerati, F. Moheimani, S.Y. Wu, A.K. Sood, S. Hua, Advances and Challenges of Liposome Assisted Drug Delivery, *Front. Pharmacol.* 6 (2015) 286. <https://doi.org/10.3389/fphar.2015.00286>.
- [165] J.G. Weers, T.E. Tarara, A.R. Clark, Design of fine particles for pulmonary drug delivery, *Expert Opin. Drug Deliv.* 4 (2007) 297–313. <https://doi.org/10.1517/17425247.4.3.297>.



- [166] M. Hoppentocht, P. Hagedoorn, H.W. Frijlink, A.H. de Boer, Developments and strategies for inhaled antibiotic drugs in tuberculosis therapy: a critical evaluation, *Eur. J. Pharm. Biopharm.* 86 (2014) 23–30. <https://doi.org/10.1016/j.ejpb.2013.10.019>.
- [167] M. Hoppentocht, P. Hagedoorn, H.W. Frijlink, A.H. de Boer, Technological and practical challenges of dry powder inhalers and formulations, *Adv. Drug. Deliv. Rev.* 75 (2014) 18–31. <https://doi.org/10.1016/j.addr.2014.04.004>.
- [168] A. Rezvankhah, Z. Emam-Djomeh, G. Askari, Encapsulation and delivery of bioactive compounds using spray and freeze-drying techniques: A review, *Drying Technology* 38 (2020) 235–258. <https://doi.org/10.1080/07373937.2019.1653906>.
- [169] P. Mehta, Imagine the Superiority of Dry Powder Inhalers from Carrier Engineering, *J. of Drug Delivery* 2018 (2018) 5635010. <https://doi.org/10.1155/2018/5635010>.
- [170] Y. Yang, M.D. Tsifansky, C.-J. Wu, H.I. Yang, G. Schmidt, Y. Yeo, Inhalable antibiotic delivery using a dry powder co-delivering recombinant deoxyribonuclease and ciprofloxacin for treatment of cystic fibrosis, *Pharm. Res.* 27 (2010) 151–160. <https://doi.org/10.1007/s11095-009-9991-2>.
- [171] R.V. Pai, R.R. Jain, A.S. Bannaliker, M.D. Menon, Development and Evaluation of Chitosan Microparticles Based Dry Powder Inhalation Formulations of Rifampicin and Rifabutin, *J. Aerosol Med. Pulm. Drug Deliv.* 29 (2016) 179–195. <https://doi.org/10.1089/jamp.2014.1187>.
- [172] D. Lu, A.J. Hickey, Liposomal dry powders as aerosols for pulmonary delivery of proteins, *AAPS PharmSciTech* 6 (2005) E641-8. <https://doi.org/10.1208/pt060480>.
- [173] G. Chai, A. Hassan, T. Meng, L. Lou, J. Ma, R. Simmers, L. Zhou, B.K. Rubin, Q.T. Zhou, P.W. Longest, M. Hindle, Q. Xu, Dry powder aerosol containing muco-inert particles for excipient enhanced growth pulmonary drug delivery, *Nanomedicine nanotechnology, biology, and medicine* 29 (2020) 102262. <https://doi.org/10.1016/j.nano.2020.102262>.
- [174] B. Porsio, E.F. Craparo, N. Mauro, G. Giammona, G. Cavallaro, Mucus and Cell-Penetrating Nanoparticles Embedded in Nano-into-Micro Formulations for Pulmonary Delivery of Ivacaftor in Patients with Cystic Fibrosis, *ACS Appl. Mater. Interfaces* 10 (2018) 165–181. <https://doi.org/10.1021/acsami.7b14992>.
- [175] Z. Huang, S.N. Kłodzińska, F. Wan, H.M. Nielsen, Nanoparticle-mediated pulmonary drug delivery: state of the art towards efficient treatment of recalcitrant respiratory tract bacterial infections, *Drug Deliv. Transl. Res.* 11 (2021) 1634–1654. <https://doi.org/10.1007/s13346-021-00954-1>.
- [176] T. Parumasivam, R.Y.K. Chang, S. Abdelghany, T.T. Ye, W.J. Britton, H.-K. Chan, Dry powder inhalable formulations for anti-tubercular therapy, *Adv. Drug. Deliv. Rev.* 102 (2016) 83–101. <https://doi.org/10.1016/j.addr.2016.05.011>.
- [177] L. Müller, X. Murgia, L. Siebenbürger, C. Börger, K. Schwarzkopf, K. Sewald, S. Häussler, A. Braun, C.-M. Lehr, M. Hittinger, S. Wronski, Human airway mucus alters susceptibility of *Pseudomonas aeruginosa* biofilms to tobramycin, but not colistin, *J. Antimicrob. Chemother.* 73 (2018) 2762–2769. <https://doi.org/10.1093/jac/dky241>.
- [178] S. Frisch, A. Boese, B. Huck, J.C. Horstmann, D.-K. Ho, K. Schwarzkopf, X. Murgia, B. Loretz, C. de Souza Carvalho-Wodarz, C.-M. Lehr, A pulmonary mucus surrogate for investigating

- antibiotic permeation and activity against *Pseudomonas aeruginosa* biofilms, *J. Antimicrob. Chemother.* 76 (2021) 1472–1479. <https://doi.org/10.1093/jac/dkab068>.
- [179] P. GEHR, M. GEISER, H.V. Im, S. SCHÜRCH, U. Waber, M. Baumann, Surfactant and inhaled particles in the conducting airways: structural, stereological, and biophysical aspects, *Microscopy research and technique* 26 (1993). <https://doi.org/10.1002/jemt.1070260510>.
- [180] P. GEHR, F.H. Green, M. GEISER, V. Im HOF, M.M. Lee, S. SCHÜRCH, Airway surfactant, a primary defense barrier: mechanical and immunological aspects, *J. Aerosol Med.* 9 (1996) 163–181. <https://doi.org/10.1089/jam.1996.9.163>.
- [181] M. Echaide, C. Autilio, E. López-Rodríguez, A. Cruz, J. Pérez-Gil, In Vitro Functional and Structural Characterization of A Synthetic Clinical Pulmonary Surfactant with Enhanced Resistance to Inhibition, *Sci. Rep.* 10 (2020) 1385. <https://doi.org/10.1038/s41598-020-58248-4>.
- [182] C. Autilio, M. Echaide, S. Shankar-Aguilera, R. Bragado, D. Amidani, F. Salomone, J. Pérez-Gil, D. de Luca, Surfactant Injury in the Early Phase of Severe Meconium Aspiration Syndrome, *Am. J. Respir. Cell Mol. Biol.* 63 (2020) 327–337. <https://doi.org/10.1165/rcmb.2019-0413OC>.
- [183] A. Sosnik, A.M. Carcaboso, R.J. Glisoni, M.A. Moretton, D.A. Chiappetta, New old challenges in tuberculosis: potentially effective nanotechnologies in drug delivery, *Adv. Drug. Deliv. Rev.* 62 (2010) 547–559. <https://doi.org/10.1016/j.addr.2009.11.023>.
- [184] B.C. Huck, D. Thiyagarajan, A. Bali, A. Boese, K.F.W. Besecke, C. Hozsa, R.K. Gieseler, M. Furch, C. Carvalho-Wodarz, F. Waldow, D. Schwudke, O. Metelkina, A. Titz, H. Huwer, K. Schwarzkopf, J. Hoppstädter, A.K. Kiemer, M. Koch, B. Loretz, C.-M. Lehr, Nano-in-Microparticles for Aerosol Delivery of Antibiotic-Loaded, Fucose-Derivatized, and Macrophage-Targeted Liposomes to Combat Mycobacterial Infections: In Vitro Deposition, Pulmonary Barrier Interactions, and Targeted Delivery, *Adv. Healthc. Mater.* (2022) e2102117. <https://doi.org/10.1002/adhm.202102117>.
- [185] A.K. Azad, M.V.S. Rajaram, L.S. Schlesinger, Exploitation of the Macrophage Mannose Receptor (CD206) in Infectious Disease Diagnostics and Therapeutics, *J. Cytol. Mol. Biol.* 1 (2014). <https://doi.org/10.13188/2325-4653.1000003>.
- [186] S.B. Cohen, B.H. Gern, J.L. Delahaye, K.N. Adams, C.R. Plumlee, J.K. Winkler, D.R. Sherman, M.Y. Gerner, K.B. Urdahl, Alveolar Macrophages Provide an Early Mycobacterium tuberculosis Niche and Initiate Dissemination, *Cell Host Microbe* 24 (2018) 439-446.e4. <https://doi.org/10.1016/j.chom.2018.08.001>.
- [187] K. To, R. Cao, A. Yegiazaryan, J. Owens, V. Venketaraman, General Overview of Nontuberculous Mycobacteria Opportunistic Pathogens: *Mycobacterium avium* and *Mycobacterium abscessus*, *J. Clin. Med.* 9 (2020). <https://doi.org/10.3390/jcm9082541>.

## 7 List of scientific publications

### Articles published in international peer-reviewed journals

1. Huck B, Thiagarajan D, Bali A, Boese A, Besecke K, Hozsa C, Gieseler R, Furch M, Carvalho-Wodarz C, Waldow F, Schwudke D, Metelkina O, Titz A, Huwer H, Schwarzkopf K, Hoppstädter J, Kiemer K, Koch M, Loretz B, Lehr C-M, *Nano-in-Microparticles for Aerosol Delivery of Antibiotic-loaded, Fucose-derivatized and Macrophage-targeted Liposomes to Combat Mycobacterial Infections: In Vitro deposition, Pulmonary Barrier Interactions and Targeted Delivery*, Adv Healthcare Mat, **2022**
2. Huck B, Murgia X, Frisch S, Hittinger M, Hidalgo A, Loretz B, Lehr C-M, *Models using native tracheobronchial mucus in the context of pulmonary drug delivery research: Composition, structure and barrier properties*, Adv Drug Del Rev, **2022**, 183: 114141
3. Metelkina O, Huck B, O'Connor J, Koch M, Manz A, Lehr C-M, Titz A, *Targeting extracellular lectins of Pseudomonas aeruginosa with glycomimetic liposomes*, J Mater Chem B, **2021**, 10:537–48
4. Huck B, Hidalgo A, Waldow F, Schwudke D, Gaede K, Feldmann C, Carius P, Autilio C, Perez-Gil J, Schwarzkopf K, Murgia X, Loretz B, Lehr C-M, *Systematic Analysis of Composition and Performance of Pulmonary Surfactant Preparations on Cellular Uptake and Cytotoxicity of Aerosolized Nanomaterials*, Small science, **2021**, 1: 2100067
5. Thiagarajan D, Huck B, Nothdurft B, Koch M, Rudolph D, Rutschmann M, Feldmann C, Hozsa C, Furch M, Besecke K, Gieseler R, Loretz B, Lehr C-M, *Spray-dried lactose-leucine microparticles for pulmonary delivery of antimycobacterial*, Drug Del Transl Rev, **2021**, 11:1766-78
6. Frisch S, Boese A, Huck B, Horstmann J, Ho D-K, Schwarzkopf K, Murgia X, Loretz B, Carvalho-Wodarz C, Lehr C-M, *A surrogate of pulmonary mucus for investigating antibiotic permeation and activity against Pseudomonas aeruginosa biofilms*, J Antimicrob Chemother, **2021**, 76:1472-79
7. Huck B, Hartwig O, Biehl A, Schwarzkopf K, Wagner C, Loretz B, Murgia X, Lehr C-M, *Macro- and microrheological properties of mucus surrogates in comparison to native intestinal and pulmonary mucus*, Biomacromolecules, **2019**, 20:3504–12

### Articles in preparation

Rautaniemi K, Richter M, Huck B, Loretz B, Lehr C-M, John T, Vuorimaa-Laukkanena E, Lisitsynaa E, Laaksonen T, *Comparing intracellular dynamics of extracellular vesicles and polymeric nanoparticles by video tracking*, Manuscript in preparation.

Tietze L, Hädrich, G, Hozsa C, Besecke K, Kollan, J, Schwudke D, Waldow, F, Markus Furch M, Gieseler R, Thiagarajan D, Huck B, Loretz B, Lehr C-M, Dailey LA. *In Vitro Assessment of Respirable Bedaquiline-Loaded Targospheres® Designed for Inhalation Therapy of Multidrug-Resistant Tuberculosis*, Manuscript in preparation.

### Poster and oral presentations

Huck B, Hartwig O, Biehl A, Schwarzkopf K, Murgia X, Loretz B, Lehr C-M. *Comparing the complex nature of native mucus and artificial mucus models: Rheological profiling and Multiple Particle Tracking*. Workshop on Pulmonary Drug Delivery **2018**, Dublin, Ireland.

Huck, B, Schüer J, Murgia X, Loretz B, Lehr C-M. *Phospholipid isolation from pulmonary mucus as a model for pulmonary surfactant*. CRS local chapter, 7+8. March **2019**, Leipzig, Germany.

Huck B, Schüer J, Schwudke D, Murgia X, Loretz B, Schwarzkopf K, Bakowsky U, Lehr C-M. *Isolation of surfactant from human tracheobronchial mucus to study particle interaction at the air-liquid interface*. International Society for Aerosols in Medicine Meeting 2.5-29. May **2019**, Montreux, Switzerland. Winner of the Winfried Möller Research Award.

Huck B, Hidalgo A, Schüer J, Murgia X, Loretz B, Schwarzkopf K, Waldow F, Schwudke D, Perez-Gil J, Bakowsky U, Lehr C.-M. *Lipid fraction extracted from tracheobronchial mucus exhibits surfactant-like properties – an alternative to pulmonary surfactant?* Poster 46. Controlled Release Society Meeting, 21-24. July **2019**, Valencia, Spain.

Huck B, Durairaj T, Schwarzkopf K, Besecke K Furch M, Gieseler R, Hosza C, Waldow F, Schwudke D, Loretz B, Lehr C-M. *Bedaquiline-loaded liposome dry powders for pulmonary treatment of mycobacterial infections*. Oral presentation + Poster; 23. International Society for Aerosols in Medicine Meeting in Boise, Idaho, USA, 22.-26. May **2021**, virtual attendance.

## 8 Scientific collaborations

This work is the result of the successful collaboration with a lot of partners, many of them, but not all, were part of the BMBF-funded ANTI-TB project. The scientific exchange, intensive discussions, fruitful meetings and hard work made this a successful project which deserves a special acknowledgement.

The collaboration with Dr. Dominik Schwudke and Dr. Franziska Waldow from Forschungszentrum Borstel (FZB) and their support on the lipidomic profiling enabled the comparison of the composition of various surfactant preparations. The cooperation with Prof. Dr. Jesus Perez-Gil and Dr. Chiara Autilio from the Complutense University Madrid helped in the biophysical analysis of the surfactant preparations. I also highly acknowledge the opportunity for a short-time research visit.

The primary cells and material used in this thesis were kindly provided by Dr. Karoline Gaede (BALF), Prof. Dr. Konrad Schwarzkopf (Mucus), Prof. Dr. Hanno Huwer (Lung tissue), Prof. Dr. Alexandra Kiemer and Dr. Jessica Hoppstädter (Buffy coats). With their expertise, they helped in discussing and interpreting the results.

Organic nanocarriers (TargoSpheres<sup>®</sup>) were produced and provided by Rodos Biotarget, thanks to Dr. Karen Besecke, Dr. Constantin Hozsa, Dr. Marcus Furch and Dr. Robert Gieseler, also for their support and discussions. Inorganic nanocarriers were provided from Prof. Dr. Claus Feldmann's lab at the Karlsruher Institute of Technology (KIT).

I further acknowledge the collaborations within the DDEL group. Dr. Christiane Carvalho-Wodarz, Dr. Annette Boese and Aghiad Bali interpreted, discussed and performed *in vitro* infection studies with *M. Abscessus*.

Flow chamber assays were performed and optimized together with Olga Metelkina and supervised by Prof. Dr. Alexander Titz. Dr. Marcus Koch from Leibniz-Institute for New Materials (INM) is thanked for his help with Cryo-TEM analysis.

## 9 Acknowledgements

Writing these words means that a big chapter is finally coming to an end. I have to deeply thank a lot of people who have encouraged me to start, to pursue and to finally finish a long journey. The time at HIPS was a time full of new experiences, both personally and scientifically, a time with ups and downs, challenges and successes. It was the people who I had the pleasure to work with, that made the past years a memorable time.

First of all, I would like to thank my Doktorvater Prof. Dr. Claus-Michael Lehr, who gave me the opportunity to perform my thesis in his group. You have supported, advised and trusted me from the very beginning and I have learned a lot from you, not only, but importantly, that collaboration is key in science. This thesis is the result of the collaboration with a lot of people and the list of co-authors is long. I'm indebted to many people and gratefully acknowledge all contributions, without which this work would not have been possible. In the following lines, I will only name a few of them.

Dr. Brigitta Loretz, you have been the continuum throughout the years, the person number one to ask about science, money, organizing whatever there was to organize, supporting me literally day and night. Thank you! Thanks to Prof. Dr. Marc Schneider for co-supervising this work. Then there are the two Spanish guys, Xabi und Alberto, who I owe a special thanks for their great support, discussions and advice. It was pleasure working with you! The same is true for Thiago. Olga and Rebekka, we shared a lot more in common than just the office! I have to thank the people "behind the scenes"; our technicians Petra, Jana, Annette and Pascal for their help in cell culture and in HPLC/LC-MS analysis, and Sarah and Karen for the office support. Working in such a big group, I'm grateful that I had the chance to meet a lot of exciting people from all over the world. Just name a few of them: Sarah<sup>3</sup>, Yun, Aghiad, Carlos, Patrick, Justus, Robert, Adriely, Mina, Sarah, Khiet, Eileen, Thomas, Lena, Max, Cristiane, Chiara, Olga and many, many more.

Zu guter Letzt möchte ich meiner Familie danken. Danke Mama und Papa, für Eure immerwährende Unterstützung, die diesen Weg möglich gemacht hat. Gleiches gilt für meine Geschwister, insbesondere meinen großen Bruder, ihr wart mir immer ein Vorbild! Zum Schluss möchte ich einer ganz besonderen Person danken. Liebe Lisa, danke für deine unermüdliche Unterstützung, deine Toleranz, Ermutigung, den Ausgleich und die Motivitionsschübe, wenn ich sie am besten brauchen konnte.